



# Indirect Constraints on Composite Higgs Models and Leptoquarks

Christoph Niehoff

Vollständiger Abdruck der von der Fakultät für Physik der Technischen Universität München zur Erlangung des akademischen Grades eines

**Doktors der Naturwissenschaften (Dr. rer. nat.)**

genehmigten Dissertation.

Vorsitzender: Prof. Dr. Bastian Märkisch

Prüfer der Dissertation: 1. Prof. Dr. Martin Beneke  
2. Prof. Dr. Andreas Weiler

Die Dissertation wurde am 03.05.2017 bei der Technischen Universität München eingereicht und durch die Fakultät für Physik am 20.06.2017 angenommen.



## Abstract

In this thesis we investigate the impact of current experimental precision measurements on the parameter spaces of concrete models for new physics. For this we consider two different but well motivated extensions of the Standard Model: composite Higgs models and leptoquark models.

We perform an extensive numerical analysis of composite Higgs models featuring partial compositeness. For this we concentrate on models in which the Higgs boson is implemented as a pseudo-Nambu-Goldstone boson of a broken global symmetry. Of particular interest in this work is a realistic description of electroweak symmetry breaking taking into account the recent discovery of the Higgs boson. Using Markov Chain Monte Carlo techniques we sample the parameter spaces of a minimal model, based on the symmetry breaking  $SO(5)/SO(4)$ , and a next-to-minimal model based on the larger coset  $SO(6)/SO(5)$ . We take into account a large variety of constraints including indirect searches (as e.g. electroweak precision observables, Higgs physics,  $Z$  couplings and flavour physics) as well as direct searches at hadron colliders. This marks the first combined numerical analysis of composite Higgs models that takes into account all relevant constraints while, at same time, generating a realistic electroweak symmetry breaking. With the found results we are able to assess the allowed parameter spaces of the models which allows us to make statements about the possible fine-tuning in these models and to make predictions for yet unobserved processes and promising experimental tests.

We further investigate leptoquarks in  $b \rightarrow s$  transitions. In the light of current experimental tensions in  $b \rightarrow s\ell^+\ell^-$  transitions we investigate the role of leptoquarks in the related modes  $B \rightarrow K^{(*)}\bar{\nu}\nu$  and  $B_s \rightarrow \mu^+\mu^-$ . For this we pay particular attention for how the related modes can be used to disentangle possible new physics contributions from leptoquarks.

## Zusammenfassung

In dieser Arbeit untersuchen wir den Einfluss aktueller, experimenteller Präzisionsmessungen auf die Parameterräume von konkreten Modellen Neuer Physik. Dazu betrachten wir zwei verschiedene aber gut motivierte Erweiterungen des Standardmodells: Composite Higgs Modelle and Leptoquark Modelle.

Wir führen eine umfassende numerische Analyse von Composite Higgs Modellen durch, welche über Partial Compositeness verfügen. Hierbei konzentrieren wir uns auf Modelle, in denen das Higgs Boson ein pseudo-Nambu-Goldstone Boson einer gebrochenen globalen Symmetrie ist. Dabei sind wir besonders an einer realistischen Beschreibung der elektroschwachen Symmetriebrechung interessiert, wobei wir die kürzliche Entdeckung des Higgs Bosons berücksichtigen. Mit Hilfe von Markov Ketten wird der Parameterraum eines minimalen Modelles, welches auf der Symmetriebrechung  $SO(5)/SO(4)$  basiert, und eines nicht-minimalen Modelles, basierend auf  $SO(6)/SO(5)$ , untersucht. Dieses ist die erste globale, numerische Analyse von Composite Higgs Modellen, welche alle relevanten Einschränkungen einbezieht und gleichzeitig zu einer realistischen Brechung der elektroschwachen Symmetrie führt. Mit den gefundenen Datenpunkten ist es möglich, Aussagen über das mögliche Feintuning in diesen Modellen zu treffen und Vorhersagen zu machen für bis jetzt ungemessene Observablen wie auch für weitere experimentelle tests.

Weiterhin betrachten wir Leptoquarks in  $b \rightarrow s$  Übergängen. In Anbetracht von momentanen experimentellen Hinweisen für mögliche neue Physik in  $b \rightarrow s\ell^+\ell^-$  Übergängen untersuchen wir Leptoquarks in den verwandten Moden  $B \rightarrow K^{(*)}\bar{\nu}\nu$  und  $B_s \rightarrow \mu^+\mu^-$ . Hierbei geben wir ein besonderes Augenmerk der Frage, wie diese verwandten Moden helfen koennen, mögliche Leptoquarkbeiträge zu unterscheiden.





## Publications within the context of this dissertation

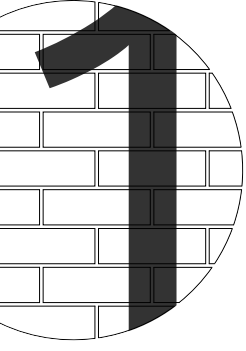
- [1] W. Altmannshofer, C. Niehoff, P. Stangl and D. M. Straub,  
*Status of the  $B \rightarrow K^* \mu^+ \mu^-$  anomaly after Moriond 2017*  
arXiv:1703.09189
- [2] W. Altmannshofer, C. Niehoff and D. M. Straub,  
 *$B_s \rightarrow \mu^+ \mu^-$  as current and future probe of new physics*  
arXiv:1702.05498
- [3] C. Niehoff, P. Stangl and D. M. Straub,  
*Electroweak symmetry breaking and collider signatures in the next-to-minimal composite Higgs model*  
published in JHEP **04** (2017) 117, arXiv:1611.09356
- [4] C. Niehoff, P. Stangl and D. M. Straub,  
*Direct and indirect signals of natural composite Higgs models*  
published in JHEP **01** (2016) 119, arXiv:1508.00569
- [5] C. Niehoff, P. Stangl and D. M. Straub,  
*Violation of lepton flavour universality in composite Higgs models*  
published in Phys. Lett. **B747** (2015) 182-186, arXiv:1503.03865
- [6] A. J. Buras, J. Girrbach-Noë, C. Niehoff and D. M. Straub,  
 *$B \rightarrow K^{(*)} \nu \bar{\nu}$  decays in the Standard Model and beyond*  
published in JHEP **02** (2015) 184, arXiv:1409.4557



# Contents

<b>1. Introduction</b>	<b>9</b>
1.1. The Standard Model . . . . .	9
1.2. Shortfalls of the Standard Model . . . . .	11
1.3. New Physics . . . . .	13
1.4. Outline of this work . . . . .	14
<b>2. Composite Higgs Models</b>	<b>15</b>
2.1. General structure of composite pNGB-Higgs models . . . . .	16
2.1.1. The composite and the elementary sector . . . . .	17
2.1.2. Composite-elementary mixings . . . . .	21
2.2. Phenomenological features . . . . .	24
2.2.1. Custodial symmetry . . . . .	24
2.2.2. Electroweak symmetry breaking . . . . .	26
2.2.3. Flavour symmetries . . . . .	32
2.2.4. Connecting flavour and the potential . . . . .	35
2.3. Composite Higgs models from extra dimensions . . . . .	37
2.3.1. Gauge-Higgs unification and the Hosotani mechanism . . . . .	38
2.3.2. Realistic GHU models . . . . .	43
2.3.3. Dimensional deconstruction . . . . .	45
2.4. Summary and a word of caution . . . . .	49
<b>3. Numerical strategy</b>	<b>51</b>
3.1. Generating viable parameter points . . . . .	51
3.2. Calculating observables . . . . .	54
3.3. Constraints . . . . .	57
3.3.1. SM parameters . . . . .	57
3.3.2. Electroweak precision observables . . . . .	61
3.3.3. $Z$ widths . . . . .	63
3.3.4. Higgs production and decay . . . . .	64
3.3.5. Flavour observables . . . . .	65
3.3.6. Electric dipole moments . . . . .	71
3.3.7. Contact interactions of light quarks . . . . .	72
3.3.8. Direct searches at colliders . . . . .	73
3.4. Summary . . . . .	77
<b>4. <math>SO(5)/SO(4)</math> – the minimal model</b>	<b>79</b>
4.1. The minimal 4d composite Higgs model . . . . .	79
4.2. The scan . . . . .	83
4.3. Electroweak symmetry breaking . . . . .	84
4.3.1. Fine-tuning . . . . .	84
4.3.2. Potential . . . . .	86
4.4. Spectra . . . . .	88
4.5. Main constraints . . . . .	91
4.6. Higgs physics . . . . .	93
4.7. Flavour physics . . . . .	93
4.7.1. Meson-antimeson mixing . . . . .	93
4.7.2. Rare decays . . . . .	99

4.8. Summary . . . . .	102
<b>5. SO(6)/SO(5) – the next-to-minimal model</b>	<b>105</b>
5.1. The next-to-minimal 4d composite Higgs model . . . . .	105
5.1.1. Nambu-Goldstone bosons in SO(6)/SO(5) . . . . .	105
5.1.2. Bosonic Lagrangian . . . . .	107
5.1.3. Fermion Lagrangian . . . . .	109
5.1.4. Flavour structure . . . . .	110
5.1.5. The effective potential and electroweak symmetry breaking . . . . .	111
5.2. The scan . . . . .	112
5.3. Fine-tuning . . . . .	112
5.4. The SO(5)/SO(4) limit . . . . .	113
5.5. Novel features . . . . .	116
5.5.1. Potential . . . . .	116
5.5.2. Higgs physics . . . . .	117
5.5.3. Flavour physics . . . . .	117
5.5.4. $CP$ violation . . . . .	118
5.5.5. Collider phenomenology of $\eta$ . . . . .	120
5.6. Summary . . . . .	120
<b>6. Leptoquarks in <math>b \rightarrow s</math> transitions</b>	<b>123</b>
6.1. $b \rightarrow s$ transitions . . . . .	123
6.2. Leptoquark basics . . . . .	124
6.3. Leptoquarks and $b \rightarrow s\bar{\nu}\nu$ . . . . .	127
6.4. Direct bounds on leptoquarks . . . . .	134
6.5. Leptoquarks and $B_s \rightarrow \mu\mu$ . . . . .	136
6.6. Summary . . . . .	143
<b>7. Conclusion</b>	<b>147</b>
<b>Appendix</b>	<b>151</b>
<b>I. Group theory</b>	<b>153</b>
I.1. SO(5) . . . . .	153
I.2. SO(6) . . . . .	154
<b>II. CCWZ formalism</b>	<b>157</b>
<b>III. Mass matrices of composite Higgs models</b>	<b>161</b>
III.1. M4dCHM . . . . .	161
III.1.1. Boson sector . . . . .	161
III.1.2. Fermion sector . . . . .	161
III.2. NM4dCHM . . . . .	164
III.2.1. Vector bosons . . . . .	164
III.2.2. Fermions . . . . .	166
<b>IV. Composite-elementary mixings</b>	<b>169</b>
IV.1. M4dCHM . . . . .	169
<b>V. Markov Chain Monte Carlo techniques</b>	<b>171</b>
<b>VI. Effective potential for NM4dCHM</b>	<b>173</b>



# Introduction

Mankind has always been driven by the desire to know what lies *beyond*. This work is no exception to this as it joins the hunt for the answer to the question of what lies beyond our present knowledge of physics at the smallest scales. By now, we have an extraordinary understanding of particle physics down to the level of quarks and leptons. The mathematical framework for this, the Standard model, is magnificently successful in passing the tests of it conducted at high energy experiments such as the Large Hadron Collider (LHC). But it is not enough to understand what we see. We want to know if this is everything and if not, we want to know what it is that lies beyond.

Such a question cannot be answered by theory alone. What is important is an interplay between theoretical ideas and experimental observation since only nature itself can tell us what it is. Such an interplay is at the heart of this work as we will investigate what experimental data can tell us about concrete models of physics beyond the Standard model. In principle, observations can impact theory through different ways. If something unexpected is measured then it can serve as a guiding light of which theory model might be the right one. But also if nothing new is measured, these null results but important constraints on the parameters of any model. In the following we will proceed from both direction.

## 1.1. The Standard Model

What today is known as the *Standard Model of particle physics* (SM) is a gauge theory describing the strong interactions as well as the electroweak unification. Quantum Chromodynamics (QCD), the theoretical description of the strong interactions, is based on the quark model proposed by Gell-Mann, Ne'eman and Zweig and was put into the mathematical framework of a non-abelian gauge theory by Fritzsche, Gell-Mann and Leutwyler [7] in the 1970s. The electroweak sector of the SM was proposed in the 1960s by Glashow [8], Weinberg [9] and Salam and has to be equipped with the mechanism of a spontaneous breaking of the gauge symmetries. The latter was also discovered in the 1960s independently by several groups [10, 11, 12, 13] and is today widely known as the Higgs mechanism.

Let us dive right away into the Lagrangian,

$$\mathcal{L}_{\text{SM}} = -\frac{1}{2} \text{tr} [G_{\mu\nu} G^{\mu\nu}] - \frac{1}{2} \text{tr} [W_{\mu\nu} W^{\mu\nu}] - \frac{1}{4} B_{\mu\nu} B^{\mu\nu} \quad (1.1a)$$

$$+ \sum_f \left\{ \bar{q}_L^f i \not{D} q_L^f + \bar{u}_R^f i \not{D} u_R^f + \bar{d}_R^f i \not{D} d_R^f + \bar{l}_L^f i \not{D} l_L^f + \bar{\ell}_R^f i \not{D} \ell_R^f \right\} \quad (1.1b)$$

$$+ (\mathcal{D}_\mu \Phi)^\dagger (\mathcal{D}^\mu \Phi) \quad (1.1c)$$

$$+ Y_{ij}^d (\bar{q}_L^i \cdot \Phi) d_R^j + Y_{ij}^u (\bar{q}_L^i \cdot \epsilon \cdot \Phi^*) u_R^j + Y_{ij}^\ell (\bar{l}_L^i \cdot \Phi) \ell_R^j + \text{h.c.} \quad (1.1d)$$

$$- V(\Phi^\dagger \Phi) \quad (1.1e)$$

and explain the individual ingredients on the fly.

The SM is a gauge theory built on the symmetry

$$G_{\text{SM}} = \text{SU}(3)_c \times \text{SU}(2)_L \times \text{U}(1)_Y. \quad (1.2)$$

This includes the strong interactions via QCD based on the group  $\text{SU}(3)_c$  as well as the electroweak sector with the symmetries  $\text{SU}(2)_L \times \text{U}(1)_Y$  that correspond to weak isospin and hypercharge, respectively. Eq. (1.1a) shows the kinetic terms for the gauge fields of this theory. In the case of the SM these

are gluon fields  $G_\mu$  corresponding to the  $SU(3)_c$  symmetry transmitting the strong interactions,  $W_\mu$  bosons connected to  $SU(2)_L$  and also an abelian gauge field  $B_\mu$  for the  $U(1)_Y$  symmetry. As the first two gauge components are non-abelian groups the kinetic terms include gauge boson self-interactions, which are of particular importance for the strong interactions as these are the origins of asymptotic freedom and confinement [14, 15].

Eq. (1.1b) shows the matter sector of the SM. An important feature of the SM is that it is a chiral theory meaning that it differentiates between left- and right-handed components of Dirac spinors,

$$\psi = \psi_L + \psi_R = \frac{1}{2}(\mathbb{1} - \gamma_5)\psi + \frac{1}{2}(\mathbb{1} + \gamma_5)\psi, \quad (1.3)$$

where in the last step we used the chiral projectors  $P_{L,R} = \frac{1}{2}(\mathbb{1} \mp \gamma_5)$  such that  $\psi_{L,R} = P_{L,R}\psi$ . This now means that under the electroweak interactions left- and right-handed components behave differently which is synonymous to assigning different representations under the SM gauge symmetry (1.2) to them. An important consequence of the chiral structure is that by gauge invariance no mass terms for the fermion fields are allowed. Putting the SM matter content into one table gives the following:

<b>Quarks</b>	$q_L^1 = \begin{pmatrix} u_L \\ d_L \end{pmatrix}$	$q_L^2 = \begin{pmatrix} c_L \\ s_L \end{pmatrix}$	$q_L^3 = \begin{pmatrix} t_L \\ b_L \end{pmatrix}$	$\in (\mathbf{3}, \mathbf{2})_{\frac{1}{6}}$
	$u_R$	$c_R$	$t_R$	$\in (\mathbf{3}, \mathbf{1})_{\frac{2}{3}}$
	$d_R$	$s_R$	$b_R$	$\in (\mathbf{3}, \mathbf{1})_{-\frac{1}{3}}$
<b>Leptons</b>	$l_L^1 = \begin{pmatrix} \nu_e \\ e_L \end{pmatrix}$	$l_L^2 = \begin{pmatrix} \nu_\mu \\ \mu_L \end{pmatrix}$	$l_L^3 = \begin{pmatrix} \nu_\tau \\ \tau_L \end{pmatrix}$	$\in (\mathbf{1}, \mathbf{2})_{-\frac{1}{2}}$
	$e_R$	$\mu_R$	$\tau_R$	$\in (\mathbf{1}, \mathbf{1})_{-1}$

This already reveals much of the structure of the SM. Matter fields can be divided according to their participation in the strong interactions, such that quarks couple to gluons while leptons are unaffected by them. Left-handed chiral fields always appear as  $SU(2)_L$  doublets, while right-handed fields are always singlets. Consequently, it is only the left-handed fields that interact with  $W_\mu$  bosons and right-handed ones are neutral under weak isospin interactions. Another important feature is the fact that nature seems to repeat itself in a threefold way such that quarks as well as leptons can be grouped into generations (or families). This is of great relevance to this work, as we will deal extensively with transitions between the different generations. In (1.1b) we introduced generational (or flavour-) indices such that we write right-handed up-type and down-type quarks as well as charged leptons in generational space as  $u_R^f = (u_R, c_R, t_R)$ ,  $d_R^f = (d_R, s_R, b_R)$  and  $\ell_R^f = (e_R, \mu_R, \tau_R)$ , respectively. Note that there are no right-handed neutrinos in the SM.

As a last ingredient the SM contains the Higgs field  $\Phi$  with the kinetic and gauge interaction term (1.1c). This is implemented as scalar doublet under  $SU(2)_L$  with quantum numbers  $\Phi \in (\mathbf{1}, \mathbf{2})_{\frac{1}{2}}$ , such that it couples to the electroweak sector but not to the strong interactions.

The Higgs can couple via the Yukawa interactions (1.1d) to the fermion sector of the SM. Phenomenologically, these terms are of utmost importance as these are the only terms in the SM distinguishing between the different fermion generations and therefore these terms are the sources of flavour transitions.

The last term (1.1e) shows one of the most important but at the same time most mysterious terms of the SM. Through the potential

$$V(\Phi^\dagger\Phi) = \mu^2\Phi^\dagger\Phi - \lambda(\Phi^\dagger\Phi)^2 = -\lambda(\Phi^\dagger\Phi - v^2)^2 \quad (1.4)$$

the Higgs field receives a non-vanishing *vacuum expectation value* ( $vev$ ),

$$\langle 0|\Phi|0\rangle = \frac{1}{\sqrt{2}}\begin{pmatrix} 0 \\ v \end{pmatrix}, \quad (1.5)$$

that does not respect the symmetries and therefore leads to a spontaneous breakdown of gauge invariance meaning that the Higgs potential induces *electroweak symmetry breaking* (*EWSB*). As a

consequence, masses for the gauge bosons and fermions are generated that were forbidden before by gauge invariance. To see this, consider the interactions (1.1c) of the Higgs field with the gauge bosons. After the Higgs assumes its vev (1.5) mass terms are generated,

$$\mathcal{L} \supset \frac{v^2}{8} \begin{pmatrix} B_\mu \\ W_\mu^3 \end{pmatrix}^t \begin{pmatrix} g_1^2 & -g_1 g_2 \\ -g_1 g_2 & g_2^2 \end{pmatrix} \begin{pmatrix} B_\mu \\ W_\mu^3 \end{pmatrix}, \quad (1.6)$$

that have to be diagonalized by a transformation

$$\begin{pmatrix} B_\mu \\ W_\mu^3 \end{pmatrix} \rightarrow \begin{pmatrix} \cos(\theta_w) & -\sin(\theta_w) \\ \sin(\theta_w) & \cos(\theta_w) \end{pmatrix} \begin{pmatrix} A_\mu \\ Z_\mu \end{pmatrix} \quad (1.7)$$

as physical states are the ones that possess a diagonal mass matrix. One of the two eigenvalues of the mass matrix (1.6) vanishes which means that due to the interactions with the Higgs vev (1.5) there is a rearrangement of gauge degrees of freedom into a massless and a massive mode. The massless mode can be identified with the photon corresponding to the unbroken electromagnetic subgroup generated by a linear combination of the original generators,

$$Q = T_3 + Y. \quad (1.8)$$

In the same manner, one sees that also masses for  $W$  boson are generated and (ignoring quantum corrections) one expects

$$m_Z = \frac{1}{2} \sqrt{g_1^2 + g_2^2} v, \quad m_W = \frac{1}{2} g_2 v \quad \text{such that} \quad \frac{m_W}{m_Z} = \cos(\theta_w), \quad (1.9)$$

where the weak mixing angle  $\tan(\theta_w) = g_1/g_2$  was introduced.

In a similar way fermion masses are generated through Yukawa interactions (1.1d) with the Higgs vacuum. Considering for simplicity only quarks<sup>1</sup>, these masses are non-diagonal in flavour-space and have to be diagonalized via unitary transformations of the quarks in flavour space,

$$u_L^i \rightarrow \mathcal{V}_{uL}^{ij} u_L^j, \quad d_L^i \rightarrow \mathcal{V}_{dL}^{ij} d_L^j, \quad u_R^i \rightarrow \mathcal{V}_{uR}^{ij} u_R^j, \quad d_R^i \rightarrow \mathcal{V}_{dR}^{ij} d_R^j. \quad (1.10)$$

This also affects the couplings of the quarks to gauge bosons. Considering for example the couplings to the  $W$  boson, these also have to be rotated into the mass basis

$$W_\mu^+ \bar{u}_L^i \gamma^\mu d_L^i \rightarrow \underbrace{\mathcal{V}_{uL}^{+ai} \mathcal{V}_{dL}^{ib}}_{=: V_{CKM}^{ab}} W_\mu^+ \bar{u}_L^a \gamma^\mu d_L^b, \quad (1.11)$$

showing that the flavour off-diagonal Yukawa couplings induce flavour transitions via  $W$  boson interactions. This is the famous Cabibbo-Kobayashi-Maskawa (CKM) mechanism [16, 17]. The SM contains  $CP$  violation through a single complex phase in CKM matrix. Note however that neutral vector bosons such as the photon, the  $Z_\mu$  as well as gluons do not induce flavour violations.

## 1.2. Shortfalls of the Standard Model

Although the SM is spectacularly successful in describing the present-day experimental data in high energy physics<sup>2</sup>, which includes the experimental confirmation of the Higgs boson in 2012 at the LHC [18, 19], it cannot be the end of the story of particle physics. There are several reasons to believe that there has to be some form of New Physics (NP) beyond the SM. These reasons can roughly be grouped into three categories. The first one regards the origin of the SM and its structure. Second there are concrete experimental observations that show that the SM, at least in its minimal version, does not describe all of the low energy degrees of freedom. And last, the SM suffers from inconsistencies due to the presence of an elementary scalar field. In what follows we will discuss these shortfalls of the SM.

<sup>1</sup>In the SM neutrinos are strictly massless such that unitary transformations in the lepton sector do not have a physical effect. Experimentally, it is, however, by now well established that neutrinos have small masses. Therefore there actually are flavour structures in the lepton sector. We will not consider this modification in this work.

<sup>2</sup>There are actually some tensions between experimental results and SM predictions in particular in flavour transitions. We will neglect them for the time being due to the overall success of the SM and come back to this issue in section 1.3

**Origin of the SM** The structure of the SM which in particular means its gauge group (1.2) and the matter content were motivated by observation, but no explanation is given as to why nature has chosen this particular option. Furthermore, the SM depends on a number of free parameters whose values are known only by observation. That in itself does not pose a problem, but the structure of the SM parameters can be seen as suggesting that there might be something going on beyond the SM. For this let us consider the Yukawa interactions (1.1d) which give rise to the two different kinds of observables: After diagonalization the singular values of the Yukawa matrices determine the masses of the fermions in the SM, such that after EWSB the fermion  $\psi$  obtains the mass  $m_\psi = \frac{1}{\sqrt{2}}y_\psi v$ , where  $y_\psi$  denotes the diagonal Yukawa coupling and  $v$  is the Higgs vev. The fermion masses show large hierarchies starting with the up- and down-masses in the MeV range all the way up to the large top mass of around 173 GeV. These large ranges of Yukawa couplings call for a dynamical explanation beyond the SM. Further, the Yukawa matrices determine the CKM matrix and therefore induce flavour transitions. Experimentally the CKM matrix is known to be strongly dominated by its diagonal elements.

A very important but not very well understood piece of the SM is the Higgs potential (1.1e). In the usual formulation this is introduced “by hand” as a parametrization of renormalizable Higgs self-interactions. Its origin and therefore the source of EWSB is currently unknown.

**Conflicts with observations** There are experimental observations that are in direct conflict with the SM that directly show that at least small extensions have to be added to it. Most and for all these are the observations of neutrino oscillations that directly show that, contrary to the assumptions of the SM, neutrinos are massive. This further necessitates an analogue of the CKM in the lepton sector, which is given by the Pontecorvo-Maki-Nakagawa-Sakata (PMNS) matrix [20, 21] and which is completely absent in the SM.

Another open question in the SM is the nature of dark matter. By now there is a lot of observational evidence, ranging from galactic rotation curves to the formation of large scale structure, that some form of dark matter should exist. SM degrees of freedom alone cannot generate the needed effects [22].

**Hierarchy and fine-tuning** For many decades the problem of the stability of the electroweak scale has been the main motivation to construct models of NP. Deep inside this consists of two separate problems that are however intimately connected.

1. Nature seems to contain at least two vastly different energy scales. One is the electroweak scale  $v = 246$  GeV that dictates the mass scale of all known elementary particles. In the SM this scale is determined by the bilinear term in the Higgs potential and, therefore, it is deeply connected to the Higgs mass. As a second scale there exists the Planck mass  $m_{\text{Pl}} \sim 10^{19}$  GeV which is the naive scale where one expects quantum gravity effects to set in. These two scales differ by many orders of magnitude leading to the question what determines the hierarchy  $v_{\text{SM}} \ll m_{\text{Pl}}$ . Assuming the Planck scale to be the fundamental one, this is the question of what is the mechanism that sets the value of the second scale and why is it so different [23]. This is the so-called *hierarchy problem*, which is not a problem per se but it is an open question to which one would like to have an answer. A different way to pose this question is by asking why the gravitational force is so much weaker than the electroweak force.
2. The second problem is more technical. It regards the consistency of the calculation of the electroweak scale (i.e. of the Higgs mass) and its robustness under very small variations in the fundamental UV parameters. Being a fundamental scalar that is not protected by a symmetry, the Higgs mass parameter receives highly UV-dependent quantum corrections [24, 25]. A priori, this is no problem as the SM is a renormalizable QFT such that the Higgs mass can consistently be calculated to all orders in the perturbative expansion. Even better, the measured Higgs mass takes a special value such that the theory can be extrapolated to high energies without running into problems such as Landau poles. However, as we have argued above the SM is not the whole story. For sure we know that there has to be some form of physics beyond the SM. Inevitably, this introduces a new energy scale. Even if this were not the case, there is at least the Planck scale that has to be considered. Having another energy scale leads to a problem for the Higgs mass as it will also get renormalized by the NP sector (at least by quantum gravity). Due to the strong sensitivity on UV



---

physics the Higgs mass renormalization will be of the order of the NP scale. Having a light Higgs mass then is only possible if there is a fragile conspiracy between the SM and the NP contributions. This is the so-called *fine-tuning problem*. Either there is the SM and some NP sector such that accidentally there is a cancellation fine-tuned to many digits such that the correct Higgs mass comes out or there is some mechanism that correlates the SM and NP contributions in such a way that a cancellation occurs *naturally* [26]. In this sense the fine-tuning problem can be understood as a guidepost for the shape of NP.

Both problems are connected, but they are not identical. While the first one is not a problem in the literal sense it is an important question to which at some point there should be an answer, even if this is in the distant future. The second problem is more acute. Of course, it is a logical possibility that nature just is fine-tuned and that the value of the electroweak scale really just is a coincidence, but this is not really satisfactory. Also, it seems hard to believe that EWSB, which is a necessary condition for the structure formation of the universe from very small to very large scales, would be hanging on a thread in such a delicate way. Therefore it is widely believed<sup>3</sup> that NP should come in a form rendering the electroweak scale natural.

### 1.3. New Physics

This work deals with the search for New Physics beyond the Standard Model. There are many different approaches to this task either from the theory side or from experiment. We will try to deal with this undertaking from a few well-motivated but different angles. In general, the goal of phenomenology in particle physics is to find correlations between observables such that experimentally verifiable predictions can be made given some input data. This goes hand in hand with the notion of a *parameter space* which gets constrained by experimental data.

On the theory side NP effects can be investigated either in concrete models or in effective theories. Concrete models are usually fully-fledged frameworks that are designed to solve some “big problem” as for example the fine-tuning problem. For this there are many models on the market. Although there are many more, the mainstream ones can be grouped into roughly two classes: There are weakly interacting models of which supersymmetric theories are the most prominent example, and there are models of new strong interactions which can often be described dually by theories on extra-dimensions. For large parts of this work we will concentrate on the second possibility and consider Composite Higgs Models (CHMs) which solve the fine-tuning problem by assuming that the Higgs boson is no fundamental object such that it decomposes into its constituents at high enough energies. The phenomenological success of such a model can even be ameliorated if the Composite Higgs is a pseudo-Nambu-Goldstone boson (pNGB) of a broken global symmetry. We are primarily interested in EWSB and flavour transitions of this kind of models.

A different theoretical approach to NP is abandoning a concrete model and the ability to solve a problem like the fine-tuning problem and supplementing the SM only with a minimal insertion of NP. In this simplified model approach one can add a single NP field or even just a single effective operator. The advantage of this approach is a loss of model-dependence but one has to assume that in the fundamental theory there is some mechanism that suppresses the effects of the remaining model. We will consider such a simplified mode by investigating leptoquark (LQ) models in which in addition to the SM there is only one extra field whose presence is one possibility that helps to explain certain experimental tensions in flavour physics.

The experimental program for searches of NP also proceeds from different angles. The obvious way is to search for NP particles directly in particle collisions at collider experiments. These searches are very important as in the end a NP particle has to be detected directly in order to be sure about its existence. However, direct searches are limited to mass ranges given by the collision energies of the accelerators. A complementary path is given by indirect searches through precision measurements of, for example, flavour changing neutral current (FCNC) processes in the flavour sector. In the SM such a processes are strongly suppressed by the Glashow-Iliopoulos-Maiani (GIM) mechanism [27]. Therefore, already very small NP contribution can lead to visible effect and hence this approach can, in principle, test much higher mass ranges than direct searches. However, the drawback is that without seeing direct evidence for NP it is hard to differentiate between models such that the hope is that signals will show up in several observables which would allow to disentangle NP contributions

---

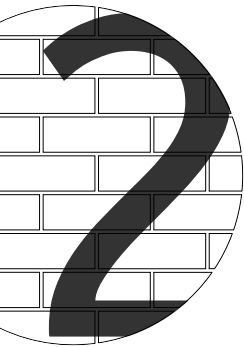
<sup>3</sup>Here, we ignore anthropic reasoning.

via correlations. In this work we will concentrate on indirect constraints on NP models. Direct constraints will be included in the analyses as they give valuable complementary bounds but for a detailed discussion we refer to [28].

## 1.4. Outline of this work

This work is based on two pillars:

1. The investigation of the impact of the Higgs discovery and flavour physics on models of a composite pNGB Higgs with partial compositeness. This will be done through an extensive numerical analysis which takes into account all relevant data from direct and indirect searches as well as a realistic breaking of the electroweak symmetries. For this we first set the stage and introduce CHMs in a detailed manner in chapter 2. In particular, we will discuss radiative EWSB through the Coleman-Weinberg potential and how such theories can emerge from extra-dimensional gauge theories. We will lay out our numerical strategy in chapter 3 and present all the bounds that we impose in the analyses. The results of the analyses will be given in chapters 4 and 5 where we will concentrate on the minimal model and a next-to-minimal variant, respectively.
2. In the last chapter 6 we will investigate the role of leptoquarks in  $b \rightarrow s$  transitions. While there are experimental tensions observed in  $b \rightarrow s\ell^+\ell^-$  decays which can be understood in terms of leptoquarks, we will investigate the impact on the related modes  $B \rightarrow K^{(*)}\bar{\nu}\nu$  and  $B_s \rightarrow \mu^+\mu^-$ . We further discuss direct bounds on leptoquark masses through collider searches for the relevant scenarios.



## Composite Higgs Models

One of the main motivations for considering CHMs is that they give a solution to the fine-tuning problem of the electroweak scale. Solutions to this problem usually embed the SM in some larger framework that explains why NP contributions to the Higgs mass should be correlated to the SM ones such that, naturally, there is a cancellation and the correct mass is generated. In the literature this problem is mostly tackled by addressing the fact that the Higgs is a *fundamental scalar* particle such that there is no symmetry which protects its mass (as e.g. a chiral symmetry for fermions or a gauge symmetry for gauge bosons). In supersymmetric models one considers the attribute “scalar” and introduces a symmetry that relates the Higgs to fermion degrees of freedom such that it inherits part of their properties (in particular, a mechanism to protect its mass). In CHMs, on the other hand, one loses the attribute “fundamental” by assuming that the Higgs is a composite object that at high enough energies decomposes into its constituents for which no fine-tuning problem exists.

Let us discuss this in greater detail and follow the arguments presented in [24]. The whole point of the fine-tuning or naturalness problem is desiring a stability of the electroweak scale under small changes in the fundamental UV parameters. If an unnatural fine-tuning up to many decimal digits takes place this clearly would not be the case. The idea behind CHMs is to reproduce the success of a theory that is known to exhibit light scalar particles without suffering from a fine-tuning problem. This theory is QCD with its hadron spectrum. The hadronic mass scale  $\Lambda_{\text{QCD}}$  is generated by the mechanism of *dimensional transmutation*, such that the value of this scale is insensitive to small changes in the fundamental QCD parameters. By itself QCD does not have any mass scale, but due to the non-abelian self-interactions quantum effects break conformal invariance such that a mass scale is generated “out of nothing”. One can see this by considering the renormalization group evolution (RGE) of the strong coupling constant that relates the value of the coupling measured at some arbitrary scale  $\mu_0$  to the value at some other scale  $Q$ ,

$$g_s^2(Q) = \frac{g_s^2(\mu_0)}{1 - 2\beta g_s^2(\mu_0) \ln\left(\frac{Q}{\mu_0}\right)}. \quad (2.1)$$

For QCD one finds that  $\beta = \frac{1}{16\pi^2} (-11 + \frac{2}{3}n_F) < 0$ . [29] The hadronic mass scale  $\Lambda_{\text{QCD}}$  is given as the value of  $Q$  at which the strong coupling constant gets large and the theory becomes confining. Although the above expression (which was calculated in a perturbative expansion) is not valid anymore in that limit, one can use it to estimate the size of  $\Lambda_{\text{QCD}}$  as the scale at which the denominator vanishes,

$$\Lambda_{\text{QCD}} \sim \mu_0 \exp\left(\frac{1}{2\beta g_s^2(\mu_0)}\right) \sim 200 \text{ MeV}. \quad (2.2)$$

Of course, this expression does not depend on which scale  $\mu_0$  one chooses but only on what value the coupling constant takes at that scale. Choosing  $\mu_0$  in the high UV, one sees that the value of the confining scale does not violently depend on the value of the coupling at high energies, in the sense that the coupling does not have to be tuned to many decimal digits. A tuning to only a few digits might be enough. Therefore, a scale generated via dimensional transmutation is reasonably insensitive to UV physics.

The mass scale of the QCD hadron spectrum is roughly given by  $\Lambda_{\text{QCD}}$ . There are, however, also mesons which are systematically lighter than the other hadrons: the pions. The reason for this lies in the fact that pions can be interpreted as the Nambu-Goldstone bosons (NGBs) of the spontaneously broken chiral symmetry. As the quark masses break chiral symmetry explicitly, the

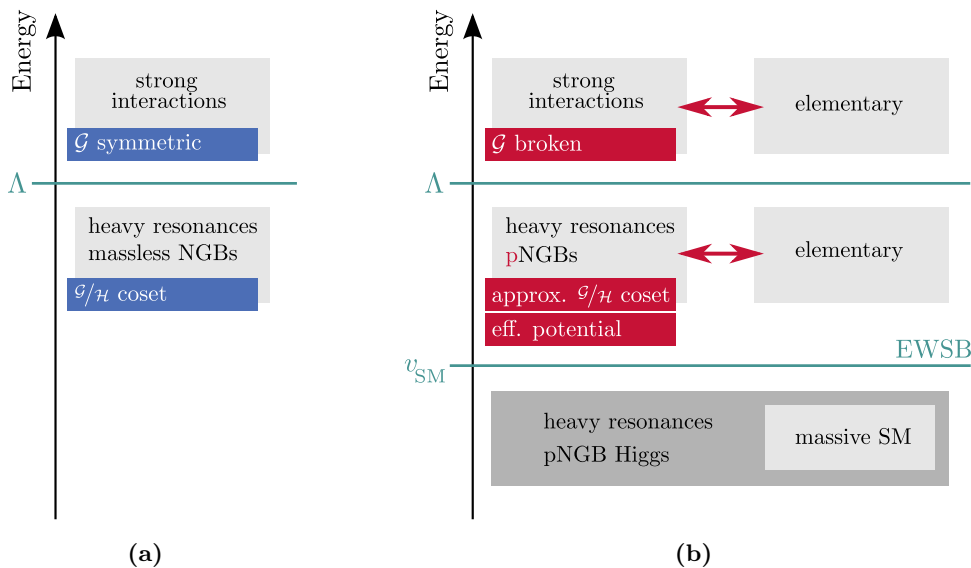


**Figure 2.1.:** Schematical structure of pNGB-CHMs. *Left:* without composite-elementary mixings. *Right:* with composite-elementary mixings.

pions are actually *pseudo*-Nambu-Goldstone bosons (pNGBs) that obtain a small mass proportional to the explicit symmetry breaking.

The main motivation behind composite Higgs models now lies in reproducing these structures at higher energies in such a way that the fine-tuning problem of the Higgs sector is solved. Imagine some non-abelian Yang-Mills theory invariant under some new strong interactions at high enough energies. By quantum effects, dimensional transmutation will generate a mass scale that is reasonably insensitive to the detailed UV physics. Then, below that mass scale the theory will appear as being “hadronized” into bound states whose masses are roughly given by the hadronization scale. These masses have to be large enough to circumvent experimental constraints. If we also assume that the UV sector is invariant under some global symmetry that is broken by some mechanism, pNGBs will appear with masses parametrically lighter than the other bound states. These Goldstone degrees of freedom can be identified with the Higgs field and its mass determines the electroweak scale that is naturally suppressed with respect to the scale where NP shows up. This scale, being generated through dimensional transmutation, is reasonably insensitive to UV physics and the fine-tuning problem is solved.

## 2.1. General structure of composite pNGB-Higgs models

In this section we introduce the general structure of Composite Higgs Models in which the Higgs is implemented as a pNGB and which feature partial compositeness. For this, the basic idea is the following: Imagine that there was a theory similar to the SM, but without a Higgs field. In addition, we assume that there is a whole sector of new physics which is confining at ‘low’ energies and will appear as a bunch of ‘hadrons’ at energies assessable to us. If both sectors interact in a suitable way we can think of the Higgs boson as one of the new hadrons and its interactions with the SM are induced by the interactions of both sectors.

Let us describe the structure of this construction using figure 2.1. Imagine the case of figure 2.1a: At high energies we assume the presence of some confining, strongly-interacting NP sector. We do not specify what it is exactly, but we will assume that this sector is well-behaved in the UV. One can think of it as some conformal theory, maybe similar to a technicolor model, or one can look at it through the dual picture of an extra-dimensional theory. No matter what this theory is, we will assume it to be invariant under a global symmetry group  $\mathcal{G}$ . At an energy scale  $\Lambda$  we will furthermore assume that something similar the chiral symmetry breaking will occur, namely that by some not further discussed mechanism this global symmetry  $\mathcal{G}$  will be broken down spontaneously to its subgroup  $\mathcal{H}$ . As a consequence, below the scale  $\Lambda$  the spectrum will contain massless NGB degrees of freedom corresponding to the coset  $\mathcal{G}/\mathcal{H}$ . Also, at low energies because of the confining character of the UV

interactions we expect the UV degrees of freedom to be “hadronized down” into composite resonances.

As a next step, we can think about adding a second sector to the theory. This we will call the “elementary sector”, since we will assume it to be neutral under the interactions of the strong sector. Consequently, there will be no resonances of the elementary fields. The elementary sector should be chiral and look similar to the SM without the Higgs boson. As a last ingredient, we will allow the elementary sector to interact weakly with the confining sector in such a way that the global symmetry  $\mathcal{G}$  is subject to a weak explicit breaking, but the elementary gauge symmetries are still preserved. Below the energy  $\Lambda$  we will then have only an approximate coset  $\mathcal{G}/\mathcal{H}$  and the corresponding NGBs turn into *pseudo*-NGBs that are still massless but not protected anymore by the Goldstone shift symmetry. At this point the theory will look just like the SM in the unbroken phase supplemented with heavy NP fields. Quantum corrections will now be able to generate a potential for the pNGBs that, given the right conditions, induces a vacuum expectation value (vev) leading to a spontaneous breaking of the remaining symmetries as in the SM. The pNGBs we will, thus, identify with the Higgs doublet and the newly generated scale is the scale of electroweak symmetry breaking. Below this energy scale, the theory should look like the SM in the broken phase embedded into a large theory with heavy composite resonances and a composite pNGB Higgs.

For the further course of this work we will be mostly indifferent to the way the theory looks in the far UV. We will work in a bottom-up approach considering only composite resonances, but not the fields they are composed from. Some model aspects can be motivated having a certain UV theory in mind, but they will prove to be more general. For example, we will motivate partial compositeness by consideration of technicolor-like theories, but as we will see in section 2.3 this feature also naturally arises in other theories such as extra dimensions. The advantage of this approach is less model dependence which allows us to investigate the general idea of compositeness and its compatibility with current experimental data. If the model does not work in the bottom-up approach then it also will not work top-down, regardless of which UV theory one is thinking about. Analyses of concrete UV completions can be found in [28].

### 2.1.1. The composite and the elementary sector

The basic structure of such a model consists of an elementary sector and composite resonances; one of which we can identify with the Higgs field. In order for the elementary particles to interact with the composite Higgs there has to be a connection between these two sectors. Schematically, the Lagrangian then has the following form:

$$\mathcal{L} = \mathcal{L}_{\text{elementary}} + \mathcal{L}_{\text{composite}} + \mathcal{L}_{\text{int}}. \quad (2.3)$$

These composite-elementary interactions then allow the elementary particles to interact indirectly with the composite Higgs, via mixing with composite fields which directly interact with the Higgs. As a consequence of this mixing with composite states the elementary particles acquire a mass and the electroweak symmetry is broken.

Let us go into detail and consider the various sectors of this kind of models.

### Elementary sector

The elementary part of the above model should resemble the well-known structure of the SM. In particular, we assume the elementary sector to be invariant under an elementary version<sup>1</sup> of the SM gauge symmetry  $G_{\text{SM}}^0 = \text{SU}(3)_c^0 \times \text{SU}(2)_L^0 \times \text{U}(1)_Y^0$ . We have to remark here that although the elementary gauge group looks just like the SM gauge group, it actually is not *the* SM gauge group. As we will see later, all SM particles will be a mixture of elementary and composite fields, such that *the* SM gauge group has to be identified with the diagonal group of the elementary and some composite gauge symmetry.

The same is also true for the elementary fermion sector. This will also look just like the SM, meaning that there are left-handed doublets and right-handed singlets under  $\text{SU}(2)_L^0$  and QCD and hypercharge quantum numbers will be just as usual.

The only thing that is missing is a scalar field, as the Higgs is assumed to be a part purely of the composite sector. Therefore, there are no masses for the elementary fermions and also all gauge bosons

<sup>1</sup>In the following we will denote elementary fields and symmetries with the index ‘0’. The SM will be denoted without an index.

are strictly massless, as there are no breaking of gauge symmetries as long as the interactions with the composite sector are turned off.

Summarizing, the elementary Lagrangian looks like the following,

$$\begin{aligned} \mathcal{L}_{\text{elementary}} = & \frac{1}{2} \text{tr} \left[ G_{\mu\nu}^0 G^{0\mu\nu} \right] + \frac{1}{2} \text{tr} \left[ W_{\mu\nu}^0 W^{0\mu\nu} \right] + \frac{1}{4} B_{\mu\nu}^0 B^{0\mu\nu} \\ & + \sum_{\text{quarks, leptons}} \sum_{\text{flavour}} \bar{\psi}^0 \not{D} \psi^0, \end{aligned} \quad (2.4)$$

where the covariant derivatives are the usual ones for  $\psi^0 = q_L^0, u_R^0, d_R^0, l_L^0, \ell_R^0$  containing weak elementary gauge couplings. Note that as there are no Yukawa couplings there is nothing that distinguishes between different generations.

The freedom in model-building for the elementary sector is limited. To see why, one could think about what would happen if the elementary sector did not look just like the SM. For example, one could consider the possibility of enlarging the symmetries and/or the matter content for the elementary fields. But, inevitably, this would introduce rather light or even massless states to the spectrum, depending on whether and how these new states interact with the composite sector. As such a scenario is phenomenologically challenging, this is not something we will pursue in the following. As an alternative the elementary sector could contain less matter than the SM. In this case, the missing SM degrees of freedom have to be purely parts of the composite sector. Consequently, these states will interact strongly with the composite Higgs, such that this option might only be viable for the top quark [30].

## Composite sector

While the elementary sector is more or less fixed, the strongly interacting NP sector offers a lot of freedom for model-building. We ignore what might happen at very high energies and just accept the fact that there are composite states, which we will simply call *resonances*. In the approach used by us the details of the composite sector are determined by its global symmetry structures. As stated above, the composite sector is subject to a symmetry breaking  $\mathcal{G}/\mathcal{H}$ . But as it turns out, this is not enough. We will see later that it is necessary to introduce couplings between the composite and elementary sectors that are *linear* in the fields. These couplings are only possible if the elementary quarks and the heavy quark resonances carry the same gauge quantum numbers. In particular, we refer here not only to electroweak quantum numbers but also to color and hypercharge. That is to say, the heavy fermion resonances that mix with the elementary quarks should be color triplets of the same QCD. To achieve this, one uses the following construction that naturally emerges in the models we are considering. Imagine, therefore, that the elementary sector is invariant under an elementary version of the SM gauge group,  $G_{\text{SM}}^0 = \text{SU}(3)_c^0 \times \text{SU}(2)_L^0 \times \text{U}(1)_Y^0$ . The composite sector we assume to be invariant under a coset  $\mathcal{G}_{\text{big}}/\mathcal{H}_{\text{big}}$  of global symmetries, such that

$$\mathcal{G}_{\text{big}} \supset \mathcal{H}_{\text{big}} \supset G_{\text{SM}}^{\text{comp}} = \text{SU}(3)_c^{\text{comp}} \times \text{SU}(2)_L^{\text{comp}} \times \text{U}(1)_Y^{\text{comp}}. \quad (2.5)$$

By introducing linear couplings between the two sectors one then effectively breaks the SM-like symmetries down to their diagonal group,

$$G_{\text{SM}}^0 \times G_{\text{SM}}^{\text{comp}} \rightarrow G_{\text{SM}}^{0+\text{comp}} \equiv G_{\text{SM}}, \quad (2.6)$$

which is then identified as *the* SM gauge group. This means that one is effectively *gauging* the  $G_{\text{SM}}$  subgroup of the composite global symmetries. This is a point that will become important later when discussing the Higgs potential. As a consequence, the resulting theory is SM gauge invariant and the heavy quark resonances carry QCD charges just as the SM quarks.

The easiest way to form such a structure is by just supplementing the coset  $\mathcal{G}/\mathcal{H}$ , that in the end is supposed to reproduce the electroweak sector, by a composite global SU(3) symmetry. As in general, the coset  $\mathcal{G}/\mathcal{H}$  might not suffice to generate the correct hypercharge quantum numbers for the composite fermions we also include a global U(1), such that ultimately hypercharge will be given as a linear combination of this U(1) and some generators of  $\mathcal{H}$ . Summarizing, we will take the global symmetries to be<sup>2</sup>

$$\mathcal{G}_{\text{big}}/\mathcal{H}_{\text{big}} = [\text{SU}(3)_c^{\text{comp}} \times \text{U}(1)_X \times \mathcal{G}] / [\text{SU}(3)_c^{\text{comp}} \times \text{U}(1)_X \times \mathcal{H}]. \quad (2.7)$$

---

<sup>2</sup> This choice is the minimal one. An example of a non-minimal example in which the composite SU(3) is embedded in a Pati-Salam symmetry is given in [31].

The extended global symmetries are a way to transmit the elementary gauge interaction to the composite sector.

### Composite scalars

As already indicated above, the Higgs scalar in this model is implemented as a NGB<sup>3</sup> of a broken global symmetry  $\mathcal{G}/\mathcal{H}$ . This is already enough to determine most of the dynamics of the NGBs. The general structure of theories of spontaneously broken global symmetries was worked out in [32, 33] and is today known as the Callan, Coleman, Wess and Zumino (CCWZ) formalism. The basics of these constructions are given in appendix II. One of the main points of this is that the spontaneous breaking of a global symmetry corresponds to a non-linear realization of  $\mathcal{G}$  that gets linear when restricted to the subgroup  $\mathcal{H}$ . In this case, the NGB modes are parametrized through matrices

$$\mathcal{U} = \exp \left[ i \frac{\sqrt{2}}{f} \pi^{\hat{a}} \mathbb{T}^{\hat{a}} \right] \quad (2.8)$$

where  $\mathbb{T}^{\hat{a}}$  are the broken coset generators and  $f$  is the Goldstone decay constant (similar to the pion decay constant). Under a general  $\mathcal{G}$ -transformation, the NGB fields  $\pi^{\hat{a}}$  transform non-linearly as<sup>4</sup>

$$\mathcal{U} \xrightarrow{g} g \mathcal{U} h(\mathcal{U}, g)^{-1} \quad \text{with } g \in \mathcal{G} \text{ and } h(\mathcal{U}, g) \in \mathcal{H}. \quad (2.9)$$

According to the CCWZ formalism, a Lagrangian for the NGB fields is best expressed in terms of the Maurer-Cartan form,

$$\omega_\mu = i \mathcal{U}^\dagger \partial_\mu \mathcal{U} =: d_\mu + E_\mu = d_\mu^{\hat{a}} \mathbb{T}^{\hat{a}} + E_\mu^a \mathbb{T}^a, \quad (2.10)$$

whose components transform under the unbroken subgroup  $\mathcal{H}$  via

$$E_\mu \rightarrow h (E_\mu + i \partial_\mu) h^\dagger, \quad d_\mu \rightarrow h d_\mu h^\dagger. \quad (2.11)$$

Using this the Goldstone kinetic Lagrangian is given as

$$\mathcal{L}_\sigma = \frac{f^2}{4} \text{tr} [d_\mu d^\mu]. \quad (2.12)$$

From this one can see the important fact that NGBs interact only through derivative terms.

### Composite vectors

Just as there are vector mesons in hadron physics one expects spin-1 resonances connected to the global symmetries to appear in the composite sector. A priori, it is not clear how these should be implemented into the theory as composite objects of some strong interactions. In the bottom-up description used in this work which stresses the similarities of the model to hadron physics one can use the same techniques as are used for introducing massive  $\rho$  mesons into low-energy strong interactions. The method builds on so-called *hidden local symmetries (HLS)* [34, 35, 36], that were developed in the late 1970s and early 80s. First investigated in the context of supersymmetry, it was soon realized that HLS are a general phenomenon in non-linear sigma models based on a coset  $\mathcal{G}/\mathcal{H}$  [37]. The basic idea here is that a coset  $\mathcal{G}/\mathcal{H}$  can be shown to be gauge equivalent to a structure  $\mathcal{G}_{\text{global}} \times \mathcal{H}_{\text{local}}$ , namely a theory with a global symmetry  $\mathcal{G}$  and a gauge symmetry  $\mathcal{H}$ . Heavy vector resonances can be introduced as dynamical gauge bosons that receive mass terms via the Higgs mechanism associated to the breaking  $(\mathcal{G}_{\text{global}} \times \mathcal{H}_{\text{local}}) \rightarrow \mathcal{G}_{\text{global}}$ .

Let us consider this in a little bit more detail. For this we closely follow [36]. Assume that we have a theory respecting a  $\mathcal{G}_{\text{global}} \times \mathcal{H}_{\text{local}}$  symmetry structure consisting of a global symmetry group  $\mathcal{G}$  and a gauge group  $\mathcal{H}$ . For this, we can introduce a field  $\xi$  transforming under these symmetries as

$$\xi(x) \rightarrow g \xi(x) h(x)^{-1} \quad \text{with } g \in \mathcal{G}_{\text{global}}, \quad h(x) \in \mathcal{H}_{\text{local}}. \quad (2.13)$$

If we introduce gauge fields  $\rho_\mu$  of  $\mathcal{H}_{\text{local}}$  then a gauge covariant derivative can be defined,

$$\mathcal{D}_\mu = \partial_\mu - i g_\rho \rho_\mu, \quad (2.14)$$

<sup>3</sup> Later, an explicit breaking of the symmetries will be introduced turning the NGBs into pNGBs with a potential and a small mass. But for our purposes right now we will just consider them as true NGBs for the time being.

<sup>4</sup> Note that this transformation becomes linear for  $g \in \mathcal{H} \subset \mathcal{G}$ .

which we use to write a Maurer-Cartan form similar to (II.15). It can then be shown that this transforms in the usual way as in (II.19). Furthermore, we are free to fix the  $\mathcal{H}_{\text{local}}$  gauge such that  $\xi(x)$  reduces to

$$\xi(x) = \exp\left[\frac{i}{f}\sigma^a(x)\mathbb{T}^a\right] \exp\left[\frac{i}{f}\pi^{\hat{a}}(x)\mathbb{T}^{\hat{a}}\right] \xrightarrow{\text{gauge fixing}} \exp\left[\frac{i}{f}\pi^{\hat{a}}(x)\mathbb{T}^{\hat{a}}\right] \quad (2.15)$$

and takes the form of a NGB matrix (5.3). There is, however, a caveat since this gauge fixing is not respected by the global  $\mathcal{G}_{\text{global}}$  symmetry, such that in general a  $g$ -transformation can spoil the above picture. This can be circumvented by performing only *simultaneous*  $g$ - and  $h(x)$ -transformations, under which  $\xi(x)$  transforms as

$$\xi(x) \rightarrow g\xi(x)h(\xi, g)^{-1}, \quad (2.16)$$

making the analogy to the CCWZ Lagrangian [33] complete.

Let us recapitulate. By introducing the field  $\xi(x)$  and fixing the symmetries in a particular way, it can be shown that the Lagrangian and the transformation properties of a theory with coset  $\mathcal{G}/\mathcal{H}$  are the same as those of one with  $\mathcal{G}_{\text{global}} \times \mathcal{H}_{\text{local}}$  symmetries, such that both theories appear to be equivalent descriptions of the same physics. Composite vector resonances appear as gauge bosons of the hidden  $\mathcal{H}_{\text{local}}$  symmetry. The gauge fixing can be understood as a breaking of the gauge symmetries  $\mathcal{G}_{\text{global}} \times \mathcal{H}_{\text{local}}$  down to a global  $\mathcal{G}$ . Connected with this is a Higgs mechanism that generates mass terms for the vector resonances. This can readily be seen by considering the kinetic terms of the  $\xi$  field. In analogy with the CCWZ construction a Cartan-Maurer form (II.15) can be defined,

$$\omega_\mu = i\xi^\dagger \mathcal{D}_\mu \xi = d_\mu^{\hat{a}} \mathbb{T}^{\hat{a}} + E_\mu^a \mathbb{T}^a, \quad (2.17)$$

that has transformation properties (II.22). Under the above gauge fixing with transformations (2.16) of  $\xi$  the Lagrangian<sup>5</sup>

$$\mathcal{L} = \frac{f^2}{4} \text{tr}[d_\mu d^\mu] + \frac{1}{4} \text{tr}[\rho_{\mu\nu} \rho^{\mu\nu}] + \frac{f_\rho^2}{2} \text{tr}[(g_\rho \rho_\mu - E_\mu)^2] \quad (2.18)$$

leads to mass terms for the vector resonances,

$$m_\rho = g_\rho f_\rho. \quad (2.19)$$

This is exactly what one would expect from a Higgs mechanism; the mass scale of the vector resonances is given by  $f_\rho \sim f$ . In this gauge, the  $\sigma$ -fields in (2.15) are eaten by the gauge bosons rendering them massive.

As seen from (2.7) also the composite  $\text{SU}(3)_c^{\text{comp}} \times \text{U}(1)_X$  symmetries belong to the unbroken directions of the coset. Therefore, utilizing HLS one also expects the presence of heavy resonances connected to these symmetries, namely heavy gluon resonances and a heavy neutral vector boson  $X_\mu$ . As the unbroken group is a direct product of several Lie groups, one has to introduce different couplings for each component. Also the mass scales can in general differ from  $f_\rho$ , but we will assume them to be all of the same order  $f_G \sim f_X \sim f_\rho \sim f$  up to  $\mathcal{O}(1)$  factors. Then, we can write the masses of these heavy vector resonances as

$$m_G = g_{\rho 3} f_G, \quad m_X = g_X f_X. \quad (2.20)$$

### Composite Fermions

Heavy fermion resonances appear in these theories just like baryons in the hadron spectrum. They are introduced in a straight-forward way as multiplets of the unbroken global symmetries of the composite sector, namely  $\text{SU}(3)_c^{\text{comp}} \times \text{U}(1)_X \times \mathcal{H}$ . As a first consequence, the composite fermion resonances can be divided into composite quarks and composite leptons depending on their representations under the

<sup>5</sup> Note here, that we introduced a new scale  $f_\rho$ . In principle, both relevant operators in (2.18) are independent structures, so one could also write

$$\mathcal{L} \subset \frac{f^2}{4} \text{tr}[d_\mu d^\mu] + a \frac{f^2}{2} \text{tr}[(g_\rho \rho_\mu - E_\mu)^2]$$

and then define  $f_\rho := \sqrt{a}f$ . This was e.g. done in [36].



global composite colour symmetry. For giving a heavy mass to the fermions these have to be vector-like. Then, these composite fermions are supplied with Dirac mass terms, which naturally should be of the order of  $f$ .

In the light of HLS the couplings between fermion and vector resonances are given by covariant derivatives (II.28), such that we can write the Lagrangian

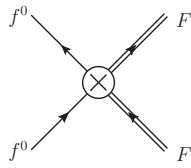
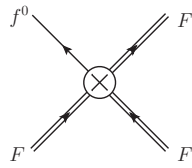
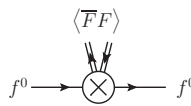
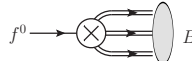
$$\mathcal{L} = \sum_i \bar{\Psi}_i (i\not{D} - m_\Psi) \Psi_i. \quad (2.21)$$

In this work we are interested in the effect of composite partners for the SM quarks. Therefore, we concentrate on that case and neglect the possibility of composite leptons.

### 2.1.2. Composite-elementary mixings

Up to now both the elementary and the composite sector of this model have been separate theories. In this section we will show how introducing composite-elementary mixing terms will push the model a far way towards phenomenological viability.

To understand the structure of these terms it is convenient to temporarily return to the picture of a strongly interacting UV theory for the composite sector. At very high energies the interactions between elementary and technifermions will appear at the non-renormalizable level in the form of 4-fermion-operators. These can take two forms that are reasonable and which are schematically given as follows:

	a)	b)
at high energies:	$\mathcal{L} \sim \frac{g}{M^2} (\bar{f}^0 f^0) (\bar{F} F)$ 	$\mathcal{L} \sim \frac{g}{M^2} (\bar{f}^0 F) (\bar{F} f^0)$ 
at low energies:	$\mathcal{L} \sim m \bar{f}^0 f^0$ 	$\mathcal{L} \sim \epsilon \bar{f}^0 B$ 

- a) In this case there is a bilinear mixing of elementary and technifermions. This is the scenario usually considered in models of *extended technicolor* (see e.g. [38]). As always the case in technicolor models, EWSB is considered as being induced by some condensate of technifermions  $\langle \bar{F} F \rangle \neq 0$ , whose interactions at low energies will introduce mass terms for the elementary fermions that depend on the techni-condensate. However, such a construction always has to struggle with strong constraints from flavour observables as these effects lead to large amounts of FCNCs, such that in practice such a construction is phenomenologically ruled out.
- b) In this case there is an interaction that mixes one elementary with three techni-fermions. As at low energies the strong sector should be confining and the techni-fermions should “hadronize” into resonances, this induces an effective linear mixing between the elementary sector and strong sector “baryons”  $B$ , i.e. quark and lepton partners. Such a mixing between the elementary and composite sectors is called *partial compositeness* [39], since in the end, all states (including the SM particles) will be mixtures of elementary states and composite resonances. Such a scenario has many advantages coming from the phenomenology side as well as from model building. Thus, partial compositeness will be the framework adopted for the remainder of this work.

Let us consider the mechanism of partial compositeness in further detail and for the time being concentrate on fermions. As we have seen above, the elementary sector by construction is invariant under a SM-like gauge symmetry, such that there are no mass terms. In the composite sector, on

the other hand, the fermions are vector-like, such that all resonances will have large masses of the order of the NP hadronization scale. Due to the interaction of both sectors the elementary states get admixtures from the composite ones and thus obtain a mass of the order of the mixing scale. To see this explicitly, let us write down a toy model for partial compositeness [40]. The elementary sector will contain left- and right-handed Weyl-fermions ( $\psi_L^0$  and  $\psi_R^0$ ) that transform as a doublet and singlet, respectively, under an elementary  $SU(2)^0$  symmetry. Now, one wants to write down mixing terms with composite resonances. As these are vectorlike, we will have to consider *two different* states ( $\Psi$  and  $\tilde{\Psi}$ ), that are a doublet and a singlet under a composite  $SU(2)^{\text{comp}}$  symmetry, respectively.

	$SU(2)^0 \times SU(2)^{\text{comp}}$		
elementary sector	$\psi_L^0 \in (\mathbf{2}, \mathbf{1})$		chiral
	$\psi_R^0 \in (\mathbf{1}, \mathbf{1})$		chiral
composite sector	$\Psi \in (\mathbf{1}, \mathbf{2})$		vectorlike
	$\tilde{\Psi} \in (\mathbf{1}, \mathbf{1})$		vectorlike

Mixing terms can be written down if spurion fields,

$$\begin{aligned} \hat{\epsilon}_L \in (\mathbf{2}, \mathbf{2}^*), \quad \hat{\epsilon}_L \rightarrow \epsilon_L \begin{pmatrix} 1 & 0 \\ 0 & 1 \end{pmatrix} \\ \hat{\epsilon}_R \in (\mathbf{1}, \mathbf{1}), \quad \hat{\epsilon}_R \rightarrow \epsilon_R \mathbb{1}, \end{aligned}$$

are introduced in such a way that the elementary and composite symmetries are broken down to the diagonal group that is then identified as the SM symmetry,  $SU(2)^0 \times SU(2)^{\text{comp}} \rightarrow SU(2)^{\text{SM}}$ . The Lagrangian for this then looks like

$$\mathcal{L} = \overline{\psi^0} i \not{\partial} \psi^0 + \overline{\Psi} (i \not{\partial} - M) \Psi + \overline{\tilde{\Psi}} (i \not{\partial} - \widetilde{M}) \tilde{\Psi} \quad (2.22)$$

$$+ \overline{\psi^0}_L \hat{\epsilon}_L \Psi_R + \overline{\psi^0}_R \hat{\epsilon}_R \tilde{\Psi}_L + \text{h.c.}, \quad (2.23)$$

In this case the fermion mass matrix has a non-diagonal form,

$$\hat{M}_\phi = \begin{pmatrix} & \psi_R^0 & \Psi_R & \tilde{\Psi}_R \\ \overline{\psi^0}_L & 0 & -\epsilon_L & 0 \\ \overline{\Psi}_L & 0 & M & 0 \\ \overline{\tilde{\Psi}}_L & -\epsilon_R^\dagger & 0 & \widetilde{M} \end{pmatrix}. \quad (2.24)$$

As physical states are defined in such a way that they possess a diagonal mass matrix, one has to diagonalize the above matrix such that the physical states will be linear combinations of elementary and composite fields. In general, this is done via a bi-unitary transformation,

$$\begin{pmatrix} \psi_L^0 \\ \Psi_L \\ \tilde{\Psi}_L \end{pmatrix} \rightarrow \begin{pmatrix} \cos(\phi_L) & -\sin(\phi_L) & 0 \\ \sin(\phi_L) & \cos(\phi_L) & 0 \\ 0 & 0 & 1 \end{pmatrix} \begin{pmatrix} \psi_L^0 \\ \Psi_L \\ \tilde{\Psi}_L \end{pmatrix} \quad (2.25a)$$

$$\begin{pmatrix} \psi_R^0 \\ \Psi_R \\ \tilde{\Psi}_R \end{pmatrix} \rightarrow \begin{pmatrix} \cos(\phi_R) & 0 & -\sin(\phi_R) \\ 0 & 1 & 0 \\ \sin(\phi_R) & 0 & \cos(\phi_R) \end{pmatrix} \begin{pmatrix} \psi_R^0 \\ \Psi_R \\ \tilde{\Psi}_R \end{pmatrix} \quad (2.25b)$$

that transforms left- and right-handed fermions separately by mixing angles that are determined by the composite-elementary-mixings and the heavy masses,

$$\tan(\phi_L) = \frac{\epsilon_L}{M}, \quad \tan(\phi_R) = \frac{\epsilon_R}{\widetilde{M}}. \quad (2.26)$$

As suggested by the mixing Lagrangian (2.23), the left-handed elementary fermions mix with the composite doublet fields  $\Psi$ , while the right-handed ones mix with the fields  $\tilde{\Psi}$ . This is now the key ingredient of partial compositeness, the SM fields are mixtures of elementary and composite fields,

$$|\text{SM}\rangle = \cos(\phi) |\text{elementary}\rangle - \sin(\phi) |\text{composite}\rangle, \quad (2.27a)$$

$$|\text{NP}\rangle = \sin(\phi) |\text{elementary}\rangle + \cos(\phi) |\text{composite}\rangle, \quad (2.27b)$$

while NP fields form the orthogonal combination. The admixture is described by a mixing angle whose sine we will call *degree of compositeness*.

Let us now consider the Higgs interactions. By construction the Higgs is part only of the composite sector and the elementary fields do not couple to it. There are only interactions of the composite Higgs with the composite resonances. For our toy model it is easiest to think of the Higgs  $\mathcal{H}$  as being a doublet of  $SU(2)^{\text{comp}}$  such that Yukawa terms can be written,

$$\mathcal{L}_{\text{comp}} \supset \mathcal{L}_{\text{yuk}} = y_{\text{comp}} \bar{\Psi} \cdot \mathcal{H} \tilde{\Psi} + \text{h.c.} . \quad (2.28)$$

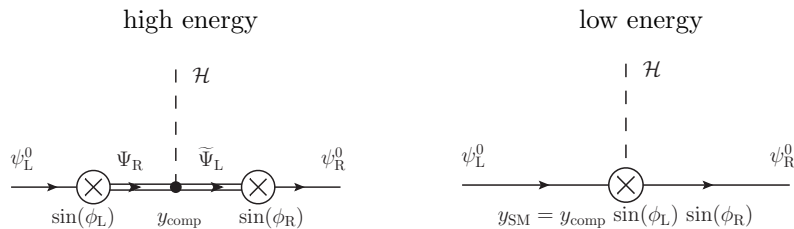
Performing the transformations (2.25), interaction terms between SM states and the Higgs are introduced,

$$\mathcal{L}_{\text{yuk}} \rightarrow y_{\text{SM}} \bar{\psi}_{\text{L}}^0 \cdot \mathcal{H} \psi_{\text{R}}^0 + \text{h.c.} + \dots, \quad (2.29)$$

where the SM Yukawa coupling is determined by the composite coupling and the degrees of compositeness,

$$y_{\text{SM}} = y_{\text{comp}} \sin(\phi_{\text{L}}) \sin(\phi_{\text{R}}). \quad (2.30)$$

This is now the SM Yukawa sector describing the interactions between the SM fermions and the Higgs boson. If one now assumes that (by whichever mechanism) a potential for the Higgs is generated in such a way that it obtains a vacuum expectation value, the masses of the SM fermions are generated in the usual way via interaction with the Higgs vacuum. Physically, the picture here is very transparent.



The elementary fields have to “oscillate” into a composite state in order to be able to interact with the Higgs. This oscillation is given by the composite-elementary-mixings and, therefore, the interactions of the Higgs with the SM fermions are governed by the degree of compositeness of the latter. If one considers more than one generation this construction allows to explain the observed flavour patterns in a natural way: The SM Yukawa couplings are determined by the degrees of compositeness of the SM fermions and the couplings of the composite fermion resonances to the composite Higgs. One could imagine that at some high scale these couplings and mixings are anarchic, meaning that they show no large hierarchies. By the RGE flow down to low energies, hierarchies in the composite-elementary mixings can be exponentially enhanced if there are sizable anomalous dimensions which is not unreasonable in a strongly interacting theory [41]. This is a further main motivation for CHMs as a dynamical explanation for flavour hierarchies can be given.<sup>6</sup> In this picture, the heavier the fermions are the more strongly they mix with states from the composite sector. However, as we will discuss in section 2.2.3 this simple picture of anarchic composite Yukawa couplings does not withstand phenomenological scrutiny such that either the scale of vector resonances has to be unnaturally high or flavour symmetries in the composite sector have to be introduced to obtain enough control over flavour transitions.

As already stated above we do not consider composite leptons in this work. The reason for this is that including composite-elementary mixings for leptons would make the model significantly more complex as the PMNS matrix would have to be reproduced. As we are mainly interested in quark flavour physics we consider the limiting case of vanishing composite-elementary mixings and treat the leptons as purely elementary.

As for the fermions, there will also be partial compositeness in the spin-1 sector that is less model-dependent since it is fixed mostly by symmetry considerations. In the spirit of HLS the couplings to the elementary sector are introduced by gauging the  $\mathcal{G}^0$  subgroup of  $\mathcal{G}_{\text{global}}$ . Then, the covariant derivative of the pNGBs changes [36],

$$\mathcal{D}_\mu \mathcal{U} = \partial_\mu \mathcal{U} - ig_\rho \rho_\mu + ig_0 A_\mu^{(0)}, \quad (2.31)$$

<sup>6</sup>A similar picture arises in dual theories on extra dimensions. In a strongly warped geometry, flavour hierarchies can be understood as being due to localizations of bulk fermion fields in the extra dimension and therefore they are determined as wavefunction-overlaps [42].

and the Lagrangian (2.18) leads to mass matrices

$$M_V^2 = f_\rho^2 \begin{pmatrix} g_0^2 & -g_0 g_\rho \\ -g_0 g_\rho & g_\rho^2 \end{pmatrix}. \quad (2.32)$$

Going to the mass basis, this mass matrix is diagonalized by a rotation

$$\begin{pmatrix} A_\mu^{\text{SM}} \\ \rho_\mu^{\text{NP}} \end{pmatrix} = \begin{pmatrix} \cos(\phi) & -\sin(\phi) \\ \sin(\phi) & \cos(\phi) \end{pmatrix} \begin{pmatrix} A_\mu^0 \\ \rho_\mu \end{pmatrix}, \quad (2.33)$$

where the degree of compositeness is given by the relative sizes of elementary and composite gauge couplings,  $\tan(\phi) = \frac{g_0}{g_\rho}$ . In this physical basis, one linear combination will obtain a large mass while the orthogonal combination remains massless,

$$m_{\text{SM}}^2 = 0, \quad (2.34)$$

$$m_\rho^2 = (g_0^2 + g_\rho^2) f_\rho^2. \quad (2.35)$$

The massless combination we will identify with the SM fields whose gauge symmetries are still preserved.

## 2.2. Phenomenological features

The above basic construction is successful in solving open questions as the fine-tuning problem or the origin of flavour hierarchies. However, to obtain a model that can be phenomenologically realistic, a few aspects have to be added. In particular, these include the notion of custodial symmetry, which will have profound consequences for the choice of the symmetry breaking patterns, electroweak symmetry breaking via the Coleman-Weinberg mechanism and the introduction of flavour symmetries that are necessary in order to have control over the flavour sector.

### 2.2.1. Custodial symmetry

The SM is a gauge theory invariant under a group  $G_{\text{SM}} = \text{SU}(3)_c \times \text{SU}(2)_L \times \text{U}(1)_Y$ . Considering the Higgs sector alone, one sees that an additional global symmetry is hidden. It is easy to show that the Higgs kinetic term and its potential can be written in an  $\text{SU}(2)_L \times \text{SU}(2)_R$  symmetric form [43]. For this one introduces a Higgs bidoublet,

$$H = (\epsilon \cdot \Phi^*, \Phi) = \frac{1}{\sqrt{2}} \begin{pmatrix} \phi_3 - i\phi_4 & \phi_1 + i\phi_2 \\ -\phi_1 + i\phi_2 & \phi_3 + i\phi_4 \end{pmatrix}, \quad (2.36)$$

which transforms as  $H \rightarrow L H R^\dagger$  under  $\text{SU}(2)_L \times \text{SU}(2)_R$ . A manifestly invariant term is given as

$$\text{tr} [H^\dagger H] = \phi_1^2 + \phi_2^2 + \phi_3^2 + \phi_4^2 = \Phi^\dagger \Phi, \quad (2.37)$$

such that the SM Higgs sector is easily seen to be invariant as well,

$$\begin{aligned} \mathcal{L}_{\text{Higgs}} &= (D_\mu \Phi)^\dagger (D_\mu \Phi) - V(\Phi^\dagger \Phi) \\ &= \text{tr} \left[ (D_\mu H)^\dagger (D_\mu H) \right] - V(\text{tr} [H^\dagger H]). \end{aligned}$$

After EWSB,  $H \rightarrow \frac{v_{\text{SM}}}{\sqrt{2}} \mathbb{1}_{2 \times 2}$ , these global symmetries are broken down to their diagonal subgroup,  $\text{SU}(2)_L \times \text{SU}(2)_R \rightarrow \text{SU}(2)_{L+R}$ . This pattern is called *custodial symmetry*. One important consequence is the well-known relation between the vector boson masses and the electroweak mixing angle (see e.g. [44]),

$$\rho = \frac{m_W^2}{m_Z^2 \cos(\theta_w)} = 1. \quad (2.38)$$

Looking at the full SM, the custodial symmetry is explicitly broken by hypercharge as well as the Yukawa couplings. This breaking introduces violations of (2.38) through quantum corrections. Deviations are however small due to the small explicit breaking of custodial symmetry.

Embedding the SM into a more fundamental theory might introduce new sources of custodial symmetry breaking. These can be controlled by the use of *electroweak precision observables* (EWPO) [45] which have been measured to a high accuracy at LEP [46] (The precision observables will be discussed in more detail in section 3.3.2). Working in an EFT approach, these correspond to Wilson coefficients of dimension-6 operators [47],

$$\mathcal{L}_{\text{EWPO}} = \frac{c_S}{\Lambda^2} \mathcal{O}_S + \frac{c_T}{\Lambda^2} \mathcal{O}_T,$$

with

$$\mathcal{O}_S = \Phi^\dagger \sigma^i \Phi W_{\mu\nu}^i B_{\mu\nu} = \text{tr} [\mathcal{H}^\dagger \sigma^i \mathcal{H} \sigma_3] W_{\mu\nu}^i B_{\mu\nu}, \quad (2.39a)$$

$$\mathcal{O}_T = |\Phi^\dagger D_\mu \Phi|^2 = \text{tr} [\mathcal{H}^\dagger (D_\mu \mathcal{H}) \sigma_3] \text{tr} [(D^\mu \mathcal{H}^\dagger) \mathcal{H} \sigma_3]. \quad (2.39b)$$

After EWSB, these operators determine the electroweak precision observables via

$$S = 4 \frac{\sin(\theta_W) \cos(\theta_W)}{\alpha} \frac{v_{\text{SM}}^2}{\Lambda^2} c_S, \quad T = -\frac{1}{2\alpha} \frac{v_{\text{SM}}^2}{\Lambda^2} c_T. \quad (2.40)$$

While the operator  $\mathcal{O}_S$  is invariant under custodial symmetry, the operator  $\mathcal{O}_T$  is not and, therefore, the  $T$  parameter measures the amount of explicit breaking of custodial symmetry. Reversing this argument, if the NP sector is invariant under the custodial symmetry, there will be no pure NP contributions to the  $T$  parameter<sup>7</sup>. As the constraints on EWPOs are very tight, it appears to be well motivated to include custodial symmetry in the NP sector in order to prevent dangerously large contributions to the  $T$  parameter while at the same time retaining an acceptable amount of fine-tuning. In CHMs, custodial symmetry is explicitly broken by the composite-elementary mixings. However, assuming the composite sector to be invariant under an  $\text{SO}(4) \cong \text{SU}(2)_L \times \text{SU}(2)_R$  symmetry assures the protection of the  $T$  parameter at tree level. NP contributions will only appear at the loop level via the exchange of heavy resonance pairs. This puts constraints on the coset of the broken global symmetries of the composite sector, as the unbroken subgroup should at least be as large as  $\text{SO}(4)$ . Demanding then that the coset is large enough to accommodate a complex doublet of Goldstone bosons gives the minimal coset for CHMs as  $\text{SO}(5)/\text{SO}(4)$  [48]. This features exactly four pNGBs that can be identified with the complex Higgs doublet.

As another feature of custodial symmetry, it was found in [49] that under certain circumstances custodial protection can also prevent dangerously large contributions to  $Z b_L b_L$  couplings. The couplings of the  $Z$  boson to a SM fermion  $\psi$  are given by

$$\frac{g}{\cos(\theta_W)} [Q_L^3 - Q_{\text{em}} \sin^2(\theta_W)] Z^\mu \bar{\psi} \gamma_\mu \psi. \quad (2.41)$$

Being interested only in non-universal corrections, NP could possibly change this coupling by contributing to the electric charge  $Q_{\text{em}}$  or to weak isospin  $Q_L^3$ . As the electric charge is protected by the electromagnetic gauge symmetries, this cannot be changed. In the SM one has  $Q_L^3 = T_L^3$ , i.e.  $Q_L^3 = \pm \frac{1}{2}$  for doublets or  $Q_L^3 = 0$  for singlets. In CHMs, however, this can be changed since due to partial compositeness the SM fermions will mix with fields with different  $\text{SU}(2)_L$  quantum numbers after EWSB. These mixings are determined by the representations of the composite resonances under global symmetries and by the way in which the SM fields are embedded into incomplete representations. As shown in [49], the corrections to  $Q_L^3$  can be protected by discrete  $P_{LR}$  symmetries if the embedding of  $\psi$  satisfies  $T_L^3 = T_R^3$ . This leads to constraints on the possible representations of the resonances under  $\text{SO}(4) = \text{SU}(2)_L \times \text{SU}(2)_R$ . One can look at the smallest representations of  $\text{SO}(5)$  and how they decompose into  $\text{SO}(4)$ ,

$$\text{spinorial} \quad \mathbf{4} = (\mathbf{2}, \mathbf{1}) \oplus (\mathbf{1}, \mathbf{2}), \quad (2.42a)$$

$$\text{fundamental} \quad \mathbf{5} = (\mathbf{2}, \mathbf{2}) \oplus (\mathbf{1}, \mathbf{1}), \quad (2.42b)$$

$$\text{anti-symmetric} \quad \mathbf{10} = (\mathbf{3}, \mathbf{1}) \oplus (\mathbf{1}, \mathbf{3}) \oplus (\mathbf{2}, \mathbf{2}), \quad (2.42c)$$

$$\text{symmetric} \quad \mathbf{14} = (\mathbf{3}, \mathbf{3}) \oplus (\mathbf{2}, \mathbf{2}) \oplus (\mathbf{1}, \mathbf{1}). \quad (2.42d)$$

If the left-handed fermion doublets can be embedded into bi-doublets of  $\text{SO}(4)$ , then their couplings to the  $Z$  boson are protected. This is not the case for the spinorial representation and, hence, we will

<sup>7</sup>There might however be a contribution due to the interaction of the NP sector with the SM in which custodial symmetry is broken explicitly.

not consider it in the following. This leaves the fundamental as the smallest representation. In the same way, it can then be seen that couplings  $Zt_L t_L$  and  $Wt_L b_L$  are not protected allowing for large NP corrections.

Summarizing, measurements of the electroweak sector have profound consequences for model-building in CHMs. Getting rid of large contributions to the  $T$  parameter forces the existence of a custodial symmetry and by that fixes the minimal coset to  $SO(5)/SO(4)$ . Also protecting the couplings of the electroweak  $Z$  boson constrains the possible choice of representations of the composite resonances under this coset, such that the minimal choice is given by the fundamental  $\mathbf{5}$ .

### 2.2.2. Electroweak symmetry breaking

A crucial point for the validity of this class of models is electroweak symmetry breaking. Experimentally, the SM and, in particular, the breaking of gauge symmetries  $SU(2)_L \times U(1)_Y \rightarrow U(1)_{em}$  is very well established and every model of NP has to incorporate a mechanism to generate this pattern. In the SM the electroweak symmetry is broken by the Higgs mechanism, i.e. by a scalar degree of freedom that gets a non-vanishing vacuum expectation value through the non-trivial structure of its potential. Although the discovery of the Higgs boson at the LHC in 2012 marked a magnificent triumph for the Higgs mechanism, it by itself does not give any explanation about the origin of EWSB as the symmetry breaking potential is merely introduced “by hand” such that it most probably is a parametrization of more fundamental physics. All we know is that the potential is there, but where it comes from is presently unknown. In CHMs with a pNGB Higgs the origin of the potential can be described in a dynamical way due to the breaking of global symmetries. Even further, the Higgs potential can actually be calculated such that predictions for the Higgs mass and the scale of EWSB can be made for a given model.

In the following sections we will review EWSB in CHMs and consider its important impact on a detailed analysis of such models. For this we first review the general notion of vacuum misalignment and then discuss the general calculation of the effective Higgs potential through the Coleman-Weinberg mechanism. After that the phenomenological consequences of the potential will be highlighted for the coset structure  $SO(5)/SO(4)$  which will be the subject of the analysis in chapter 4.

#### Vacuum misalignment

In CHMs a solution to this question is given through the mechanism of *vacuum misalignment* [50], which allows the potential to be generated dynamically through quantum corrections. The basic idea here is that the Goldstone shift symmetry of the composite sector is explicitly broken via interactions with the elementary fields, which allows the true vacuum of the theory to deviate from the directions respecting the  $G_{SM}$ -symmetry, thus breaking it down to  $U(1)_{em}$ . In turn, the SM particles receive their masses and a Higgs boson emerges as a massive scalar particle.

To see this in more detail, consider the basic structure of CHM. There is an elementary sector invariant under a  $G_{SM}^0 = SU(2)^0 \times U(1)^0$  gauge symmetry. Furthermore, we have a confining, strongly interacting sector that we assume to be “hadronized” into an effective theory with heavy vector and fermion resonances. This sector is subject to a global symmetry breaking  $\mathcal{G}/\mathcal{H}$  such that NGB states  $\pi^{\hat{a}}$ , implemented through the combination

$$\mathcal{U}(x) = \exp\left(i\frac{\sqrt{2}}{f}\pi^{\hat{a}}(x)\mathsf{T}^{\hat{a}}\right), \quad (2.43)$$

appear in the spectrum, which we later identify with the Higgs. By the general construction of appendix II Goldstone bosons are subject to a *shift symmetry*,  $\pi^{\hat{a}}(x) \rightarrow \pi^{\hat{a}}(x) + c$ , such that they can only appear via derivative terms. In particular, this means that no mass term and no potential can arise as long as this shift symmetry is exact. The physical vacuum exhibits an infinite degeneracy that is characterized by

$$\langle \mathcal{U} \rangle = \exp\left(i\frac{\sqrt{2}}{f}\langle \pi_{\hat{a}}(x) \rangle \mathsf{T}^{\hat{a}}\right), \quad (2.44)$$

where the the vevs  $\langle \pi_{\hat{a}}(x) \rangle$  can take any real value. By the shift symmetry it then follows that in this case  $\langle \pi_{\hat{a}}(x) \rangle = 0$  in full generality.

So, one sees that if both sectors are separated no breaking of the electroweak symmetry occurs. This changes if one turns on interactions between both sectors. In CHMs there are two sources of explicit symmetry breaking:

1. In the gauge sector there are linear interactions between elementary gauge bosons and composite vector resonances. This means that the elementary gauge symmetry  $G_{\text{SM}}^0 = \text{SU}(2)^0 \times \text{U}(1)^0$  and the  $\text{SU}(2) \times \text{U}(1)$  subgroup of the unbroken composite global symmetry  $\mathcal{H}$  are broken down to their diagonal group,

$$G_{\text{SM}}^0 \times \underbrace{G_{\text{SM}}^{\text{comp}}}_{\subset \mathcal{H}} \rightarrow G_{\text{SM}}^{0+\text{comp}} \equiv G_{\text{SM}}, \quad (2.45)$$

that we then identify with the SM gauge group. Effectively this means that one is *gauging a subgroup of the global symmetries* of the composite sector. This inevitably leads to a breaking of the global symmetries. At first sight, this might seem counter-intuitive, but the point is just that if one assumes the gauging of the subgroup to be exact then the global symmetry of the larger group cannot be present anymore, as a global symmetry transformation would break gauge invariance.<sup>8</sup>

2. The fermions of the elementary sector do not appear in full  $\mathcal{H}$  representations, but rather in  $\text{SU}(2)$  doublets and singlets according to their quantum numbers. As a consequence, one has to couple the composite fermion resonances to elementary states embedded into *incomplete representations* of the composite global symmetries. Later, this will turn out to be the dominant mechanism for generating EWSB.

In conclusion, the effect of the interactions between the composite and elementary sector is that the global symmetries are explicitly broken and the theory is invariant only under a gauge symmetry that we identify with *the* SM gauge symmetry. The explicit breaking of global symmetries turns the NGB fields into pNGBs such that, in particular, a potential and mass terms are allowed for them. The potential, of course, has to respect the  $G_{\text{SM}}$  gauge symmetry, but the crucial point is that the true vacuum of the theory does not. In general, the degeneracy in (2.44) is lifted and the physical vacuum picks some  $\langle \pi_{\hat{a}}^* \rangle = \langle \pi_{\hat{a}}^* \rangle \neq 0$ , such that

$$\langle \mathcal{U} \rangle = \exp \left( i \frac{\sqrt{2}}{f} \langle \pi_{\hat{a}}^*(x) \rangle \mathbf{T}^{\hat{a}} \right) \neq \mathbb{1}, \quad (2.46)$$

and no shift symmetry is present that forces the vevs to vanish. This is the mechanism of vacuum misalignment [50]: One can interpret the vevs  $\langle \pi_{\hat{a}}^* \rangle$  as parameterizing the deviation between the physical vacuum of the theory and the symmetry restoring vacuum  $\langle \mathcal{U} \rangle = \mathbb{1}$ .

### The Coleman-Weinberg effective potential

On the classical level there is no potential for the pNGBs. Therefore, vacuum misalignment is a quantum phenomenon in this case, in the sense that the potential is only generated dynamically through radiative corrections. The framework for this was developed in the early 80s as the Coleman-Weinberg (CW) potential [52] (see also [53]). The idea of it is that in contrast to the ordinary action (which gives the dynamics on the classical level) the effective action gives the full quantum corrected dynamics. As a lowest order in a derivative expansion the effective action contains the effective potential which determines the physical vacuum of the theory. Its general form is given as [52]

$$V_{\text{eff}}(\varphi) = \frac{1}{\mathcal{V}} \sum_n \frac{1}{n!} \int_{\mathcal{V}} d^4 x_1 \dots d^4 x_n \Gamma^{(n)}(x_1, \dots, x_n) \varphi(x_1) \dots \varphi(x_n), \quad (2.47)$$

which shows that, essentially, the coefficient of the  $\varphi^n$ -term in the effective potential is given by the *1-particle irreducible vertex*  $\Gamma^{(n)}$  with vanishing external momentum. This also shows how to calculate

<sup>8</sup>In general, gauging of a subgroup breaks the global symmetries down to the largest subgroup that contains the gauged subgroup as an ideal (see [51, Footnote 2]). This will become important in the later parts of this work (see chapter 5) when we will consider non-minimal CHMs.





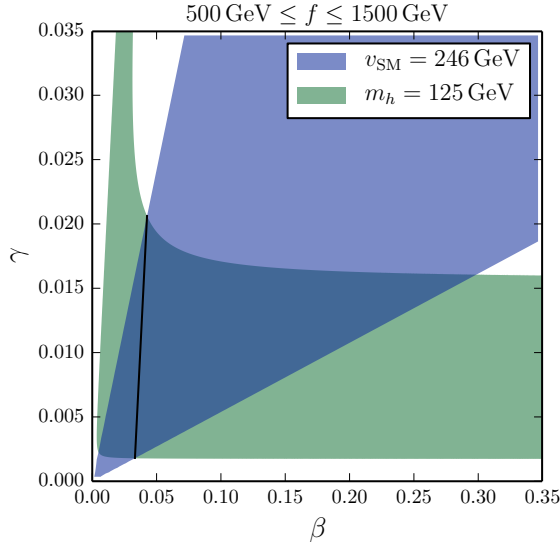


**Figure 2.2.:** Allowed values for  $\gamma$  and  $\beta$  that can reproduce the experimental values for the Higgs vev and its mass. In this plot the scale  $f$  is varied between 500 GeV and 1500 GeV. The black line indicates the points where both constraints are satisfied on the same time.

### Structure of the potential for SO(5)/SO(4)

Let us now discuss the structure of the effective potential in greater detail. For this we choose as an example the minimal option based on the coset SO(5)/SO(4) which will be the subject of investigation in chapter 4. Using the generators of SO(5) which are given in appendix I.1 and going to SM unitary gauge, in which  $\pi^{\hat{a}} = (0, 0, 0, h)$  such that the Higgs field is the only remaining scalar degree of freedom, one can write the Goldstone-matrix as follows

$$\mathcal{U} := \exp \left[ i \frac{\sqrt{2}}{f} \pi^{\hat{a}}(x) T^{\hat{a}} \right] = \begin{pmatrix} 1 & 0 & 0 & 0 & 0 \\ 0 & 1 & 0 & 0 & 0 \\ 0 & 0 & 1 & 0 & 0 \\ 0 & 0 & 0 & \cos\left(\frac{h}{f}\right) & \sin\left(\frac{h}{f}\right) \\ 0 & 0 & 0 & -\sin\left(\frac{h}{f}\right) & \cos\left(\frac{h}{f}\right) \end{pmatrix}. \quad (2.54)$$

This explicitly demonstrates the role of  $h/f$  as an angle of misalignment between the physical vacuum and the symmetry restoring vacuum  $\langle \mathcal{U} \rangle = \mathbb{1}$ .

As we will see later on, the hierarchy between the NP scale  $f$  and the Higgs vev  $v_{\text{SM}}$  in the SM will be given by the value  $s_h^*$  of  $s_h$  at the minimum of the potential, i.e.  $v_{\text{SM}} = f s_h^*$ . Therefore, assuming  $f$  to be of  $\mathcal{O}(\text{TeV})$  one generally expects that  $s_h^*$  is a number smaller than 1, which suggests an expansion of the effective potential in terms of  $s_h$  such that one can write the potential as [55]

$$V_{\text{eff}}(s_h) = (-\gamma s_h^2 + \beta s_h^4 + \dots) f^4. \quad (2.55)$$

In this expansion the minimum of the potential and the Higgs mass can be calculated as

$$s_h^* = \sqrt{\frac{\gamma}{2\beta}}, \quad m_h^2 = \left. \frac{\partial^2 V_{\text{eff}}(s_h)}{\partial h^2} \right|_{s_h=s_h^*} = 4\gamma \left( 1 - \frac{\gamma}{2\beta} \right) f^2. \quad (2.56)$$

Figure 2.2 shows the allowed ranges for the coefficients  $\gamma$  and  $\beta$  that are needed to generate the correct values for the two measured parameters of EWSB: the SM Higgs vev  $v_{\text{SM}}$  and the Higgs mass  $m_h$ . Generally, one needs  $\beta \gtrsim \gamma$  to trigger EWSB and a rather small  $\gamma$  to explain the hierarchy  $m_h \ll f$ .

As discussed above, the effective potential for the pNGBs is generated by the explicit breaking of the global symmetries. Because of this, a large amount of information about the qualitative structure of the potential can be obtained utilizing a so-called *spurion analysis*. For this one promotes the symmetry breaking parameters in the Lagrangian to fictitious fields with well-defined transformation

properties under the given symmetries. In this formalism the symmetry breaking is parametrized by “vacuum expectation values” that one allows the spurions to obtain. Such a spurion analysis for the given effective composite Higgs potential has been performed extensively in the literature (see e.g. [56, 57, 58, 59]); we will repeat the results here as in the following they will be important in many occasions.

From the discussion above we know that there are two qualitatively very different sources of explicit symmetry breaking for the considered theories: gauging the  $G_{\text{SM}}$ -subgroup of the global symmetries and coupling the composite fermion resonances to elementary fermions that do not form full  $\text{SO}(5)$  multiplets. Let us consider both contributions separately in greater detail.

**Gauge contributions:** In the gauge sector the global symmetries are broken explicitly by the couplings of the pNGBs to the elementary gauge fields, such that effectively only a subgroup of larger global symmetries is gauged. Therefore, it is instructive to elevate the elementary gauge fields to a fictitious complete  $\text{SO}(5)$  adjoint by writing [60],

$$g_\rho V_\mu = \mathbf{g}_{aA} W_\mu^a \mathbb{T}^A + \mathbf{g}'_A B_\mu \mathbb{T}^A, \quad (2.57)$$

where  $A$  and  $a$  are  $\text{SO}(5)$ - and  $\text{SU}(2)$ -indices, respectively. The original theory is obtained if the spurions take the vevs

$$\mathbf{g}_{aA} \mathbb{T}^A \rightarrow g_0 \mathbb{T}_L^a, \quad \mathbf{g}'_A \mathbb{T}^A \rightarrow g'_0 \mathbb{T}_R^3. \quad (2.58)$$

The whole point of the spurion analysis is that before taking their vevs the spurions can only appear in symmetry-preserving combinations which allows to deduce the qualitative structure of the potential in an expansion in terms of the (presumably small) symmetry breaking parameters  $\epsilon$ ,

$$V_{\text{eff}}(s_h) = f^4 \sum_n c_n \mathcal{I}_n(s_h) \epsilon^n. \quad (2.59)$$

In this notation, the coefficients  $c_n$  cannot be fixed by the spurion analysis and have to be determined by an explicit calculation, but naturally they are assumed to be  $\mathcal{O}(1)$  numbers. For the case at hand, the symmetry breaking parameters  $\epsilon \sim g_0/g_\rho$  are given by the relative strength of composite and elementary gauge couplings. This also shows that there are no gauge contributions to the potential in the limit of vanishing elementary gauge couplings. The functions  $\mathcal{I}_n(s_h)$  are given by invariant structures between pNGBs and spurion fields and lead to a non-trivial form of the potential after the spurions take their vevs. To lowest order these invariant structures appear with two insertions of spurions and are given as [60, 55]<sup>9</sup>

$$\mathcal{I}_2(s_h) = (\mathcal{U}^t \mathbf{g}_{aA} \mathbb{T}^A \mathbf{g}_{aB} \mathbb{T}^B \mathcal{U})_{55} \rightarrow \frac{3}{4} s_h^2, \quad (2.60a)$$

$$\mathcal{I}_2(s_h) = (\mathcal{U}^t \mathbf{g}'_A \mathbb{T}^A \mathbf{g}'_B \mathbb{T}^B \mathcal{U})_{55} \rightarrow \frac{1}{4} s_h^2. \quad (2.60b)$$

One observes that at this order in the spurion expansion only the coefficient  $\gamma$  of the potential (2.55) is generated, such that the coefficient  $\beta$  only appears with one further suppression by elementary gauge couplings [55],

$$\gamma_{\text{gauge}} \sim c_2 \left(\frac{g_0}{g_\rho}\right)^2, \quad \beta_{\text{gauge}} \sim c_4 \left(\frac{g_0}{g_\rho}\right)^4 \sim \left(\frac{g_0}{g_\rho}\right)^2 \gamma \ll \gamma, \quad (2.61)$$

which shows that gauge contributions alone are not enough to satisfy the necessary condition  $\beta \gtrsim \gamma$  to generate a non-trivial minimum for the potential. Therefore, fermion contributions are essential to trigger EWSB.

**Fermion contributions:** In (4.12) the global symmetries are broken explicitly by embedding the elementary fermions into incomplete  $\text{SO}(5)$  representations. In the language of spurions an alternative formulation is useful by introducing spurion fields  $\Delta$  such that the Lagrangian is written as

$$\mathcal{L} \supset \bar{q}_L^0 \Delta_{uL} \Psi_{uR} + \bar{q}_L^0 \Delta_{dL} \Psi_{dR} + \bar{u}_R^0 \Delta_{uR} \tilde{\Psi}_{uL} + \bar{d}_R^0 \Delta_{dR} \tilde{\Psi}_{dL} + \text{h.c.}, \quad (2.62)$$

<sup>9</sup> Note that the  $\mathcal{I}_n$  become  $s_h$ -independent if the spurions take vevs in  $\text{SO}(5)$ -preserving directions,

$$\mathbf{g}^{(\prime)} \rightarrow g_0^{(\prime)} \mathbf{1},$$

showing that in this case the symmetry is not explicitly broken and no potential for the pNGBs is generated by the gauge sector.

where the appearing fields have the following quantum numbers under  $SU(2)_L^0 \times U(1)_Y^0 \times SO(5) \times U(1)_X$ :<sup>10</sup>

$$q_L^0 \in \left( \mathbf{2}_{\frac{1}{6}}, \mathbf{1}_0 \right), \quad u_R^0 \in \left( \mathbf{1}_{\frac{2}{3}}, \mathbf{1}_0 \right), \quad d_R^0 \in \left( \mathbf{1}_{-\frac{1}{3}}, \mathbf{1}_0 \right), \quad (2.63a)$$

$$\Psi_u \in \left( \mathbf{1}_0, \mathbf{5}_{\frac{2}{3}} \right), \quad \Psi_d \in \left( \mathbf{1}_0, \mathbf{5}_{-\frac{1}{3}} \right), \quad \tilde{\Psi}_u \in \left( \mathbf{1}_0, \mathbf{5}_{\frac{2}{3}} \right), \quad \tilde{\Psi}_d \in \left( \mathbf{1}_0, \mathbf{5}_{-\frac{1}{3}} \right), \quad (2.63b)$$

$$\Delta_{uL} \in \left( \mathbf{2}_{\frac{1}{6}}, \mathbf{5}_{-\frac{2}{3}}^* \right), \quad \Delta_{dL} \in \left( \mathbf{2}_{\frac{1}{6}}, \mathbf{5}_{\frac{1}{3}}^* \right), \quad \Delta_{uR} \in \left( \mathbf{1}_{\frac{2}{3}}, \mathbf{5}_{-\frac{2}{3}}^* \right), \quad \Delta_{dR} \in \left( \mathbf{1}_{-\frac{1}{3}}, \mathbf{5}_{\frac{1}{3}}^* \right), \quad (2.63c)$$

where the spurions carry elementary as well as composite charges such that they can communicate with both sectors.

The original Lagrangian is reproduced if the spurions take the vevs

$$\Delta_{uL} \rightarrow \frac{1}{\sqrt{2}} \begin{pmatrix} 0 & 0 & 1 & i & 0 \\ 1 & -i & 0 & 0 & 0 \end{pmatrix} \epsilon_{uL}, \quad \Delta_{uR} \rightarrow \begin{pmatrix} 0 & 0 & 0 & 0 & 1 \end{pmatrix} \epsilon_{uR}, \quad (2.64a)$$

$$\Delta_{dL} \rightarrow \frac{1}{\sqrt{2}} \begin{pmatrix} 1 & i & 0 & 0 & 0 \\ 0 & 0 & -1 & i & 0 \end{pmatrix} \epsilon_{dL}, \quad \Delta_{dR} \rightarrow \begin{pmatrix} 0 & 0 & 0 & 0 & 1 \end{pmatrix} \epsilon_{dR}. \quad (2.64b)$$

Just as for the gauge boson case one finds that also the lowest order in the fermionic spurion expansion for this case only gives contributions to the  $\gamma$  coefficient of the potential,<sup>11</sup>

$$\mathcal{I}_2^L(s_h) = \left( \mathcal{U}^t \Delta_L^\dagger \Delta_L \mathcal{U} \right)_{55} = -\frac{1}{2} |\epsilon_L|^2 s_h^2 + (u \leftrightarrow d) \quad (2.65a)$$

$$\mathcal{I}_2^R(s_h) = \left( \mathcal{U}^t \Delta_R^\dagger \Delta_R \mathcal{U} \right)_{55} = |\epsilon_R|^2 (1 - s_h^2) + (u \leftrightarrow d) \quad (2.65b)$$

Terms of order  $s_h^4$  (that correspond to the  $\beta$ -coefficient in (2.55)) only appear with a higher number of spurion insertions<sup>12</sup>

$$\mathcal{I}_4^{LL}(s_h) = \mathcal{I}_2^L(s_h) \mathcal{I}_2^L(s_h) = \frac{1}{4} |\epsilon_L|^4 s_h^4 + (u \leftrightarrow d) \quad (2.66a)$$

$$\mathcal{I}_4^{RR}(s_h) = \mathcal{I}_2^R(s_h) \mathcal{I}_2^R(s_h) = |\epsilon_R|^4 (1 - s_h^2)^2 + (u \leftrightarrow d) \quad (2.66b)$$

$$\mathcal{I}_4^{LR}(s_h) = \mathcal{I}_2^L(s_h) \mathcal{I}_2^R(s_h) = -\frac{1}{2} |\epsilon_L|^2 |\epsilon_R|^2 (1 - s_h^2) s_h^2 + (u \leftrightarrow d) \quad (2.66c)$$

As a consequence, formally sub-leading terms in the spurion expansion have to become comparable to leading order terms in order to satisfy the necessary condition  $\beta \gtrsim \gamma$  for having a non-trivial minimum of the potential. Contrary to the gauge sector, where the amount of explicit symmetry breaking is always small ( $g_0 \ll g_\rho$ ), this is possible in the fermion sector as the more complicated parametric dependencies allow for a certain amount of fine-tuning to be present. This strongly depends on the details of the confining UV theory, but is accessible for explicit calculations in the EFT. Therefore, one can identify a source of necessary fine-tuning needed in this model [61]. This tuning is less severe for large composite-elementary mixings, such that one expects the potential to be generated mostly by the heavy top quark (and to a lesser degree by the bottom quark).

Summarizing, the above spurion analysis shows that the effective potential,

$$V_{\text{eff}}(s_h) = \left( -(\gamma_{\text{fermion}} + \gamma_{\text{gauge}}) s_h^2 + \beta_{\text{fermion}} s_h^4 + \dots \right) f^4, \quad (2.67)$$

gets contributions from the fermion as well as from the gauge sector. While EWSB is induced by loops of quarks with a large degree of compositeness an interplay between the gauge and fermion sectors is necessary to determine the exact location of the minimum as well as the value of the Higgs mass. Assuming all massive parameters of the strong sector to be roughly of the same order

<sup>10</sup> The fermion contributions are model-dependent since they depend on the representations of the fermion resonances under the global symmetries. In this section we only consider the simplest case of fundamentals under  $SO(5)$ , but larger representations are possible and can lead to different conclusions, in particular about fine-tuning. For a review see e.g. [56, 59].

<sup>11</sup> This is not true in general. If the fermion resonances are e.g. embedded into a symmetric  $\mathbf{14}$ -representation of  $SO(5)$  then  $s_h^4$ -terms appear already at this level in the spurion expansion and no further tuning is necessary. [56, 59]

<sup>12</sup> Terms of the form  $\mathcal{U}^t \Delta^\dagger \Delta \Delta^\dagger \Delta \mathcal{U}$  either vanish or give  $s_h$ -independent contributions to the potential.

$m_\Psi \sim m_{\tilde{\Psi}} \sim f$  one would expect that the potential also gets contributions of that order such that  $\gamma = \gamma_{\text{fermion}} + \gamma_{\text{gauge}} = \mathcal{O}(1)$ . This, however, is in tension with a light Higgs mass that by (2.56) instead forces  $\gamma \sim \frac{m_{\tilde{\Psi}}^2}{f^2} \ll 1$ . To achieve the needed suppression of  $\gamma$  parameter, an unnatural cancellation between the a priori largely uncorrelated gauge and fermion contributions has to take place such that

$$\gamma_{\text{fermion}} \approx -\gamma_{\text{gauge}} \quad \text{and} \quad \gamma_{\text{fermion}} + \gamma_{\text{gauge}} \ll 1. \quad (2.68)$$

Phenomenologically, this is of great relevance as including the Higgs mass leads to non-trivial correlations between the gauge and fermion sectors of the theory. For our work, this has profound consequences as because of these correlations it is not possible to constrain the different sectors of the theory separately, but one has to perform a global analysis including all constraints at the same time to account for the interplay between the different parts of the theory. In the end, such different things as flavour observables and EWPOs could be connected in a subtle way.

For composite pNGB Higgs models with fermions in the fundamental representation of  $\text{SO}(5)$  there are two sources of fine-tuning. The first one originates from generating the hierarchy between the electroweak scale  $v_{\text{SM}}$  and the NP scale  $f$ . This is the minimal tuning which is present in all cases. It is usually estimated as  $\Delta^{\text{min}} \sim \frac{f^2}{v_{\text{SM}}^2}$ , so for  $1 \text{ TeV} \leq f \leq 2.5 \text{ TeV}$  this roughly corresponds to a tuning at the 10% – 1% level. As discussed above, for fermions in the fundamental representation a further source of tuning is given due to the fact that formally sub-leading terms in the spurion expansion should become of the order of the leading terms in order to induce EWSB. Because of this the real tuning is actually parametrically enhanced such that the so-called double-tuning is estimated as

$$\Delta^{\text{double-tuning}} \sim \frac{1}{\epsilon^2} \frac{f^2}{v_{\text{SM}}^2}, \quad (2.69)$$

where  $\epsilon$  is a generic spurion expansion parameter. This is hard to quantify, but due to the presence of the top quark contributions this parameter should not be too small, and it also should not be too large for the spurion expansion to make sense. For the remainder of this work we will make an educated guess and use an example value  $\epsilon = 0.5$ . This corresponds to a tuning at the 10% – 1% level only for smaller values of  $0.5 \text{ TeV} \leq f \leq 1.2 \text{ TeV}$ .

We have to note that the above conclusions can be significantly relaxed if one considers a lepton sector with significant degrees of compositeness [59]. In this case the leptons can give non-negligible contributions to the effective potential that can soften the strong correlations between the quark and vector sector. As remarked above, we do not consider composite leptons in this work.

### 2.2.3. Flavour symmetries

If one wants to investigate a realistic model it is inevitable to include flavour. Effectively this means that the above parameters (like masses and composite-elementary mixings) become  $3 \times 3$  matrices in flavour space. In the end, their flavour structure will have to reproduce the known CKM structures of the SM. This can be done in manifold ways, but it has to be ensured that no new unobserved large deviation from the experimental measurements occur. A major motivation for CHMs is their ability to explain flavour hierarchies in a dynamical way (see the discussion in section 2.1.2) with an anarchic flavour structure in the composite sector. Although such a setup is very elegant it was realized that this scenario notoriously leads to problems with  $CP$  observables in the flavour sector such as e.g.  $\epsilon_K$ , the measure of indirect  $CP$  violation in the kaon system [62, 63], calling for compositeness scales of  $\mathcal{O}(20 \text{ TeV})$ . Therefore, to avoid dangerously large flavour effects while still keeping an acceptable level of fine-tuning it is well-motivated to assume the presence of some flavour symmetry that is only weakly broken such that the observed flavour pattern can be traced back to this breaking [64]. In this section we will briefly introduce the concept of flavour symmetries and explain how these are implemented in this work. For this we will closely follow [65] and use their description of flavour symmetries for CHMs.

The concept of flavour symmetries is introduced most easily using models of Minimal Flavour Violation (MFV) [66, 67], where we will concentrate on quark flavour. We will also, for the time being, only consider SM degrees of freedom and discuss CHMs only at the end of this section. If the SM did not include the Higgs there was nothing that distinguishes between between the quark generations and therefore it would be subject to a global symmetry

$$\mathcal{G}_{\text{MFV}} = \text{U}(3)^3 = \text{U}(3)_{q_L} \times \text{U}(3)_{u_R} \times \text{U}(3)_{d_R} \quad (2.70)$$

which acts on the flavour indices of the quarks in the following way:

$$[q_L]_i = \left[ \begin{pmatrix} u_L \\ d_L \end{pmatrix}, \begin{pmatrix} c_L \\ s_L \end{pmatrix}, \begin{pmatrix} t_L \\ b_L \end{pmatrix} \right] \in (\mathbf{3}, \mathbf{1}, \mathbf{1}), \quad (2.71a)$$

$$[u_R]_i = [u_R, c_R, t_R] \in (\mathbf{1}, \mathbf{3}, \mathbf{1}), \quad (2.71b)$$

$$[d_R]_i = [d_R, s_R, b_R] \in (\mathbf{1}, \mathbf{1}, \mathbf{3}). \quad (2.71c)$$

However, in the presence of Yukawa interactions with the Higgs this symmetry can only be approximate as it gets broken explicitly. In MFV models one assumes that the SM Yukawa couplings are the only source of such a breaking.

Bilinears of the quark fields can be formed if one introduces spurion fields that transform under  $\mathcal{G}_{\text{MFV}}$  in the following way:

$$Y_u \in (\mathbf{3}, \bar{\mathbf{3}}, \mathbf{1}) \quad \text{and} \quad Y_d \in (\mathbf{3}, \mathbf{1}, \bar{\mathbf{3}}). \quad (2.72)$$

Yukawa couplings to the Higgs are then written as  $\mathcal{G}_{\text{MFV}}$ -singlets involving the spurions,

$$\mathcal{L}_{\text{yuk}} = \bar{q}_L \cdot Y_d \cdot d_R \mathcal{H} + \bar{q}_L \cdot Y_u \cdot u_R \tilde{\mathcal{H}} + \text{h.c.} \quad (2.73)$$

This symmetry is broken by the large top mass and in a weak way by the observed flavour hierarchies and CKM patterns. To parametrize this breaking the spurions take the following vevs

$$Y_u \rightarrow V_{\text{CKM}}^\dagger \text{diag}(y_u, y_c, y_t), \quad Y_d \rightarrow \text{diag}(y_d, y_s, y_b), \quad (2.74)$$

where we went into a flavour basis that is convenient for processes involving down-type quarks and used the experimental input for the Yukawa couplings and CKM mixings.

The assumption of MFV has profound consequences on the flavour structure of higher dimensional operators. In the spirit of the above construction, these operators have to be formally invariant under  $\mathcal{G}_{\text{MFV}}$  before the spurions take their vevs. Assuming MFV this has to be true even including NP contributions. As an example, let us consider a dim-6 operator from the SMEFT [68],

$$\mathcal{L}^{6-\text{dim}} \supset \frac{[C_{\ell d}]_{ij;kl}}{\Lambda^2} \left( \bar{d}_R^i \gamma^\mu d_R^j \right) \left( \bar{\ell}_L^k \gamma_\mu \ell_L^l \right). \quad (2.75)$$

Neglecting the lepton flavour and assuming  $\mathcal{G}_{\text{MFV}}$ -invariance, the Wilson coefficient has to be written as

$$[C_{\ell d}]_{ij} = a_0 \mathbb{1}_{ij} + a_2 [Y_d^\dagger Y_d]_{ij} + a_4 [Y_d^\dagger Y_d Y_d^\dagger Y_d]_{ij} + a'_4 [Y_d^\dagger Y_u Y_u^\dagger Y_d]_{ij} + \mathcal{O}(Y^6). \quad (2.76)$$

This is an expansion of the Wilson coefficients in terms of the symmetry breaking spurion fields. Note that FCNC couplings only appear starting with the  $a'_4$ -term when the spurions take their vevs. Assuming that the  $a_i$  coefficients take  $\mathcal{O}(1)$  values this determines the hierarchy of the flavour violating couplings which is given solely in terms of the CKM matrix.

As a flavour symmetry,  $U(3)^3$  is the maximal example. Considering the large mass splitting between the first two and the third generation, a alternative is given by a smaller flavour group [65]

$$\mathcal{G}_f = U(2)^3 = U(2)_{q_L} \times U(2)_{u_R} \times U(2)_{d_R}, \quad (2.77)$$

under which one assumes only the first two generations to form a doublet while the third generation is a singlet,

$$[q_L]_i = \left[ \begin{array}{l} \mathbf{q}_L = \left[ \begin{pmatrix} u_L \\ d_L \end{pmatrix}, \begin{pmatrix} c_L \\ s_L \end{pmatrix} \right] \in (\mathbf{2}, \mathbf{1}, \mathbf{1}) \\ q_L^3 = \begin{pmatrix} t_L \\ b_L \end{pmatrix} \in (\mathbf{1}, \mathbf{1}, \mathbf{1}) \end{array} \right], \quad (2.78)$$

$$[u_R]_i = \left[ \begin{array}{l} \mathbf{u}_R = [u_R, c_R] \in (\mathbf{1}, \mathbf{2}, \mathbf{1}) \\ t_R \in (\mathbf{1}, \mathbf{1}, \mathbf{1}) \end{array} \right], \quad (2.79)$$

$$[d_R]_i = \left[ \begin{array}{l} \mathbf{d}_R = [d_R, s_R] \in (\mathbf{1}, \mathbf{1}, \mathbf{2}) \\ b_R \in (\mathbf{1}, \mathbf{1}, \mathbf{1}) \end{array} \right]. \quad (2.80)$$

Analogously to the  $U(3)^3$  case spurion fields have to be introduced to write down bilinears in the quark fields [65],

$$Y_u \in (\mathbf{2}, \bar{\mathbf{2}}, \mathbf{1}), \quad Y_d \in (\mathbf{2}, \mathbf{1}, \bar{\mathbf{2}}), \quad \mathbf{V} \in (\mathbf{2}, \mathbf{1}, \mathbf{1}). \quad (2.81)$$

With the help of these, Yukawa terms are given as

$$\begin{aligned} \mathcal{L}_{\text{Yuk}} &= \bar{q}_L \cdot \mathbf{Y}_d \cdot d_R \mathcal{H} + \bar{q}_L \cdot \mathbf{Y}_u \cdot u_R \tilde{\mathcal{H}} + \text{h.c.} \\ &= (a_d^1 \bar{q}_L^3 b_R + a_d^2 \bar{q}_L \cdot \mathbf{V} b_R + a_d^3 \bar{q}_L \cdot Y_d \cdot \mathbf{d}_R + \dots) \mathcal{H} \\ &\quad + (a_u^1 \bar{q}_L^3 t_R + a_u^2 \bar{q}_L \cdot \mathbf{V} t_R + a_u^3 \bar{q}_L \cdot Y_u \cdot \mathbf{u}_R + \dots) \tilde{\mathcal{H}} \\ &\quad + \text{h.c.}, \end{aligned} \quad (2.82)$$

where we neglected terms of higher order in the spurion expansion, such as e.g.  $\bar{q}_L^3 \mathbf{V}^\dagger \cdot Y_d \cdot \mathbf{d}_R$ . It was found in [65] that the spurion vevs that are necessary to reproduce the observed flavour pattern are given as

$$Y_u \rightarrow \mathbf{R}(\alpha_u) Y_u^{\text{diag}}, \quad Y_d \rightarrow \text{diag}(e^{i\phi_d}, 1) \mathbf{R}(\alpha_d) Y_d^{\text{diag}}, \quad \mathbf{V} = (0, \epsilon)^t, \quad (2.84)$$

where unphysical parameters and phases have been rotated away by  $\mathcal{G}_f$  rotations. With  $\mathbf{R}(\alpha)$  we denote a  $2 \times 2$  rotation matrix by the angle  $\alpha$ . Absorbing the  $\mathcal{O}(1)$  coefficients  $a_{u,d}^i$  into the spurion vevs, the Yukawa matrices can then be written as

$$\mathbf{Y}_u = \begin{pmatrix} c_u Y_u^1 & -s_u Y_u^2 & 0 \\ s_u Y_u^1 & c_u Y_u^2 & \epsilon \\ 0 & 0 & Y_u^3 \end{pmatrix}, \quad \mathbf{Y}_d = \begin{pmatrix} c_d Y_d^1 e^{i\phi} & -s_d Y_d^2 e^{i\phi} & 0 \\ s_d Y_d^1 & c_d Y_d^2 & \epsilon \\ 0 & 0 & Y_d^3 \end{pmatrix}, \quad (2.85)$$

where  $s_{u,d} = \sin(\alpha_{u,d})$  and  $c_{u,d} = \cos(\alpha_{u,d})$ .

In the end, we want to consider CHMs with full flavour structure. For this we consider the above introduced flavour symmetries and assumed the whole composite sector to be exactly invariant under a flavour symmetry group  $\mathcal{G}_f$ , which we take to be either of  $U(3)$ -type or of  $U(2)$ -type. Only the couplings of the composite sector to the elementary fields will in the end break this symmetry explicitly, therefore generating the known CKM structure. The idea of implementing flavour symmetries in CHMs was introduced in [69, 64] and further worked out in [65, 70].

To discuss this in further detail let us write down the schematic Lagrangian of a CHM (where we neglect the gauge and Higgs interactions as these do not influence the considerations here),<sup>13</sup>

$$\begin{aligned} \mathcal{L} &= \mathcal{L}_{\text{elem}} + \mathcal{L}_{\text{comp}} + \mathcal{L}_{\text{mix}} \\ &\supset \bar{q}_L^0 i \not{\partial} q_L^0 + \bar{u}_R^0 i \not{\partial} u_R^0 + \bar{d}_R^0 i \not{\partial} d_R^0 + \bar{\Psi}_u (i \not{\partial} - M_u) \Psi_u + \bar{\Psi}_d (i \not{\partial} - M_d) \Psi_d \\ &\quad + \mathcal{L}_{\text{mix}}. \end{aligned} \quad (2.86)$$

If  $\mathcal{L}_{\text{mix}} = 0$  then the above theory is invariant under a flavour symmetry<sup>14</sup>

$$\mathcal{G}_f = U(n)_{\text{elem}}^3 \times U(n)_{\text{comp}}^2 = U(n)_{q_L} \times U(n)_{u_R} \times U(n)_{d_R} \times U(n)_U \times U(n)_D, \quad (2.87)$$

where  $n = 2, 3$  depending on which flavour scenario one wants to look at. This symmetry contains a direct product of the  $U(n)_{\text{elem}}^3$  flavour symmetry of the chiral elementary sector and the  $U(n)_{\text{comp}}^2$  symmetry for the vector-like composite sector.

If  $\mathcal{L}_{\text{mix}} \neq 0$  then the above symmetry is explicitly broken. Schematically, the mixing Lagrangian can be written as

$$\mathcal{L}_{\text{mix}} = \Delta_{uL} \bar{q}_L^0 \Psi_{uR} + \Delta_{dL} \bar{q}_L^0 \Psi_{dR} + \Delta_{uR} \bar{u}_R^0 \Psi_{uL} + \Delta_{dR} \bar{d}_R^0 \Psi_{dL} + \text{h.c.}, \quad (2.88)$$

showing that the symmetry breaking can either come from left- or right-handed mixings, or from both. As (2.30) suggests it is enough that the breaking stems only from one chirality to reproduce the SM flavour patterns. This means there are two distinct scenarios:

<sup>13</sup>Note that in this notation  $\Psi_u$  and  $\Psi_d$  do not have to be a single multiplet. It could contain several different fermion states with the same quantum numbers arising e.g. in composite models with more than two sites. In this case, the matrices  $M_u$  and  $M_d$  are general mass mixing matrices. As an example consider the scenario which will be investigated in chapter 4: left- and right-handed elementary fermions mix different composite resonances  $\Phi$  and  $\tilde{\Psi}$ . In an abuse of notation we denote both by  $\Psi$  as mixing terms of the form  $\bar{\Psi} \tilde{\Psi}$  will enforce the same transformation properties under flavour symmetries for both fields.

<sup>14</sup>In general, the flavour symmetry depends on the representations of the composite resonances under the global symmetry of the composite sector. Here, we have a particular scenario in mind which will be investigated in chapter 4: we consider the minimal coset in which fermion resonances appear as singlets and bidoublets of  $SO(4)$ .

- **left-compositeness (LC)**: In this scenario one assumes the left-handed composite-elementary mixings to be flavour-diagonal, such that effectively the flavour symmetry reduces to

$$U(n)_{LC}^3 = U(n)_{q_L+U+D} \times U(n)_{u_R} \times U(n)_{d_R} \quad (2.89)$$

and all the flavour breaking will be given by the right-handed mixings.

- **right-compositeness (RC)**: In this scenario one assumes the right-handed composite-elementary mixings to be flavour-diagonal, such that effectively the flavour symmetry reduces to

$$U(n)_{RC}^3 = U(n)_{q_L} \times U(n)_{u_R+U} \times U(n)_{d_R+D} \quad (2.90)$$

and all the flavour breaking will be given by the right-handed mixings.

This means there are 4 scenarios to be considered: LC and RC for U(3) and U(2).

Including flavour symmetries has a profound impact on the compositenesses of the SM quarks. In general, (2.30) must hold such that, assuming nearly flavour degenerate composite Yukawa couplings as in an anarchic scenario, the SM mass hierarchies have to be generated by the product of left- and right-handed degrees of compositeness,  $y_{SM}^i \sim \sin(\phi_L^i) \sin(\phi_R^i)$ . A flavour structure implemented in the above way can have two effects: First, and this is particularly relevant for U(2) symmetries, a flavour structure can enforce also a structure on the composite Yukawas such that the SM hierarchies do not have to be generated by the degrees of compositeness alone anymore. Second, choosing either LC or RC gives a hierarchy between the left- and right-handed degrees of compositeness. Generally, one would expect the spurions to transmit a not too large breaking of the flavour symmetries for the whole framework to make sense. This then implies that the degrees of compositeness responsible for flavour breaking should be small compared to the symmetry conserving ones. This justifies the nomenclature introduced above: In LC the left-handed composite-elementary mixings respect the flavour symmetries while the right-handed ones break them. Therefore, one expects the left-handed degrees of compositeness to be larger than the right-handed ones. For RC the opposite scenario is true. In U(3) scenarios the degrees of compositeness of the light quarks are directly linked to that of third generation quarks. Hence, to generate the masses of the heavy quarks one expects also for light quarks in this scenario that one chirality is significantly composite while the other chirality is mostly elementary such a degree that a mass low enough is generated. In U(2) scenarios this only holds to a much weaker degree, since here the third generation is effectively decoupled from the first two.

## 2.2.4. Connecting flavour and the potential

If light quarks can have one significantly composite chirality then it is an interesting question what influence this has on the effective Higgs potential. As this potential is induced by the composite-elementary mixings which break the global symmetries explicitly one would expect the contributions to the potential to be correlated to the mixings. Also, as the composite-elementary mixings are responsible for both, EWSB and flavour, it is interesting whether this leads to correlations between both sectors. To assess this question we generalized the spurion analysis of eqs. (2.62) – (2.66) for the example of SO(5)/SO(4) to include also the breaking of flavour symmetries. Such a spurion analysis can only give a rough qualitative understanding of the effects which can be very helpful. A proper analysis of the effective potential, however, can only be done numerically. This we will perform in chapter 4, but the results obtained in this section will help to interpret the numerical results.

Starting from the general mixing Lagrangian (2.62) we can introduce flavour indices transforming under the flavour symmetries in addition to the quantum numbers (2.63a). Considering first the U(3) case<sup>15</sup> we assign representations under  $\mathcal{G}_f = U(3)_{q_L} \times U(3)_{u_R} \times U(3)_{d_R} \times U(3)_U \times U(3)_D$  in the following way

$$\begin{aligned} q_L^0 &\sim ((\mathbf{3}, \mathbf{1}, \mathbf{1}), (\mathbf{1}, \mathbf{1})), & u_R^0 &\sim ((\mathbf{1}, \mathbf{3}, \mathbf{1}), (\mathbf{1}, \mathbf{1})), & d_R^0 &\sim ((\mathbf{1}, \mathbf{1}, \mathbf{3}), (\mathbf{1}, \mathbf{1})), \\ \tilde{\Psi}_u &\sim ((\mathbf{1}, \mathbf{1}, \mathbf{1}), (\mathbf{3}, \mathbf{1})), & \tilde{\Psi}_d &\sim ((\mathbf{1}, \mathbf{1}, \mathbf{1}), (\mathbf{1}, \mathbf{3})), & \Psi_{uR} &\sim ((\mathbf{1}, \mathbf{1}, \mathbf{1}), (\mathbf{3}, \mathbf{1})), & \Psi_{dR} &\sim ((\mathbf{1}, \mathbf{1}, \mathbf{1}), (\mathbf{1}, \mathbf{3})), \\ \Delta_{uL} &\sim ((\mathbf{3}, \mathbf{1}, \mathbf{1}), (\bar{\mathbf{3}}, \mathbf{1})), & \Delta_{dL} &\sim ((\mathbf{3}, \mathbf{1}, \mathbf{1}), (\mathbf{1}, \bar{\mathbf{3}})), & \Delta_{uR} &\sim ((\mathbf{1}, \mathbf{3}, \mathbf{1}), (\bar{\mathbf{3}}, \mathbf{1})), & \Delta_{dR} &\sim ((\mathbf{1}, \mathbf{1}, \mathbf{3}), (\mathbf{1}, \bar{\mathbf{3}})). \end{aligned}$$

This means the spurions carry four indices,

$$[\Delta_{uL}]_{ijab} = [\epsilon_{uL}]_{ab} \otimes [P_{uL}]_{ij} f, \quad (2.92)$$

<sup>15</sup>The U(2) case works in complete analogy with obvious replacements  $3 \leftrightarrow 2$ .

where  $i, j$  are indices under  $SU(2)_L^0 \times SO(5)$  and  $a, b$  are indices for the elementary and composite flavour groups. Note that we factored out the mass scale  $f$  to obtain dimensionless spurions. Although the composite-elementary mixings parametrize the breaking of both the global/gauge symmetries as well as the flavour symmetries, these are independent, such that the 4-index tensor factorizes into a part  $\epsilon$  describing flavour breaking and a part  $P_{L,R}$  describing the breaking of the Goldstone symmetries responsible for generating the effective potential. When assuming the spurion vevs the  $P_{L,R}$  will be given by the matrices written in (2.64) while the  $\epsilon$  parts will take the vevs dictated by the assumed flavour structure. The explicit forms are given in appendix IV.

For the given vevs we can now identify the scalar invariants contributing to the effective potential in analogy to eqs. (2.65) and (2.65). Due to the factorization (2.92) we find that qualitatively the form of the invariants stays the same but one has to replace  $|\epsilon|^2 \rightarrow \text{tr}[\epsilon^\dagger \epsilon]$ . In terms of the invariants the effective potential can be written as

$$V(s_h) \propto \sum_X c_X \mathcal{I}_X(s_h), \quad (2.93)$$

where  $c_X$  are unknown coefficients that have to be determined by an explicit calculation. From these expressions we can determine the parametric dependence of the parameters  $\gamma$  and  $\beta$  in the expansion (2.55),

$$\begin{aligned} \gamma &\sim \left[ \frac{1}{2} c_2^{uL} \text{tr}[\epsilon_{uL}^\dagger \epsilon_{uL}] + c_2^{uR} \text{tr}[\epsilon_{uR}^\dagger \epsilon_{uR}] + 2c_4^{uRR} \text{tr}[\epsilon_{uR}^\dagger \epsilon_{uR}]^2 + \frac{1}{2} c_4^{uLR} \text{tr}[\epsilon_{uL}^\dagger \epsilon_{uL}] \text{tr}[\epsilon_{uR}^\dagger \epsilon_{uR}] + (u \leftrightarrow d) \right] \\ \beta &\sim \left[ \frac{1}{4} c_4^{uLL} \text{tr}[\epsilon_{uL}^\dagger \epsilon_{uL}]^2 + c_4^{uRR} \text{tr}[\epsilon_{uR}^\dagger \epsilon_{uR}]^2 + \frac{1}{2} c_4^{uLR} \text{tr}[\epsilon_{uL}^\dagger \epsilon_{uL}] \text{tr}[\epsilon_{uR}^\dagger \epsilon_{uR}] + (u \leftrightarrow d) \right]. \end{aligned}$$

Using these expressions we can obtain the following very rough estimate: Assuming either LC or RC one could make use of the hierarchies between left-handed and right-handed composite-elementary mixings and neglect the small  $\epsilon$ 's while setting the larger ones to  $\epsilon = 1$  which seems to be justified at least for the top quark. In this case one finds

$$\begin{array}{ll} \text{LC} & \gamma \sim \frac{1}{2} c_2^L, & \frac{\gamma}{\beta} \sim \frac{2c_2^L}{c_4^{LL}}, \\ \text{RC} & \gamma \sim c_2^R + 2c_4^{RR}, & \frac{\gamma}{\beta} \sim \frac{c_2^R + 2c_4^{RR}}{c_4^{RR}}. \end{array}$$

Assuming that the coefficients are of  $\mathcal{O}(1)$  and keeping in mind that in order to obtain EWSB and a light Higgs mass one needs  $\gamma \ll 1$  and  $\beta \gtrsim \gamma$ , this seems to suggest that LC fulfills these requirements more naturally, thus one would expect that the fine-tuning of the effective potential in the case of LC could be less severe. This is of course only a very rough estimate as factors of a few could easily be present in the  $c$  coefficients changing the whole picture. Therefore, an explicit calculation is essential and this will be done in section 4.3.1.

Going back to the scalar invariants of (2.93) we can calculate the factors of  $\text{tr}[\epsilon^\dagger \epsilon]$  using the explicit expressions of appendix IV.1. This gives for the U(3) case:

LC:

$$\text{tr}[\epsilon_{uL}^\dagger \epsilon_{uL}] f^2 = 3 (\Delta_{uL}^{123})^2, \quad \text{tr}[\epsilon_{dL}^\dagger \epsilon_{dL}] f^2 = 3 (\Delta_{dL}^{123})^2, \quad (2.95a)$$

$$\text{tr}[\epsilon_{uR}^\dagger \epsilon_{uR}] f^2 = (\Delta_{uR}^1)^2 + (\Delta_{uR}^2)^2 + (\Delta_{uR}^3)^2, \quad \text{tr}[\epsilon_{dR}^\dagger \epsilon_{dR}] f^2 = (\Delta_{dR}^1)^2 + (\Delta_{dR}^2)^2 + (\Delta_{dR}^3)^2, \quad (2.95b)$$

RC:

$$\text{tr}[\epsilon_{uL}^\dagger \epsilon_{uL}] f^2 = (\Delta_{uL}^1)^2 + (\Delta_{uL}^2)^2 + (\Delta_{uL}^3)^2, \quad \text{tr}[\epsilon_{dL}^\dagger \epsilon_{dL}] f^2 = (\Delta_{dL}^1)^2 + (\Delta_{dL}^2)^2 + (\Delta_{dL}^3)^2, \quad (2.95c)$$

$$\text{tr}[\epsilon_{uR}^\dagger \epsilon_{uR}] f^2 = 3 (\Delta_{uR}^{123})^2, \quad \text{tr}[\epsilon_{dR}^\dagger \epsilon_{dR}] f^2 = 3 (\Delta_{dR}^{123})^2. \quad (2.95d)$$

Similarly for the U(2) flavour symmetries we find:



LC:

$$\begin{aligned} \text{tr} \left[ \epsilon_{uL}^\dagger \epsilon_{uL} \right] f^2 &= 2 (\Delta_{uL}^{12})^2 + (\Delta_{uL}^3)^2, & \text{tr} \left[ \epsilon_{dL}^\dagger \epsilon_{dL} \right] f^2 &= 2 (\Delta_{dL}^{12})^2 + (\Delta_{dL}^3)^2, & (2.96a) \\ \text{tr} \left[ \epsilon_{uR}^\dagger \epsilon_{uR} \right] f^2 &= (\Delta_{uR}^1)^2 + (\Delta_{uR}^2)^2 + (1 + \epsilon_u^2) (\Delta_{uR}^3)^2, & \text{tr} \left[ \epsilon_{dR}^\dagger \epsilon_{dR} \right] f^2 &= (\Delta_{dR}^1)^2 + (\Delta_{dR}^2)^2 + (1 + \epsilon_d^2) (\Delta_{dR}^3)^2, & (2.96b) \end{aligned}$$

RC:

$$\text{tr} \left[ \epsilon_{uL}^\dagger \epsilon_{uL} \right] f^2 = (\Delta_{uL}^1)^2 + (\Delta_{uL}^2)^2 + (1 + \epsilon_u^2) (\Delta_{uL}^3)^2, \quad \text{tr} \left[ \epsilon_{dL}^\dagger \epsilon_{dL} \right] f^2 = (\Delta_{dL}^1)^2 + (\Delta_{dL}^2)^2 + (1 + \epsilon_d^2) (\Delta_{dL}^3)^2, \quad (2.96c)$$

$$\text{tr} \left[ \epsilon_{uR}^\dagger \epsilon_{uR} \right] f^2 = 2 (\Delta_{uR}^{12})^2 + (\Delta_{uR}^3)^2, \quad \text{tr} \left[ \epsilon_{dR}^\dagger \epsilon_{dR} \right] f^2 = 2 (\Delta_{dR}^{12})^2 + (\Delta_{dR}^3)^2. \quad (2.96d)$$

From this we can see several things. Assuming again the dominance of the flavour symmetry conserving composite-elementary mixings, there is an additional factor of 3 compared to the one-flavour case for the U(3) scenario. Keeping in mind that there has to be a cancellation between fermion and vector contributions to the effective potential, an increase in the fermion contributions also means an increase of needed fine-tuning with the vector sector. This is however not so severe for the U(2) symmetry as in this case the contributions from the symmetry preserving couplings are the sum of the contributions from the first two and the third generation. As for this flavour structure the third generation is decoupled, the first two generations can contribute at a weaker level. This leads to the expectation of a milder fine-tuning in U(2) theories.

A further point we observe is that the parameters describing flavour mixing cancel in the combination  $\text{tr} [\epsilon^\dagger \epsilon]$ . Taking the spurion expansion serious this leads to the expectation that the effective potential is correlated to mass of the quarks and in particular to the top quark mass but one might not expect to see correlations with flavour observables. This is of course only a rough qualitative estimate that has to be validated by explicit calculations in chapter 4.

### 2.3. Composite Higgs models from extra dimensions

In this section let us pursue a seemingly totally different road to composite Higgs models, namely a construction inspired by extra dimensions. This has several advantages. Embedding a CHM into an extra-dimensional theory allows to inherit all the benefits of the higher-dimensional model. In particular, this includes having a framework to explain the gauge hierarchy problem by geometry. Also the vastly different couplings that in the end lead to the measured flavour patterns can have a simple geometrical origin if there are additional spatial dimensions [42]. The main advantage for this work is of a slightly more technical nature. It is possible to implement the pNGB Higgs as a component of an extra-dimensional gauge field such that its potential becomes calculable. In other words, the main reason for considering such theories in this work is that the extra-dimensional gauge symmetry ensures that the Weinberg sum rules (2.52) are satisfied, because otherwise the predictive power of such a model would rather low.

At this point we want to stress explicitly that what we are investigating are CHMs *inspired* by extra dimensions, but we are not considering actual extra-dimensional theories. The important point in this work is that the models considered have a structure suggested by extra dimensions that ensures the calculability of the Higgs potential. In the following we analyze the models by sampling their parameter spaces. At no point do we want to make the statement that the found parameter points translate into a concrete extra-dimensional model with some given geometry. In this sense we are even more general, we want to judge the status of CHMs while ignoring possible correlations between parameters that would be present in a higher-dimensional framework.

The idea of supplementing the known spacetime by additional space dimensions is already quite old. More than 100 years ago Nordström started an idea [71] that a few years later would become the so-called Kaluza-Klein theory [72]. Herein, an additional space dimension was introduced as an auxiliary construct to unify gravitation and electromagnetism into the metric of a hypothetical five-dimensional manifold. Physical sense could be made from these additional dimensions by compactifying them to small ‘circles’ and thus reconciling them with the observed four spacetime dimensions [73]. Then, for quite a long time extra dimensions were rather marginal appearing only as an artifact in string theory

constructions. The big reintroduction of extra dimensions into the mainstream started in the late 1990s with the formulation of the AdS/CFT conjecture [74], which allowed to mathematically connect four-dimensional strongly interacting theories (like the composite Higgs) with perturbative theories on higher dimensional spacetimes. Shortly after, it was realized the extra dimensions can give natural solutions to the hierarchy problem via geometrical mechanisms. In these scenarios the apparent weakness of gravitation is explained by the assumption that it penetrates the whole extra-dimensional spacetime while all the SM fields are confined to four-dimensional subspaces, so-called branes. The first model of this kind was the Arkani-Hamed - Dimopoulos - Dvali (ADD) model [75] using large, flat extra dimensions. As a more elegant approach the idea of a highly-curved spacetime was introduced in the Randall-Sundrum (RS) models [76, 77]. In this scenario of warped extra dimensions the electroweak scale is connected to the Planck-scale purely by the geometry of spacetime itself,

$$m_{\text{EW}} \sim e^{-kr_c\pi} m_{\text{Pl}}, \quad (2.97)$$

via an exponential factor depending only on the scale of warping  $k$  and the radius of the fifth dimension  $r_c$ , such that effectively the hierarchy problem is reduced to a problem of order  $kr_c \approx \mathcal{O}(10)$ .

Very shortly after that it was also realized that extra dimensions can solve yet another open question of the SM, namely the flavour puzzle. The important ingredient for solving the hierarchy problem is that the Higgs is localized on (or at least near) a brane, but the other fields can propagate through the entire higher-dimensional spacetime. This opens the possibility to localize the fermions along the extra dimension giving effective control over how strongly they interact with the Higgs field and thus over the values for the entries of the Yukawa matrices [42, 78, 79].

In the following we will briefly review extra-dimensional theories and the Hosotani mechanism which is the crucial ingredient for models of Gauge-Higgs unification (GHU). Using the procedure of dimensional deconstruction, the extra-dimensional theory can be approximated by a CHM in four spacetime dimensions. In the end, this leads to the so-called Minimal 4d Composite Higgs Model (M4dCHM) which will be the subject of investigation for the remainder of this work. In this section we will give a review about such constructions and show how these are related to the models that will be subject of the analyses performed in this work. Thus, this section does not contain new results but we think that it is important for understanding the detailed structure and our motivation for the considered model.

### 2.3.1. Gauge-Higgs unification and the Hosotani mechanism

In extra-dimensional theories one considers the four-dimensional Minkowski spacetime as part of a higher-dimensional manifold. Therefore, every spacetime point can be described by coordinates  $x_M = (x_\mu, x_m)$ , where the first ones are the usual 4d coordinates and the last ones are in the extra dimensions. As the known world obviously only has 4 dimensions the others have to be *compactified* to be somewhat “small”, such that at low energies (large wavelengths) these small extra dimensions cannot be resolved and the spacetime effectively appears four-dimensional.<sup>16</sup> Simple examples for these “compactified spaces” are a circle  $S^1$  for one extra-dimension, a sphere  $S^2$  or a torus  $S^1 \times S^1$  for two dimension, and so on. But also much more complicated objects are possible.

The geometric structure of the spacetime is encoded in its metric  $ds^2 = g_{MN} dx^M dx^N$ . As simple examples for this with only one extra-dimension, one can consider the ADD model [75] or the RS model [76] (which uses a non-factorizable geometry):

$$ds^2 = \eta_{\mu\nu} dx^\mu dx^\nu - r_c^2 d\phi^2 \quad \text{ADD model} \quad (2.98)$$

$$ds^2 = e^{-2kr_c\phi} \eta_{\mu\nu} dx^\mu dx^\nu - r_c^2 d\phi^2 \quad \text{RS model} \quad (2.99)$$

Here,  $\phi$  denotes the coordinate on an extra dimension that takes the form of a circle with compactification radius  $r_c$ .

One further ingredient is of a slightly more technical nature, namely the fact that the SM as the low energy limit is a *chiral* theory. For extra-dimensional models with an odd number of dimensions it is well known that the Dirac representation of the Poincaré group is not reducible such that the Dirac spinors do not decompose into chiral Weyl spinors. Formally, these higher-dimensional spinors can still be projected onto their left- and right-handed components via  $P_{L/R} = \frac{1}{2} (1 \pm \gamma^5)$ , but these

<sup>16</sup>In full generality, this statement is not true. One can have an infinite extra dimension which then has to be strongly curved as for example in the RS2 scenario [77].

components will not be independent and one certainly cannot assign different quantum numbers to them. Such a theory can only contain *vector-like* fermions. A way out is given by introduction of certain discrete symmetries. As an example let us consider the case of only one extra dimension having the form of a circle  $S^1$ . By the circular periodicity one has to identify fields at the coordinates  $\phi$  and  $\phi + 2\pi$ ,

$$\Psi(x, \psi) = \Psi(x, \phi + 2\pi). \quad (2.100)$$

In addition, one can introduce a  $\mathbb{Z}_2$  symmetry connecting the points  $\phi \leftrightarrow -\phi$ , giving rise to a special kind of geometry (for a review see e.g. [80]). Since this symmetry operation connects the region  $\phi \in [0, \pi]$  to the region  $\phi \in [\pi, 2\pi]$  in a unique way, we can restrict ourselves to the former. Effectively, this reduces the circle  $S^1$  to the line element  $S^1/\mathbb{Z}_2$ , a process called *orbifolding*. On this orbifold the  $\mathbb{Z}_2$  acts as a parity operation, such that for an invariant theory one can classify fields as being *odd* or *even*,

$$\Psi(x, -\phi) = \Psi(x, \phi) \quad \text{even}, \quad (2.101a)$$

$$\Psi(x, -\phi) = -\Psi(x, \phi) \quad \text{odd}. \quad (2.101b)$$

A special emphasis has to be given to the points  $\phi = 0$  and  $\phi = \pi$  as these remain invariant under the orbifold parity operation, they are *orbifold fixed points*. For an orbifold odd field this means that it has to vanish at the fixed points. If the field is orbifold even one can always construct an odd field by acting on it with a derivative along the extra dimension. Thus, we can identify two different *boundary conditions* for field on orbifolds,

$$\Psi(x, \phi)|_{\phi=0, \pi} = 0 \quad \text{odd}, \quad (2.102a)$$

$$\partial_\phi \Psi(x, \phi)|_{\phi=0, \pi} = 0 \quad \text{even}. \quad (2.102b)$$

In a Kaluza-Klein (KK) decomposition, in which one performs a Fourier transformation in the discrete extra-dimensional component of momentum such that the effective theory takes the form of an infinite tower of four-dimensional theories, one can easily see that zero modes, which are identified with SM fields, vanish in case of an odd orbifold parity. Consequently, one can obtain a chiral low-energy limit from extra-dimensional vector-like fermions by imposing orbifold parities in a particular way such that the KK spectrum is given by

$$\left. \begin{array}{l} \text{RH odd: } \bar{\psi}_{L,0} i \not{\partial} \psi_{L,0} \\ \text{LH odd: } \bar{\psi}_{R,0} i \not{\partial} \psi_{R,0} \end{array} \right\} + \sum_{n=1}^{\infty} \int d^4x \left[ (\bar{\psi}_L + \bar{\psi}_R)_n i \not{\partial} (\psi_L + \psi_R)_n - m_n (\bar{\psi}_{L,n} \psi_{R,n} + \bar{\psi}_{R,n} \psi_{L,n}) \right]. \quad (2.103)$$

This now allows to construct chiral theories, but one does not have one 5d fermion per SM fermion, but rather one extra-dimensional field for each SM chirality. In a minimal example for describing, say, a  $u$ -quark one needs two 5d fermions. One will be part of an  $SU(2)$  doublet and RH odd. Its zero mode will be identified with the left-handed  $u_L$  chiral field. In addition, one will also need a 5d  $SU(2)$  singlet which has LH odd boundary conditions. That zero mode then describes the right-handed  $u_R$  component of the  $u$ -quark. So, for each SM fermion there will be *four* separate towers of KK resonances.

## Hosotani mechanism

In the following we shortly review the Hosotani mechanism [81] which acts as the source of EWSB in GHU theories. This discussion is based on the review [82].

Let us now go further and consider the case when there is a (non-abelian) gauge symmetry  $\mathcal{G}$  in the extra dimension. This means one has to introduce gauge fields [83, 84, 85],

$$A_M(x, \phi) = A_M^a(x, \phi) \Gamma^a = (A_\mu^a(x, \phi), A_5^a(x, \phi)) \Gamma^a. \quad (2.104)$$

As is well known, these carry a group index  $a$  and a space-time index  $M$ . Since by definition the theory is invariant under four-dimensional Lorentz-transformations, the higher-dimensional gauge field has to decompose into representations of the 4d Poincaré group. In 5 dimensions we thus get a four-vector field  $A_\mu$  and additionally a scalar  $A_5$ , both of which have different towers of KK modes,

$$A^{a\mu}(x, \phi) = \sum_{n=0}^{\infty} A_n^{a\mu}(x) \frac{h_{(a),n}(\phi)}{\sqrt{r_c}}, \quad A^{a5}(x, \phi) = \sum_{n=0}^{\infty} A_n^{a5}(x) \frac{h_{(a),n}^5(\phi)}{\sqrt{r_c}}. \quad (2.105)$$

Note here that there is also an independent KK tower for each generator of the gauge field. Given some geometry  $g^{MN}$ , one can write the Lagrangian as

$$\mathcal{L} = -\frac{1}{4} \int d^4x \int r_c d\phi \sqrt{|g|} g^{MR} g^{NS} \text{tr} [F_{MN} F_{RS}], \quad (2.106)$$

where the field-strength tensor of the (non-abelian) gauge field takes the usual form

$$F_{MN}(x, \phi) = \partial_M A_N(x, \phi) - \partial_N A_M(x, \phi) + ig [A_M(x, \phi), A_N(x, \phi)]. \quad (2.107)$$

Regarding the orbifold parities of the gauge boson field, one can observe that the above Lagrangian contains terms of the form <sup>17</sup>

$$\mathcal{L} \supset g^{5\nu} g^{\mu 5} F_{5\mu} F_{\nu 5} \supset g^{5\nu} g^{\mu 5} (\partial_\phi A_\mu^a) (\partial_\nu A_5^a), \quad (2.108)$$

which shows that for each group component the vector  $A_\mu^a$  and the scalar component  $A_5^a$  have to have the opposite parities for the Lagrangian to be invariant under orbifold parity. As a consequence, only one of both can have a zero mode appearing in the spectrum. But what does it mean when there are no massless gauge bosons appearing? For this let us take a closer look at the boundary conditions.

The Hosotani mechanism [81, 86] is the observation that on spacetimes that are not simply-connected<sup>18</sup> a dynamical rearrangement of gauge symmetries can occur. Similarly to the Aharonov-Bohm effect, phases of the gauge field along non-contractible paths can become physical, leading to a breaking of symmetries. The key point here is that on a periodic spacetime, quantum fields do not have to be single-valued if there is a symmetry in the theory. Only physical observables have to have a definite value. To see this, one has to remember that a circle actually is the covering space  $\mathbb{R}$  equipped with an identification  $f(x + 2\pi r_c) = f(x)$ . If there is e.g. a gauge symmetry then field values at identified points do not have to coincide; all that is required in order to get well-defined observables is that quantum fields coincide up to a gauge transformation [86, 87]:

$$\begin{aligned} A_M(x, y + 2\pi r_c) &= g A_M(x, y) g^\dagger, \\ \psi(x, y + 2\pi r_c) &= \exp(i\beta) \hat{\rho}(g) \psi(x, y), \end{aligned}$$

where  $g \in \mathcal{G}$  and  $\hat{\rho}(g)$  is a transformation of  $g$  in the appropriate representation of  $\psi$ . Thus, boundary conditions on the fields can be labeled by  $(g, \beta)$ . Of course, field values change under gauge transformations, and therefore also boundary conditions. If sets of boundary conditions are connected by such a gauge transformation they lead to the same physics and so, one can define equivalence classes of boundary conditions  $(g, \beta) \sim (g', \beta')$ . A physical symmetry is now given by transformations that leave the boundary conditions invariant, all other symmetries are broken by choosing an explicit set of conditions. In general, these symmetries differ from the whole set of gauge transformations, leading to an effective reduction of symmetries by the choice of boundary conditions.

In addition, Wilson lines

$$\mathcal{W}_{\mathcal{C}} = \mathcal{P} \exp \left( ig \int_{\mathcal{C}} dx^M A_M \right) = \mathcal{P} \exp \left( ig \int dz A_5 \right) \quad (2.109)$$

along non-contractible paths  $\mathcal{C}$  in the extra dimension do not vanish and thus become dynamical quantities. Then, the physical vacuum of the theory is determined by the expectation values of these Wilson line phases.

This is of course not the whole story, since the above statements are subject to quantum corrections. For this it is more convenient to change to boundary conditions that are (semi-)trivial [88] using the above gauge equivalence. Then the dynamical symmetry reduction is described by the Wilson lines, which develop a Coleman-Weinberg-like effective potential on the quantum level (which depends on the boundary conditions  $(g, \beta)$ ) that determines the physical vacuum. For an orbifolded extra dimension

<sup>17</sup>Remember that a metric tensor has to be symmetric  $g^{5\nu} = g^{\nu 5}$  and that  $g^{5\mu}$  and  $g^{5\nu}$  have to have the same orbifold parity due to Lorentz invariance. So, a structure of the form  $g^{5\nu} g^{\mu 5}$  has to be orbifold *even*.

<sup>18</sup>The definition of *simply-connected* is given in many textbooks on topology: A simply-connected space is a topological space in which every loop can be contracted to a point. For example, on a 2d-sphere  $S^2$  every loop on the surface can be shrunk to a point, but on a circle  $S^1$  this cannot be done for a loop winding along the circle. Effectively, a simply-connected space is a space without “holes”.

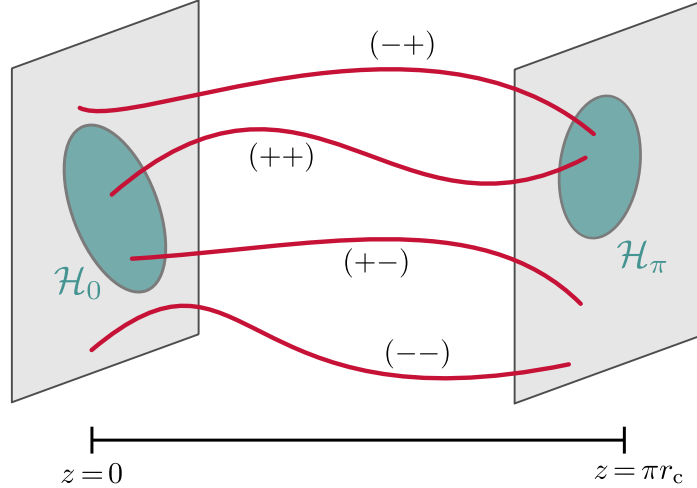


**Figure 2.3.:** Illustration of symmetry reduction via boundary conditions. On the boundaries the bulk gauge group  $\mathcal{G}$  gets broken down to subgroups  $\mathcal{H}_0$  and  $\mathcal{H}_\pi$ . Only for  $(++)$  boundary conditions there will be massless gauge fields in the spectrum. Goldstone bosons correspond to  $(--)$  conditions.

it is not possible, in general, to switch to totally trivial boundary conditions. One still has orbifold parities which leads to a kind of explicit reduction of the symmetries at the orbifold fixed points [88].

To be more concrete, let us start with a  $\mathcal{G}$  gauge theory on a five-dimensional spacetime  $\mathcal{M}_4 \times S^1/\mathbb{Z}_2$ . The most general boundary conditions compatible with the orbifold can be of the following forms [41, 80]<sup>19</sup>

$$(++) : \quad \partial_z A_\mu^a(x, z)|_{z=0} = 0, \quad \partial_z A_\mu^a(x, z)|_{z=\pi r_c} = 0, \quad (2.110a)$$

$$(+-) : \quad \partial_z A_\mu^a(x, z)|_{z=0} = 0, \quad A_\mu^a(x, z)|_{z=\pi r_c} = 0, \quad (2.110b)$$

$$(-+) : \quad A_\mu^a(x, z)|_{z=0} = 0, \quad \partial_z A_\mu^a(x, z)|_{z=\pi r_c} = 0, \quad (2.110c)$$

$$(--): \quad A_\mu^a(x, z)|_{z=0} = 0, \quad A_\mu^a(x, z)|_{z=\pi r_c} = 0. \quad (2.110d)$$

These boundary conditions can be chosen independently for each group component  $A^a$ . So, one sees that by appropriate choices of boundary conditions one can reduce the number of gauge fields appearing on the two sides of the extra-dimensional interval. Note that for consistency the symmetries on the boundary still have to form a group. Effectively, what is done is a reduction (i.e. a breaking) of the bulk gauge group  $\mathcal{G}$  down to subgroups  $\mathcal{H}_0$  and  $\mathcal{H}_\pi$  at the boundaries located at  $z = 0$  and  $z = \pi r_c$ , respectively. For an illustration see figure 2.3.

This amounts to an actual breaking of symmetries. Since a gauge transformation should not change the boundary conditions of the fields, the theory is not invariant anymore under the group  $\mathcal{G}$ , but rather under the somewhat smaller group

$$\mathcal{G}' = \{g(x, z) \in \mathcal{G} \mid g(x, z = 0) \in \mathcal{H}_0, g(x, z = \pi r_c) \in \mathcal{H}_\pi\}. \quad (2.111)$$

So, we cannot consider general  $\mathcal{G}$ -transformations anymore, but only transformations that reduce the respective subgroups at the boundary.

The physical spectrum of the theory depends on the above boundary conditions. For the  $(+, +)$ -fields, the spatial components will have zero modes giving rise to massless gauge bosons. For the coset fields with  $(--)$ -boundary conditions there will be zero modes for the scalar components appearing as Wilson lines. Due to quantum effects, there will be an effective potential that (depending on the detailed boundary conditions  $(g, \beta)$  as well as on the matter content of the theory) can lead to a non-trivial vacuum expectation value for the scalars and thus to a dynamical breaking of gauge symmetries.

In this setup one can now describe the structure of electroweak symmetry breaking. The Wilson lines are what has to be identified with the Higgs bosons. Then the Higgs mechanism is described via the dynamical symmetry reduction of the Hosotani mechanism. Since one wants at least four massless

<sup>19</sup>For a very nice, more formal discussion in terms of orbifold parities we refer to [82].

gauge bosons in the unbroken phase, one has to embed  $\mathcal{H}_0 \cap \mathcal{H}_\pi \supset G_{\text{SM}}$ . The remaining symmetries will lead to additional heavy resonances in the spectrum. This setup is what is called *Gauge-Higgs unification* [81].

### Holographic gauge fixing

For making the connection between extra-dimensional GHU models and four-dimensional models with a composite Higgs a powerful tool is given by *holography*. We will review this in the following where we will make extensive use of [89] and [90]. In holography the key element is to separate bulk from boundary degrees of freedom, such that the latter ones are interpreted as four-dimensional fields interacting with the bulk fields living inside the extra dimension. Thinking more formally in terms of partition functions, the extra-dimensional theory is described via a path integral [89]

$$\mathcal{Z} = \int \mathcal{D}\Phi|_{\text{b.c.}} \exp(iS[\Phi]), \quad (2.112)$$

where the integral is understood as ranging over all field configurations on the extra-dimensional spacetime that satisfy the given boundary conditions. In the spirit of holography one can single out the field values at, say, the  $z = 0$ -boundary and treat them as source fields for the bulk degrees of freedom. This means that the measure of the path integral in some sense ‘factorizes’ into a boundary and a bulk part, such that

$$\mathcal{Z} = \int \mathcal{D}\phi \int \mathcal{D}\Phi|_{\Phi(z=0) \equiv \phi} \exp(iS[\Phi]), \quad (2.113)$$

where now  $\phi$  is a four-dimensional field living *on* the boundary  $z = 0$ . For consistency with the above boundary conditions of the extra-dimensional field  $\Phi$ , the integral measure  $\mathcal{D}\phi$  of the boundary field has to be understood in such a way that only the fields allowed by the boundary conditions are propagating while all others are set to zero.

When considering an extra-dimensional gauge theory as above, the gauge field can likewise be separated into boundary and bulk field. We can also think of the the gauge symmetry  $\mathcal{G}$  as decomposing into a bulk part  $\mathcal{G}_B$  and a symmetry  $\mathcal{H}_0$  at the boundary, namely

$$\mathcal{G} = \mathcal{H}_0 \times \mathcal{G}_B, \quad (2.114)$$

where (cf. (2.111))

$$\mathcal{G}_B = \{g(x, z) \in \mathcal{G} | g(x, z = \pi) \in \mathcal{H}_\pi, g(x, z = 0) = \mathbb{1}\}. \quad (2.115)$$

To make the physical spectrum of the theory manifest, it is convenient to adopt a gauge where in particular the scalar degrees of freedom,  $A_5^a(x, z)$ , take a rather simple form. Pretending for the time being that the symmetries are not reduced at the boundaries then the extra-dimensional gauge component,  $A_5^a(x, z)$ , can be made to vanish everywhere if the corresponding gauge transformation is chosen to be the Wilson line stretching from one boundary to the other. However, for general boundary conditions this is not possible, since then the Wilson lines do not reduce to the correct subgroups at the boundary and thus, such a transformation is not an element of the bulk gauge symmetry. This drawback can be circumvented by modifying the boundary conditions in such a way that superficially the whole  $\mathcal{G}$ -invariance is restored all over the extra dimension. To this end, non-linear  $\sigma$ -model fields are introduced at the  $z = \pi$  boundary, such that the new boundary conditions now read

$$\left[ F_{\mu 5}^{(\Sigma^{-1})}(x, z = \pi) \right]^a = 0 \quad \text{for the unbroken directions} \quad \text{and} \quad (2.116)$$

$$\left[ A_\mu^{(\Sigma^{-1})}(x, z = \pi) \right]^{\hat{a}} = 0 \quad \text{for the broken directions.} \quad (2.117)$$

Here,  $A_\mu^{(\Sigma^{-1})} = \Sigma^{-1}(A_\mu + i\partial_\mu)\Sigma$  denotes the boundary gauge field transformed by  $\Sigma^{-1} \in \mathcal{G}$ , which transforms like a Goldstone boson (II.12)

$$\Sigma \rightarrow g\Sigma h^{-1}(g, \Sigma), \quad (2.118)$$

such that the boundary conditions are invariant under general transformations  $g \in \mathcal{G}$ . Having done this, it is now possible to adopt the gauge where  $A_5 \equiv 0$  everywhere, such that it vanishes completely

from the spectrum. The price one has to pay for this was the introduction of Goldstone-like fields on the  $z = \pi$  boundary.

In the following it will be convenient to perform one further gauge transformation that moves the  $\Sigma$ -fields from  $z = \pi$  to the other boundary, i.e. to the location where the holographic fields live [90]. Effectively, this gauge amounts to setting

$$A_5(x, z) = \begin{cases} \text{“}\Sigma(x)\text{”} & \text{at } z = 0 \\ 0 & \text{everywhere else.} \end{cases} \quad (2.119)$$

### 2.3.2. Realistic GHU models

Putting the above arguments together one can now write down a realistic GHU model. For this we will very closely follow [48].

Some important points were already discussed in the preceding sections. One of the most important was that the necessity to have a chiral low-energy theory forces us to consider orbifolded extra dimensions, the simplest one being  $S^1/\mathbb{Z}_2$ . Hence, let us in the following consider the case of a five-dimensional space  $\mathcal{M} = \mathcal{M}_4 \times S^1/\mathbb{Z}_2$ . Regarding the metric, we do not want to be too specific, as for our general purposes this will not be of much importance. In principle, one can consider flat or warped geometries; we will have some curved spacetime in our mind due to the ability to explain the flavour hierarchies by localization in the extra dimension (see e.g. [42]).

The symmetry breaking structure determines the particle spectrum. So, let us recapitulate what requirements one has. In our setup some extra-dimensional gauge group  $\mathcal{G}$  is broken to the subgroups  $\mathcal{H}_0$  and  $\mathcal{H}_\pi$  by boundary conditions at the orbifold fixed points. SM fields corresponding to gauge boson zero modes appear for gauge components with  $(+, +)$  boundary conditions, i.e. for elements of the subgroup  $\mathcal{H}_0 \cap \mathcal{H}_\pi$ . Then the simplest possibility is choosing  $\mathcal{H}_\pi \supset \mathcal{H}_0 = G_{\text{SM}}$ . Restrictions from electroweak precision observables suggest to include a custodial protection of oblique corrections (see section 2.2.1). Therefore, we consider an enlarged symmetry and impose  $\text{SU}(2)_R \times \text{SU}(2)_L \subset \mathcal{H}_\pi$ . The simplest choice is then given by  $\mathcal{H}_\pi = \text{SO}(4) \cong \text{SU}(2)_R \times \text{SU}(2)_L$ . The coset  $\mathcal{G}/(\mathcal{H}_0 \cap \mathcal{H}_\pi) = \mathcal{G}/\mathcal{H}_\pi$  determines the Goldstone boson fields. For these the minimal requirement is that they include an  $\text{SU}(2)_L$  doublet, which can be identified with the Higgs. A minimal group satisfying this is  $\text{SO}(5)$ , as for this the coset contains *four* real degrees of freedom transforming as a bidoublet  $(\mathbf{2}, \mathbf{2})$  under the custodial symmetry group.<sup>20</sup> To summarize, this fixes the coset to be  $\text{SO}(5)/\text{SO}(4)$ .

The gauge bosons are determined by the  $\text{SO}(5)$  gauge theory in the bulk, that gets reduced to  $G_{\text{SM}}$  and  $\text{SO}(4)$  at the two boundaries, such that there is a bulk gauge field in the adjoint representation. It is convenient to group the generators into the  $\text{SO}(4) \cong \text{SU}(2)_L \times \text{SU}(2)_R$  subgroups. Schematically, the gauge field then ‘decomposes’ into

$$\text{SO}(5) \sim [\text{SU}(2)_L \times \text{SU}(2)_R \times \text{SO}(5)/\text{SO}(4)], \quad (2.120)$$

i.e. into left and right  $\text{SU}(2)$  fields and coset fields,

$$\rho_\mu^A = (\rho_{L\mu}^a, \rho_{R\mu}^a, \mathbf{a}_\mu^{\hat{a}}), \quad (2.121)$$

and similarly for the 5-component. Here, the indices range over  $a = 1, 2, 3$  and  $\hat{a} = 1, 2, 3, 4$ , giving 10 gauge components in total.

These symmetries are not enough to obtain a realistic theory. First of all one also has to include  $\text{SU}(3)_c$  as a bulk gauge symmetry to obtain colored fields. This symmetry should not be broken at the boundaries such that SM particles feel the strong interaction. Furthermore, as we will see shortly, an additional  $\text{U}(1)_X$  symmetry has to be included to get the correct hypercharges for the fermions. Hypercharge quantum numbers will correspond to a linear combination of the  $\text{U}(1)_X$  charge and the  $\text{T}_R^3$  component of  $\text{SO}(5)$ . Therefore, it is more convenient to express the corresponding gauge bosons by the same combination,

$$(\rho_{R\mu}^3, X_\mu) \leftrightarrow (B_\mu, \rho_{R\mu}^3), \quad (2.122)$$

such that we can assign boundary conditions in such a way that hypercharge has a zero mode. Effectively, this means that the bulk gauge symmetry  $\mathcal{G} = \text{SU}(3)_c \times \text{SO}(5) \times \text{U}(1)_X$  is broken to  $\mathcal{H}_0 = \text{SU}(3)_c \times \text{SU}(2)_L \times \text{U}(1)_Y$  and  $\mathcal{H}_\pi = \text{SU}(3)_c \times \text{SO}(4) \times \text{U}(1)_X$  at the boundaries. The boundary conditions are given in table. 2.1. The low-energy spectrum consists of zero modes for the

<sup>20</sup>In particular, this implies that some components transform as a doublet under  $\text{SU}(2)_L$ .

colour	$SU(3)_c$	$G_\mu^a(+, +)$	$G_5^a(-, -)$
electroweak	$SO(4) \times U(1)_X$	$\rho_{L\mu}(+, +)$	$\rho_{L5}(-, -)$
		$\rho_{R\mu}^\pm(-, +)$	$\rho_{R5}^\pm(+, -)$
		$B_\mu(+, +)$	$B_5(-, -)$
		$\rho_{R\mu}^3(-, +)$	$\rho_{R5}^3(+, -)$
coset	$SO(5)/SO(4)$	$\mathfrak{a}_\mu^{\hat{a}}(-, -)$	$\mathfrak{a}_5^{\hat{a}}(+, +)$

**Table 2.1.:** Boundary conditions for gauge boson fields.

vector components corresponding to  $G_{SM} = SU(3)_c \times SU(2)_L \times U(1)_Y$  as well as zero modes for the extra-dimensional scalars for the coset fields. The latter are identified with the complex Higgs doublet.

After choosing the symmetries let us now consider the matter content the theory should have. As already discussed earlier, every SM chirality should be embedded into its own five-dimensional field. So, for each generation we introduce *four* bulk fermions. Fermions should come in irreducible representations of the bulk gauge group  $\mathcal{G} = SO(5)$ . In principle, one is free to choose whatever representation one likes, but there is the restriction to reproduce the SM fermion content, in the sense that doublets and singlets of  $SU(2)$  should emerge. In addition to this, it turns out that there is a subset of representations that is favorable as they provide a built-in mechanism protecting from dangerous corrections of  $Zbb$ -vertices (see section 2.2.1). An overview of the smallest representations of  $SO(5)$  is given in eq. (2.42). The simplest one providing the needed features is given by the fundamental  $\mathbf{5}$ , as under the  $SO(4)$  subgroup it decomposes as  $\mathbf{5} = (\mathbf{2}, \mathbf{2}) \oplus (\mathbf{1}, \mathbf{1})$  into a bidoublet and a singlet.

As mentioned above in order to obtain realistic hypercharges an additional  $U(1)_X$  symmetry is included such that

$$\hat{Y} = \hat{T}_R^3 + \hat{X}, \quad (2.123)$$

similar to the definition of the electric charge. Introducing such a  $U(1)$  charge now has profound implications on the embedding of the SM fields into higher-dimensional bulk fields. In order to match the weak interactions at low energies, right-handed chiralities have to be parts of the singlet component of  $SO(5)$  fundamentals. By the same reasoning, the left-handed SM fermions have to be embedded into the bi-doublet components. Assigning the  $U(1)_X$  charges in such a way that hypercharge is reproduced then leads to the fact that one will not be able to write down Higgs interactions for up-type as well as down-type quarks, if the left-handed SM doublet  $q_L$  is identified with only *one* extra-dimensional fermion multiplet [91]. This means that for one generation of SM quarks the fields will be embedded as follows,

$$q_L^0 \sim \begin{cases} \Psi_u \in \mathbf{5}_{\frac{2}{3}} \\ \Psi_d \in \mathbf{5}_{-\frac{1}{3}} \end{cases}, \quad u_R^0 \sim \tilde{\Psi}_u \in \mathbf{5}_{\frac{2}{3}}, \quad d_R^0 \sim \tilde{\Psi}_d \in \mathbf{5}_{-\frac{1}{3}}, \quad (2.124)$$

meaning that the SM quark doublet is identified with the zero mode of the linear combination  $\Psi_u + \Psi_d$ .<sup>21</sup> Later, when matching to a CHM, this will reflect in the fact that the left-handed elementary quarks will both be embedded into two different separate incomplete  $SO(5)$  representations  $\xi_{uL}$  and  $\xi_{dL}$ .

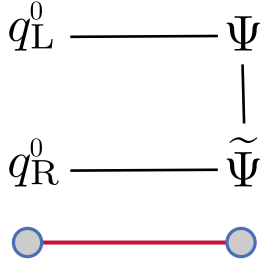
### Discrete Composite Higgs model

Let us use this opportunity and consider a different possibility for constructing GHU models. In the above construction each SM chirality was embedded into *its own* extra-dimensional  $SO(5)$ -multiplet. But as an alternative one could think of embedding for each SM fermion both chiralities into the same multiplet. This can e.g. easily be done for a fundamental  $\mathbf{5} = (\mathbf{2}, \mathbf{2}) \oplus (\mathbf{1}, \mathbf{1})$  when the right-handed

<sup>21</sup>The zero mode of the orthogonal combination we do not want to have in the low-energy spectrum. One can get rid of this via giving it a large mass by introducing right-handed localized fermion fields that have mass mixings with it [91]. The exact mechanism is not important at this point. We just assume these fields to be absent.



M4dCHM @ 2 sites



DCHM @ 3 sites

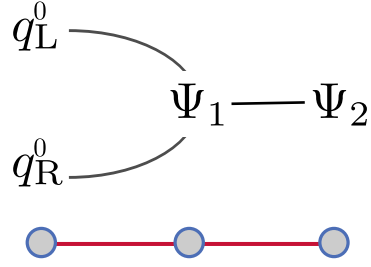


**Figure 2.4.:** Comparison of the basic structures of the fermion mixings of M4dCHM and DCHM. The black lines denote mass mixings of the fermion which are realized either as composite-elementary mixings or as couplings inside the composite sector. In the M4dCHM chiral elementary quarks mix with separate resonances of the composite sector while in the DCHM both elementary chiralities couple to the same composite fermion resonance.

singlet is identified with the zero mode of the singlet component and the LH fermions are part of the bidoublet. In this case only one  $u$ - and one  $d$ -type partner are needed in the extra dimension for each quark generation. This is the structure used in the so-called Discrete Composite Higgs Model (DCHM) [60]. The basic structure of the mixing terms in the M4dCHM, which we will use in the present work, and the DCHM are compared in figure 2.4. The DCHM only gives a finite (i.e. calculable) Higgs potential if there are at least three sites. At each site a separate level of composite resonances is introduced for fermion as well as boson fields. The fermions only interact with the vector resonances of the corresponding site<sup>22</sup>.

### 2.3.3. Dimensional deconstruction

There are different ways to perform calculations in field theories on extra dimensions. For example, one can directly work in the higher-dimensional setup and define propagators through the extra dimension. For this one typically works in a mixed momentum/position framework where position space is used for the extra dimensions. Calculations of this kind have been performed (see e.g. [85, 92, 93, 94, 95, 96] for calculations in the RS geometry with one extra-dimension), however they are rather involved. Therefore it is often more convenient to transform the higher-dimensional theory into a four-dimensional one and perform the calculation using ordinary Feynman diagram techniques. The standard approach for doing so is the above mentioned KK reduction, where the higher-dimensional fields are expanded in a generalized Fourier series with respect to the discrete extra-dimensional momentum and the four-dimensional Fourier coefficients are interpreted as ordinary four-dimensional quantum fields. Proceeding this way, a higher-dimensional field takes the form of an infinite tower of four-dimensional fields, which one can tackle using standard techniques.

In the following we will review an alternative approach that is more suited to holography and allows to construct models with partial compositeness and a pNGB Higgs that are inspired by extra-dimensional theories and inherit a lot of advantages from them. In particular, these models feature a calculable Higgs potential which is necessary to make predictive calculations. This idea of *dimensional deconstruction* was developed by Arkani-Hamed, Cohen and Georgi [97, 54] in the beginning of this century. The basic idea is to discretize the extra dimensions into individual points and then use lattice gauge theory to describe the physics. Schematically this is visualized in figure 2.5. At each discrete point in the extra dimension one encounters a separate 4d theory that corresponds to one level of composite resonances. The complete higher-dimensional theory is restored in the continuum limit when the spacing between the discrete points vanishes, but the approximation of the whole extra dimension by only a few lattice points is already enough to construct a theory that resembles all the important properties of the extra dimensions.

<sup>22</sup>In the original paper [60] a slightly different construction is used which not really corresponds to a dimensionally deconstructed model: They treat the  $U(1)_X$  symmetry as external to the cosets. So, the  $B$  fields interact with every site. See footnote 9 therein.

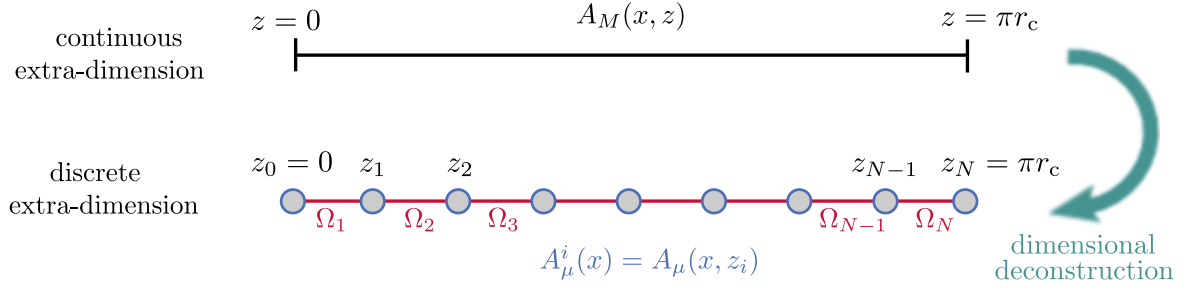


**Figure 2.5.:** Method of dimensional deconstruction. A continuous extra dimension is discretized into individual points. Gauge invariance is restored by connecting the spacetime points through link fields  $\Omega_i$ . At each point  $z_i$  there is a 4d theory with gauge fields  $A_\mu^i(x) \equiv A_\mu(x, z_i)$ .

In gauge theories on a discrete spacetimes one usually encounters the problem that fields at different lattice points transform differently under the gauge symmetry such that interactions cannot be introduced in a consistent way. To circumvent this, one has to introduce so-called *link fields*  $\Omega_i = \Omega(z_{i-1}, z_i)$  which are Wilson lines (2.109) connecting lattice points  $z_{i-1}$  and  $z_i$  [98]. Under the gauge symmetries the link fields transform as  $\Omega_i \rightarrow g(z_{i-1}) \Omega_i g(z_i)^{-1}$ , such that they can be used to connect fields at neighboring points. The picture that dimensional deconstruction gives for an extra-dimensional gauge theory then is the following: Due to discretization one obtains a tower of  $N$  different 4d gauge theories that are connected by link fields (see figure 2.5). In the 4d theory with gauge symmetry  $\mathcal{G}^N$  these link fields then encode the information about the extra-dimensional gauge invariance.

In the context of CHMs, the procedure to implement such a structure was described in [99, 100], which we want to follow in this section. For every discrete extra-dimensional coordinate point a coset  $(\mathcal{G}_L \times \mathcal{G}_R) / \mathcal{G}_{L+R}$  of *global* symmetries is introduced with a NGB-like field  $\Omega$  transforming as

$$\Omega \rightarrow g_L \Omega g_R^{-1}. \quad (2.125)$$

Let us now consider the situation depicted in the first diagram of figure 2.6 in which we have a total number  $N$  of such cosets; then the Lagrangian is manifestly invariant under  $2N$  global symmetries  $\mathcal{G}_{L,R}^i$  with  $i = 1 \dots N$ . Resonances can be introduced by gauging the diagonal groups of  $\mathcal{G}_R^i$  and  $\mathcal{G}_L^{i+1}$  to form a *site*, i.e. a gauge theory that describes one level of composite resonances. These sites are connected by the fields  $\Omega_i$  that function as the link fields from lattice gauge theory. By the gauging, the global symmetries  $\mathcal{G}_R^i$  and  $\mathcal{G}_L^{i+1}$  are broken down to their diagonal group. The occurring Goldstone bosons from this breaking will be eaten by the gauge fields at each site in order to obtain a mass.

Subtleties arise at the boundaries as the second diagram of 2.6 shows. Using the holographic point of view, we identify the left boundary with the elementary sector of the theory. For the time being, we do not specify this, leave it open and just treat the fields in the leftmost  $\sigma$ -model as source fields for the rest of the theory. At the right boundary, as we know, the symmetry is reduced to  $\mathcal{H} = \mathcal{H}_\pi$  by the boundary conditions of the higher-dimensional gauge fields. Therefore we introduce a  $\sigma$ -model parameterizing the breaking  $\mathcal{G}/\mathcal{H}$  by the Goldstone matrix  $\Omega^*$  transforming as usual as

$$\Omega^* \rightarrow g \Omega^* h^{-1}. \quad (2.126)$$

From (2.125) one can infer the transformation properties of the  $\Omega$ -fields under the symmetries,

$$\begin{cases} \Omega_1 \rightarrow g_L^1 \Omega_1 g_1^{-1}(x), \\ \Omega_i \rightarrow g_{i-1}(x) \Omega_i g_i^{-1}(x) \quad \text{for } 2 \leq i \leq N, \\ \Omega^* \rightarrow g_N(x) \Omega^* h^{-1}, \end{cases} \quad (2.127)$$

where  $g_L^1 \in \mathcal{G}_L^1$  is the remaining global symmetry at the left boundary and  $g_i(x) \in \mathcal{G}_i$  are the gauge symmetries at the sites. From these it follows that in addition to the gauge symmetries at each site the theory gives rise to a *global* symmetry breaking  $\mathcal{G}_L^1/\mathcal{H}$  parametrized by

$$\mathcal{U} := \Omega_1 \Omega_2 \dots \Omega_N \Omega^*, \quad (2.128)$$

which transforms as

$$\mathcal{U} \rightarrow g_L^1 \mathcal{U} h^{-1}. \quad (2.129)$$

This corresponds to the Wilson line along the extra dimension.

These symmetries are exact for vanishing source fields at the left boundary and thus the Goldstone bosons are exactly massless. But eventually we want to introduce SM-like elementary fields on this boundary. This means we gauge the  $SU(2) \times U(1)$  subgroup of the global  $\mathcal{G}_L^1$  and introduce matter fields in incomplete representations. As a consequence, the global pattern  $\mathcal{G}/\mathcal{H}$  gets *explicitly* broken by the interactions with the elementary sector at the left boundary, turning  $\mathcal{U}$  into a *pseudo*-Goldstone matrix.

Using this construction, the pure bosonic Lagrangian then takes the form

$$\mathcal{L}_{\text{boson}} = \underbrace{\frac{1}{4} \text{tr} [F_0^{\mu\nu} F_{\mu\nu}^0]}_{\text{elementary}} + \underbrace{\frac{1}{4} \sum_{i=1}^{N-1} \text{tr} [\rho_i^{\mu\nu} \rho_{i\mu\nu}]}_{\text{composite}} + \underbrace{\frac{f^2}{4} \text{tr} [d_\mu^{\hat{a}} d^{\hat{a}\mu}]}_{\text{symmetry breaking}} + \underbrace{\sum_{i=1}^N \frac{f_i^2}{4} \text{tr} [(\mathcal{D}_\mu \Omega_i)^{-1} (\mathcal{D}^\mu \Omega_i)]}_{\text{link fields}}. \quad (2.130)$$

It consists of kinetic terms for the elementary gauge bosons as well as for the composite vector resonances  $\rho_\mu^i$ . The symmetry breaking  $\mathcal{G}/\mathcal{H}$  is described by the  $d$ -symbols for  $\Omega^*$  of the CCWZ formalism (see appendix II) and furthermore, there are the link fields  $\Omega_i$  that encode the higher-dimensional gauge invariance. The gauge covariant derivatives are given as

$$\begin{cases} \mathcal{D}_\mu \Omega_1 = \partial_\mu \Omega_1 - ig_0 A_\mu^0 \Omega_1 + ig_\rho^1 \Omega_1 \rho_\mu^1 \\ \mathcal{D}_\mu \Omega_i = \partial_\mu \Omega_i - ig_\rho^{i-1} \rho_\mu^{i-1} \Omega_i + ig_\rho^i \Omega_i \rho_\mu^i \text{ for } 2 \leq i \leq N \end{cases} \quad (2.131)$$

in accordance with (2.127) and where  $A_\mu^0$  denotes the collection of elementary gauge fields.

In this construction one can easily draw a connection to the holographic gauge fixing discussed in section 2.3.1. Making use of the transformation rules (2.127) a gauge at every site can be chosen in such a way that  $\Omega^* = \Omega_N = \dots = \Omega_2 = \mathbb{1}$ . There are, however, not enough gauge symmetries to set every Goldstone matrix to  $\mathbb{1}$ . At the leftmost site the above gauge choices lead to  $\Omega_1 \rightarrow \Omega_1 \Omega_1 \dots \Omega_N \Omega^* = \mathcal{U}$ , where (2.128) was used. One further finds that under the remaining global symmetries this Goldstone matrix transforms exactly via (2.129), which shows that the whole Goldstone structure is moved to one boundary. This is in exact accordance with holography as discussed in (2.119) which makes the connection to extra-dimensional theories transparent. We will use this gauge choice in the following and refer to it as *holographic gauge*,

$$\Omega_1 = \mathcal{U}(x) = \exp \left( i \frac{\sqrt{2}}{f_1} \pi_{\hat{a}}(x) T^{\hat{a}} \right), \quad \Omega_2 = \dots = \Omega_N = \Omega^* = \mathbb{1}. \quad (2.132)$$

Including fermions in this set-up is straightforward. The value of the higher-dimensional fermion at each discrete point of the extra dimension  $\Phi_i(x) \equiv \Phi(x, z_i)$  is interpreted as a four-dimensional, vector-like resonance transforming under the symmetries of the corresponding site. From the holographic point of view it is then clear that one 5d fermion decomposes into a bunch of resonances (which we will call composite) and possibly a chiral elementary field. Hence, all the fermion resonances belonging to the same 5d field have to be in the same representation at each site.

The elementary sector is introduced as source fields on the leftmost site. On this site there formally is a global  $\mathcal{G}$  invariance. But also, a subgroup was gauged down to the  $\mathcal{H}_0 \supset G_{\text{SM}}^0$  gauge group. This means that the  $\mathcal{H}_0$  multiplets have to be embedded into incomplete  $\mathcal{G}$  representations, introducing an further source of explicit symmetry breaking.

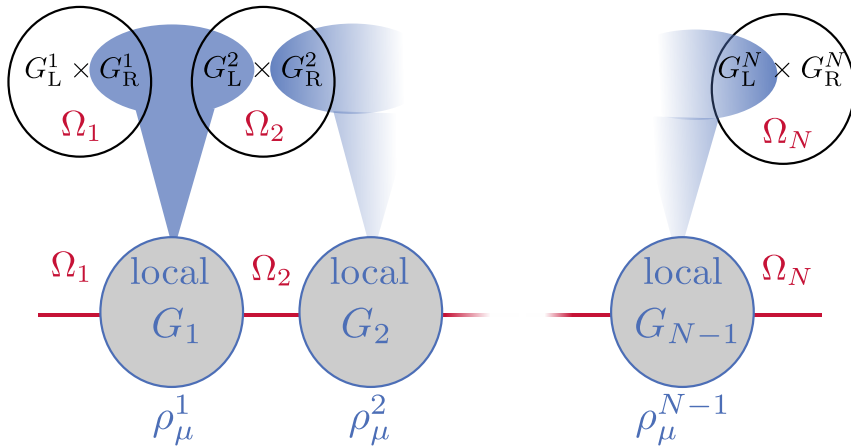
Having chosen a representation for the resonances it is then clear how to build the Lagrangian of the composite sector: One simply has to write down the most general terms invariant under the symmetries given the bosonic and fermionic fields. Then the fermion Lagrangian has the form,

$$\mathcal{L}_{\text{fermion}} = \mathcal{L}_{\text{kin}}^{(\text{elem})} \quad (2.133a)$$

$$+ \sum_{i=1}^N \bar{\Psi}_i^{(r)} \left( i \not{D}^{(r)} - m_i^{(r)} \right) \Psi_i^{(r)} \quad (2.133b)$$

$$+ \epsilon^{(r)} \bar{q}_0^{(r)} \Omega_1 \Psi_1^{(r)} + \sum_{i=1}^N \Delta_L^{(r)} \bar{\Psi}_{iL}^{(r)} \Omega_{i+1} \Psi_{i+1R}^{(r)} + \text{h.c.} \quad (2.133c)$$

a)



b)

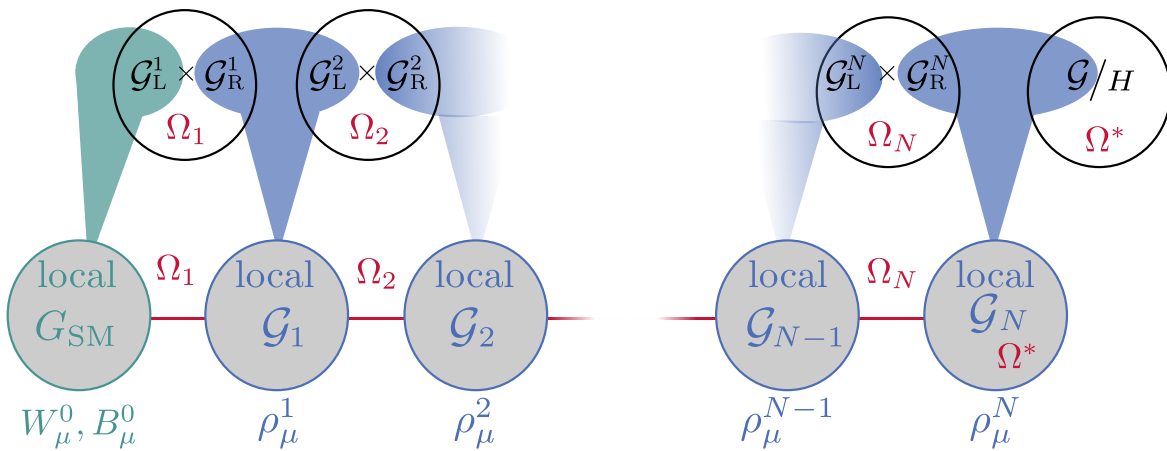


**Figure 2.6.:** Schematic of the symmetry structure. a) Inside the bulk there are a number of cosets  $(G_L \times G_R) / G_{L+R}$ . Diagonal subgroups are gauged in order to form a site with vector resonance  $\rho_\mu^i$ . The  $\Omega$ -matrices act as link fields between the sites. b) Including the boundaries the symmetry breaking  $G/H$  is introduced at the right boundary. Gauging the elementary  $G_{SM}$  subgroup of  $G_L^1$  introduces an explicit breaking of the global  $G$  symmetry causing massive pseudo Goldstone bosons.

This is a rather compressed notation, so let us explain this in a bit more detail. There are kinetic terms for the massless elementary fields, interacting as in the SM with the gauge bosons of the elementary, SM-like gauge group. The composite resonances were all combined into one symbol  $\Psi^{(r)}$  where  $r$  is an index ranging over different particle species as well as over different representations of  $\mathcal{H}$ .<sup>23</sup> They interact with the vector resonances via covariant derivatives

$$\mathcal{D}_\mu \Psi_i^{(r)} = \partial_\mu \Psi_i^{(r)} - ig_\rho^{(i)} \rho_\mu^i \Psi_i^{(r)}. \quad (2.134)$$

Furthermore, as the fermion resonances are vector-like, one can write down mass terms for them. The last line of the above Lagrangian describes the interactions between different sites. As this means, interactions between different discrete points in the extra dimension, link fields  $\Omega_i$ , have to be involved. The first term describes the mixing between the elementary fermions and the composite resonances of the second site. Additionally, there can be mixing terms between fermion resonances.

## 2.4. Summary and a word of caution

In this chapter we gave a review about Composite Higgs models, their advantages and their structure. The main motivation in considering such models lies in the fine-tuning problem since if the Higgs is a composite object whose ingredients are well-behaved at high energies then its mass does not get too large quantum corrections. More formally, in analogy to QCD, one expects the NP scale to be generated via dimensional transmutation such that it is stable against small changes in the initial parameters. The separation between the electroweak scale and the NP scale can be explained if the Higgs is a pNGB of an explicitly broken global symmetry. In models of partial compositeness there is a linear coupling between the composite and the elementary sector that transmits the needed explicit symmetry breaking. SM fields are mixtures of elementary and composite fields in this framework and their coupling strengths to the Higgs boson are determined by the amount of composite admixtures they carry.

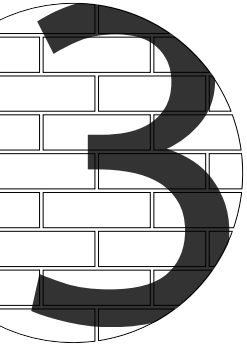
To have a phenomenologically successful model one has to introduce some further structures. Dangerous contributions to EWPOs and  $Z$  boson couplings can be avoided if the model contains custodial symmetry  $SU(2)_L \times SU(2)_R$ , which gives constraints on the possible symmetry breaking structures such that the minimal coset is given by  $SO(5)/SO(4)$ . Flavour transitions can be brought under control by assuming that the composite sector respects a flavour symmetry that is broken only by interactions with elementary fields such that the complete flavour structure is determined by the composite-elementary mixings. In this work we consider  $U(3)^3$  and  $U(2)^2$  flavour structures that get broken by either left-handed or right-handed mixings.

Great emphasis is given in this work on EWSB. This is generated in CHMs radiatively through the Coleman-Weinberg mechanism. In general, it depends on the details of the model whether the effective potential can be calculated consistently. Considering the potential at the one-loop order, we ensure calculability by considering models whose structure is inspired by theories in which the Higgs is implemented as a component of an extra-dimensional gauge field. By this the predictivity of the potential is guaranteed by gauge invariance.

There is, however, a word of caution that is in order. CHMs are in general non-renormalizable such that the results can be strongly affected by UV contributions. These theories are usually expected to have a low cutoff  $\Lambda \sim 4\pi f = \mathcal{O}(10 \text{ TeV})$ , such that considerable theoretical uncertainties are to be expected. In this work we only include constraints that can be calculated without a strong UV sensitivity and thus we are able to apply the experimental bounds in a meaningful way. Further, one should keep in mind that in the construction of the above model some truncations were made. This means a truncation in the number of levels of resonances as well as a truncation in the derivative expansion of the non-linear  $\sigma$ -model. Also the fact that CHMs are strongly interacting theories might lead to considerable uncertainties in perturbatively calculated observables. This could in particular affect the Higgs potential such that two-loop contributions can be important. In the course of this work we assume rather conservative estimates for theory uncertainties to cope with possibly relevant higher-order contributions. It will be the general philosophy of these analyses that we carefully try not to exclude model points that might predict the correct experimental observables when taking into account higher orders in the theory calculation.

<sup>23</sup>For example, an  $SO(5)$  fundamental field decomposes into a fundamental  $\mathbf{4}$  and a singlet  $\mathbf{1}$  under  $SO(4)$ . The index  $r$  is supposed to range over both representations.





## Numerical strategy

In this chapter we present the details of the numerical analyses performed in this work. The central objects are *parameter points*

$$\vec{\Theta} = (g_0, \dots, f, \dots, g_{\text{comp}}, \dots, m_{\text{comp}}, \dots, \epsilon, \dots), \quad (3.1)$$

which are collections of all real numbers necessary to characterize the model parameters, such as symmetry breaking scales, elementary and composite couplings, composite mass matrices or composite-elementary mixing matrices. A given parameter point defines a concrete instantiation of the model that allows to calculate all observables.

The main goal of this analysis is generating large sets of parameter points that are compatible with all available experimental data. Such parameter points we will denote as ‘viable’ in the following. With these as input it will then be possible to identify the allowed parameter space of the model. Furthermore we will be able to give predictions for yet unobserved processes and classify observables that are very sensitive probes of these models, such that future measurements might help to efficiently reduce the allowed parameter space or (in the best case) find a signal. This section is devoted to laying out the approach used by us to efficiently find viable parameter points.

This chapter is organized as follows: In section 3.1 we discuss our general numerical approach for finding viable parameter points. In the following section 3.2 we describe how given a certain parameter point, we calculate physical observables. But we will wait until section 3.3 to be specific and list all the physical observables implemented in the analysis.

### 3.1. Generating viable parameter points

In general, putting constraints on the parameter space of CHMs is a non-trivial task. Due to partial compositeness the parameter space is heavily ‘entangled’, meaning that it does not factorize into a SM and a NP part that can be constrained separately. This is generally the case in models with partial compositeness. A further source of entanglement stems from including the effective Higgs potential (see section 2.2.2). Via this, strong correlations between the fermion and gauge sectors will have to be fulfilled, although a priori they are (to a certain degree) independent in our approach. Remember that the position  $s_h^*$  of the minimum of the effective potential profoundly depends on cancellations between spin-1 and spin- $\frac{1}{2}$  contributions. In turn, the particle masses and couplings in the mass basis depend on the exact value of  $s_h^*$  and, therefore, in the end all observables will depend on it. This leads to the fact that effectively every observable is a complicated function of basically all the model parameters. As a consequence, partial compositeness necessitates performing a global analysis that simultaneously takes into account all constraints at once. Including a realistic EWSB even strengthens this demand.

The traditional approach for such an analysis is to scan the parameter space on the grid or to draw random numbers. Both procedures become inapplicable if the parameter space has a high dimensionality and is entangled in the above ways. In the models investigated in this work there are around 30-50 free parameters, and so demanding a sufficient coverage of parameter space would require an extraordinary large number of points which is not doable using present computing power. Also, finding solutions that are fine-tuned to a certain degree appears to be a hard task as by large volume effects in the high-dimensional parameter space it gets increasingly improbable to pick such a point. For these reasons we are forced to use a numerically much more sophisticated approach. Our method is based on an idea put forward in [101]. In that reference the parameter space of a

CHM was sampled using Markov Chain Monte Carlo (MCMC) techniques as implemented in the Metropolis-Hastings algorithm [102, 103]. A MCMC is a standard tool for optimization, numerical integration and Bayesian statistical inference. It is a simple algorithm that performs a random walk in the parameter space that is strongly pulled towards the region of viable points. Therefore, the Markov chain finds viable parameter points automatically and subsequently samples that region to efficiently generate a large number of viable points. We present some details of MCMCs in appendix V.

A key element for using MCMCs is defining a scalar measure that quantifies how well a given parameter point  $\vec{\Theta}$  agrees with the experimental data. This is given by the *likelihood*  $\mathcal{L}(\vec{\Theta}) = \exp(-\chi^2(\vec{\Theta})/2)$ , where the so-called  $\chi^2$ -function is defined in analogy with the method of least-squares,

$$\chi^2(\vec{\Theta}) \sim \sum_{\mathcal{O} \in \text{observables}} \frac{(\mathcal{O}_{\text{theo}}(\vec{\Theta}) - \mathcal{O}_{\text{exp}})^2}{\sigma_{\mathcal{O}}^2}. \quad (3.2)$$

Here,  $\sigma_{\mathcal{O}}^2$  denotes the uncertainty of the observable  $\mathcal{O}$ . We are interested in finding parameter points  $\vec{\Theta}$  that *maximize* the likelihood which is equivalent to *minimizing* the  $\chi^2$ . These are the points for which the theory predictions  $\mathcal{O}_{\text{theo}}(\vec{\Theta})$  are generally close to the experimental measurements  $\mathcal{O}_{\text{exp}}$ . This means our problem of finding viable parameter points generalizes to finding the minima of  $\chi^2(\vec{\Theta})$  on the parameter space. This optimization problem can be solved using MCMCs.

What (3.2) does not take into account yet are possible correlations between different observables. These can come either from experiment or from theory. In practice, we will account for correlations only in a few cases, but for these the correlations are very important. Effectively this means that one has to replace the uncertainties  $\sigma_{\mathcal{O}}^2$  by the full covariance matrix  $C^2$ , so that the  $\chi^2$  takes the form

$$\chi^2(\vec{\Theta}) \sim \sum_{\mathcal{O}^i, \mathcal{O}^j \in \text{observables}} (\mathcal{O}_{\text{theo}}^i(\vec{\Theta}) - \mathcal{O}_{\text{exp}}^i) [C^2]_{ij}^{-1} (\mathcal{O}_{\text{theo}}^j(\vec{\Theta}) - \mathcal{O}_{\text{exp}}^j). \quad (3.3)$$

An observable is subject to two types of uncertainties. First, there is the error of the experimental measurement. Furthermore, also the theoretical calculation is subject to uncertainties. These can be uncertainties of input parameters (such as e.g. CKM elements or hadronic parameters calculated by lattice QCD) or also neglected higher-order terms (which can be particularly relevant in strongly-interacting theories). Therefore, what we want to investigate is the convolution of the experimental and theoretical likelihood that takes into account both types of uncertainties simultaneously. For this, we take the covariance matrix  $C^2$  in (3.3) to be the sum of experimental and theoretical covariance,

$$C^2 = C_{\text{exp}}^2 + C_{\text{theo}}^2. \quad (3.4)$$

We will describe the observables which enter the  $\chi^2$  function in section 3.3.

After having defined the  $\chi^2$  in (3.3), what is left to do is to find its minima and sample the parameter space around them. A priori it is not clear how many different minima there are, as this depends on the detailed model and the detailed constraints. There could be only one continuous region of good  $\chi^2$ , but also it could be the case that there are several regions scattered all over the parameter space. To account for this it is necessary to start a number of chains which is large enough to find all regions. Even if there is only one region starting a large number of chains gives good access to different subregions within this region. We found it practical to separate the optimization and the sampling into different steps. In our experience the Markov chains did not perform very well for points very far away from a minimum. That is why we used the global optimization tool `NLOpt`[104] to burn in into a region of ‘reasonably good’  $\chi^2$  and used that as a starting point for the Markov Chain. In general, global optimizers need some starting point provided by the user. For this we randomly generated parameter points until we found one that fulfilled some very basic requirements. Most random points do not feature EWSB for example, as for this the parameters of the boson and fermion sectors have to be correlated to a certain degree. It usually takes  $\mathcal{O}(5 - 10 \text{ min})$  to find a random point with non-vanishing  $s_h^*$  and some other rudimentary consistency conditions such as e.g.  $g_0 < g_{\text{comp}}$ . Such a point can in principle have an arbitrarily high  $\chi^2$ -value; in our scans it usually was  $\chi^2 = \mathcal{O}(10^6)$ . With this as input the global optimizer is able to find regions of parameter space where the  $\chi^2$ -value is as low as  $\mathcal{O}(5000)$ .<sup>1</sup> This usually takes  $\mathcal{O}(30 \text{ min})$ . The package `NLOpt` offers a

<sup>1</sup>In our final numerics we will include around 60 individual  $\chi^2$ -contributions from different observables and we will have 30-50 parameters.



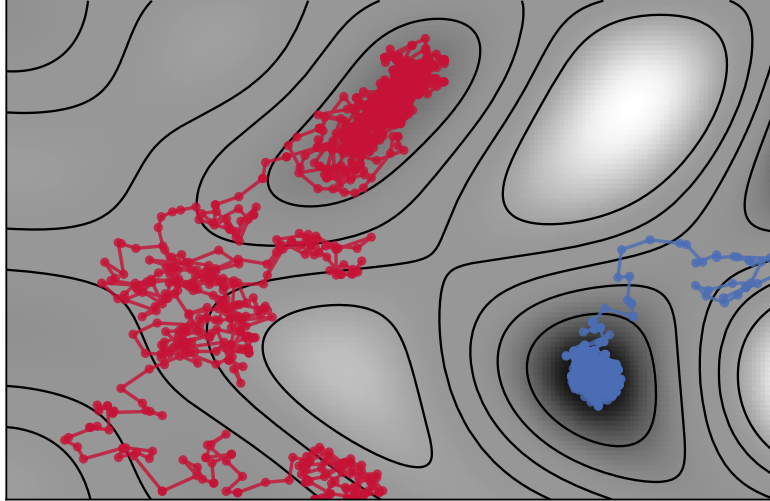


**Figure 3.1.:** Example of the behaviour of Markov chains in 2d. We show some  $\chi^2$  function with maxima (*white*) and minima (*black*). Two Markov chains are started. The deep minimum is found by the *blue* chain right away and the region of good  $\chi^2$  is sampled. The other local minimum, which is not so deep, takes longer to be found, but in the end it is also sampled efficiently by the *red* chain.

variety of different optimization algorithms, each best suited for a certain problem. In our experience the ‘subplex’ algorithm NLOPT\_LN\_SBPLX [105] worked best for our task. In such a region of parameter space it is now possible to start the Markov chain. We used adaptive Markov chains implemented in the package `pymc` [106]. In long runs of  $\mathcal{O}(50\text{ h})$  the Markov chain samples the parameter space and finds viable points with  $\chi^2$  as low as  $\mathcal{O}(30)$ , which given the number of observables and free parameters marks a very good agreement with the experimental data.

The main purpose of the Markov chain is not finding the minimum, but sampling the  $\chi^2$  around it. An example for this is shown in figure 3.1. We show an example of a  $\chi^2$  function in 2d that is sampled by Markov chains. One sees that after a certain burn-in phase the Markov chains find regions of good  $\chi^2$ . For our purposes it is not enough to simply find the minima, we also want to extract many points in the neighbourhood of the minimum as all of them could in principle be of interest for us. Furthermore, it is not clear what a minimum looks like in 30 dimensions. It could be strongly constraining in one direction of the parameter space but flat in another direction. Therefore, qualitatively different solutions could be reached while sampling one minimum.

Figure 3.1 also shows a different characteristic of adaptive Markov chains. If the chain is burned-in into a certain local minimum, then it samples that particular minimum, but it is not very probable that the chain leaves the minimum again to find another one. In the limit of infinitely many steps the chain should show this behaviour but for a finite run time the transition probability gets smaller the further apart the two minima are from each other. In practice, we do not have any a priori information about the shape and the number of disjoint minima. This is an inherent problem of Markov chains, but it can easily be solved by simply starting a large number of different chains all starting at random initial points and in the end combining the results of all chains. Another reason for starting a large number of different chains is that the approach described above does not always succeed. Only in about one third of attempts does the global minimizer achieve a reduction of  $\chi^2$  in a sufficient way such that Markov chains can be started. Also the chain itself can get stuck in a local minimum that does not allow for points good enough to be considered in our analysis. This need for extensive computational power is the reason we performed the numerics at the *Computational Center for Particle and Astrophysics* (C2PAP) [107] which is part of the Excellence Cluster Universe located in Munich. At this high-performance computing cluster we were able to start  $\mathcal{O}(1000)$  scans per model giving us a reasonable coverage of the parameter space.

For a Markov chain subsequent points always lie somewhat ‘close’ to each other. As a consequence, performing an MCMC scan will inevitably introduce a large autocorrelation between the found points. This is cured in part by starting many different scans, but to deal with autocorrelation in one chain,

we thin out the data and consider only every 10th point in our analysis.

In principle, there are many different ways to define a criterion for determining when a point is ‘good enough’ to be considered in our analysis. One could, for example, define a cut on the total  $\chi^2$  and only consider points with  $\chi^2$  below that value. This, however, theoretically allows for large deviations in one single observable at the price of agreeing with all the other ones very well. We decided to pose conditions on *individual*  $\chi^2$  contributions. As stated above, the covariance matrix in (3.3) is mostly diagonal such that we can write the total  $\chi^2$  as a sum over individual contributions

$$\chi^2(\vec{\Theta}) = \sum_{\mathcal{O} \in \text{observables}} \chi_{\mathcal{O}}^2(\vec{\Theta}). \quad (3.5)$$

For these we impose the conditions

$$\chi_{\mathcal{O}}^2(\vec{\Theta}) < 9 \quad \forall \mathcal{O} \quad (3.6)$$

on all viable parameter points which roughly corresponds to considering only points that satisfy the constraints on every observables at the  $3\sigma$ -level.<sup>2</sup> It is a property of MCMCs that the found points will be statistically distributed according to the sampled likelihood. Therefore, the viable points will only have a small number of individual constraints violated by more than  $2\sigma$ . We will quantify this later when discussing the concrete analyses.

To summarize our approach for generating large sets of viable parameter point includes the following steps:

1. Generate a random point that only fulfills basic requirements such as e.g. a non-vanishing Higgs vev.
2. Run a global optimization algorithm to reduce the  $\chi^2$ .
3. Burn in into regions of good  $\chi^2$  and sample the parameter space using Markov chains.
4. Thin out the found point and keep every parameter points which respects all individual constraints on the  $3\sigma$  level.

Let us note at this place that although MCMCs are a technique often used in statistics, we do not intend to make any statistical statements about probabilities of model parameters. We only use the Markov chains as efficient tools for generating large numbers of viable points. We cannot make statistical statements as for this the coverage of the global parameter space is far too low.

## 3.2. Calculating observables

In the above chapter 2 the Lagrangian of the CHMs was defined in the interaction basis which is the natural description dictated by the given symmetry structures. But partial compositeness as well as EWSB leads to mixings between particles in the form of non-diagonal mass matrices. Having said that, physical observables are always defined in the physical basis where all mass matrices are diagonal. Therefore, in order to calculate physical observables one has to rotate the Lagrangian to the physical mass basis which, in the end, will lead to massive SM fields and flavour mixings in interactions. As spin and electromagnetic charge are good quantum numbers even after EWSB, the mass matrices can be grouped into separate matrices for charged and neutral vector bosons and also up- and down-type quarks.

The schematic procedure for calculating the physical masses and couplings is shown in figure 3.2. A parameter point is given by a collection of parameter values  $\vec{\Theta}$ , which include dimensionless parameters (such as gauge couplings etc.) as well as massive parameters (resonance masses, composite-elementary mixings, symmetry breaking scales, etc.). Given all these values the Lagrangian of the model determines the mass and coupling matrices in the gauge basis (gb). To illustrate this, let us consider collections of fields

$$\Psi^{(\text{gb})} = (\psi_1^0, \psi_2^0, \dots, \Psi_1^{\text{comp}}, \Psi_2^{\text{comp}}, \dots)^t, \quad (3.7)$$

$$\mathbf{V}_{\mu}^{(\text{gb})} = (A_{1\mu}^0, A_{2\mu}^0, \dots, \rho_{1\mu}^{\text{comp}}, \rho_{2\mu}^{\text{comp}}, \dots)^t, \quad (3.8)$$

---

<sup>2</sup>Quantifying the cut by  $3\sigma$  is technically not accurate if the individual  $\chi^2$  contains two correlated observables (this is e.g. the case for electroweak precision observables as will be discussed in section 3.3.2). In that case a  $3\sigma$  (= 99.73% CL) bound would mean  $\chi^2 < 11.83$  [108]. We will ignore this and continue calling it a ‘ $3\sigma$  bound’ although meaning (3.6).

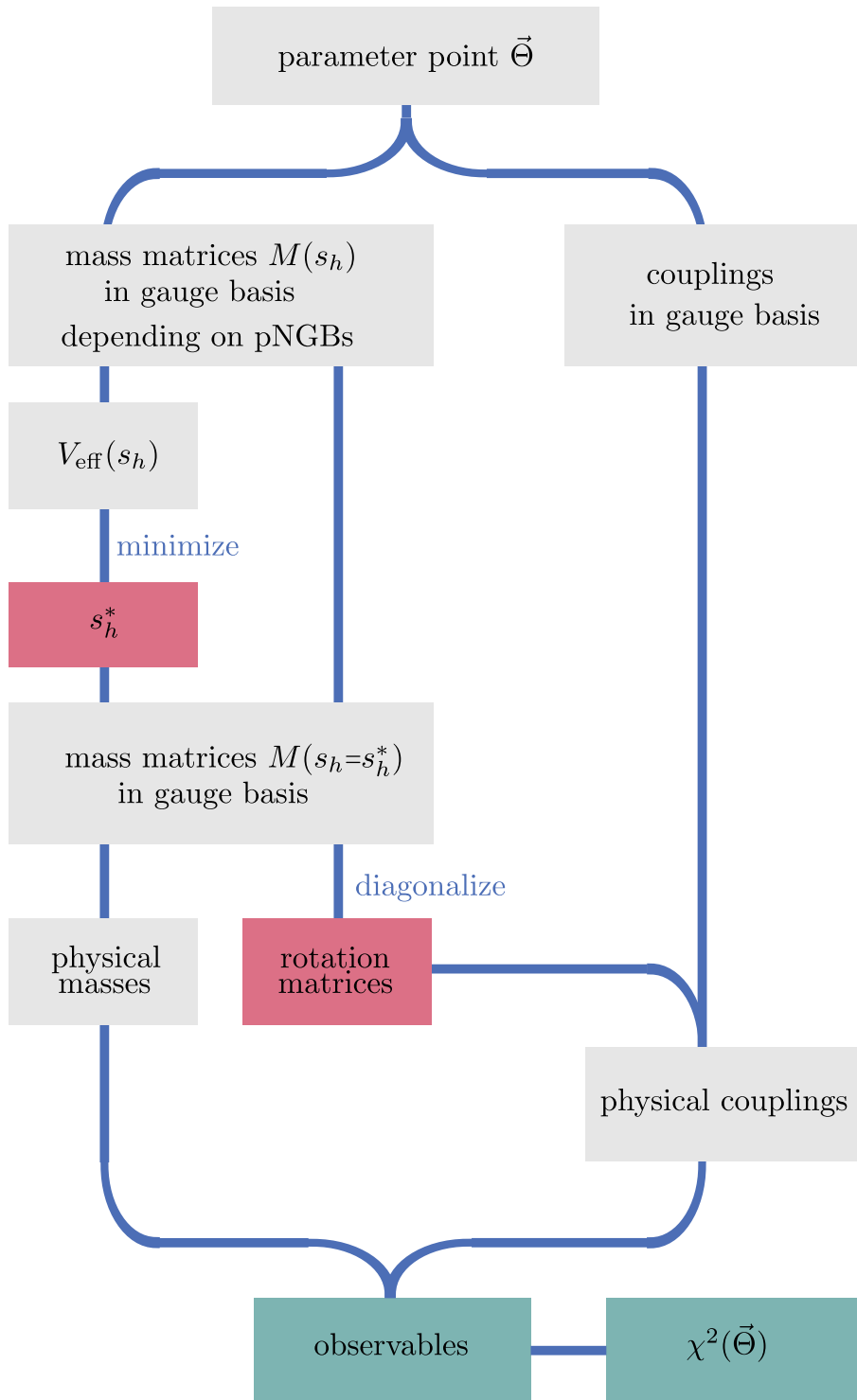


**Figure 3.2.:** Schematic algorithm for calculating physical masses and couplings.

that are vectors containing elementary as well as composite fields all of the same charge. For these fields one can write a general Lagrangian in the gauge basis in the following form

$$\begin{aligned} \mathcal{L}_{\text{gb}} = & \bar{\Psi}_i^{(\text{gb})} i \not{\partial} \Psi_i^{(\text{gb})} - \left[ M_{(\text{gb})}^{\Psi}(\vec{\Theta}; s_h) \right]_{ij} \bar{\Psi}_i^{(\text{gb})} \Psi_j^{(\text{gb})} \\ & - \frac{1}{4} \text{tr} \left[ \mathbf{V}_{\mu\nu}^{(\text{gb})i} \mathbf{V}_i^{(\text{gb})\mu\nu} \right] + \frac{1}{2} \left[ M_{(\text{gb})}^V(\vec{\Theta}; s_h) \right]_{ij} \mathbf{V}_i^{(\text{gb})\mu} \mathbf{V}_{j\mu}^{(\text{gb})} \\ & + \left[ g_{(\text{gb})}^{\text{LL}}(\vec{\Theta}) \right]_{ijk} \bar{\Psi}_{L i}^{(\text{gb})} \gamma_{\mu} \Psi_{L j}^{(\text{gb})} \mathbf{V}_k^{(\text{gb})\mu} + \left[ g_{(\text{gb})}^{\text{RR}}(\vec{\Theta}) \right]_{ijk} \bar{\Psi}_{R i}^{(\text{gb})} \gamma_{\mu} \Psi_{R j}^{(\text{gb})} \mathbf{V}_k^{(\text{gb})\mu}, \end{aligned} \quad (3.9)$$

where the precise form of the mass matrices and the couplings is dictated by the particular theory and its symmetries. The mass matrices depend on the parameters  $\vec{\Theta}$  and on the pNGB fields through  $s_h$ . A possible dependence of the couplings on  $s_h$  is not considered, as this will not appear in the concrete models considered in this work. After EWSB the pNGBs get a vev  $s_h \rightarrow s_h^*$ , such that the mass matrices are given as

$$M_{(\text{gb})}(\vec{\Theta}) = M_{(\text{gb})}(\vec{\Theta}; s_h = s_h^*).$$

The pNGB-vev can be calculated as the minimum of the effective potential (2.53), which is again a function of the parameters  $\vec{\Theta}$ . So, after the intermediate step of minimizing the effective potential the mass matrices and couplings are completely determined by the parameters  $\vec{\Theta}$ .

In general, the mass mixing matrices  $M_{(\text{gb})}(\vec{\Theta})$  contain particle mixings and have to be diagonalized to go to the mass basis (mb) for the fields. Just as in the SM, this can be done via bi-unitary transformations for the fermions and orthogonal rotations for the vector bosons,

$$\Psi_{L i}^{(\text{gb})} = [\mathcal{V}_{\Psi L}]_{ia} \Psi_{L a}^{(\text{mb})}, \quad (3.10a)$$

$$\Psi_{R i}^{(\text{gb})} = [\mathcal{V}_{\Psi R}]_{ia} \Psi_{R a}^{(\text{mb})}, \quad (3.10b)$$

$$\mathbf{V}_i^{(\text{gb})} = [\mathcal{V}_V]_{ia} \mathbf{V}_a^{(\text{mb})}, \quad (3.10c)$$

such that the physical masses are given as the eigenvalues or singular values of the mixing matrices. In this basis the above Lagrangian takes the form

$$\begin{aligned} \mathcal{L}_{\text{mb}} = & \bar{\Psi}_a^{(\text{mb})} \left( i \not{\partial} - \left[ M_{(\text{mb})}^{\Psi}(\vec{\Theta}) \right]_{aa} \right) \Psi_a^{(\text{gb})} \\ & - \frac{1}{4} \text{tr} \left[ \mathbf{V}_{\mu\nu}^{(\text{mb})a} \mathbf{V}_a^{(\text{mb})\mu\nu} \right] + \frac{1}{2} \left[ M_{(\text{mb})}^V(\vec{\Theta}) \right]_{aa} \mathbf{V}_a^{(\text{mb})\mu} \mathbf{V}_{a\mu}^{(\text{mb})} \\ & + \left[ g_{(\text{mb})}^{\text{LL}}(\vec{\Theta}) \right]_{abc} \bar{\Psi}_{L a}^{(\text{mb})} \gamma_{\mu} \Psi_{L b}^{(\text{mb})} \mathbf{V}_c^{(\text{mb})\mu} + \left[ g_{(\text{mb})}^{\text{RR}}(\vec{\Theta}) \right]_{abc} \bar{\Psi}_{R a}^{(\text{mb})} \gamma_{\mu} \Psi_{R b}^{(\text{mb})} \mathbf{V}_c^{(\text{mb})\mu}, \end{aligned} \quad (3.11)$$

where the mass basis couplings are defined as

$$\left[ g_{(\text{mb})}^{\text{LL}}(\vec{\Theta}) \right]_{abc} = \left[ g_{(\text{gb})}^{\text{LL}}(\vec{\Theta}) \right]_{ijk} [\mathcal{V}_{\Psi L}^{\dagger}]_{ia} [\mathcal{V}_{\Psi L}]_{jb} [\mathcal{V}_V]_{kc}, \quad (3.12)$$

$$\left[ g_{(\text{mb})}^{\text{RR}}(\vec{\Theta}) \right]_{abc} = \left[ g_{(\text{gb})}^{\text{RR}}(\vec{\Theta}) \right]_{ijk} [\mathcal{V}_{\Psi R}^{\dagger}]_{ia} [\mathcal{V}_{\Psi R}]_{jb} [\mathcal{V}_V]_{kc}. \quad (3.13)$$

This Lagrangian can now be used to extract the Feynman rules for a given parameter point and with these, one can calculate observables.

For calculating observables given a parameter point we developed the package `pypngb` in the programming language Python. This automatically performs the operations laid out in figure 3.2. For this the couplings and mass matrices in the gauge basis are calculated from the given parameters, the effective potential is calculated and minimized, the mass matrices are diagonalized and all the couplings are rotated into the mass basis. With these as input, all observables (which will be discussed in the next section) can be calculated and combined into a  $\chi^2$  function (3.3).

At this place let us remark on the parameters and the ranges in which we allow them to vary. We give this information in table 3.1. The symmetry breaking scales are bound to lie in a reasonable region suggested by naturalness arguments. Further, we impose consistency conditions motivated by the partial unitarization of Goldstone boson scattering [55]. An important fact it that we do not scan the massive parameters of the composite sector directly. We rather use their logarithms as input parameters, since otherwise we would have a strong bias for large values and it would be difficult to draw random values is small as it is needed to reproduce the hierarchies in the SM flavour parameters. Additionally, we constrain all massive parameters to be below the cutoff of the EFT which we identify with  $4\pi f$ .

	parameter	scanning method	range	remark
elementary couplings	$g_0, g'_0$ $g_3^0$	linear	0 – 1 0 – 2	
symmetry breaking scales	$f$ $f_1, f_X, f_G$	linear	(250 – 3000) GeV	$1 < \frac{f_1}{f} < \sqrt{3}$ $\frac{1}{2} \leq \frac{f_{X,G}}{f_1} \leq 2$
composite couplings	$g_\rho, g_X, g_G$	linear	1 – $4\pi$	$m_{\rho,X,G} < 4\pi f$
composite masses	$m_Q, m_{\tilde{Q}},$ $m_{Y_Q}, m_{Y_{\tilde{Q}}} + Y_Q$	logarithmic	$(e^1 - e^{10})$ GeV	$< 4\pi f$
composite-elementary mixings	$\Delta_L, \Delta_R$ angles & phases	logarithmic linear	$(e^{-30,-10} - e^{+10})$ GeV – $\pi$ – $+\pi$	$< 4\pi f$

**Table 3.1.:** Details on the model parameters. We show the considered ranges, the scanning method (i.e. whether we scanned the parameters or their logarithms) and we show further consistency conditions.

### 3.3. Constraints

In the following we will discuss in detail the experimental constraints that will be imposed in the analyses that are presented in chapters 4 and 5. These are investigations of a minimal (chapter 4) and a next-to-minimal CHM (chapter 5) that were conducted in 2015 and 2016, respectively. In the time between the two analyses many observables received updates. Either new experimental data were presented or more precise theoretical input data (e.g. results from lattice QCD) became available. If this is the case, we will present both numbers in the following.

#### 3.3.1. SM parameters

##### Electroweak symmetry breaking

In this analysis much attention is given to a realistic electroweak symmetry breaking. As discussed in section 2.2.2 the effective Higgs potential is generated dynamically at loop-level via the Coleman-Weinberg mechanism. We calculate the potential using (2.53) and determine its minimum numerically. The minimum is what in the end will determine the electroweak scale  $v_{\text{SM}}$  and, in particular, the hierarchy  $v_{\text{SM}} \ll f$ . As an example, in the M4dCHM one has

$$v_{\text{SM}} = s_h^* f, \quad (3.14)$$

where  $s_h^* = \sin(\langle h \rangle / f)$  denotes the minimum of the effective potential. Depending on the model the potential will not only be a function of the Higgs boson alone but also of a (possibly) extended scalar sector, such that the electroweak scale is a function depending on each scalar vev. Experimentally, the vev of the Higgs field is extracted through the Fermi constant  $G_\mu = \frac{1}{2\sqrt{2}} \frac{1}{v_{\text{SM}}^2}$  via muon decay  $\mu^\pm \rightarrow e^\pm \nu_\mu \bar{\nu}_e$ . In the SM this process is mediated at tree-level via the exchange of a  $W$  boson. In extensions of the SM NP can also contribute to this process such that the extraction of  $v_{\text{SM}}$  is affected by NP contaminations. In CHMs these NP contributions are also present on tree level and come from the exchange of heavy charged vector resonances as well as effective right-handed  $W$  couplings. Since we only consider a trivial lepton sector in our setup, we do not have to care about the second possibility and we can define

$$G_\mu = \frac{1}{2\sqrt{2}} \sum_a \frac{|g_{W^a \mu\nu} g_{W^a e\nu}^*|}{m_{W^a}^2}, \quad (3.15)$$

where the index  $a$  sums over the SM  $W$  as well as over contributions from heavy charged vectors. This observable can be compared to the experimental value which is measured to an extreme precision [108],

$$G_\mu^{\text{exp}} = (1.1663787 \pm 0.0000006) \times 10^{-5}. \quad (3.16)$$

We conservatively add a theory uncertainty of 1% to account for ignored loop corrections to  $G_\mu$ .

A second observable that is determined by the effective potential is the mass of the Higgs boson, which is given as the curvature at the minimum of the potential. In the general case  $V_{\text{eff}}$  depends on a variety of scalar fields  $\phi_i$ , such that the curvature is described by the Hessian matrix

$$\mathbf{H}_{mn} = \partial_m \partial_n V_{\text{eff}}(\phi_i)|_{\phi_i=\langle\phi_i\rangle}. \quad (3.17)$$

This matrix then represents the full leading-order mass mixing matrix for the scalar fields such that the Higgs mass is identified with the smallest eigenvalue of the Hessian. Going back to the case of the M4dCHM, the problem is much simpler and the Higgs mass is simply given as the second derivative of the potential,

$$m_h^2 = \partial_h^2 V_{\text{eff}}(h)|_{h=\langle h\rangle} = \frac{1-s_h^2}{f^2} \partial_{s_h}^2 v_{\text{eff}}(s_h) \Big|_{s_h=s_h^*}. \quad (3.18)$$

Experimentally the Higgs mass has been by now well established by the LHC and its value is cited as [108]

$$m_h^{\text{exp}} = (125.09 \pm 0.24) \text{ GeV}. \quad (3.19)$$

We interpret the calculated Higgs mass as a running mass at the scale  $\mu = m_t$ . By this we neglect higher order corrections which can be substantial in the strongly interacting theory. For this we add a theory uncertainty of 5%, which means that effectively we allow for Higgs masses in quite a large range  $m_h \in [106, 144] \text{ GeV}$ .

### Particle masses

The most salient constraint is, of course, reproducing the masses, couplings and CKM mixings of the SM. As already discussed above, due to partial compositeness elementary fermions mix with composite resonances, which is described by large mass mixing matrices. These mixings depend on the minimum of the effective Higgs potential. After diagonalization the SM fields are linear combinations of composite and elementary fields. We interpret the masses in this basis as  $\overline{\text{MS}}$  running masses at the scale  $\mu = m_t$ .

The masses of the lighter quarks are measured not at the electroweak scale, but at some hadronic scale  $\mu_{\text{low}}$ . Although they are fundamental parameters of the theory, they cannot be measured directly as quarks are confined into hadrons. Therefore, quark masses have to be extracted indirectly by fits to hadronic observables. This is particularly difficult for the first generation quarks since they are small. However, due to chiral symmetry breaking masses and mass differences of pNGBs (pions, kaons and etas) are sensitive to up- and down-quark masses. Thus, they can be determined with the help of lattice QCD computations; we use the values provided in [109]. For the masses of the other quarks we use the PDG averages [110]. A further subtlety arises for the top quark mass. This is determined by fitting to the outcome of Monte Carlo parton shower generators. Therefore, what is actually measured is  $m_t^{\text{MC}}$ , a parameter of the Monte Carlo generators. Rigorously it is not precisely known how this is related to the pole mass, but both are estimated to coincide within 1 GeV [111]. We add this as an additional theory uncertainty.

The values of the masses at  $\mu = \mu_{\text{low}}$  and  $\mu = m_t$  are related via the RGE running. We use the 4-loop RGE results as implemented in the code `RunDec` [112] to obtain the masses at the low scale from the eigenvalues of the mass matrices, which then can be compared to the measured values. The masses of  $t$ ,  $Z$  and  $W$  we directly interpret as masses at  $\mu = m_t$ . The used experimental values are shown in table 3.2.

We calculate the masses at tree-level. One could, in principle, calculate the one-loop corrections to the masses, but for this we would have to calculate the full one-loop corrections to the mass mixing matrices. Unfortunately, as the fermion mass matrices are quite large ( $27 \times 27$  in the simplest case), this approach is not feasible for us because of computations times in the numerical scans. Therefore, we add a relative theory error of 5% for  $t$ ,  $Z$  and  $W$  and 1% for the light quarks.

### Couplings

In models with partial compositeness the elementary gauge group and the SM-like subgroup of the global symmetries are broken down to their diagonal subgroup, which is then identified with the SM

	low scale $\mu_{\text{low}}$	$m(\mu_{\text{low}})$	$m(\mu_{\text{high}})$
$m_u$	2 GeV	$(2.16 \pm 0.11)$ MeV [109]	$(1.18 \pm 0.06)$ MeV
$m_d$	2 GeV	$(4.68 \pm 0.16)$ MeV [109]	$(2.55 \pm 0.09)$ MeV
$m_c$	$m_c$	$(1.275 \pm 0.025)$ GeV [110]	$(0.613 \pm 0.012)$ GeV
$m_s$	2 GeV	$(95 \pm 5)$ MeV [110]	$(52 \pm 3)$ MeV
$m_b$	$m_b$	$(4.18 \pm 0.03)$ GeV [110]	$(2.58 \pm 0.02)$ GeV
$m_t$	—	—	$(173.21 \pm 0.87 \pm 1.00)$ GeV [110]
$m_W$	—	—	$(80.385 \pm 0.015)$ GeV [110]
$m_Z$	—	—	$(91.1876 \pm 0.0021)$ GeV [110]
$m_h$	—	—	$(125.09 \pm 0.24)$ GeV [108]

**Table 3.2.:** Experimental input values for SM masses. Quark masses (except for the top mass) are evolved up to the high scale  $\mu_{\text{high}} = m_t$  while the top and vector boson masses are interpreted as masses at the high scale.

gauge symmetry 2.2.2. Therefore, the SM gauge couplings are determined by the elementary and composite gauge couplings,

$$\frac{1}{g'^2} = \frac{1}{g_0'^2} + \frac{1}{g_\rho^2} + \frac{1}{g_X^2}, \quad \frac{1}{g^2} = \frac{1}{g_0^2} + \frac{1}{g_\rho^2}. \quad (3.20)$$

In the SM, these couplings are of utmost importance for the shape of the electroweak sector and are extracted from electroweak observables. Assuming the SM tree-level relation

$$\rho = \frac{m_Z \cos(\theta_w)}{m_W} = 1 \quad (3.21)$$

to hold, it would in principle suffice to fix  $m_W/m_Z$  and  $m_W/v_{\text{SM}}$  for demanding to reproduce the correct values for the gauge couplings. Beyond the SM this relation is not ensured. This is why one has to constrain the electroweak couplings redundantly, and we add the electromagnetic coupling

$$\alpha_{\text{em}} = \frac{e^2}{4\pi} = \frac{1}{4\pi} \left( \frac{g_{\gamma ee}^L + g_{\gamma ee}^R}{2} \right)^2 \quad (3.22)$$

as an additional observable.<sup>3</sup> This observable has been measured very accurately at LEP and Tevatron. Since the RGE running of the electromagnetic coupling is rather small for the considered energy ranges we can simply use the measured value at  $\mu = m_Z$  [113]

$$\alpha_{\text{em}}^{-1}(\mu = m_t) \approx \alpha_{\text{em}}^{-1}(\mu = m_Z) = 128.962 \pm 0.014. \quad (3.23)$$

To include the uncertainty due to the RGE running (and due to possible NP contributions to the RGE running) we conservatively add a theory error of 2%. Note that quantum corrections to  $\rho$  (3.21) are effectively brought under control by the (loop-induced)  $T$  parameter (rf. section 3.3.2).

### CKM mixings

In CHMs reproducing the measured values of the CKM matrix is a powerful constraint. Due to partial compositeness the SM quarks are mixtures of elementary and composite fields. Therefore, including the full flavour sector, does not lead only to a mixing of the 3 SM generations. There are also mixings of SM fields with composite resonances, such that the CKM matrix is embedded as a  $3 \times 3$  submatrix

<sup>3</sup>Note that the above relation is only valid when considering a purely elementary lepton sector, as we will do in this work.

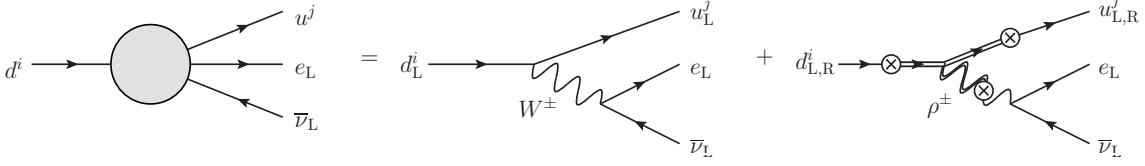


**Figure 3.3.:** Extraction of CKM matrix elements in CHMs from tree-level  $W$  mediated decays. There is a SM contribution as well as a NP contamination with heavy resonance exchange and/or right-handed currents.

into the large  $W$  couplings matrix. Writing down the interaction Lagrangian in the mass basis gives

$$\begin{aligned} \mathcal{L}_{\text{int}} = & \left[ \mathcal{V}_{uL}^\dagger \right]_{iI} \left[ \mathcal{V}_{dL} \right]_{jJ} \left[ \mathcal{V}_W \right]_{KW} \left[ g_{W\psi\psi}^L \right]_{IJK} \bar{U}_L^i \gamma^\mu D_L^j W_\mu^+ \\ & + \left[ \mathcal{V}_{uR}^\dagger \right]_{iI} \left[ \mathcal{V}_{dR} \right]_{jJ} \left[ \mathcal{V}_W \right]_{KW} \left[ g_{W\psi\psi}^R \right]_{IJK} \bar{U}_R^i \gamma^\mu D_R^j W_\mu^+ + \text{h.c.} \end{aligned} \quad (3.24a)$$

$$\begin{aligned} = & \frac{g_2^{\text{SM}}}{\sqrt{2}} \left( \begin{array}{c} [\bar{u}_L^{\text{SM}}] \\ [\bar{\Psi}_{uL}^{\text{NP}}] \end{array} \right)_i \gamma^\mu \underbrace{\left( \begin{array}{cc} [V_{\text{CKM}}^{\text{SM}}]_{ij} & * \\ * & * \end{array} \right)}_{=V_{\text{CKM,L}}^{\text{total}}} \left( \begin{array}{c} [d_L^{\text{SM}}] \\ [\Psi_{dL}^{\text{NP}}] \end{array} \right)_j W_\mu^+ \\ & + \frac{g_2^{\text{SM}}}{\sqrt{2}} \left( \begin{array}{c} [\bar{u}_R^{\text{SM}}] \\ [\bar{\Psi}_{uR}^{\text{NP}}] \end{array} \right)_i \gamma^\mu [V_{\text{CKM,R}}^{\text{total}}] \left( \begin{array}{c} [d_R^{\text{SM}}] \\ [\Psi_{dR}^{\text{NP}}] \end{array} \right)_j W_\mu^+ + \text{h.c.}, \end{aligned} \quad (3.24b)$$

where left-handed as well as right-handed couplings are generated. Both couplings are described by large CKM-like matrices,  $V_{\text{CKM,L}}^{\text{total}}$  and  $V_{\text{CKM,R}}^{\text{total}}$ , that by construction have to be unitary. The SM CKM matrix  $V_{\text{CKM}}^{\text{SM}}$ , being a submatrix, is *not* unitary, so the only thing we can demand is that it looks ‘unitary enough’ to pass all experimental constraints such as e.g. the unitary triangle. This puts strong constraints on the mixings between quarks and quark partners and accordingly acts as an upper bound on the quark degrees of compositeness.

Experimentally, the CKM elements are extracted from decays that are mediated at tree-level via a  $W$ -exchange, or from meson-antimeson mixing. Both extractions are plagued by NP contaminations that affect the determination of the SM parameters. For the tree-level decay there are also contributions from the exchange of heavy vector resonances as well as right-handed charged currents. Although they are suppressed by the heavy resonance mass and the quark degrees of compositeness we include these effects. We define CKM matrix element which can be compared to the values measured in experiment via ratios of  $W$  couplings,

$$|V_{ij}| = \frac{|g_{Wu_i d_j}^L|}{|g_{W e \nu}^L|}. \quad (3.25)$$

For the extraction of  $V_{ud}$  and  $V_{us}$  the above expression is sufficient as possible right-handed NP contributions are negligible. In the case of CKM elements involving the third generation we numerically include the right-handed NP contributions. Note that the above definition explicitly only holds for a trivially modeled lepton sector as considered in this work.

Using this prescription, we can compare the calculated CKM elements to the experimental values:

- The CKM elements  $|V_{ud}|$  and  $|V_{us}|$  are extracted from the superallowed  $0^+ \rightarrow 0^+$  nuclear  $\beta$ -decay and from  $K \rightarrow \pi \ell \nu$ , respectively. Their values are strongly constrained by first-row CKM unitarity, which is strongly supported by experiment,

$$1 = |V_{ud}|^2 + |V_{us}|^2 + |V_{ub}|^2 \approx |V_{ud}|^2 + |V_{us}|^2, \quad (3.26)$$

where  $|V_{ub}|$  is negligibly small.

- For both  $|V_{ub}|$  and  $|V_{cb}|$ , there is the long-standing issue of a discrepancy between the determinations from inclusive and exclusive  $B$  decays. The matrix element  $|V_{ub}|$  can be extracted from inclusive  $B \rightarrow X_u \ell \nu$  decays as well as from exclusive  $B \rightarrow \pi \ell \nu$ . Similarly,  $|V_{cb}|$  is obtained from  $B \rightarrow X_c \ell \nu$  inclusively and from  $B \rightarrow D^{(*)} \ell \nu$  exclusively. Currently, the determinations



	2015	2016
$V_{ud}$	(0.97417 ± 0.00021) [117]	
$V_{us}$	(0.2249 ± 0.0008) [109]	(0.2243 ± 0.0010) [118]
$V_{ub}^{\text{excl}}$	$(3.72 \pm 1.9 \times 0.16) \times 10^{-3}$ [119]	$(3.62 \pm 2.3 \times 0.14) \times 10^{-3}$ [118]
$V_{ub}^{\text{incl}}$	$(4.33 \pm 1.9 \times 0.28) \times 10^{-3}$ [120]	$(4.33 \pm 2.3 \times 0.28) \times 10^{-3}$ [120]
$V_{cb}^{\text{excl}}$	$(3.904 \pm 2.9 \times 0.075) \times 10^{-2}$ [121]	$(3.927 \pm 2.7 \times 0.074) \times 10^{-2}$ [118]
$V_{cb}^{\text{incl}}$	$(4.221 \pm 2.9 \times 0.078) \times 10^{-2}$ [121]	$(4.221 \pm 2.7 \times 0.078) \times 10^{-2}$ [118]
$V_{tb}$	(0.998 ± 0.041) [122]	
$\gamma$	(72.85 ± 6.65) <sup>o</sup> [123]	

**Table 3.3.:** Experimental input for the CKM matrix used in the scans. We give the data for scans performed in 2015 and 2016. For  $V_{ub}$  and  $V_{cb}$  the experimental uncertainties are scaled to account for tensions in the inclusive vs. exclusive determination.

from both channels differ by several  $\sigma$  for both CKM elements (see e.g. the discussion in [114]). These tensions cannot be resolved in our model, which is why we include the inclusive and exclusive determinations as separate observables. For this we implemented the model-independent contributions from NP given in [114] (which includes right-handed  $W$  couplings) for the theory calculation and used the PDG prescription to rescale the uncertainties of discrepant measurements [108].

- Since top-quarks do not form bound states, the above method cannot be applied to extract  $|V_{tb}|$ . This CKM element is determined from the  $t$ -channel single-top-quark production cross section at the LHC. In this process the top quark is produced in association with a  $b$  quark and light quarks. Therefore, one is sensitive only to the combination  $V_{ud} V_{tb}$ .
- We include the angle  $\gamma$  of the unitary triangle [108]. A particularly clean way to obtain this observable experimentally is via the interference of  $b \rightarrow c\bar{u}s$  and  $b \rightarrow u\bar{c}s$  amplitudes in  $B \rightarrow DK$  [115, 116]. Neglecting possible contributions from right-handed  $W$  couplings, we calculate this CKM angle through

$$\gamma = -\arg \left( \frac{\sum_a (g_{W^a cb}^L g_{W^a us}^{L*}) / m_{W^a}^2}{\sum_a (g_{W^a ub}^L g_{W^a cs}^{L*}) / m_{W^a}^2} \right). \quad (3.27)$$

- The CKM elements  $|V_{td}|$  and  $|V_{ts}|$  cannot be determined from tree-level  $t$  decays. Having fixed the value of  $|V_{tb}|$ , these matrix elements can be included indirectly through  $B_{(s)}$  mixing and rare  $B$  decays (see section 3.3.5).

During the time the scans were performed the experimental values were updated such that we give values from 2015 used in the scan of the M4dCHM as well as values used in the analysis of the NM4dCHM in Tab. 3.3.

### 3.3.2. Electroweak precision observables

As already mentioned in section 2.2.1, modifications to the electroweak sector can be parametrized by the so-called electroweak precision observables (EWPO) [45, 124]. These describe the oblique corrections, i.e. the vacuum polarizations, of the electroweak vector bosons. EWPOs are an important constraint for strongly-coupled models of EWSB and, in particular, they put high tension on technicolor models. Therefore, it is important to include these constraints in an analysis of CHMs.

As a first step one defines the transverse parts of the vacuum polarizations<sup>4</sup> of the SM electroweak

<sup>4</sup>Here, the vacuum polarizations include only NP contributions.

vector bosons,

$$\begin{aligned}\Pi_{\gamma\gamma}(q^2) &= q^2\Pi'_{\gamma\gamma}(q^2=0) + \dots, \\ \Pi_{Z\gamma}(q^2) &= q^2\Pi'_{Z\gamma}(q^2=0) + \dots, \\ \Pi_{ZZ}(q^2) &= \Pi_{ZZ}(p^2=0) + q^2\Pi'_{ZZ}(q^2=0) + \dots, \\ \Pi_{WW}(q^2) &= \Pi_{WW}(p^2=0) + q^2\Pi'_{WW}(q^2=0) + \dots,\end{aligned}$$

which then allows to give a definition for the  $S$  and  $T$  parameters,<sup>5</sup>

$$\alpha_{\text{em}}S = 4\sin^2(\theta_W)\cos^2(\theta_W)\left[\Pi'_{ZZ}(q^2=0) - \frac{\cos^2(\theta_W) - \sin^2(\theta_W)}{\sin(\theta_W)\cos(\theta_W)}\Pi'_{Z\gamma}(q^2=0) - \Pi'_{\gamma\gamma}(q^2=0)\right], \quad (3.28a)$$

$$\alpha_{\text{em}}T = \frac{\Pi_{WW}(q^2=0)}{m_W^2} - \frac{\Pi_{ZZ}(q^2=0)}{m_Z^2}, \quad (3.28b)$$

which coincide with the definitions given in (2.39a).

By construction, the  $T$  parameter does not receive tree-level corrections as we imposed a custodial protection through the used coset (rf. section 2.2.1). On the one-loop level there are several different contributions. As Yukawa couplings and the gauging of hypercharge break custodial symmetry explicitly, loops of quark vector resonances will contribute to the  $T$  parameter. In [55] these contributions have been estimated in a general parametrization of CHMs and the vector loops have been found to be subdominant with respect to the fermion ones. Therefore, we will only include the fermion one-loop contributions to the transverse vacuum polarizations, which are given as

$$-16\pi^2\Pi_{VV} = \sum_{f_i, f_j} H(m_{f_i}^2, m_{f_j}^2) \left( |g_{Vf_i f_j}^L|^2 + |g_{Vf_i f_j}^R|^2 \right) + 4m_{f_i}m_{f_j}B_0(m_{f_i}^2, m_{f_j}^2) \text{Re}\left(g_{Vf_i f_j}^{L*}g_{Vf_i f_j}^R\right),$$

where one sums over all SM fermions and quark resonances. The Passarino-Veltman function is defined as in [125] and the function  $H$  can be found e.g. in [126]. We explicitly checked that for the considered models the above one-loop contributions lead to a finite result. Further, in CHMs there are also corrections to the couplings of the Higgs to SM vector bosons that contribute to oblique corrections with Higgs loops. As a consequence, there appears an incomplete cancellation between Higgs and Goldstone diagrams [127, 128],

$$g \log\left(\frac{\Lambda}{m_Z}\right)\Big|_{\text{Goldstones}} + (g + \delta g) \log\left(\frac{\Lambda}{m_h}\right)\Big|_{\text{Higgs}} \sim g \log\left(\frac{m_h}{m_Z}\right) + \delta g \log\left(\frac{\Lambda}{m_h}\right), \quad (3.29)$$

such that an explicit UV dependence through the cutoff  $\Lambda$  remains. As this ‘IR-log’ contribution is not straight-forwardly calculable (but it has been estimated in [70]), we will later include it as an uncertainty of the calculation.

The  $S$  parameter is not protected by custodial symmetry and therefore it already appears at tree-level. For this it is not useful to work with the vacuum polarizations (3.28), but fortunately the tree-level  $S$  parameter can be related to the shift in the coupling of the  $Z$  boson to leptons,

$$g_{Zee} = \sqrt{g_1^2 + g_2^2} (\mathbb{T}_L^3 - \sin^2(\theta_{\text{eff}})Q),$$

in models that feature a vanishing  $T$  parameter a tree-level. Then, the NP contribution to the  $S$  is given numerically as

$$\alpha_{\text{em}}S|_{T=0} = 4(s_W^2 - \sin^2(\theta_{\text{eff}})), \quad (3.30)$$

where  $s_W^2 = 1 - m_W^2/m_Z^2$  and the effective weak mixing angle is defined via the leptonic forward-backward asymmetry,<sup>6</sup>

$$\sin^2\theta_{\text{eff}} = \frac{1}{4} \left( 1 + \frac{g_{Zee}^R + g_{Zee}^L}{g_{Zee}^R - g_{Zee}^L} \right). \quad (3.31)$$

<sup>5</sup>One could also define the so-called  $U$  parameter, but this one is suppressed in NP models as it corresponds to a dimension-8 operator.

<sup>6</sup>We have to note that this approach is only possible since we modeled the lepton sector in a trivial way as purely elementary. If the lepton were partially composite then the  $Zee$  coupling would receive non-oblique corrections, such that the  $S$  parameter could not be extracted.

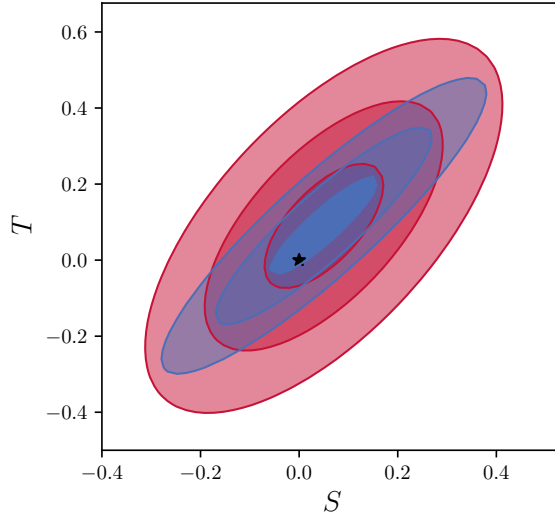


**Figure 3.4.:** Allowed  $1\sigma$ -,  $2\sigma$ -,  $3\sigma$ -regions for the electroweak precision observables  $S$  and  $T$ . *Blue:* Values allowed by the global electroweak fit [46]. *Red:* Allowed region used by us. The uncertainties were blown up to account for theory uncertainties. The black star marks the SM prediction.

Experimentally, the  $S$  and  $T$  parameters are extracted from a global electroweak fit [46], which finds

$$S = 0.05 \pm 0.11, \quad T = 0.09 \pm 0.13 \quad (3.32)$$

with a correlation coefficient of  $+0.9$ . In our analysis we inflate the uncertainties to account for the neglected contributions in the calculation (‘IR-log’ contributions for  $S$  and  $T$  as well as vector boson loop corrections for  $T$ ). To be conservative, we assume uncorrelated theory uncertainties of  $0.05$  for  $S$  and  $0.10$  for  $T$  which we combine with the experimental uncertainties. The values are chosen to match the typical size of the ‘IR-log’ contributions (see e.g. [70]). The allowed regions are shown in figure 3.4. The strong correlation between the  $S$  and  $T$  parameters is quite important as this means that a large contribution to one parameter implies also a large contribution to the other observable. This is not trivial since the tree-level  $S$  parameter is determined by the gauge sector of the theory, while the one-loop contributions to the  $T$  are dominated by the fermion resonances.

To estimate the impact of the constraint given by the  $S$  parameter, we can look at the approximate result given in [99],

$$S \approx 4\pi v_{\text{SM}}^2 \left( \frac{1}{m_\rho^2} + \frac{1}{m_a^2} \right). \quad (3.33)$$

This shows that effectively, the  $S$  acts as a lower bound on the masses of the composite vector resonances. Assuming degenerate vector resonance masses, the  $3\sigma$  bound of figure 3.4 gives a rough lower bound on the vector masses

$$m_\rho \gtrsim 1.9 \text{ TeV}. \quad (3.34)$$

### 3.3.3. $Z$ widths

Decays of the  $Z$  boson have been measured to a very high accuracy at LEP [129]. Therefore these results are sensitive probes of variations of couplings of the  $Z$  to SM fermions. By partial compositeness these couplings get corrections when going to the mass basis,

$$g_{Zf_i f_j}^{\text{mb}} = V_{iI}^\dagger V_{jJ} V_{ZK}^{\text{boson}} [g^{\text{gb}}]_{IJK} = \sum_{I=1}^3 V_{iI}^\dagger V_{jI} g_{Z}. \quad (3.35)$$

If the admixtures of composite resonances are large (which just means that if the SM fermions have a large degree of compositeness) then the  $3 \times 3$  submatrix of the total fermion mixing matrix will be significantly non-unitary, meaning that the couplings get sizable corrections and even flavour-offdiagonal  $Z$ -couplings are introduced. Such a sizable degree of compositeness is to be expected even for the lighter quarks in models with a slightly broken flavour symmetry.

As discussed in section 2.2.1, the  $Z$  couplings to SM fermions are subject to a custodial protection, if the SM are embedded into  $SO(5)$  multiplets in such a way that  $T_L^3 = T_R^3$  is satisfied. Looking at the explicit form of the embeddings (4.12) one observes that for the particular model we are analyzing not the whole  $Z d_L^i d_L^j$  coupling is protected but rather only the contribution to this coupling that is induced by the admixture of ‘up-type’ composite resonances into the ‘down-type’ SM quarks. But this is actually very important since it is the up-type contribution that due to the large degree of compositeness of the top is expected to be dangerous. It can be seen from the mass matrices that this contribution is not suppressed by the Higgs vev  $s_h^*$  (see appendix III). Therefore, despite having a custodial protection mechanism it is very important to include the constraint coming from  $Z$  coupling modifications. We also note that by the same reasoning for the  $Z u_L^i u_L^j$  coupling the protection works for the subleading contributions by admixtures of down-type resonances. The right-handed couplings are always protected as after EWSB they are related only to the electromagnetic coupling which is protected by gauge invariance.

Experimentally, the  $Z$  widths have been measured as ratios [129, 130],

$$R_b = \frac{\Gamma(Z \rightarrow b\bar{b})}{\Gamma(Z \rightarrow q\bar{q})} = 0.21629 \pm 0.00066, \quad R_c = \frac{\Gamma(Z \rightarrow c\bar{c})}{\Gamma(Z \rightarrow q\bar{q})} = 0.1721 \pm 0.0030,$$

$$R_\ell = \frac{\Gamma(Z \rightarrow q\bar{q})}{\Gamma(Z \rightarrow \ell^+ \ell^-)} = \begin{cases} 20.804 \pm 0.050 & \text{for } \ell = e \\ 20.785 \pm 0.033 & \text{for } \ell = \mu \\ 20.764 \pm 0.045 & \text{for } \ell = \tau \end{cases} .$$

where  $\Gamma(Z \rightarrow q\bar{q})$  implies a sum over all quarks except the top. Especially,  $R_b$  is measured to a very high accuracy such that this gives an important bound on the bottom degree of compositeness. As in our analysis the lepton sector is purely elementary, the leptonic  $Z$  widths can effectively be seen as constraints on the total hadronic width  $\Gamma(Z \rightarrow q\bar{q})$ . In particular when imposing a flavour symmetry the degrees of compositeness (of one chirality) of the light quarks can be significant, which could possibly lead to sizable effects in the hadronic  $Z$  width.

In our analysis we calculate the partial widths of the SM  $Z$  boson at tree-level with zero momentum. Contributions beyond this limit are discussed in [131]. These results contain the tree-level SM contributions. To match the measured values we add by hand NNLO SM contributions including QCD corrections [130].

### 3.3.4. Higgs production and decay

In the SM, the coupling of the Higgs to the other fields is predicted to be proportional to their mass. It is apparent that such a drastic change in the Higgs sector as present in CHMs can easily modify these relations. Therefore, it is important to control the deviations in the Higgs sector such that it is in accordance with the experimental data.

Higgs couplings are often measured in terms of *signal strengths*,

$$\mu_X^{gg} = \frac{\sigma(gg \rightarrow h) \times \text{BR}(h \rightarrow X)}{\sigma(gg \rightarrow h) \times \text{BR}(h \rightarrow X)|_{\text{SM}}}, \quad (3.36)$$

which are the product of production and decay into a particular channel  $h \rightarrow X$  normalized to the SM prediction. As the Higgs is predominantly produced via gluon fusion we assume this as the sole production mechanism.

Higgs production and decay were already discussed quite frequently in the literature. The general EFT description of a strongly-interacting light Higgs (SILH), as it is appropriate for a composite pNGB Higgs, has been developed in [132]. There, the relevant effective dimension-6 operators for Higgs production were identified as

$$\mathcal{L}_{\text{SILH}} \supset \frac{c_H}{f^2} \partial_\mu (H^\dagger H) \partial^\mu (H^\dagger H) + \frac{c_y}{f^2} (H^\dagger H) \bar{f}_R H f_L + \frac{c_g}{f^2} (H^\dagger H) \text{tr}[G_{\mu\nu} G^{\mu\nu}] + \text{h.c.} \quad (3.37)$$

These correspond to three different NP contributions that are diagrammatically shown in figure 3.5. The first one is a modification of the Higgs kinetic term induced by the non-linear pNGB nature of the Higgs in this kind of models. The second contribution describes modifications of the Higgs Yukawas to the SM fermions. And finally, NP particles running in the loop can also contribute. It was found

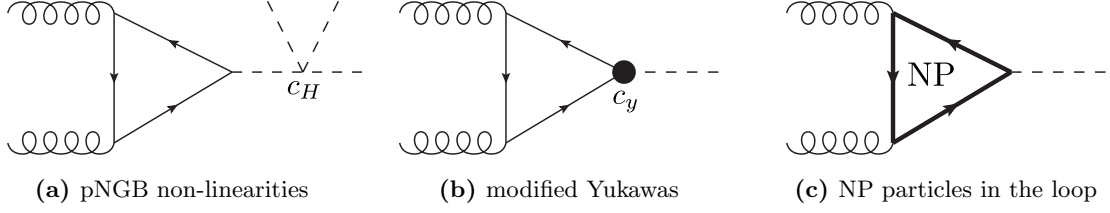


**Figure 3.5.:** Contributions to Higgs production via gluon fusion.

in [133] that the last two contributions cancel to a large degree. In particular, the effective Higgs-Gluon coupling is independent of the spectrum of the NP sector and is for the most part dominated by the non-linear character of the pNGB Higgs.<sup>7</sup>

The signal strengths can be expressed as

$$\mu_X^{gg} = \frac{r_{gg} r_X}{r_{\text{total}}} \quad (3.40)$$

where the partial width ratios  $r_i = \Gamma_i/\Gamma_i^{\text{SM}}$  are used. Due to the Higgs non-linearities the partial widths are modified as [132]

$$\Gamma(h \rightarrow X) = \left(1 - c_X \frac{v_{\text{SM}}^2}{f^2}\right) \Gamma(h \rightarrow X)_{\text{SM}} \quad (3.41)$$

with respect to the SM prediction, where the  $c_X$  are channel dependent constants. With this one finds for the signal strengths (3.40)

$$\mu_X^{gg} = 1 - (c_{gg} + c_X - c_{\text{tot}}) \frac{v_{\text{SM}}^2}{f^2} + \mathcal{O}\left(\frac{v_{\text{SM}}^4}{f^4}\right), \quad (3.42)$$

so that in general one expects a reduction that depends on the value of the symmetry breaking scale  $f$  and is more pronounced the smaller this scale is.

This is not true anymore if the light quarks are considerably composite as was shown in [135]. In this case the cancellation between Yukawa modifications and NP loops is not complete anymore and new terms for light quarks arise that can be non-negligible for large degrees of compositeness. Depending on the chosen flavour structure this case is well achievable and violations of (3.41) can appear.

In the analysis we include leading order contributions to the partial widths. In particular, we include the channels  $h \rightarrow \{WW, ZZ, \tau^+\tau^-\}$  at tree-level and  $h \rightarrow \gamma\gamma$  at one-loop level (where the loop counting here refers to the decay). Signal strengths in the channel  $h \rightarrow b\bar{b}$  have not been measured yet in the gluon fusion production channel.

The experimental input data are shown in figure 3.6. Unfortunately, the experimental uncertainties are still rather large

### 3.3.5. Flavour observables

#### Meson-antimeson mixing

Particle-antiparticle mixings of neutral mesons are a very powerful tool in constraining NP models. In the SM these processes occur via box diagrams involving electroweak gauge bosons that are further suppressed by the GIM mechanism [27]. In CHMs already tree-level exchanges of heavy vector resonances can contribute substantially. Therefore it is very important to include these constraints in the analysis, especially as we are interested in the flavour structure.

<sup>7</sup> This can also be understood from the fact that the radiative Higgs-vector boson coupling can be written as [134]

$$c_{hVV} \propto \frac{\partial_v \det(M)}{\det(M)}, \quad (3.38)$$

with  $M$  the fermion mass matrix. For the models considered here, the determinant of the mass matrix factorizes as

$$\det(M) = F(v/f) \times P(Y, M, f), \quad (3.39)$$

such that for the effective coupling all dependence on the mass parameters and couplings drops out and the Higgs non-linearities remain as the only contribution.

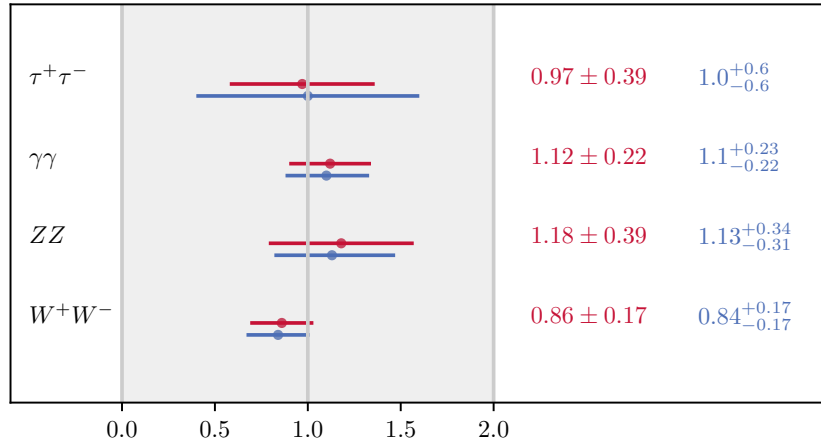


**Figure 3.6.:** Input data for the Higgs signal strengths. We show values for the 2015 analysis (*red*, values taken from [136, 137] and for the 2016 analysis (*blue*, values taken from [138]).

Mesons and antimesons can oscillate into each other. There are a lot of reviews on this topic; e.g. [139, 140, 141, 142]. Basically, this means that a meson  $\mathcal{M}$  (where  $\mathcal{M} = K, B_d, B_s, D$ ) can propagate into its antiparticle  $\bar{\mathcal{M}}$ ,

$$|\mathcal{M}(t)\rangle = f(t) |\mathcal{M}\rangle + \bar{f}(t) |\bar{\mathcal{M}}\rangle. \quad (3.43)$$

The time evolution of the coefficients is determined by a Schrödinger equation

$$i \frac{d}{dt} \begin{pmatrix} f(t) \\ \bar{f}(t) \end{pmatrix} = \left[ \begin{pmatrix} M_{\text{diag}} & M_{12} \\ M_{12}^* & M_{\text{diag}} \end{pmatrix} - \frac{i}{2} \begin{pmatrix} \Gamma_{\text{diag}} & \Gamma_{12} \\ \Gamma_{12}^* & \Gamma_{\text{diag}} \end{pmatrix} \right] \begin{pmatrix} f(t) \\ \bar{f}(t) \end{pmatrix}, \quad (3.44)$$

where it is a consequence of the  $CPT$  theorem that the diagonal elements are the same.

The mass matrix  $M$  then has two eigenvalues  $M_H$  and  $M_L$ , whose corresponding eigenstates are linear combinations of the flavour eigenstates. The mixing of the flavour states is characterized by the mass difference

$$\Delta M = M_H - M_L = 2 |M_{12}|. \quad (3.45)$$

Of great importance is the  $CP$ -violating phase  $\phi_{\mathcal{M}} = \arg(M_{12})$  of the mixing matrix element. In the SM this is determined by the phases in the CKM matrix and, therefore, it is a powerful tool for testing the CKM mechanism and for constructing the unitarity triangle. At this point we are mainly interested in  $M_{12}$  and  $\phi_{\mathcal{M}}$ , but the effects of  $\Gamma_{12}$  will be discussed in 6 in the context of different models for NP.

The calculation of the above observables is best done in an operator product expansion which separates UV and IR contributions,

$$M_{12}^{\mathcal{M}} = \frac{1}{2m_{\mathcal{M}}} \langle \bar{\mathcal{M}}^0 | \mathcal{H}_{\text{eff}}^{\Delta F=2} | \mathcal{M}^0 \rangle = (M_{12}^{\mathcal{M}})_{\text{SM}} + \sum_a C_a^{q_i q_j}(\mu_{\text{low}}) \langle \bar{\mathcal{M}}^0 | \mathcal{O}_a^{q_i q_j}(\mu_{\text{low}}) | \mathcal{M}^0 \rangle, \quad (3.46)$$

where  $q$  can be  $u$  or  $d$  and the loop-induced SM contribution is discussed e.g. in [143]. The  $\Delta F = 2$  effective Hamiltonian is given as [144]

$$\mathcal{H}_{\text{eff}}^{\Delta F=2} = \frac{G_F^2}{16\pi^2} M_W^2 \sum_a \lambda_{\text{CKM}}^a C_a^{q_i q_j}(\mu) \mathcal{O}_a^{q_i q_j}. \quad (3.47)$$

Here  $\lambda_{\text{CKM}}^a$  denote meson dependent CKM structures. The four-quark operators, which are generated in the considered models, are then given by<sup>8</sup>

$$\mathcal{O}_{\text{VLL}}^{q_i q_j} = (\bar{q}_L^i \gamma^\mu q_L^j)(\bar{q}_L^i \gamma^\mu q_L^j), \quad \mathcal{O}_{\text{VRR}}^{q_i q_j} = (\bar{q}_R^i \gamma^\mu q_R^j)(\bar{q}_R^i \gamma^\mu q_R^j), \quad (3.48a)$$

$$\mathcal{O}_{\text{VLR}}^{q_i q_j} = (\bar{q}_L^i \gamma^\mu q_L^j)(\bar{q}_R^i \gamma^\mu q_R^j), \quad \mathcal{O}_{\text{SLR}}^{q_i q_j} = (\bar{q}_R^i q_L^j)(\bar{q}_L^i q_R^j). \quad (3.48b)$$

<sup>8</sup>There are also tensor operators that could possibly contribute. But as we will only consider tree-level NP contributions tensor operators will not be generated.

In CHMs these operators are already generated at tree level by the exchange of neutral vector resonances. These include heavy  $Z'$  bosons as well as heavy gluon partners that couple to the composite admixture of the SM quarks. After rotation into the mass basis their couplings become flavour off-diagonal as they couple in a different way to elementary and composite fermions. Therefore, the Wilson couplings can easily be calculated from the mass basis couplings and the resonance masses,<sup>9</sup> (see e.g. [63] for a derivation in extra-dimensional models)

$$C_{VLL}^{q_i q_j}(\mu = m_t) = -\frac{1}{2} \sum_k \left( \frac{g_{\rho_k^0 q_i q_j}^L}{m_{\rho_k^0}} \right)^2 - \frac{1}{6} \left( \frac{g_{\rho_G q_i q_j}^L}{m_{\rho_G}} \right)^2, \quad (3.50a)$$

$$C_{VRR}^{q_i q_j}(\mu = m_t) = C_{VLL}^{q_i q_j} \Big|_{L \rightarrow R}, \quad (3.50b)$$

$$C_{VLR}^{q_i q_j}(\mu = m_t) = -\sum_k \frac{g_{\rho_k^0 q_i q_j}^L g_{\rho_k^0 q_i q_j}^R}{m_{\rho_k^0}^2} + \frac{1}{6} \frac{g_{\rho_G q_i q_j}^L g_{\rho_G q_i q_j}^R}{m_{\rho_G}^2}, \quad (3.50c)$$

$$C_{SLR}^{q_i q_j}(\mu = m_t) = \frac{g_{\rho_G q_i q_j}^L g_{\rho_G q_i q_j}^R}{m_{\rho_G}^2}. \quad (3.50d)$$

Here  $\rho^0$  denote the  $Z'$  and  $\rho_G$  the heavy gluon contributions. By our general rationale we interpret these effective couplings as Wilson coefficients at the high scale  $\mu = m_t$ . For calculating the contributions to meson-antimeson mixing they have to be evaluated at the low scale appropriate for the particular process. The general forms of the RGE equations are given in [144],

$$\vec{C}(\mu_{\text{low}}) = \hat{U}(\mu_{\text{low}}, \mu_{\text{high}} = m_t) \vec{C}(\mu_{\text{high}} = m_t). \quad (3.51)$$

We use them to evolve the Wilson coefficients down to the low scales ( $\mu_{\text{low}} = m_b$  for  $B_{d,s}$  mixing,  $\mu_{\text{low}} = 3 \text{ GeV}$  for  $D$  mixing and  $\mu_{\text{low}} = 2 \text{ GeV}$  for  $K$  mixing). The relevant evaluations of  $\alpha_s$  at various different scales is performed using the code `RunDec` [112] including 4-loop contributions.

The matrix elements appearing in (3.46) are non-perturbative objects and can be determined using lattice QCD. They depend on the meson decay constants and bag parameters

$$\langle \overline{\mathcal{M}}^0 | \mathcal{O}_a^{q_i q_j}(\mu_{\text{low}}) | \mathcal{M}^0 \rangle = m_{\mathcal{M}} f_{\mathcal{M}}^2 \mathcal{B}_a^{\mathcal{M}}(\mu_{\text{low}}), \quad (3.52)$$

where

$$\mathcal{B}_{VLL}^{\mathcal{M}} = \mathcal{B}_{VRR}^{\mathcal{M}} = \frac{1}{3} B_1^{\mathcal{M}}(\mu_{\text{low}}), \quad (3.53a)$$

$$\mathcal{B}_{VLR}^{\mathcal{M}} = -\frac{1}{6} \left( \frac{m_{\mathcal{M}}}{m_{q_i} + m_{q_j}} \right)^2 B_5^{\mathcal{M}}(\mu_{\text{low}}), \quad \mathcal{B}_{SLR}^{\mathcal{M}} = \frac{1}{4} \left( \frac{m_{\mathcal{M}}}{m_{q_i} + m_{q_j}} \right)^2 B_4^{\mathcal{M}}(\mu_{\text{low}}). \quad (3.53b)$$

The lattice predictions for the decay constants as well as the bag parameters  $B_i$  depend on the meson. We use ref. [109]<sup>10</sup> for  $B_d$  and  $B_s$  mixing. For the kaon bag parameters we use ref. [146]. Putting all the formulae (3.50), (3.51) and (3.52) together, the  $\Delta F = 2$  mixing amplitude  $M_{12}^{\mathcal{M}}$  can be calculated through (3.46).

We include the following observables for  $\Delta F = 2$  processes

**$B_{(s)}$  mesons:** We include in our analysis the mass differences in the  $B_d$  and  $B_s$  systems. For these we use the world averages provided by the HFAG collaboration [148]<sup>11</sup>

$$\Delta M_d = 2 \left| M_{12}^{B_d} \right| = (0.510 \pm 0.003) \text{ ps}^{-1}, \quad (3.54)$$

$$\Delta M_s = 2 \left| M_{12}^{B_s} \right| = (17.761 \pm 0.022) \text{ ps}^{-1}. \quad (3.55)$$

<sup>9</sup>The numerical prefactors of the heavy gluon contributions are determined by a color Fierz transformation

$$\text{T}_{ab}^A \text{T}_{cd}^A = -\frac{1}{6} \delta_{ab} \delta_{cd} + \frac{1}{2} \delta_{ad} \delta_{cb}, \quad (3.49)$$

where  $\text{T}^A$  denote the QCD generators.

<sup>10</sup>In the later part of the analysis new lattice QCD results on the  $B_{(s)}$  bag parameters became available. Therefore, in the analysis of the non-minimal model with coset  $\text{SO}(6)/\text{SO}(5)$  (see chapter 5) we used the newer results [145] that have considerably reduced uncertainties.

<sup>11</sup>These numbers are the world averages as they were in early 2015, when these scans were performed. The up to date numbers of 2017,  $\Delta M_d = (0.5064 \pm 0.0019) \text{ ps}^{-1}$  and  $\Delta M_s = (17.757 \pm 0.021) \text{ ps}^{-1}$  as given in [149], differ not too much, but  $\Delta M_d$  has a somewhat smaller uncertainty. However, these changes are small as compared to the theory uncertainties.

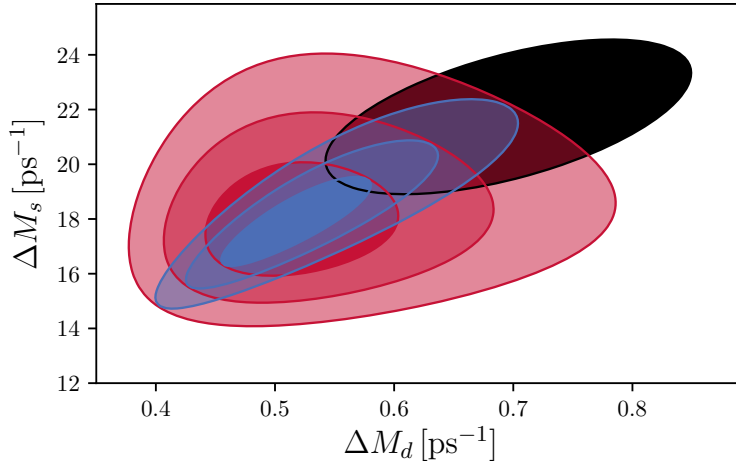


**Figure 3.7.:** Contour plots of the  $\chi^2$  function used in the scans for the correlated observables  $\Delta M_d$  and  $\Delta M_s$ . These include the convolution of experimental and theoretical uncertainties. We show the  $1\sigma$ -,  $2\sigma$ - and  $3\sigma$ -contours. *Red:* ‘Old’ likelihood used in the SO(5)/SO(4) scan. *Blue:* ‘New’ likelihood used in the SO(6)/SO(4) scan. *Black:*  $1\sigma$  SM prediction, calculated with `flavio` [147]

On the theory side, the main uncertainty is associated with the values of the hadronic matrix elements calculated on the lattice. We do not have to include uncertainties of the CKM elements, since these are varied in our scans. Since the hadronic parameters are extracted from global fits to lattice QCD calculations, they are correlated. During our analyses, there was a steady progress in extracting these numbers, such that we used the updated numbers for the later scans. For the analysis of the CHM with the SO(5)/SO(4) coset we used the results of [109] and assumed relative uncertainties of 10.2% for  $\Delta M_d$  and 7.6% for  $\Delta M_s$  with a correlation factor 0.17. In the more recent analysis of the SO(6)/SO(5) coset we implemented the results of [145]. For this we assumed relative uncertainties of 8% for  $\Delta M_d$  and 6% for  $\Delta M_s$  with a correlation factor 84.5%. The impact of the different theory errors<sup>12</sup> is illustrated in figure 3.7, where we compare the  $\chi^2$  contours for both cases.

To constrain the complex phases of  $M_{12}^{B_{d,s}}$  we include measurements of mixing phases. These are extracted as mixing-induced  $CP$  asymmetries in  $B_q$  decays into  $CP$  eigenstates. We include the process  $B_d \rightarrow J/\psi K_S$  for  $B_d$  and the decays  $B_s \rightarrow J/\psi K^+ K^-$  and  $B_s \rightarrow J/\psi \pi^+ \pi^-$  and the  $B_s$  system. In the SM these observables correspond to (combinations of) the angles of the unitary triangle. For  $S_{\psi K_S}$  we use the HFAG average [148]<sup>13</sup> while for  $\phi_s$  we use a combination provided by the LHCb collaboration [150],

$$S_{\psi K_S} = \sin \left( \arg \left( M_{12}^{B_d} \right) \right) = 0.682 \pm 0.019, \quad (3.56a)$$

$$\phi_s = \arg \left( M_{12}^{B_s} \right) = -0.010 \pm 0.039 \text{ rad}. \quad (3.56b)$$

These values correspond to an angle  $\phi_d = 43.0^\circ \pm 1.5^\circ$  and  $\phi_s = -0.6^\circ \pm 2.2^\circ$  for  $B_d$  and  $B_s$ , respectively. The extraction of these phases from  $CP$  asymmetries is plagued by additional contributions stemming from hard-to-calculate diagrams with penguin topologies. To account for this so-called penguin pollution [151] we include theoretical errors of  $0.68^\circ$  for  $B_d$  and  $1^\circ$  for  $B_s$ .

**K mesons:** In the  $K$  system the SM determination of the mass difference,

$$\Delta M_K = 2\text{Re} \left( M_{12}^K \right), \quad (3.57)$$

<sup>12</sup>The uncertainties can be estimated by naively adding in quadrature the uncertainties of the individual input parameters. In a more dedicated analysis, the uncertainties and correlation coefficients can be extracted by generating random numbers for the input parameters with a probability distribution taking into account the correlations provided by the lattice collaborations. This however results in similar numbers.

<sup>13</sup>The used value differs only minimally from the up-to-date value  $S_{\psi K_S} = 0.691 \pm 0.017$  given in [149].



is plagued by large hadronic uncertainties. Therefore, we take a conservative standpoint and allow the NP contribution to the mass difference to maximally saturate the experimental central value at  $1\sigma$ . To be concrete, we define the NP contribution as a ‘pseudo-observable’ which we constrain to

$$\Delta M_K^{\text{NP}} = (0 \pm 3.483) \times 10^{-15}. \quad (3.58)$$

Here, the uncertainty corresponds to the PDG average given in [110]. This procedure only sets a loose bound on the NP contribution, but it assures that no obscure fine-tuned cancellation between SM and NP contributions happens.

In contrast to the mass difference, indirect  $CP$  violation in the  $K$  system is theoretically under better control. The well-known  $\epsilon_K$  parameter acts as a constraint on the imaginary part of the mixing matrix element,

$$|\epsilon_K| = \kappa_\epsilon \frac{\text{Im}(M_{12}^K)}{\sqrt{2} \Delta M_K}, \quad (3.59)$$

where  $\kappa_\epsilon = 0.923$  parametrizes long-distance effects [152] and for  $\Delta M_K$  we use the experimental value. To account for uncertainties due to long-distance effects, hadronic parameters as well as the bad scale-dependence of the perturbative calculation we assume a theory error of 11% [153]. We take the PDG average for the experimental measurements [110],

$$|\epsilon_K|_{\text{exp}} = (2.228 \pm 0011) \times 10^{-3}. \quad (3.60)$$

**$D$  mesons:** In [65] it was shown that in CHMs with a weakly broken  $U(2)$  flavour symmetry, like in our setup, one cannot expect to find large effects in  $D^0$  mixing observables. Therefore, we refrain from using them as bounds in our analysis.

### Rare $B$ decays

Semi-leptonic  $b \rightarrow s$  transitions are a powerful tool for testing the SM and constraining NP scenarios. In the SM these flavour-changing neutral currents (FCNC) are strongly suppressed and only appear via loop-diagrams while in NP models these processes can already appear at tree-level such that SM and NP could be of comparable size. Thus, this is one of the first places where NP can show up and, turning the argument around, measurements of these processes give strong constraints on the parameter space of NP models.

The FCNC transitions  $b \rightarrow s$  are usually described by the weak Hamiltonian

$$\mathcal{H}_{\text{eff}} = \sum_{a=1}^6 C_a \mathcal{O}_a - \frac{4G_F}{\sqrt{2}} V_{tb} V_{ts}^* \sum_i C_i \mathcal{O}_i \quad (3.61)$$

where the operators  $\mathcal{O}_{a=1\dots 6}$  describe hadronic effects that should be unaffected by NP. Generally, in NP models one expects contributions to the effective operators  $\mathcal{O}_i$  which are given as

$$\mathcal{O}_7 = \frac{e}{16\pi^2} m_b (\bar{s}_L \sigma^{\mu\nu} b_R) F_{\mu\nu}, \quad \mathcal{O}'_7 = \frac{e}{16\pi^2} m_b (\bar{s}_R \sigma^{\mu\nu} b_L) F_{\mu\nu}, \quad (3.62a)$$

$$\mathcal{O}_8 = \frac{g_s}{16\pi^2} m_b (\bar{s}_L \sigma^{\mu\nu} T^a b_R) G_{\mu\nu}^a, \quad \mathcal{O}'_8 = \frac{g_s}{16\pi^2} m_b (\bar{s}_R \sigma^{\mu\nu} T^a b_L) G_{\mu\nu}^a, \quad (3.62b)$$

$$\mathcal{O}_9 = \frac{e^2}{16\pi^2} (\bar{s}_L \gamma_\mu b_L) (\bar{\mu} \gamma_\mu \mu), \quad \mathcal{O}'_9 = \frac{e^2}{16\pi^2} (\bar{s}_R \gamma_\mu b_R) (\bar{\mu} \gamma_\mu \mu), \quad (3.62c)$$

$$\mathcal{O}_{10} = \frac{e^2}{16\pi^2} (\bar{s}_L \gamma_\mu b_L) (\bar{\mu} \gamma_\mu \gamma_5 \mu), \quad \mathcal{O}'_{10} = \frac{e^2}{16\pi^2} (\bar{s}_R \gamma_\mu b_R) (\bar{\mu} \gamma_\mu \gamma_5 \mu), \quad (3.62d)$$

$$\mathcal{O}_S = \frac{e^2}{16\pi^2} m_b (\bar{s}_L b_R) (\bar{\mu} \mu), \quad \mathcal{O}'_S = \frac{e^2}{16\pi^2} m_b (\bar{s}_R b_L) (\bar{\mu} \mu), \quad (3.62e)$$

$$\mathcal{O}_P = \frac{e^2}{16\pi^2} m_b (\bar{s}_L b_R) (\bar{\mu} \gamma_5 \mu), \quad \mathcal{O}'_P = \frac{e^2}{16\pi^2} m_b (\bar{s}_R b_L) (\bar{\mu} \gamma_5 \mu). \quad (3.62f)$$

In CHMs (at least for the minimal coset  $SO(5)/SO(4)$ ) scalar operators are not generated, as there are no heavy scalars in the theory. The dipole operators  $\mathcal{O}_{7,8}^{(\prime)}$  encode flavour violating couplings of photons to SM quarks. These can be constrained by the dipole transition  $b \rightarrow s\gamma$ . For operators with

a vector structure there are many processes to which they contribute. Especially in the light of recent experimental anomalies in  $b \rightarrow s\ell\ell$  transitions (see section 6.5) we do not want to be too restrictive as we want to judge the ability to accommodate these effects in CHMs. For this reason we chose to impose only the rare decay  $B_s \rightarrow \mu^+\mu^-$  as a constraint on  $C_{10}^{(\prime)}$  and leave  $C_9^{(\prime)}$  basically unconstrained to give predictions for its possible size (given all other constraints).

### The dipole transition $b \rightarrow s\gamma$

The dipole transition  $b \rightarrow s\gamma$  is a powerful tool to constrain the dipole operators  $\mathcal{O}_7^{(\prime)}$  and  $\mathcal{O}_8^{(\prime)}$ . Since electromagnetism as well as QCD are good, unbroken gauge symmetries, these transitions (even for CHMs) first arise only at one-loop level. Analytical expressions for the Wilson coefficients in terms of loop functions are given in [154, Appendix B]. We include NP contributions stemming from fermion and vector resonances in the loop (where the latter is subdominant for most regions of parameter space [154]) as well as contributions originating from the non-linear structure of the pNGB Higgs.

According to our general rationale we interpret these contributions as Wilson coefficients at the high scale  $\mu_{\text{high}} = m_t$ , such that the RGE flow down to the low scale  $\mu_{\text{low}} = m_b$  has to be included. Considering LO QCD renormalization, there is mixing between the dipole operators [155, 154],<sup>14</sup>

$$\begin{pmatrix} C_7^{(\prime)}(\mu = m_b) \\ C_8^{(\prime)}(\mu = m_b) \end{pmatrix} = \begin{pmatrix} \eta_{\gamma\gamma} & \eta_{\gamma g} \\ 0 & \eta_{gg} \end{pmatrix} \begin{pmatrix} C_7^{(\prime)}(\mu = m_t) \\ C_8^{(\prime)}(\mu = m_t) \end{pmatrix}, \quad (3.63)$$

such that numerically

$$C_7^{(\prime)}(\mu = m_b) = 0.597C_7^{(\prime)}(\mu = m_t) + 0.318C_8^{(\prime)}(\mu = m_t). \quad (3.64)$$

Then, the branching ratio of the  $b \rightarrow s\gamma$  transition normalized to the SM value can be written as [156]

$$\frac{\text{Br}(b \rightarrow s\gamma)}{\text{Br}(b \rightarrow s\gamma)_{\text{SM}}} = \frac{|C_7^{\text{eff}}(\mu = m_b)|^2 + |C_7'(\mu = m_b)|^2 + N_\gamma}{|C_7^{\text{eff}}(\mu = m_b)_{\text{SM}}|^2 + N_\gamma}, \quad (3.65)$$

where  $N_\gamma = 3.6 \times 10^{-3}$  is a non-perturbative correction [157]. To obtain renormalization scheme independent expressions for the Wilson coefficients of dipole operators, one introduces the effective operators [158] (explicit formulae can be found e.g. in [159])

$$C_7^{\text{eff}}(\mu = m_b) = C_7(\mu = m_b) - 0.156 - 0.05387, \quad (3.66)$$

where the first numerical value is the NLO correction [155] and the second value was chosen to match the NNLO result given in [156]. We use the SM prediction [160]  $\text{Br}(b \rightarrow s\gamma)_{\text{SM}} = (3.36 \pm 0.23) \times 10^{-4}$ .

On the experimental side we use the present HFAG average [148]

$$\text{Br}(b \rightarrow s\gamma)_{\text{exp}} = (3.43 \pm 0.22) \times 10^{-4} \quad (3.67)$$

which is in very good agreement with the above SM prediction. We add the the experimental and theoretical uncertainties in quadrature. The resulting uncertainty of  $\sim 8\%$  leaves only little room for NP interfering with the SM.

### $B_s \rightarrow \mu^+\mu^-$

The rare decay  $B_s \rightarrow \mu^+\mu^-$  is an important probe for models beyond the SM as it is sensitive to scalar as well as vector effective operators. We will discuss the detailed structure of the branching ratio in greater detail in section 6.5, but here it suffices to remark that the structure of the dependence is given as follows (see e.g. [161])

$$\frac{\text{Br}(B_s \rightarrow \mu^+\mu^-)}{\text{Br}(B_s \rightarrow \mu^+\mu^-)_{\text{SM}}} = \frac{|(C_{10} - C'_{10}) + \kappa_1(C_P - C'_P)|^2 + |\kappa_2(C_S - C'_S)|^2}{|C_{10}^{\text{SM}}|^2}. \quad (3.68)$$

<sup>14</sup> As mentioned in [154] there is also the possibility of four-fermion operators mixing into the dipole operators. However, these contributions are suppressed by the composite-elementary mixings and therefore neglected.

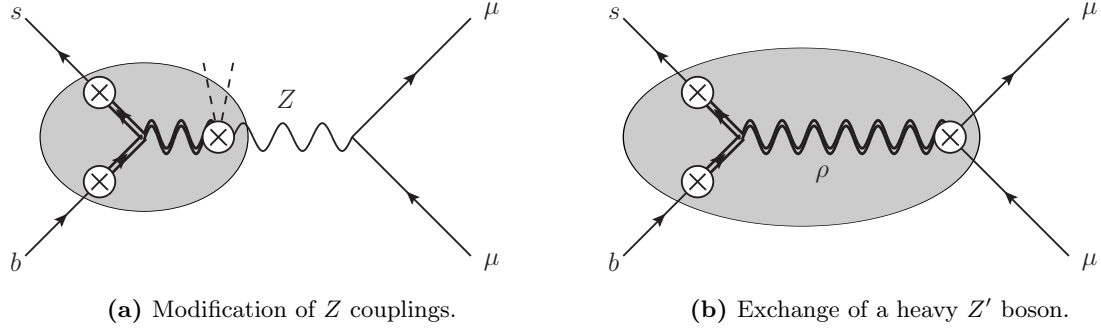


**Figure 3.8.:** Tree-level contributions to vector effective operators. There are two qualitatively different contributions: (a) through a change in the SM  $Z$  boson couplings or (b) through the exchange of a heavy vector resonance.

With  $\kappa_{1,2}$  we denote kinematic prefactors that enhance the contributions by scalar operators. However, as already mentioned above, scalar operators are not generated in this model, therefore one can write the correction of the branching ratio simply as

$$\frac{\text{Br}(B_s \rightarrow \mu^+ \mu^-)}{\text{Br}(B_s \rightarrow \mu^+ \mu^-)_{\text{SM}}} = \frac{|C_{10} - C'_{10}|^2}{|C_{10}^{\text{SM}}|^2}. \quad (3.69)$$

The SM prediction reads [162]

$$\text{Br}(B_s \rightarrow \mu^+ \mu^-)_{\text{SM}} = (3.65 \pm 0.23) \times 10^{-9}. \quad (3.70)$$

In the SM this FCNC process occurs only as a loop process and is heavily suppressed by the GIM mechanism. In CHMs the vector operators  $C_{10}$  and  $C'_{10}$  are, however, already generated at tree-level by the exchange of a heavy  $Z'$  boson or by modification of  $Z$  couplings to SM fermions (see figure 3.8) [163],

$$C_{bs\mu\mu} \sim -\frac{g_{Zbs}g_{Z\mu\mu}}{m_Z^2} - \sum_i \frac{g_{\rho_i bs}g_{\rho_i \mu\mu}}{m_{\rho_i}^2}. \quad (3.71)$$

**$Z$  exchange:** After EWSB the  $Z$  boson mixes with heavy resonances that couple to the composite admixtures of the SM quarks. This contribution is suppressed by a factor  $\frac{v^2}{f^2}$ . As the coupling between the  $Z$  and the leptons is SM like, one expects  $C_9^{(\prime)} \sim (1 - 4 \sin^2(\theta_w))C_{10}^{(\prime)} \approx 0.08C_{10}^{(\prime)}$ , such that this is mainly a contribution to  $C_{10}^{(\prime)}$ .

**$\rho$  exchange:** The exchange of a heavy vector resonance is suppressed by the heavy vector mass  $\frac{m_Z^2}{m_\rho^2} \sim \frac{g_0^2}{g_\rho^2} \frac{v^2}{f^2}$  and therefore formally of the same order as the  $Z$  exchange. However, there is an additional suppression by  $g_0^2/g_\rho^2$  which can be understood by the fact that the coupling of elementary leptons to the vector resonance has to go via mixing with elementary gauge bosons.

The RGE evolution of semi-leptonic four-fermion operators is known to be very mild as they are not renormalized by QCD [143] and QED renormalization is suppressed by  $\alpha_{\text{em}}$ . Therefore we neglect RGE running and treat these operators directly as generated at a suitable scale for  $B$  mesons.

Experimentally, the measured value for this decay [164],

$$\text{Br}(B_s \rightarrow \mu^+ \mu^-)_{\text{exp}} = (2.8_{-0.6}^{+0.7}) \times 10^{-9}. \quad (3.72)$$

as given in a combination of LHCb and CMS data agrees very well with the SM prediction.

### 3.3.6. Electric dipole moments

In CHMs with a mildly broken flavour symmetry the flavour structure is induced by the composite-elementary mixings (see section 2.2.3). Potentially, they can introduce a significant number of new  $CP$ -violating complex phases. Additionally, as will be seen in chapter 5, the effective potential can

generate a spontaneous breaking of  $CP$  if some  $CP$ -odd scalar field receives a vev. In such a case  $CP$ -violation should show up in the electric dipole moment of the neutron (nEDM).

The nEDM describes NP contributions to the imaginary parts of Wilson coefficients of dipole operators that are analogous to the operators  $\mathcal{O}_7^{(\prime)}$  and  $\mathcal{O}_8^{(\prime)}$  in (3.62) where only first-generation quarks are considered [165],

$$\mathcal{L} \subset -\frac{i}{2} \sum_{q=u,d} d_q^\gamma (\bar{q} \sigma^{\mu\nu} \gamma_5 q) F_{\mu\nu} - \frac{i}{2} \sum_{q=u,d} d_q^g (\bar{q} \sigma^{\mu\nu} \gamma_5 T^a q) G_{\mu\nu}^a. \quad (3.73)$$

In complete analogy with the calculation of  $b \rightarrow s\gamma$  in section 3.3.5 we calculate the relevant Wilson coefficients at the scale  $\mu_{\text{high}} = m_t$ . We use the RGE (3.3.5) to run the Wilson coefficients down to the low scale, this time the hadronic scale  $\mu_{\text{low}} = \mu_h = 1 \text{ GeV}$ . In terms of these Wilson coefficients the nEDM can be calculated as [165, 166, 154]

$$d_n = (1.0_{-0.7}^{+0.5}) [1.4 (d_d^\gamma(\mu_h) - 0.25 d_u^\gamma(\mu_h)) + 1.1e (d_d^g(\mu_h) + 0.5 d_u^g(\mu_h))] \frac{\langle \bar{q}q \rangle}{(225 \text{ MeV})^3}, \quad (3.74)$$

where the numerical factors are the outcome of QCD sum rules calculations [165]. With  $\langle \bar{q}q \rangle$  we denote the QCD quark condensate.

Experimentally the nEDM is quite strongly constrained [167],

$$d_n^{\text{exp}} = (-0.2 \pm 1.6) \times 10^{-26} e \text{ cm}, \quad (3.75)$$

and tiny. On the theory side there are large hadronic uncertainties, which is why we conservatively choose the low value 0.3 for the prefactor of the bracket in (3.74).

In principle, there could also be an effect on leptonic observables such as the electron EDM. But since we consider a purely elementary lepton sector this can only be generated at a higher loop level. For example, in the non-minimal model considered in chapter 5 which features an extended scalar sector, the electron EDM can be generated via a 2-loop Barr-Zee process [168]. We, however, find this observable to be subleading with respect to the nEDM, which is why we will not consider it further.

### 3.3.7. Contact interactions of light quarks

Until now we mostly put constraints on the degrees of compositeness of heavy quarks. But in some regions of parameter space also light quarks can have one chirality that might be strongly composite. This is particularly relevant for models with a  $U(3)^3$  flavour symmetry, since in that case the compositeness of the  $u$ -quark is directly linked to the one of the  $t$ -quark. If first-generation quarks are considerably composite then four-fermion operators (very similar to the  $\Delta F = 2$  operators discussed in section 3.3.5) are generated that contribute to the emission of jets in hadronic colliders. In particular, the angular distribution of dijet events at the LHC has proven to be a powerful tool in constraining these scenarios.

The angular distribution of dijet events is usually given in terms of the variable

$$\chi = \frac{1 + |\cos(\theta^*)|}{1 - |\cos(\theta^*)|}, \quad (3.76)$$

where  $\theta^*$  is the scattering angle in the dijet center-of-mass frame, in which the two jets are back-to-back. A low value of  $\chi \approx 1$  means a scattering orthogonal to the beam axis, while a larger value describes scattering more alongside the beam direction. Then, the dijet cross section for emission into a specific range of  $\chi$  is a helpful observable.

Experiments usually quote their results as bounds on the compositeness scale assuming that only a single NP operator is present. In a full treatment, however, a large number of four-quark operators is actually active. Therefore, to include the effects of other operators we make use of the LO calculation of the dijet cross section. This can be used to obtain a bound on dijet events that is independent of normalization (such as  $k$ -factors), thus exactly reproducing the experimental bound (which was obtained using NLO simulations) but including also other four-quark operators. The LO calculation of the dijet cross section into a given  $\chi$ -bin was performed in [169]. For this one needs the effective Hamiltonian for  $uu \rightarrow uu$ ,  $dd \rightarrow dd$  and  $ud \rightarrow ud$  transitions<sup>15</sup>

$$\mathcal{H}_{\text{eff}} = \sum_i \frac{c_i}{\Lambda^2} \mathcal{O}_i + \text{h.c.} \quad (3.77)$$

<sup>15</sup>Here one only considers quarks of the first generation as contributions from higher generations are suppressed by the parton distribution functions.

with

$$\mathcal{O}_{uu}^{(1)} = (\bar{u}_R \gamma_\mu u_R) (\bar{u}_R \gamma^\mu u_R), \quad \mathcal{O}_{dd}^{(1)} = (\bar{d}_R \gamma_\mu d_R) (\bar{d}_R \gamma^\mu d_R), \quad (3.78a)$$

$$\mathcal{O}_{ud}^{(1)} = (\bar{u}_R \gamma_\mu u_R) (\bar{d}_R \gamma^\mu d_R), \quad \mathcal{O}_{ud}^{(8)} = (\bar{u}_R \gamma_\mu \Gamma^A u_R) (\bar{d}_R \gamma^\mu \Gamma^A d_R), \quad (3.78b)$$

$$\mathcal{O}_{qq}^{(1)} = (\bar{q}_L \gamma_\mu q_L) (\bar{q}_L \gamma^\mu q_L), \quad \mathcal{O}_{qq}^{(8)} = (\bar{q}_L \gamma_\mu \Gamma^A q_L) (\bar{q}_L \gamma^\mu \Gamma^A q_L), \quad (3.78c)$$

$$\mathcal{O}_{qu}^{(1)} = (\bar{q}_L \gamma_\mu q_L) (\bar{u}_R \gamma^\mu u_R), \quad \mathcal{O}_{qu}^{(8)} = (\bar{q}_L \gamma_\mu \Gamma^A q_L) (\bar{u}_R \gamma^\mu \Gamma^A u_R), \quad (3.78d)$$

$$\mathcal{O}_{qd}^{(1)} = (\bar{q}_L \gamma_\mu q_L) (\bar{d}_R \gamma^\mu d_R), \quad \mathcal{O}_{qd}^{(8)} = (\bar{q}_L \gamma_\mu \Gamma^A q_L) (\bar{d}_R \gamma^\mu \Gamma^A d_R). \quad (3.78e)$$

Then, the NP contribution to the dijet cross section into a range  $\chi < \chi_0$  and with a cut on the invariant dijet mass  $m_{jj} > m_{jj}^{\text{cut}}$  can be written as

$$\sigma_{jj}^{\text{NP}} (\chi < \chi_0, m_{jj} > m_{jj}^{\text{cut}}) = \int_1^{\chi_0} d\chi \int_{m_{jj}^{\text{cut}}}^s d\hat{s} \int_{Y_{\text{min}}}^{Y_{\text{max}}} dY \, x_1 f_1(x_1) x_2 f_1(x_2) \left. \frac{d\sigma_{\text{part}}}{d\hat{t}} \frac{\hat{t}^2}{\hat{s}^2} \right|_{\substack{x_{1,2} = \sqrt{\frac{\hat{s}}{s}} \exp(\pm Y) \\ \hat{t} = -\hat{s}/(1+\chi)}}, \quad (3.79)$$

where the partonic cross section can be found in [169] and  $f_i(x)$  denote parton distribution functions. The integrations can be done numerically, leading to

$$\sigma_{jj}^{\text{NP}} (\chi < \chi_0, m_{jj} > m_{jj}^{\text{cut}}) = -\frac{1}{\Lambda^2} \vec{\mathcal{P}} \cdot \vec{A}(c_i) + \frac{1}{\Lambda^4} \vec{\mathcal{Q}} \cdot \vec{B}(c_i), \quad (3.80)$$

where the vectors  $\vec{A}(c_i)$  and  $\vec{B}(c_i)$  are specific combinations of Wilson coefficients given in [169, eq. (11)], while the elements of  $\vec{\mathcal{P}}$  and  $\vec{\mathcal{Q}}$  are purely numerical factors, that depend on the details of the particular experimental analysis. This form is suitable for implementation in our numerical scan.

As stated above, the experiments usually do not give their results in terms of the above cross section, but they rather assume a NP model where only one of the operators (3.78) is active (usually they choose  $c_{qq}^{(1)}$ ) and give a 95% CL bound on the NP scale  $\Lambda$  for a fixed value of the Wilson coefficient. We can calculate the cross section that corresponds to the bound on  $c_{qq}^{(1)}/\Lambda^2$  and we use this as 95% CL upper bound on  $\sigma_{jj}^{\text{NP}}$  as calculated above.<sup>16</sup> To cope with the fact that only an upper bound is given (while a  $\chi^2$  functions usually contains measurements, i.e. a central value with some error interval) we include the bound on the cross section as a ‘pseudo-measurement’ which is centered around 0 and has an uncertainty of half the experimental upper bound.

Contrary to meson-antimeson mixing, contact interactions involve much higher energies. While e.g.  $B$  mixing has an energy scale of around the  $b$  mass, the processes leading to dijet events happen at energies that are of the order of the hadronic collisions, i.e. possibly of the order of several TeV. Since the effective theory approach is basically an expansion in  $p^2/\Lambda_{\text{NP}}^2$  (where  $p$  is the energy scale of the contact interaction) this raises the question whether it is meaningful to extract constraints on the EFT coefficients if the expansion parameter is not small and, in principle, higher order corrections should be taken into account. In fact, the analysis in [170] suggests that in such a case the constraints are considerably weaker than a naive analysis would suggest. We take this into account and use the prescription given in that reference. We rescale each individual contribution to the four-quark operators by a factor  $(1 + (1.3 \text{ TeV})^2/m_\rho^2)^{-2}$ , where  $m_\rho$  is the mass of the exchanged heavy resonance. The numerical factor is an estimation obtained by analyzing toy models in [170]. The effect of this approach is that contributions from lighter resonances are weakened such that their bounds are not overestimated.

In our numerical scan we used an analysis provided by ATLAS [171] using  $17.3 \text{ fb}^{-1}$  of run 1 data. Prior to the scan of the non-minimal CHM an ATLAS analysis [172] using  $3.6 \text{ fb}^{-1}$  of run 2 data became available. We give details on the used analyses in Table 3.4.

### 3.3.8. Direct searches at colliders

Besides the above indirect constraints on the parameter space very important constraints on the theory come from direct searches for new particles at colliders. If they are sufficiently light and they have

<sup>16</sup>Note that by doing this, the absolute normalization of the cross section (such as missing  $k$ -factor in the LO calculation) drop out and we obtain a bound that is independent from global rescaling factors.

analysis	$\sqrt{s}$	$\int dt \mathcal{L}$	$\chi^0$	$m_{jj}^{\text{cut}}$	bound on $\Lambda$	$\sigma_{jj}^{95\% \text{ CL}}$
ATLAS [171]	8 TeV	17.3 fb <sup>-1</sup>	$\chi < 3.32$	$m_{jj} > 3.2$ TeV	12.0 TeV	0.28 pb
ATLAS [172]	13 TeV	3.6 fb <sup>-1</sup>	$\chi < 2$	$m_{jj} > 5.4$ TeV	17.5 TeV	0.06 pb

**Table 3.4.:** Details on the used experimental analyses of the dijet angular distribution. From left to right we give the center-of-mass energy and the integrated luminosity. This is followed by the cuts on the angular parameter  $\chi$  and the dijet mass  $m_{jj}$ . Lastly we quote the given bound on the NP scale  $\Lambda$  (assuming  $c_{qq}^{(1)} = 2\pi$ ) as well as the corresponding 95% CL bound on the NP cross section.

non-negligible couplings to the SM sector, the composite resonances should show up at these direct searches. An analysis of direct constraints on CHMs is usually performed assuming couplings only to 3rd generation SM quarks. In this work we want to include these searches in a more general way since we are considering full flavour structures such that there can be several relevant decay channels. To this end, we calculate all branching ratios for all resonances into all experimentally relevant channels and compare them to the recent exclusion limits provided by the experiments. Here, we only very briefly review our approach. For a more elaborated discussion we refer to [28].

In experimental searches one is looking for resonances that can be either heavy vector-like quarks, heavy vector bosons or (in the case of a non-minimal scalar sector) heavy scalars. The resonances have to decay in to SM particles since only these are visible to the detector.

**Quark partners** To produce a signature that is detectable<sup>17</sup> by the experiments a heavy fermion resonance has to decay into a SM fermion and a SM boson, i.e. either a Higgs or an electroweak vector boson. In principle, there are three sources the fermion resonance can come from: It can be produced singly or as a pair, or can be part of a cascade decay in which it was produced by another even heavier resonance. Out of these possibilities only the pair production is model-independent. The other two production channels depend on the detailed couplings of the resonances and can therefore not be implemented efficiently into our scan. We will thus only consider the case of pair production from gluons and take the conservative standpoint that we ignore constraints originating from the other production mechanisms. In this case the production rate only depends on the value of the strong coupling constant and the mass of the resonance. Since we do not assume any significant deviation in the strong coupling, the production is determined only by the resonance mass and it is calculated at NNLO in QCD using *Hathor* [173].

Direct searches in the relevant channels have been performed by ATLAS and CMS but also by CDF at Tevatron and there exist old bounds from LEP. A complete list of the used channels can be found in [4, Table 2] and [3, Table 1].

**Vector resonances** At hadron colliders heavy vector resonances  $\rho$  are singly produced via a Drell-Yang-like process with a hadronic cross section

$$\sigma(pp \rightarrow \rho) = \frac{4\pi^2}{3} c_\rho \sum_{q_1, q_2} \frac{\Gamma(\rho \rightarrow q_1 \bar{q}_2)}{s m_\rho} \mathcal{L}_{q_1 \bar{q}_2}. \quad (3.81)$$

In this expression the narrow width approximation (NWA) was employed to account for the parton distribution functions via the parton luminosities

$$\mathcal{L}_{q_1 \bar{q}_2} = \int_{\hat{s}/s}^1 \frac{dx}{x} f_{q_1}(x) f_{\bar{q}_2}(\hat{s}/(xs)), \quad (3.82)$$

and the coefficient  $c_\rho$  in (3.81) is a color factor whose value depends on whether the resonance is a heavy gluon or a partner of an electroweak gauge boson. The advantage of using the NWA is that the parton luminosities can be calculated and stored model-independently allowing for a fast computation of the full hadronic cross section which is essential for a numeric scan. To be

<sup>17</sup>We neglect the possibility of cascade decays of heavy resonances into SM fields and other resonances, since such a signature is hard to be included in our framework.

visible in the detector, the heavy vector resonances can decay either into a pair of SM fermions or SM bosons. Complete lists of the used decay channels are provided in [4, Table 3] and [3, Table 3].

A problem appears if the decay into two fermion resonances is kinematically allowed. Since fermion and vector resonances are strongly coupled to each other this case would lead to very broad resonances that can no longer be captured in the experimental analyses. Therefore, we only include the constraints from direct searches if  $\Gamma_\rho/m_\rho < 5\%$ . This goes along with our general philosophy of being conservative.

**Heavy scalars** In the non-minimal CHM to be considered in chapter 5 the Higgs sector is non-trivial and a heavy composite scalar appears. In general, heavy scalars have similar production modes as the Higgs. At hadron colliders the dominant production is via gluon fusion. But we also consider production directly from quark-antiquark pairs as well as vector boson fusion (VBF). The production cross section can be calculated similarly to the case of a heavy vector resonance. For VBF we employ the ‘effective  $W$  approximation’ [174, 175, 176, 177] to treat the electroweak vector bosons as ‘partons’, such that parton distribution functions can be defined for them.

A heavy scalar resonance can decay into pairs of SM fermion or bosons. In particular, direct searches for the decay into two Higgs bosons are available. A complete list of the decay channels considered can be found in [3, Table 2]. We note that in the non-minimal model of chapter 5 the scalar resonance is a pNGB such that it is relatively light and therefore a decay into heavy resonances is kinematically not allowed for the most parameter points.

To evaluate the compatibility of one parameter point with direct searches we now use the following approach. For each resonance  $R$  we calculate the production cross section as well as the partial widths  $\Gamma(R \rightarrow x)$  for the decays into all possible final states  $x$ . For some particular channel  $R \rightarrow X$  the branching ratio of  $R$  is then calculated via

$$\text{Br}(R \rightarrow X) = \frac{\Gamma(R \rightarrow X)}{\sum_x \Gamma(R \rightarrow x)}. \quad (3.83)$$

The experimental collaborations usually give their results as so-called ‘brazil band plots’, i.e. 95% CL upper bounds on the product  $\sigma_{\text{prod}} \times \text{Br}_{\text{decay}}$  for a resonance in a mass range typically between a few hundred GeV and a few TeV. For producing the plots the experiments usually assume  $\text{Br}_{\text{decay}} = 1$  for the particular channel. This means that the experimental bounds have to be rescaled by the value of the theoretical branching ratio such that they can be compared to the  $\sigma_{\text{prod}} \times \text{Br}_{\text{decay}}$  predicted for a particular parameter point.<sup>18</sup> We digitize these plots using the package `svg2data` [178], which extracts the exact experimental numbers from a vector-graphics file.

To be able to judge the viability of a parameter point we define a  $\chi^2$  function in the following way. One can interpret the experimental 95% CL bounds as ‘measurements’ which give  $\sigma_{\text{prod}} \times \text{Br}_{\text{decay}} = 0$  and have an uncertainty that at the  $2\sigma$ -level coincides with the quoted bound  $\mathbf{B}(m_R)$  for the mass  $m_R$  of the resonance. Then, the  $\chi^2$  takes the form

$$\chi^2 = \left( \frac{(\sigma\text{Br})_{\text{exp}} - (\sigma\text{Br})_{\text{theo}}}{\text{uncertainty}} \right)^2 = \left( \frac{0 - (\sigma\text{Br})_{\text{theo}}}{\mathbf{B}(m_R)/2} \right)^2 = 4 \frac{(\sigma\text{Br})_{\text{theo}}^2}{\mathbf{B}(m_R)^2} \quad (3.84)$$

In this approach  $\chi^2 = 4$  means that the theory prediction lies directly on the experimental limit corresponding to a 95% CL exclusion. The so-defined  $\chi^2$  function still depends on the resonance and on the particular decay channel. We group the experimental analyses according to the experiment, the center-of-mass energy and the spins of the resonances and calculate for each group the maximum of all  $\chi^2$  for all resonances and all channels. This gives us a set of combined  $\chi^2$  values for each experiment, each LHC run and each resonance spin, which we assume to be uncorrelated and on which we can separately apply the  $\chi^2 < 9$  cut (3.6).

	non-linearity $f$	flavour mixing	electro- weak	light quark LH dipoles	quark compositeness 4quark	heavy quark dipoles	quark compositeness 4quark	semilept.	$CP$ V	quark resonances	vector resonances mass	Br	scalar resonances mass	resonances mixing
<b>SM</b>														
CKM		✓		✓										
gauge couplings			✓ (tree)											
$T$			✓ (loop)											
$S$											✓			
$Z$ width				✓	✓		✓	✓						
Higgs decays	✓													✓
<b>Flavour</b>														
meson mixing		✓					✓							
$b \rightarrow s\gamma$		✓						✓						
$B_s \rightarrow \mu\mu$		✓						✓						
nEDM					✓				✓					✓
contact interactions						✓								
<b>direct</b>														
spin- $\frac{1}{2}$										✓				
spin-1											✓	✓		
spin-0													✓	

Table 3.5.: This table summarizes which constraint is sensitive to what aspect of CHMs.



---

## 3.4. Summary

In this chapter we presented our general strategy for constraining the parameter spaces of composite Higgs models. Our approach is a completely numerical parameter scan that does not make use of analytical approximations. By this we have the power to include special cases that are not accessible using approximate formulae. A software framework was developed in the programming language Python that takes as input general mass and coupling matrices, rotates them into the physical mass basis and uses these as input for the calculation of observables. As an important step our code includes the calculation and minimization of the one-loop effective Coleman-Weinberg potential, which is essential for including a realistic EWSB into the analysis.

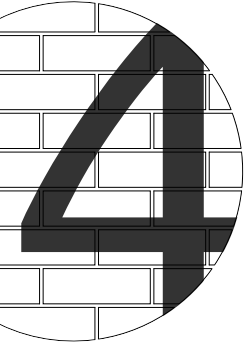
Viable parameter points were generated utilizing a least-squares fit in which the problem reduces to finding the minima of a  $\chi^2$  function on the parameter space of the model. For an efficient scanning result we employed a two-staged approach in which a global minimization tool is used to burn-in into a good parameter region and after that adaptive Markov chains were used to sample the parameter space.

Although the above code is fairly model-independent the included experimental constraints were chosen to obtain bounds covering all model aspects of CHMs in the best possible way. The included constraints are summarized in table 3.5.

---

<sup>18</sup>For the quark resonances there is a subtlety: As they are assumed to be pair-produced, the experiments can either assume that one or both resonances decay in a particular channel, which changes the corresponding rescaling factor. This, however, depends on the analysis under consideration.





## SO(5)/SO(4) – the minimal model

After introducing CHMs on rather general grounds in chapter 2 and presenting our general strategy for an analysis in chapter 3 we are now in the position to conduct dedicated numerical analyses of CHMs. In the following chapter we investigate a well-motivated model that is minimal in the number of newly introduced free parameters as well as in the number of appearing NP states. At the same time the considered model is fully realistic as it includes the complete flavour structure as well as a calculable EWSB and avoids dangerous corrections to EWPOs.

In the following we will first introduce the concrete model which we are investigating and which is the minimal version of the construction described in 2.3. After that we immediately discuss the results of the analysis. These are large collections of parameter points that fulfill all experimental constraints imposed on the model. We present the results as scatter plots of the viable parameter points such that the magnitude of possible NP effects in physical observables becomes visible. Our discussions of results will include EWSB and fine-tuning, mass spectra for the heavy resonances, an identification of the strongest experimental bounds (such that an increase in experimental accuracy in these observables can efficiently reduce the allowed parameter space in the future) as well as modifications of observables in Higgs and flavour physics.

### 4.1. The minimal 4d composite Higgs model

In this section we introduce the so-called *minimal 4d composite Higgs model* (M4dCHM) by De Curtis, Redi and Tesi [99], which is the minimal version of the dimensionally deconstructed model introduced in section 2.3, and generalize it to include a full flavour structure. This model will be the subject of the following analysis. The minimal model has the advantage that it is still realistic in the sense that the Higgs potential is calculable and severe phenomenological constraints are avoided. In the following chapter 5 we will generalize this model to the next-to-minimal case. For a more detailed discussion of the model we refer the interested reader to the original publication [99] and for a broader context which includes the relation to similar models a good reference is given by [55].

#### Bosonic part

As discussed in section 2.2.1 the minimal coset featuring a custodial protection of EWPO's and  $Z$  couplings as well as a  $SU(2)_L$  doublet NGB-Higgs is given by  $SO(5)/SO(4)$ . Including also QCD and hypercharge this means that we will work with a group  $\mathcal{G}_{\text{big}} = SU(3)_c \times SO(5) \times U(1)_X$  broken down to  $\mathcal{H}_{\text{big}} = SU(3)_c \times SO(4) \times U(1)_X$ . By interacting with a SM-like elementary sector these symmetries will subsequently break down spontaneously to  $SU(3)_c \times U(1)_{\text{em}}$  by strong dynamics.

Although at first sight it might appear to be a very crude approximation, this model has the feature that realistic physics is already reproduced by a maximal discretization. This means that, one can go to the extreme case and approximate the extra-dimensional theory by only *two* sites, which we will refer to as the elementary and the composite site. Hence, we will be dealing with the SM supplemented by only one level of composite resonances. Along the lines of section 2.3.3 the minimal symmetry structure is depicted in figure 4.1. The model consists of two non-linear  $\sigma$ -models, one of which describes a coset  $(SO(5)_L^1 \times SO(5)_R^1) / SO(5)_{L+R}^1$  with NGBs  $\Omega_1$  while the other represents the breaking  $SO(5)/SO(4)$  with a NGB matrix  $\Omega^*$ , where for the sake of simplicity we did not write explicitly the  $SU(3) \times U(1)_X$  components. The symmetries  $SO(5)_R^6$  and  $SO(5)$  are gauged to their diagonal group to form a site of composite resonances. Without elementary fields this model still

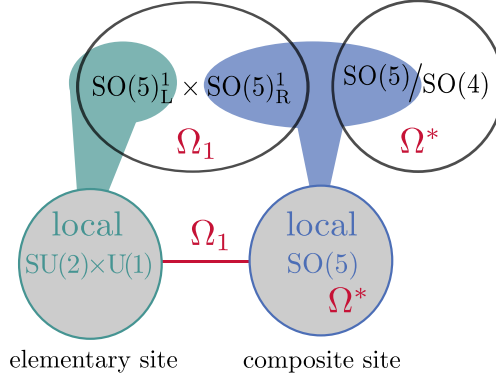


**Figure 4.1.:** Symmetry pattern of the M4dCHM with two sites. There is an elementary sector and one level of composite resonances  $\rho_\mu$ , interacting with each other via a link field  $\Omega_1$ . The symmetry breaking  $\text{SO}(5)/\text{SO}(4)$  is parametrized by the Goldstone matrix  $\Omega^*$ . This is the minimal version of the structure shown in figure 2.6.

features a global symmetry breaking structure  $\text{SO}(5)_L^1/\text{SO}(4)$  which is parametrized by  $\mathcal{U} = \Omega_1 \Omega^*$  which is the NGB matrix defined in (2.128).

Associated with the composite site there are heavy vector resonances  $\rho_\mu^A$  which are described as gauge bosons. Because of this they are adjoints of  $\text{SO}(5)$  such that they can be written as

$$\underbrace{\rho_\mu^A}_{\mathbf{10}} = \underbrace{\rho_{L\mu}^a \mathbb{T}_L^a}_{(\mathbf{3},\mathbf{1})} + \underbrace{\rho_{R\mu}^a \mathbb{T}_R^a}_{(\mathbf{1},\mathbf{3})} + \underbrace{\alpha_\mu^{\hat{a}} \mathbb{T}_{(\mathbf{2},\mathbf{2})}^{\hat{a}}}_{(\mathbf{2},\mathbf{2})}, \quad (4.1)$$

where we decomposed them into  $\text{SO}(4) = \text{SU}(2)_L \times \text{SU}(2)_R$  components and the  $(\mathbf{3}, \mathbf{1})$  components have the right quantum numbers to act as heavy partners of the  $W_\mu$  bosons. Also at the composite site there are gauge symmetries connected with color and the  $U(1)_X$  such that heavy gluons  $\rho_{G\mu}$  and  $X_\mu$  resonances appear.

On the elementary site in figure 4.1 the global  $\text{SO}(5)_L^1$  interacts with SM-like elementary fields such that the global symmetries are gauged down to  $\text{SU}(2) \times \text{U}(1)$ . As a consequence, the elementary gauge fields directly interact with the  $\sigma$ -model field  $\Omega_1$  which transmits the interactions to the composite sector and therefore induces partial compositeness for the vector bosons.

Putting everything together, the effective Lagrangian of the boson sector is written as

$$\mathcal{L}_{\text{boson}} = \mathcal{L}_{\text{gauge}} + \mathcal{L}_{\text{NGB}}, \quad (4.2)$$

which is the minimal version of the general Lagrangian (2.130). Here, the gauge Lagrangian,

$$\begin{aligned} \mathcal{L}_{\text{gauge}} &= -\frac{1}{4} \text{tr} [G_{\mu\nu}^0 G^{\mu\nu}] - \frac{1}{4} \text{tr} [W_{\mu\nu}^0 W_0^{\mu\nu}] - \frac{1}{4} B_{\mu\nu}^0 B_0^{\mu\nu} && \text{(elementary)} \\ &- \frac{1}{4} \text{tr} [\rho_{G\mu\nu} \rho_G^{\mu\nu}] - \frac{1}{4} \text{tr} [\rho_{\mu\nu} \rho^{\mu\nu}] - \frac{1}{4} X_{\mu\nu} X^{\mu\nu} && \text{(composite)} \\ &+ \frac{f_G^2}{4} (g_3^0 G_\mu^0 - g_{\rho 3} \rho_{G\mu})^2 + \frac{f_X^2}{4} (g'_0 B_\mu^0 - g_X X_\mu)^2, && \text{(mixing)} \end{aligned} \quad (4.3)$$

contains kinetic terms for the elementary gauge fields and heavy vector resonances. Further, we explicitly included mass terms that act as composite-elementary mixings for composite gluon and  $X_\mu$  resonances with their elementary counterparts. These depend on effective scales  $f_G$  and  $f_X$  as well as on effective gauge couplings  $g_{\rho 3}$  and  $g_X$  and were chosen to closely resemble the general form (2.33). The coupling strength of the resonances associated with  $\text{SO}(5)$  is denoted by  $g_\rho$ . For the Goldstone fields the Lagrangian takes the form given in (2.130) which in its minimal version reduces to

$$\mathcal{L}_{\text{NGB}} = \frac{f_1^2}{4} \text{tr} [(\mathcal{D}_\mu \Omega_1)^\dagger (\mathcal{D}^\mu \Omega_1)] + \frac{f_2^2}{2} [(\mathcal{D}_\mu \Omega^*)^\dagger (\mathcal{D}^\mu \Omega^*)]_{55}. \quad (4.4)$$

While the link field  $\Omega$  couples to elementary as well as to composite vectors, the other NGB matrix  $\Omega^*$  only has interactions with the composite spin-1 resonances. Both fields do not interact with colour

or  $X_\mu$  resonances as these are not part of the underlying symmetry breaking structure. Therefore, the covariant derivatives of the  $\sigma$ -model fields are given as

$$\mathcal{D}_\mu \Omega_1 = \partial_\mu \Omega_1 - i (g_0 W_\mu^{0a} \mathbb{T}_L^a + g'_0 B_\mu^0 \mathbb{T}_R^3) \Omega_1 + i g_\rho \Omega_1 \rho_\mu, \quad (4.5a)$$

$$\mathcal{D}_\mu \Omega^* = \partial_\mu \Omega^* - i g_\rho \rho_\mu \Omega^*. \quad (4.5b)$$

In the following we adopt the holographic gauge (2.132),

$$\Omega_1(x) = \mathcal{U} = \exp \left[ i \frac{\sqrt{2}}{f_1} \pi_{\hat{a}}(x) \mathbb{T}^{\hat{a}} \right] \quad \text{and} \quad \Omega^*(x) = \mathbb{1}_5. \quad (4.6)$$

This moves all dependencies on the NGB fields of the  $\text{SO}(5)/\text{SO}(4)$  breaking to the left link field such that composite-elementary mixings proceed through insertions of  $\mathcal{U}$ . Note further that in this gauge the NGBs associated with the breaking of  $(\text{SO}(5)_R^1 \times \text{SO}(5)) / \text{SO}(5)_{\text{diag}}$  through gauging are absent. In this gauge the NGB matrix takes the form

$$\mathcal{U} := \exp \left[ i \frac{\sqrt{2}}{f_1} \pi_{\hat{a}}(x) \mathbb{T}^{\hat{a}} \right] = \begin{pmatrix} 1 & & & & \\ & 1 & & & \\ & & 1 & & \\ & & & \cos \left( \frac{h(x)}{f_1} \right) & \sin \left( \frac{h(x)}{f_1} \right) \\ & & & -\sin \left( \frac{h(x)}{f_1} \right) & \cos \left( \frac{h(x)}{f_1} \right) \end{pmatrix}, \quad (4.7)$$

where the SM unitary gauge was used to set  $\pi_{\hat{a}}(x) = (0, 0, 0, h(x))$ .

Writing the Lagrangian as above in holographic gauge leads to a mixing term between the Higgs and the fourth component of the coset vector resonances of the form

$$\frac{1}{\sqrt{2}} g_\rho f_1 \mathbf{a}_4^\mu \partial_\mu h. \quad (4.8)$$

One can get rid of this term by a field redefinition,

$$\mathbf{a}_4^\mu \rightarrow \mathbf{a}_4^\mu - \frac{\sqrt{2}}{g_\rho} \frac{f}{f_2^2} \partial^\mu h, \quad h \rightarrow \frac{f_1}{f} h, \quad (4.9)$$

where  $f$  is given by  $f^{-2} := f_1^{-2} + f_2^{-2}$ . By this transformation the mixing term vanishes and the composite Higgs kinetic term gets canonically normalized. This is a general phenomenon in non-linear  $\sigma$ -model with gauge symmetries that was already mentioned in the early paper [33]. As a result, all dependencies on the Higgs field are given via

$$s_h = \sin \left( \frac{h}{f} \right). \quad (4.10)$$

The above Lagrangian leads to the mass mixing matrices given in appendix III.1.1.

## Fermionic part

We now include the fermionic states. As we are considering the case of only two sites, this is just the minimal version of (2.133) with elementary fields and one level of composite resonances living in the fundamental representation of  $\text{SO}(5)$ , where the fundamental was chosen as this can give a custodial protection of  $Z$  couplings (rf. section 2.2.1). Under the  $\text{SO}(4)$  subgroup this decomposes into a bidoublet  $Q$  and a singlet  $S$ ,  $\mathbf{5} = (\mathbf{2}, \mathbf{2}) \oplus (\mathbf{1}, \mathbf{1})$ . When using the basis of generators introduced in appendix I.1, the singlet can be placed in the 5th component and then the whole 5-plet is written as

$$\mathbf{5} = \left( \begin{bmatrix} Q^{++} & Q^{+-} \\ Q^{-+} & Q^{--} \\ S^{00} \end{bmatrix} \right), \quad (4.11)$$

where the indices are used to denote the quantum numbers under  $\hat{\mathbb{T}}_L^3$  and  $\hat{\mathbb{T}}_R^3$ . Eventually, the explicit breaking of global symmetries in the fermion sector is introduced by embedding the elementary chiral

states into incomplete fundamentals of  $\text{SO}(5)$  in such a way that the SM gauge group is respected but  $\text{SO}(4)$  is explicitly broken. Therefore, the left-handed quark doublets have to be included as the  $\text{SU}(2)_L$ -doublet components of the  $\mathbf{5}$ , while the right-handed singlet states are implemented as the singlet components. By the definition of hypercharge in these models (2.123), the quantum numbers of the  $\text{U}(1)_X$ -symmetry are already fixed to  $q_X = \frac{2}{3}$  and  $q_X = -\frac{1}{3}$  for up- and down-type quarks, respectively. Then, the embeddings of the elementary quarks are written as (see section I.1)

$$q_L^0 \rightarrow \xi_{uL} = \left( \begin{bmatrix} 0 & u_L^0 \\ 0 & d_L^0 \\ & 0 \end{bmatrix} \right) = \frac{1}{\sqrt{2}} \begin{pmatrix} d_L^0 \\ -i d_L^0 \\ u_L^0 \\ i u_L^0 \\ 0 \end{pmatrix}, \quad q_L^0 \rightarrow \xi_{dL} = \left( \begin{bmatrix} u_L^0 & 0 \\ d_L^0 & 0 \\ & 0 \end{bmatrix} \right) = \frac{1}{\sqrt{2}} \begin{pmatrix} u_L^0 \\ i u_L^0 \\ -d_L^0 \\ i d_L^0 \\ 0 \end{pmatrix}, \quad (4.12a)$$

$$u_R^0 \rightarrow \xi_{uR} = \left( \begin{bmatrix} 0 & 0 \\ 0 & 0 \\ & u_R^0 \end{bmatrix} \right) = \begin{pmatrix} 0 \\ 0 \\ 0 \\ 0 \\ u_R^0 \end{pmatrix}, \quad d_R^0 \rightarrow \xi_{dR} = \left( \begin{bmatrix} 0 & 0 \\ 0 & 0 \\ & d_R^0 \end{bmatrix} \right) = \begin{pmatrix} 0 \\ 0 \\ 0 \\ 0 \\ d_R^0 \end{pmatrix}. \quad (4.12b)$$

Here we explicitly used the fact the left-handed quarks can be embedded in both,  $\xi_{uL}$  and  $\xi_{dL}$  (see the discussion below eq. (2.124)).

The composite resonances have to come in  $\text{SO}(5)$  fundamentals with the same  $\text{U}(1)_X$  charge assignment in order to be able to mix with the elementary states. Then, written in components, one has

$$\Psi_u = \left( \begin{bmatrix} Q_{\frac{5}{3}} & Q_{\frac{2}{3}} \\ Q_{\frac{2}{3}} & Q_{-\frac{1}{3}} \\ & S_{\frac{2}{3}} \end{bmatrix} \right) \in \mathbf{5}_{\frac{2}{3}}, \quad \Psi_d = \left( \begin{bmatrix} Q_{\frac{2}{3}} & Q_{-\frac{1}{3}} \\ Q_{-\frac{1}{3}} & Q_{-\frac{4}{3}} \\ & S_{-\frac{1}{3}} \end{bmatrix} \right) \in \mathbf{5}_{-\frac{1}{3}}. \quad (4.13)$$

Here, the indices denote the electromagnetic charges after EWSB given by

$$Q = \mathbb{T}_L^3 + Y = \mathbb{T}_L^3 + \mathbb{T}_R^3 + X. \quad (4.14)$$

This shows that the physical spectrum contains states of exotic charges  $q = \frac{5}{3}$  and  $q = -\frac{4}{3}$ .

As seen for the extra-dimensional model in section 2.3, left-handed elementary fields mix with a fundamental  $\Psi$ , while the right-handed states mix with a fundamental  $\tilde{\Psi}$  (rf. eq. (2.124)). With this in mind it is now possible to write down the most general form of the fermion Lagrangian in which the composite sector is invariant under a coset  $\text{SO}(5)/\text{SO}(4)$  that is broken explicitly only by the couplings to the elementary sector:

$$\mathcal{L}_{\text{fermion}} = \mathcal{L}_{\text{fermion}}^{(\text{elem})} \quad (4.15a)$$

$$+ \bar{\Psi}_u (i\mathcal{D} - m_U) \Psi_u + \bar{\tilde{\Psi}}_u (i\mathcal{D} - \tilde{m}_U) \tilde{\Psi}_u \quad (4.15b)$$

$$- Y_u \bar{\Psi}_{uL} \phi_2^t \tilde{\Psi}_{uR} - m_{Y_u} \bar{\Psi}_{uL} \tilde{\Psi}_{uR} + \text{h.c.} \quad (4.15c)$$

$$+ \Delta_{uL} \bar{\xi}_{uL} \Omega_1 \Psi_u + \Delta_{uR} \bar{\xi}_{uR} \Omega_1 \tilde{\Psi}_u + \text{h.c.} \quad (4.15d)$$

$$+ (u \leftrightarrow d). \quad (4.15e)$$

Neglecting for a moment the composite-elementary mixings, the breaking  $\text{SO}(5) \rightarrow \text{SO}(4)$  is parametrized by  $\phi_2 := \Omega^* \cdot (0, 0, 0, 0, 1)$ . If this vanishes then the full global  $\text{SO}(5)$  symmetry is manifest. But if, on the other hand, this has a non-vanishing value then it leads to a mass splitting between singlet and bidoublet components, which can be understood as the composite Yukawa coupling appearing in (2.28).

Assuming holographic gauge (4.6) the fermion Lagrangian takes the form:

$$\mathcal{L}_{\text{fermion}} = \mathcal{L}_{\text{fermion}}^{(\text{elem})} \quad (4.16a)$$

$$+ i\bar{Q}_u \not{D} Q_u + i\bar{\tilde{Q}}_u \not{D} \tilde{Q}_u + i\bar{S}_u \not{D} S_u + i\bar{\tilde{S}}_u \not{D} \tilde{S}_u \quad (4.16b)$$

$$- m_U (\bar{Q}_u Q_u + \bar{S}_u S_u) - \tilde{m}_U (\bar{\tilde{Q}}_u \tilde{Q}_u + \bar{\tilde{S}}_u \tilde{S}_u) \quad (4.16c)$$

$$- (m_{Y_u} + Y_u) \bar{S}_{uL} \tilde{S}_{uR} - m_{Y_u} \bar{Q}_{uL} \tilde{Q}_{uR} + \text{h.c.} \quad (4.16d)$$

$$+ \Delta_{uL} \bar{\xi}_{uL} \mathcal{U} (Q_{uR} + S_{uR}) + \Delta_{uR} \bar{\xi}_{uR} \mathcal{U} (\tilde{Q}_{uL} + \tilde{S}_{uL}) + \text{h.c.} \quad (4.16e)$$

$$+ (u \leftrightarrow d). \quad (4.16f)$$

This Lagrangian leads to the mass mixing matrices given in appendix III.1.2.

As already stated earlier, we are mainly interested in the interplay between quark flavour measurements and the Higgs potential, we do not consider effects of partial lepton compositeness in this work. Furthermore, if the compositeness of the left- and right-handed lepton chiralities are comparable, they have to be small due to the small masses of the leptons and their impact on the observables to be considered below is expected to be small. Moreover, flavour-changing interactions are strongly constrained by negative searches for charged lepton flavour violating processes. Therefore, we simply consider elementary leptons with direct bilinear couplings to the Higgs field,

$$\mathcal{L}_{\text{lepton}} = i\bar{l}_L^0 \not{D} l_L^0 + i\bar{l}_R^0 \not{D} l_R^0 - \frac{m_{\text{SM}}}{v} \bar{l}_L^0 \cdot \begin{pmatrix} 0 \\ h \end{pmatrix} l_R^0 + \text{h.c.}, \quad (4.17)$$

where, just as for the elementary quarks, the covariant derivatives are understood as couplings to the elementary  $\text{SU}(3)^0 \times \text{SU}(2)^0 \times \text{U}(1)^0$  gauge fields.

## Flavour structure

As discussed in section 2.2.3 we consider the case that the composite sector is invariant under a flavour symmetry. We assume that these symmetries are explicitly broken by either left-handed or right-handed composite-elementary mixings. As a consequence, the composite-elementary mixings are not general matrices in flavour space but their explicit forms are determined by a spurion expansion. In this analysis we consider the following four flavour structures: MFV-like flavour symmetries  $\text{U}(3)_{\text{LC}}^3$  or  $\text{U}(3)_{\text{RC}}^3$ , in which either left-handed or right-handed composite elementary mixings preserve this symmetry while the right-handed mixing break it explicitly, and flavour structures  $\text{U}(2)_{\text{LC}}^3$  or  $\text{U}(2)_{\text{RC}}^3$ , in which the third generation is independent from the first two.

We give the explicit forms of the composite-elementary mixings in appendix IV.1.

## 4.2. The scan

Using the scanning method laid out in section 3.1 we started  $\mathcal{O}(1000)$  scans for each of the 4 considered flavour structures,  $\text{U}(2)_{\text{LC}}^3$ ,  $\text{U}(2)_{\text{RC}}^3$ ,  $\text{U}(3)_{\text{LC}}^3$ ,  $\text{U}(3)_{\text{RC}}^3$ . In the end this gave us the following number of viable parameter points that fulfill each individual constraint on the  $3\sigma$  level:

$\text{U}(2)_{\text{LC}}^3$	$\text{U}(2)_{\text{RC}}^3$	$\text{U}(3)_{\text{LC}}^3$	$\text{U}(3)_{\text{RC}}^3$
431507	128066	0	410321

One very important observation is that we did not find any viable parameter point for the  $\text{U}(3)_{\text{LC}}^3$  structure. This is reasonable as a qualitative analysis of CHMs with this flavour symmetry already revealed a significant tension with experimental constraints [70]. We therefore conclude that this flavour structure is strongly disfavoured in CHMs when combining flavour and electroweak constraints with a realistic EWSB and in the following we will not include it anymore into the analysis.

For the remaining three successful flavour structures we found large numbers of viable parameter points. We have to remind the reader that these are the numbers of point that successfully pass *all* constraints. The total number of all sampled points is much higher. These numbers as well as the following results show that all reasonable regions of parameter space were sampled which allow to

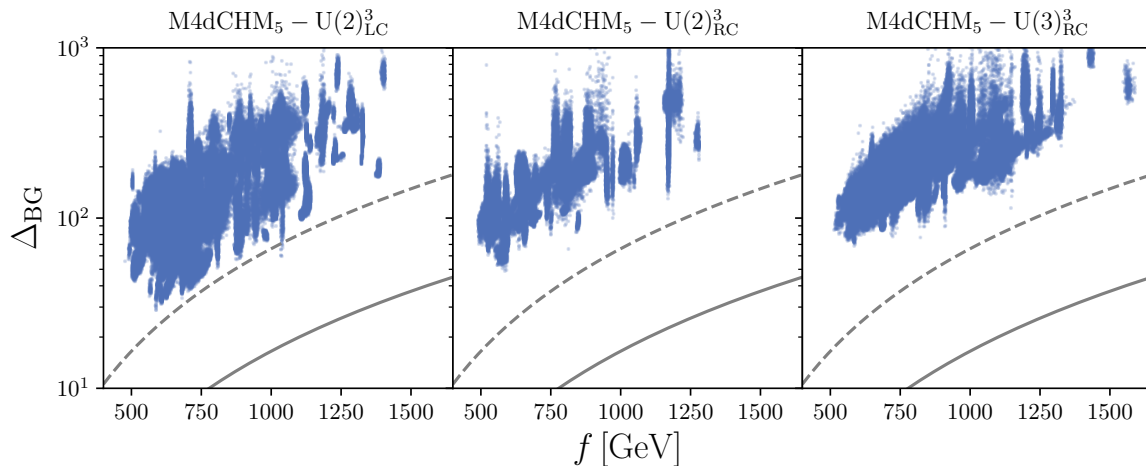


**Figure 4.2.:** Barbieri-Giudice measure of fine-tuning for the three flavour models. The solid gray line shows the naive expectation  $\Delta \sim f^2/v_{\text{SM}}^2$ . The dashed line shows the same expectation but including double tuning,  $\Delta \sim (1/\epsilon^2) \times f^2/v_{\text{SM}}^2$ , with an example value  $\epsilon = 0.5$ .

satisfy the given constraints. But we again want to stress that our results are not intended to and do not allow us to draw statistical conclusions about the parameter space. We used Markov chains simply as a handy tool for generating viable parameter points in an efficient way.

For all three models we find that the total  $\chi^2$  of the viable parameter points almost always lies in the region  $\chi_{\text{total}}^2 \sim 15 - 60$  with a peak around  $30 - 40$ . Given a number of 52 individual (uncorrelated) constraints imposed and a number of free parameters of 44 for  $U(2)$  and 30 for  $U(3)$ , we see that we actually find good a good agreement with the experimental data. We further see that for the majority of viable points only one or two individual constraints are violated at the  $2\sigma$  level. For less than 10% of the points more than 4 individual constraints are violated at that level. These constraints are most often the top mass (as will be discussed in section 4.3.1). But also  $\Delta F = 2$  observables as well as direct constraints are often in tension.

### 4.3. Electroweak symmetry breaking

One of the main points of this work is a realistic reproduction of EWSB. In this section we therefore discuss the results we find for the effective Higgs potential. For this we first discuss the fine-tuning of the potential. After that the potential itself, its minimum and its generation are addressed.

#### 4.3.1. Fine-tuning

At this point let us assess the fine-tuning needed to generate the hierarchy  $v_{\text{SM}} \ll f$ . A quantitative measure for the stability of the electroweak scale is given by the Barbieri-Giudice measure [179],

$$\Delta_{\text{BG}} = \max_{\lambda \in \text{parameters}} \left| \frac{\partial \log(m_Z)}{\partial \log(\lambda)} \right|, \quad (4.18)$$

which directly quantifies the sensitivity of the electroweak scale against small variations in the fundamental parameters. Present-day analyses of this measure in SUSY models [180, 181, 182] result in values  $\Delta_{\text{BG}} \sim \mathcal{O}(\text{few hundred})$ , where the value can go down to as low as 10 for some non-minimal models. A similar situation is found for CHMs [183]. We are interested in the question what the present-day situation is for CHMs when all current constraints are included in a global analysis. Having identified parameter points with low fine-tuning will also allow us to judge whether predictions made by the viable points require fine-tuning.

For CHMs with minimal coset  $\text{SO}(5)/\text{SO}(4)$  this Barbieri-Giudice measure is readily calculated from the effective potential via [56]

$$\Delta_{\text{BG}} = \max_{\lambda \in \text{parameters}} \left| \frac{2\lambda}{s_h} \frac{c_h^2}{f^2 m_h^2} \frac{\partial^2 V_{\text{eff}}}{\partial \lambda \partial s_h} \right|. \quad (4.19)$$



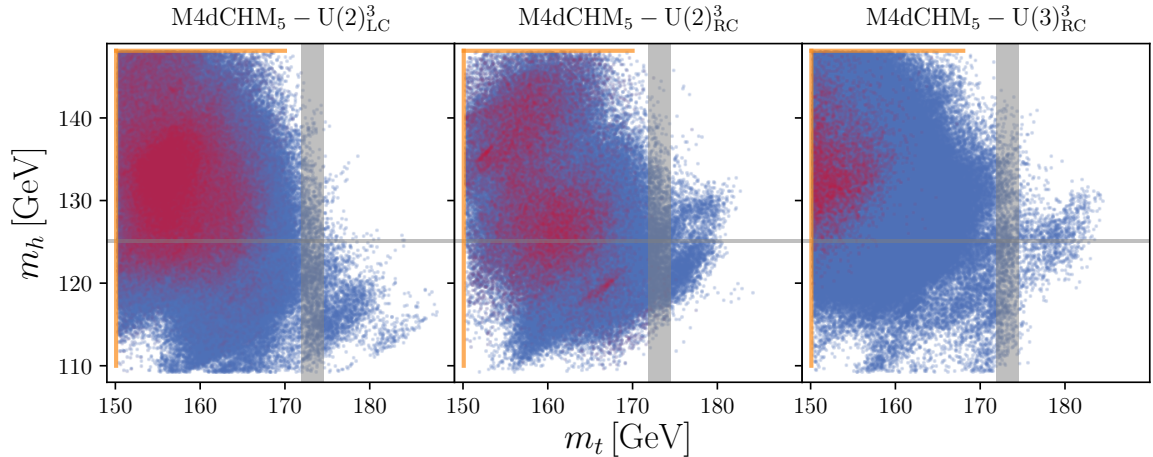


**Figure 4.3.:** Predicted values for Higgs and top mass in all three viable flavour structures. The red points have  $\Delta_{\text{BG}} < 100$  and the gray band mark the experimental  $1\sigma$  measurements of the masses. To guide the eye orange lines are drawn where these constraints cut into the parameter space of the model.

We calculate this number for every found parameter point that satisfies the constraints (3.6). As can be seen in figure 4.2, we find values of  $\Delta_{\text{BG}}$  that vary over a broad range, but their distribution is peaked around  $\Delta_{\text{BG}} \sim 100 - 200$  for all three models. We find the following minimal values<sup>1</sup>

$$\Delta_{\text{BG}}^{\text{min}} = \begin{cases} 29 & \text{for } U(2)_{\text{LC}}^3 \\ 50 & \text{for } U(2)_{\text{RC}}^3 \\ 70 & \text{for } U(3)_{\text{RC}}^3 \end{cases} . \quad (4.20)$$

As expected we find the fine-tuning to be correlated with the symmetry breaking scale  $f$ . A tuning better than the percent-level is certainly still possible for all three flavour structures as long as  $f \lesssim 1100 \text{ GeV}, 800 \text{ GeV}, 700 \text{ GeV}$  for  $U(2)_{\text{LC}}, U(2)_{\text{RC}}, U(3)_{\text{RC}}$ , respectively.

In figure 4.2 also the naive expectation for minimal tuning,  $\Delta \sim f^2/v_{\text{SM}}^2$  is shown. As discussed in section 2.2.2, for fermions embedded into the fundamental representation of  $SO(5)$ , one actually expects an increased tuning, the so-called double-tuning  $\Delta \sim (1/\epsilon^2) \times f^2/v_{\text{SM}}^2$ , due to the fact that formally subleading terms in the spurion expansions (2.65) and (2.66) have to be tuning to the size of the leading order contributions to obtain a realistic EWSB [56]. Figure 4.2 also shows this expectation for an example value  $\epsilon = 0.5$ , which shows that our results are compatible with double-tuning.

Let us note that in figure 4.2 one can identify individual chains as lines of constant  $f$  the reason for this is the following: As discussed in section 2.2.2 the effective potential necessitates the occurrence of cancellations between fermion and vector contributions to the effective potential. While the vector contributions are essentially given by the scale  $f$ , the fermion contributions depend on a large number parameters. Therefore, the value of  $f$  remains constant to a large degree within one Markov chain as a change in  $f$  would imply a simultaneous and coordinated change of the parameters of the fermion sector, which is hard to find for a Markov chain.

Such low levels of fine-tuning (4.20) unfortunately come at a price. CHMs have the known tendency to predict a rather high Higgs mass and a somewhat low top mass. We find that points with low fine-tuning follow this trend as shown in figure 4.3. We remind the reader that we define the viability of a parameter point by passing a  $3\sigma$  constraint assuming convoluted experimental and theoretical errors. Especially for the top mass we assumed a theory uncertainty of 5% such that we allow for large deviation with respect to the experimental value. It is however not a priori clear whether higher order corrections will lift this tension.

These estimations of fine-tuning have to be taken with a grain of salt. In our bottom-up approach we treat all effective parameters as being independent. In a more complete theory, however, the effective parameters could be strongly correlated, such that the fine-tuning in the parametrization of the fundamental theory might in fact be lower.

<sup>1</sup>We remark that relative values for the fine-tuning in the different flavour structures fit the very naive expectation we obtained using a spurion analysis in section 2.2.4

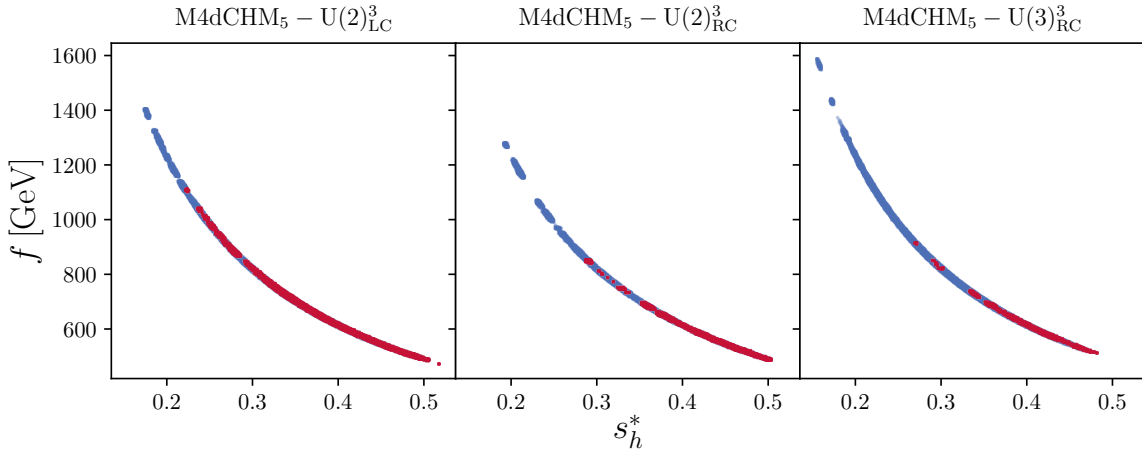


**Figure 4.4.:** Found minima  $s_h^*$  of the effective Higgs potential. These are strongly correlated with the symmetry breaking scale  $f$  via  $f s_h^* = v_{\text{SM}} = 246 \text{ GeV}$ . The blue points mark all viable parameter points and the red points have  $\Delta_{\text{BG}} < 100$ .

### 4.3.2. Potential

In figure 4.4 we present the found values for the minimum  $s_h^*$  of the effective potential. As expected these are strongly correlated with the symmetry breaking scale  $f$  through  $f s_h^* = v_{\text{SM}} = 246 \text{ GeV}$ . Model-independently we find roughly the same allowed ranges  $s_h^* \sim 0.2 - 0.6$ , which correspond to values of  $f$  in the range  $f \sim (500 - 1500) \text{ GeV}$ . Larger values of  $f$  (corresponding to smaller values of  $s_h^*$ ) are not excluded per se, but raising this scale to the ballpark of 2 TeV quickly introduces a tuning at the permille level as can be seen by extrapolating from figure 4.2.

In (2.55) we introduced an expansion of the effective potential in powers of  $s_h$ ,

$$V_{\text{eff}}(s_h) = (-\gamma s_h^2 + \beta s_h^4 + \dots) f^4, \quad (2.55)$$

and saw that in order to generate the correct scale of EWSB and the correct Higgs mass, one has to find the coefficients  $\beta$  and  $\gamma$  in the ballpark shown in figure 2.2. Roughly speaking, one needs  $\beta \approx 0.04$  and  $\gamma \lesssim 0.03$ . For each of our viable parameter points we are able to fit this expansion to the effective potential and by this extract the predictions for  $\beta$  and  $\gamma$  for a given parameter point. In general, we find a good agreement between the fit and the full potential indicating a small coefficient of a possible  $s_h^6$ -term in (2.55). Comparing our results on  $\beta$  and  $\gamma$  with the expectations given in section 2.2.2 we find a good agreement between the found points and the expectations. In particular, we see that all points are clustered around the black line given in figure 2.2, which marks a non-trivial consistency check.

To retrieve more information we are able to extract the coefficients  $\beta$  and  $\gamma$  separately for each contribution to the potential given by up-type or down-type quarks or by charged and neutral vector resonances. Regarding  $\beta$  we find that the contribution  $\beta_U$  from top partners is always the dominant one. This is exactly the behaviour predicted in section 2.2.2. For the coefficient  $\gamma$  the usual folklore is that it gets a largely positive<sup>2</sup> contribution by the fermions (in particular, from top partners) which has to be counteracted by vector contributions in order to obtain the desired small positive value [55]. On the whole we can confirm this behaviour in our numerical scan and further we can identify three qualitatively different scenarios for the relative ratios of up-type and down-type contributions,  $\gamma_U$  and  $\gamma_D$ .

scenario (I): The up-type quark resonances give a strong positive contribution while  $\gamma_D$  is rather small. In this scenario EWSB is triggered by top-partners alone and the correct value of the vev is given by a cancellation between up-type and vector contributions. This scenario marks the one with small tuning as it only needs a cancellation between two independent contributions.

scenario (II): Again EWSB is triggered by the up-type quark resonances. However in this case down-type resonances give a significant negative contribution that counteracts  $\gamma_U$ . Although now the

<sup>2</sup>One should keep in mind that in the expansion (2.55) the coefficient  $\gamma$  is defined with a negative sign. Therefore, a positive value of  $\gamma$  is needed in order to have a non-trivial minimum.

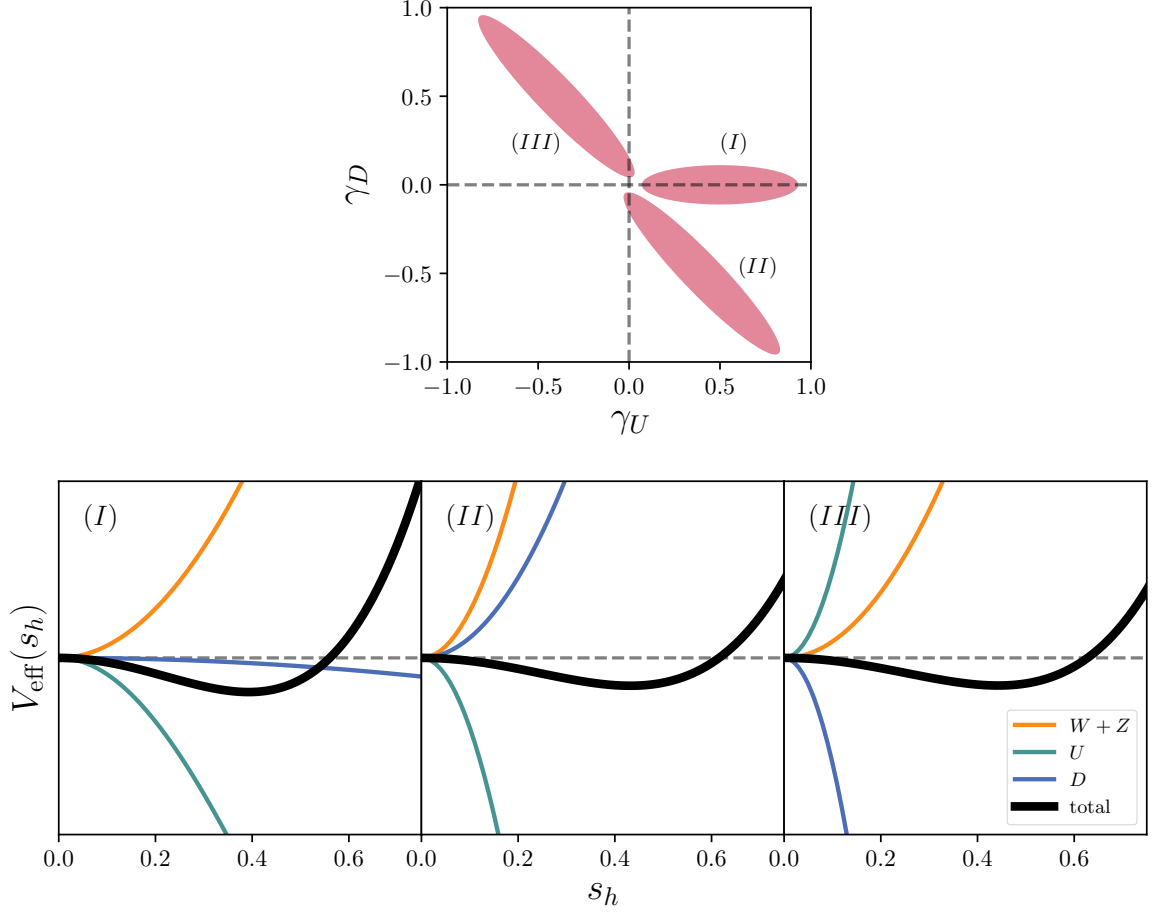


**Figure 4.5.:** Different scenarios for the relative contributions of up-type and down-type fermion resonances to the coefficient  $\gamma$  of the effective potential. *Top row:* Schematic separation of the  $\gamma_U - \gamma_D$  plane into the scenarios of interest. *Bottom row:* Individual contributions to the effective potential for the three scenarios. The contributions generated by up-type and down-type quarks are shown in green and blue, respectively. Orange marks the contributions from vector resonances which are always positive. The black line shows the full effective Higgs potential, i.e. the sum of the individual  $U$ -  $D$  and  $W + Z$ -contributions.

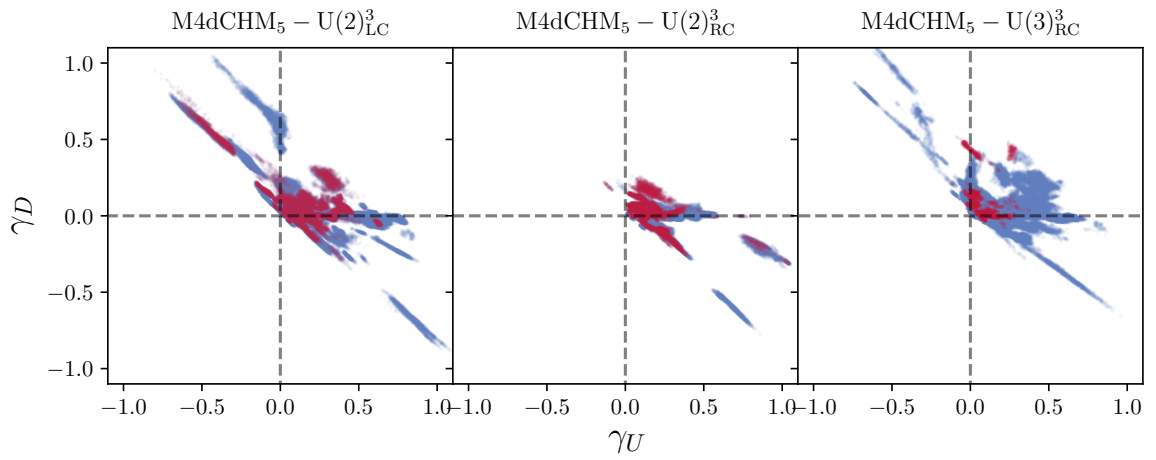


**Figure 4.6.:** Found values for the contributions  $\gamma_U$  and  $\gamma_D$  to the effective potential. The blue points mark all viable parameter points and the red points have  $\Delta_{BG} < 100$ .

cancellations that have to be maintained by the vector resonances are smaller, this scenario is more fine-tuned as it involves cancellations between three independent contributions.

scenario (*III*): In this scenario the roles of up-type and down-type contributions are exchanged with respect to scenario (*II*). EWSB is induced by bottom-partners, while the top-partners counteract this effect. Also for this case we expect a considerable amount of tuning needed.

Schematically, these are shown in figure 4.5. Generally, we find that the contributions from charged and neutral vector resonances to  $\gamma$  are strongly correlated due to custodial symmetry. Further, these contributions are always negative, such that vector contributions alone cannot give a non-trivial minimum for the potential.

A further possibility where top- and bottom-partners simultaneously trigger EWSB is disfavoured as it would imply a large amount of fine-tuning, since then the vector contributions would have to overcome the combined effect of the fermion sector.

We show the distributions found for  $\gamma_U$  and  $\gamma_D$  in figure 4.6. They roughly fall into the above scenarios although also superpositions are possible for a small fraction of points. We note that for  $U(2)_{\text{RC}}^3$  we did not find any points corresponding to scenario (*III*).

## 4.4. Spectra

As already mentioned in section 3.3.8 CHMs have an interesting and rich collider phenomenology. Although included as a vital part of this analysis we will not discuss constraints and prospects for direct searches of composite resonances in this work. We rather refer the interested reader to [28] where these topics are elaborated in great detail.

To get a feeling for the mass ranges of the composite resonances which are still allowed after applying all constraints coming from EWSB, indirect constraints and direct searches we present the mass spectra in figure 4.7. In this figure, the mass distributions of the lightest resonances for each class of composite states (up-type- and down-type partners, exotically charged resonances, neutral and charged vector resonances and gluon resonances) are shown. We find that in each class the light composite resonances are often nearly mass-degenerate (at least for the composite fermions) such that the distributions shown in figure 4.7 are valid for the lightest couple of resonances. Model-independently we observe that the masses of the lightest up-type and down-type partners are always below 2 TeV, which is well within the reach of the LHC, so that these states will be tested in near-future collider searches. Note that kinematically the light fermion resonances can only have branching ratios into SM final states. The masses of charged and neutral vector resonances vary over a much larger range. We find most spin-1 resonances with masses of several TeV which can go down to roughly 2 TeV (with an exception for  $U(2)_{\text{LC}}^3$  where the masses can be a little bit smaller).<sup>3</sup> For the neutral vector resonances we also find very small masses below 1 TeV. These correspond to anomalous light states mainly composed of the  $X_\mu$  resonance that does not contribute to oblique corrections and is therefore not constrained by the  $S$  parameter. These states will be relevant for rare  $B$  decays as will be discussed in section 4.7.2. Last, we find gluon resonances with masses up to 16 TeV.

Apart from the mass spectra it is interesting to see how the assumed flavour structures determine the degrees of compositeness of the SM quarks. For this one first has to define what is actually meant by a degree of compositeness for the given model. The naive formulae (2.26) are clearly not applicable in our case, as the elementary fields are allowed to mix with several composite resonances (even in a flavour off-diagonal way). In general, the SM quarks are mixtures of elementary and composite fields,

$$\psi_i^{\text{SM}} = \mathcal{V}_{ij}^{0-0} \psi_j^0 + \mathcal{V}_{iJ}^{0\text{-comp}} \Psi_J^{\text{comp}}, \quad (4.21)$$

where  $\mathcal{V}^{0-0}$  and  $\mathcal{V}^{0\text{-comp}}$  are elements of the rotation matrices that are defined in (3.10) and due to unitarity one has  $\sum_j |\mathcal{V}_{ij}^{0-0}|^2 + \sum_J |\mathcal{V}_{iJ}^{0\text{-comp}}|^2 = 1$ . Then for each chiral SM quark one can define a degree of compositeness of a particle  $i$  via

$$\text{degree of compositeness} = \sum_J |\mathcal{V}_{iJ}^{0\text{-comp}}|^2. \quad (4.22)$$

---

<sup>3</sup>This is in contrast to lattice calculations of the vector resonance spectrum in CHMs [184], where values larger by one order of magnitude were found. In these lattice calculations, however, specific fermionic 4d UV completions are assumed. Our EFT approach is model-independent and implicitly assumes the existence of a high energy theory allowing for low vector resonance masses.

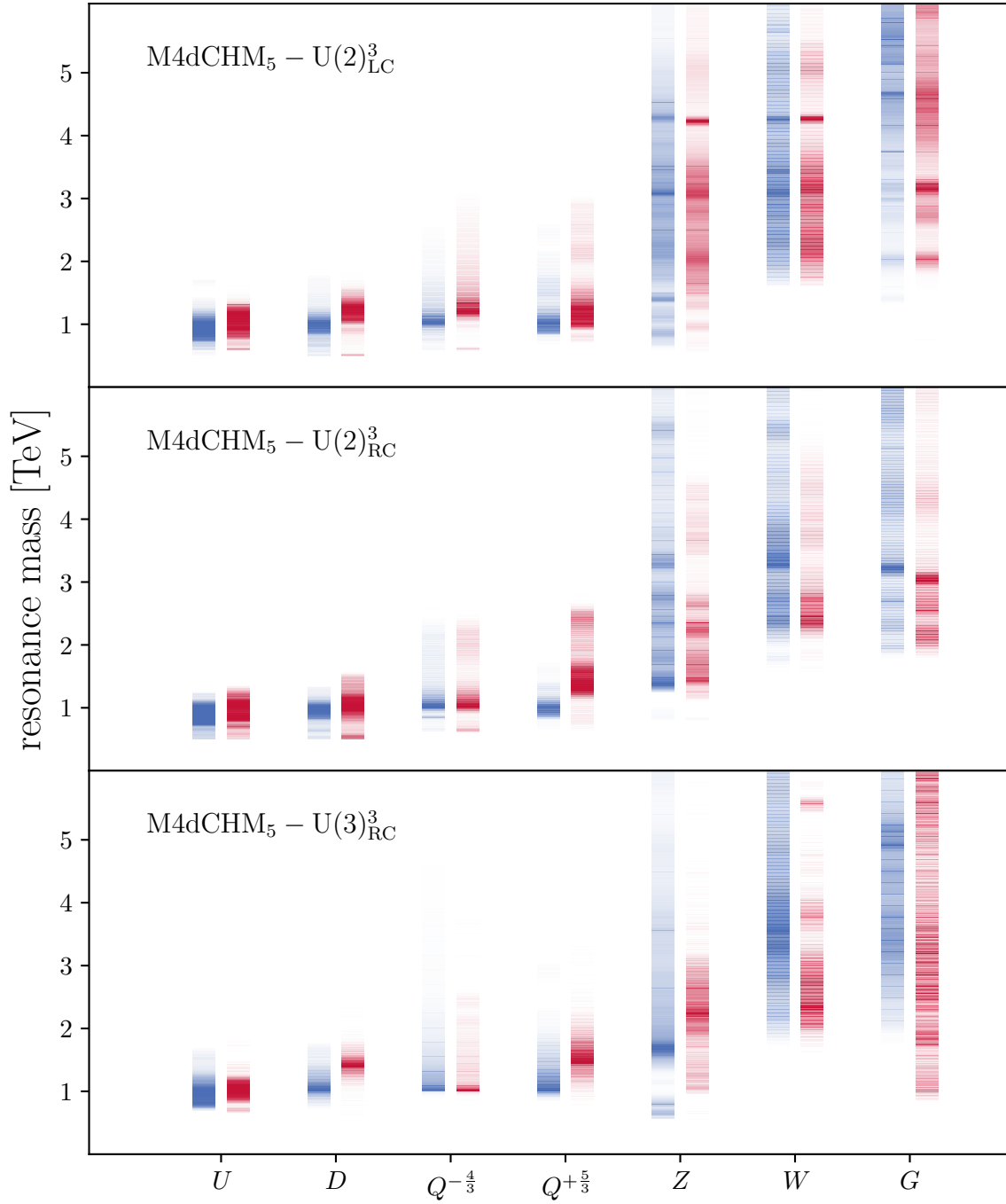


**Figure 4.7.:** Found mass spectra for the three successful flavour structure. For each class of composite resonances (up-type- and down-type partners, exotically charged resonances, neutral and charged vector resonances and gluon resonances) the mass distribution of the *lightest resonance* is shown by color shading. The distributions including all viable parameter points are shown in blue while red shows the same but only including parameter points with  $\Delta_{BG} < 100$ .

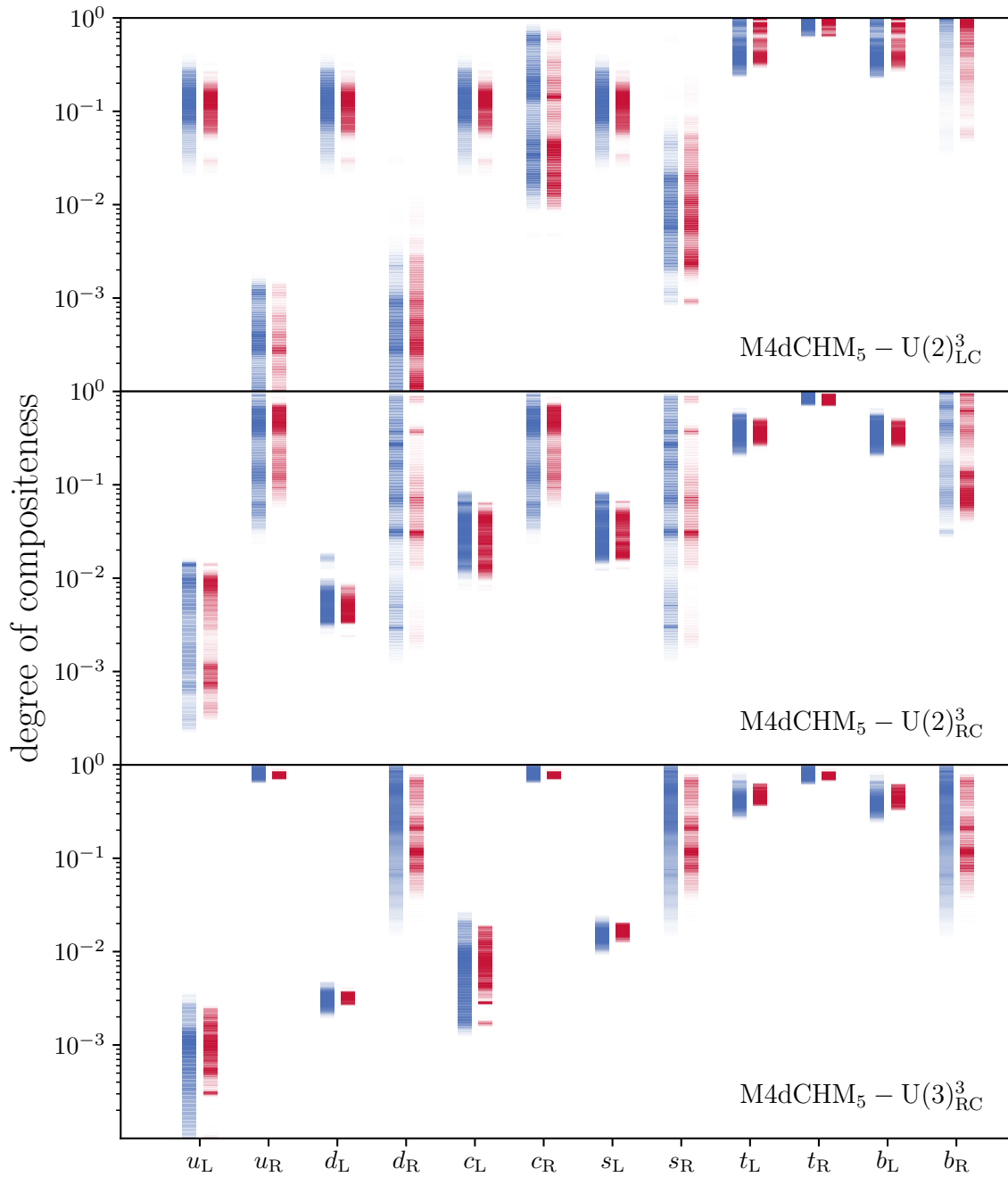


**Figure 4.8.:** Found degrees of compositeness for the SM quarks. The distributions including all viable parameter points are shown in blue while red shows the same but only including parameter points with  $\Delta_{\text{BG}} < 100$ .

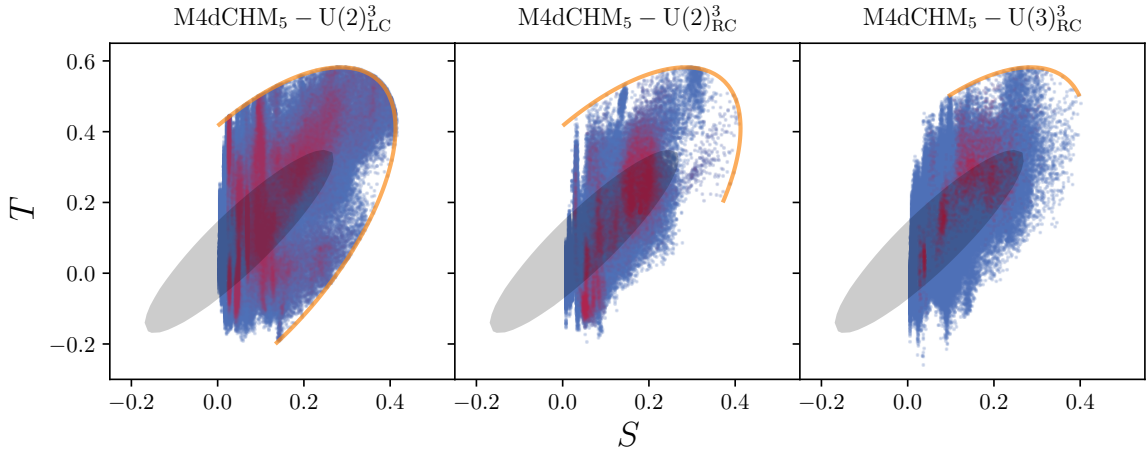


**Figure 4.9.:** Oblique parameters  $S$  and  $T$ . We only show the NP contributions. All viable parameter points are shown in blue, while red points have  $\Delta_{\text{BG}} < 100$ . In gray we show the experimental  $2\sigma$  contour. To guide the eye orange lines are drawn where these constraints cut into the parameter space of the model.

We present the distributions for the compositeness of the SM quarks in figure 4.8. This nicely demonstrates the impact of the flavour structures on the degrees of compositeness.

- $\mathbf{U(2)_{LC}^3}$  We find the left-handed compositenesses of the first two generations to be strongly correlated. As a consequence the hierarchies of the masses have to be generated by the right-handed degrees of compositeness alone. The third generation is decoupled and for top and bottom we find both chiralities to be considerably composite.
- $\mathbf{U(2)_{RC}^3}$  For right-handed compositeness the picture is similar. Here the right-handed compositenesses of the first and second generation quarks are large and correlated, while the left-handed ones generate the mass hierarchies. In the third generation we find a less composite bottom and an almost entirely composite  $t_R$ .
- $\mathbf{U(3)_{RC}^3}$  A slightly broken  $\mathbf{U(3)}$  flavour symmetry is qualitatively very different. Here the degrees of compositeness of all three generations are correlated leading to almost completely composite  $u_R$  and  $d_R$  quarks. The freedom to generate the correct masses is much more restricted leading to sharply peaked distributions.

We find these results in perfect agreement with what one would expect from these flavour structures.

## 4.5. Main constraints

In this section we want to identify the most constraining bounds on this model. EWPOs are known to be a major constraint on strongly coupled theories like CHMs or technicolor [38]. We present the found values for these observables in figure 4.9. One can see that although most parameter points with reasonable fine-tuning predict only moderate contributions to the  $S$  and  $T$  parameters, these observables pose a relevant bound for all three flavour structures. According to (3.33) the NP contribution to the  $S$  parameter is always positive. The contribution to the  $T$  parameter can have either sign, but for a positive  $S$  parameter also a positive  $T$  parameter is preferred by the experimental data.

In section 3.3 we implemented CKM unitarity, the hadronic  $Z$  width and contact interactions as constraints on the compositeness of light quarks. We show results on these observables in figure 4.10. First-row CKM unitarity is a relevant constraint for left-compositeness. In this flavour model the left-handed quark chiralities are considerably composite leading to large deviations in  $W$  couplings which modifies the extraction of CKM elements. The impact of this constraint is nicely seen as horizon and vertical edges in the distribution of the viable parameter points. These mark the  $3\sigma$  bound (3.6) imposed by us and they show that CKM unitarity is a constraint that deeply cuts into the parameter space of models with left-handed compositeness. Being such a strong constraint we can

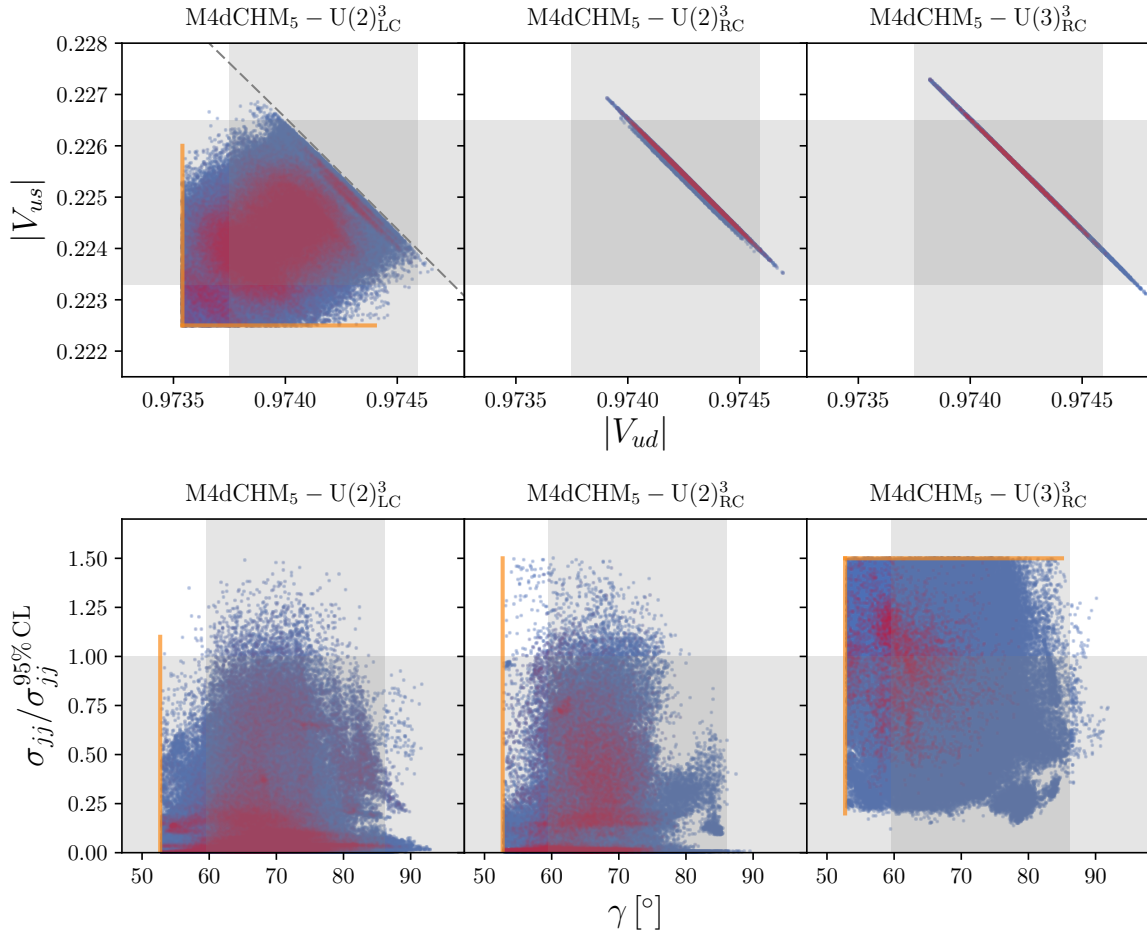


**Figure 4.10.:** Constraints on the quark compositeness. Scatter plot including all viable points (blue). In red we mark all points with  $\Delta_{\text{BG}} < 100$ . The gray bands are experimental  $2\sigma$  constraints. To guide the eye orange lines are drawn where these constraints cut into the parameter space of the model via (3.6). *Top row:* Constraints coming from first row CKM unitarity. The black lines denotes the unitarity line  $|V_{ud}|^2 + |V_{us}|^2 \approx 1$ . *Bottom row:* Constraints stemming from the CKM angle  $\gamma$  and contact interactions contributing to the dijet angular distribution. For the latter we normalize to the experimental 95% CL bound, such that  $\sigma_{jj}/\sigma_{jj}^{95\% \text{ CL}} = 1$  marks a  $2\sigma$  constraint.

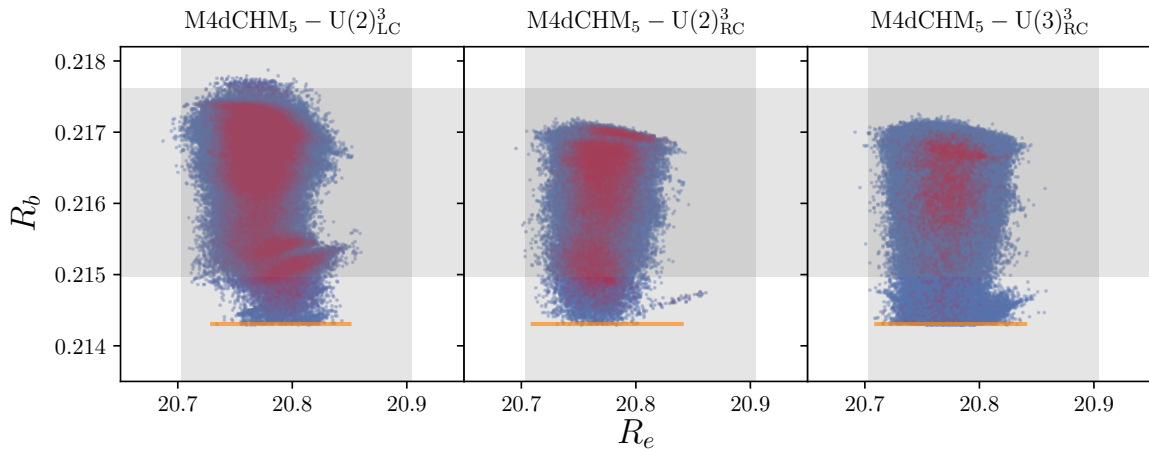


**Figure 4.11.:** Constraints of  $Z$  width measurements into charm- and bottom quarks. In blue we show all viable parameter points, while red points have  $\Delta_{\text{BG}} < 100$ . In gray we show the experimental  $2\sigma$  bands.



identify it as one of the main reasons why a  $U(3)_{\text{LC}}^3$  flavour symmetry is not viable. In such a model the compositeness of the left-handed chiralities of the light quarks is directly connected to that of the 3rd generation, leading to too large deviations in the CKM elements. In models with right-handed compositeness, on the other hand, there is no large left-handed degree of compositeness, making this constraint virtually non-existing.

In the second row of figure 4.10 we present constraints coming from the CKM angle  $\gamma$  and from contact interactions. For  $U(2)_{\text{LC}}^3$  contact interactions are not constraining at the moment but they can become important provided the experimental upper bounds on the dijet angular distributions will decrease in the future. Especially for  $U(3)_{\text{RC}}^3$  contact interactions lead to a significant bound that cuts into the parameter space. For this flavour structure also the light quarks have one strongly composite chirality such that one generally finds large contributions to the dijet cross section that are often near the experimental limits. This is in contrast to the  $U(2)$  flavour models where the dijet cross section tends to be small, but can become sizable for some points. We find the CKM angle  $\gamma$  to be relevant in all three flavour structures.

We show the constraints coming from  $Z$  width deviations in figure 4.11. For left- and right-compositeness the hadronic  $Z$  width is not a very sensitive probe yet. The hadronic width  $R_e = \sum_q \Gamma(Z \rightarrow \bar{q}q) / \Gamma(Z \rightarrow ee)$  was identified in [70] as a strong bound on the compositeness of left-handed light quarks such that this constraint is particularly important for a  $U(3)_{\text{LC}}^3$  flavour structure. We, however, find that this constraint is not violated by more than  $2\sigma$  such that there are more significant bounds on light quark compositeness, such as e.g. CKM unitarity. Assuming partial compositeness also for charged leptons, the hadronic  $Z$  width can become an important constraints if the leptons are significantly composite. We find further that the coupling of  $Z$  to the bottom quark,  $R_b$ , gives a bound for low values of the  $Z$  width in all three flavour structures, indicating that the large degree of compositeness of the 3rd generation can give significant contributions in this observable.

## 4.6. Higgs physics

It is intuitive that due to the non-linear realization of the Higgs in pNGB-theories its couplings to SM fields can get significant modifications. This can be measured in terms of Higgs signal strengths as discussed in section 3.3.4. We present the outcome for these observables in figure 4.12. As the top row of this figure shows the general dependence of the signal strengths on the scale  $f$  roughly fits the expectation (3.42). Deviations from this expectation are possible if light quarks have a significant degree of compositeness, as discussed in section 3.3.4. We find this confirmed by the fact that the curves for  $U(3)_{\text{RC}}^3$  generally appear to be more “washed out”, as for this flavour structure a large compositeness also for light quarks is to be expected.

We find that the Higgs signal strengths in the channels  $h \rightarrow WW, ZZ$  and  $h \rightarrow \tau^+\tau^-$  do not pose a strong bound at the moment. However, we also see that the decay into photons is already able to rule out points with very small values of  $f$  for  $U(3)_{\text{RC}}^3$ , as can be seen in the bottom row of figure 4.12. Currently, the signal strength in this mode is measured with an uncertainty of around 20%. In the future, both experiments, ATLAS and CMS, expect to reach a sensitivity of around 10% and 5% for  $300 \text{ fb}^{-1}$  and for a high-luminosity phase with  $3000 \text{ fb}^{-1}$ , respectively [185, 186, 187]. This shows that in the future this channel will give significant constraints on the symmetry breaking scale  $f$  even for the other flavour structures.

One can also see that the effects in  $h \rightarrow \bar{b}b$  are generally larger than in other channels. Presently, there is no observation in this channel yet, but it is expected after  $100 \text{ fb}^{-1}$  of Run 2 data are accumulated. As prospects the CMS experiment gives expected uncertainties of 10 – 15% for  $300 \text{ fb}^{-1}$  and even below 5% for  $3000 \text{ fb}^{-1}$ , respectively [188, 186]. With such an accuracy the decay  $h \rightarrow \bar{b}b$  will become a very important constraint that can potentially rule out  $f \lesssim 1 \text{ TeV}$  after a high-luminosity phase, provided a SM-like value will be measured.

## 4.7. Flavour physics

### 4.7.1. Meson-antimeson mixing

In our analysis meson-antimeson mixing was included to obtain control over the CKM structure of the model. Furthermore, due to the presence of many neutral vector resonances as well as possibly large

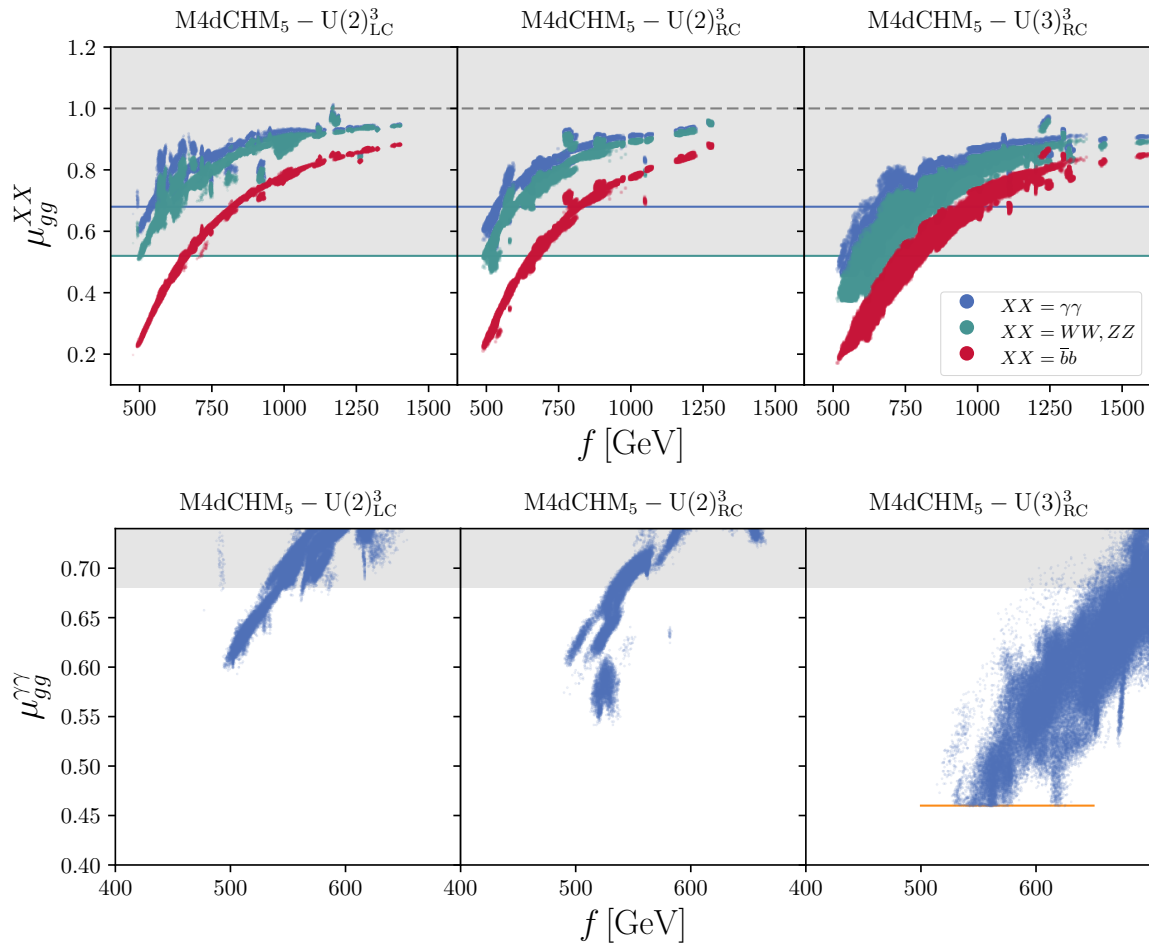


**Figure 4.12.:** Higgs signal strengths (3.40) in the channels  $h \rightarrow WW, ZZ$  (both are the same due to custodial symmetry),  $h \rightarrow \gamma\gamma$  and  $h \rightarrow \bar{b}b$  as functions of the symmetry breaking scale  $f$ . The gray bands and colored horizontal lines mark the  $2\sigma$  experimental limits. *Top row:* Signal strengths in all relevant channels. We refrained from showing results for  $h \rightarrow \tau^+\tau^-$  as due to the yet large experimental uncertainties this does not pose any constraint at the moment. *Bottom row:* Zoomed picture for  $h \rightarrow \gamma\gamma$ . To guide the eye orange lines are drawn where this constraint cuts into the parameter space.

degrees of compositeness for the SM quarks these observables can potentially get large modifications. Before presenting the results of our analyses let us first shortly discuss the expectation one has for the  $\Delta F = 2$  parameters given the assumed flavour structures. The consequences of  $U(2)^3$  and  $U(3)^3$  flavour symmetries using a general EFT framework were elaborated in [65] (see also [189] for a derivation in a supersymmetric context). In these references remarkably simple correlations between the  $\Delta F = 2$  parameters in  $B_d$ -,  $B_s$ - and  $K$ -mixing were found at leading order in the spurion expansion:

**U(3)**

$$\frac{\Delta M_d}{\Delta M_d^{\text{SM}}} = \frac{\Delta M_s}{\Delta M_s^{\text{SM}}}, \quad \phi_d^{\text{NP}} = \phi_s^{\text{NP}} = 0, \quad \frac{\epsilon_K}{\epsilon_K^{\text{SM}}} = (1 - \alpha) + \alpha \frac{\Delta M_d}{\Delta M_d^{\text{SM}}}, \quad (4.23a)$$

where  $\alpha = \epsilon_K^{\text{SM}(tc+cc)}/\epsilon_K^{\text{SM}}$  is the ratio of the sub-leading top-charm and charm-charm contribution to the full SM prediction for  $\epsilon_K$ . Thus, for this MFV-like flavour structure one expects highly correlated NP contributions to  $\Delta F = 2$  observables.

**U(2)**

$$\frac{\Delta M_d}{\Delta M_d^{\text{SM}}} = \frac{\Delta M_s}{\Delta M_s^{\text{SM}}}, \quad \phi_d^{\text{NP}} = \phi_s^{\text{NP}}, \quad \frac{\epsilon_K}{\epsilon_K^{\text{SM}}} = (1 - \alpha) + \alpha \frac{|1 + h_K|}{|1 + h_B|} \frac{\Delta M_d}{\Delta M_d^{\text{SM}}}, \quad (4.23b)$$

where  $h_{K,B} \approx 0.009 \text{ TeV}^2 C_{VLL}^{K,B}$  and the Wilson coefficients  $C_{VLL}^{K,B}$  were defined in (3.47)<sup>4</sup>. The correlation between  $\epsilon_K$  and  $\Delta M_d$  is model-dependent and depends (roughly speaking) on the ratio of the left-handed vector-interactions  $C_{VLL}^{K,B}$ .

We present our results on the  $\Delta F = 2$  observables in figures 4.13, 4.14 and 4.15. The first row in each of these figures shows the predictions on the total values of the observables, which can be compared directly with the experimental bounds. We observe that in all observables large effects, up to saturating the experimental constraints on the  $3\sigma$  level, are possible. In the mass differences in the  $B_d$  and  $B_s$  systems (shown in figure 4.13) we mostly find an enhancement while a negative NP contribution is disfavoured. We find parameter points giving the whole range allowed for the mixing phases (rf. figure 4.14), but we also see that the scans prefer a slight positive shift  $\phi_d$  and a negative shift of  $\phi_s$  with respect to the experimental value. In  $U(2)$  flavour structures we observe an enhancement of  $\epsilon_K$  up to saturating the  $3\sigma$  bound. In  $U(3)_{\text{RC}}^3$  we find a similar effect but it is less pronounced as the correlations with  $\Delta M_d$  are stronger.

We have to remind the reader that in our scans also the CKM elements are allowed to vary. Therefore, all correlations between NP contributions between  $\Delta F = 2$  observables are obscured by the variation of CKM elements. In the bottom rows of figures 4.13, 4.14 and 4.15 we present the above results normalized to the SM values, i.e. to the values obtained by forbidding heavy resonances to contribute to the observable. Because of this the variations of the CKM elements drop out and a connection to the expectations (4.23) can be drawn. We find that for a  $U(3)_{\text{RC}}^3$  flavour structure the MFV expectations are satisfied to an excellent degree. But for the mass differences and mixing phases in  $U(2)$  flavour structures we also find that large violations of the leading-order expectations (4.23a) are possible. This is due to enhanced sub-leading contributions which are not considered in (4.23a). Most notably these are due to enhancements of the Wilson coefficient  $C_{\text{SLR}}^{bs}$  defined in (3.47). But we also find that the expected relations are satisfied by the majority of points, meaning a large density of points around the dashed lines in that figures.

A very interesting feature can be observed for the correlations between  $\frac{\epsilon_K}{\epsilon_K^{\text{SM}}}$  and  $\frac{\Delta M_d}{\Delta M_d^{\text{SM}}}$  shown in figure 4.15. The three flavour structures show qualitatively very different results. While the MFV relation is satisfied to a good degree in  $U(3)_{\text{RC}}^3$ , there is generally either a suppression or an enhancement of  $\frac{\epsilon_K}{\epsilon_K^{\text{SM}}}$  with respect to  $\frac{\Delta M_d}{\Delta M_d^{\text{SM}}}$  for left-composite and right-composite  $U(2)$ , respectively. Experimentally, this gives a clear discriminator for the flavour structures.

A remarkable feature of the predictions given in figures 4.13, 4.14 and 4.15 is that the parameter points with an acceptable fine-tuning  $\Delta_{\text{BG}} < 100$  are mostly clustered around the experimentally preferred values (an exception might be  $\Delta M_s$  in  $U(3)_{\text{RC}}^3$ ). This is important as it shows that there is no tension between the effective potential and  $\Delta F = 2$  flavour observables, which might have been there since flavour breaking as well as EWSB is induced by the composite-elementary mixing. This very well meets the expectations we obtained in section 2.2.4 through a spurion analysis, namely that the connection between the the potential and flavour transitions should be small.

<sup>4</sup>Note that our normalization of the effective operators is different to the one used in [65]

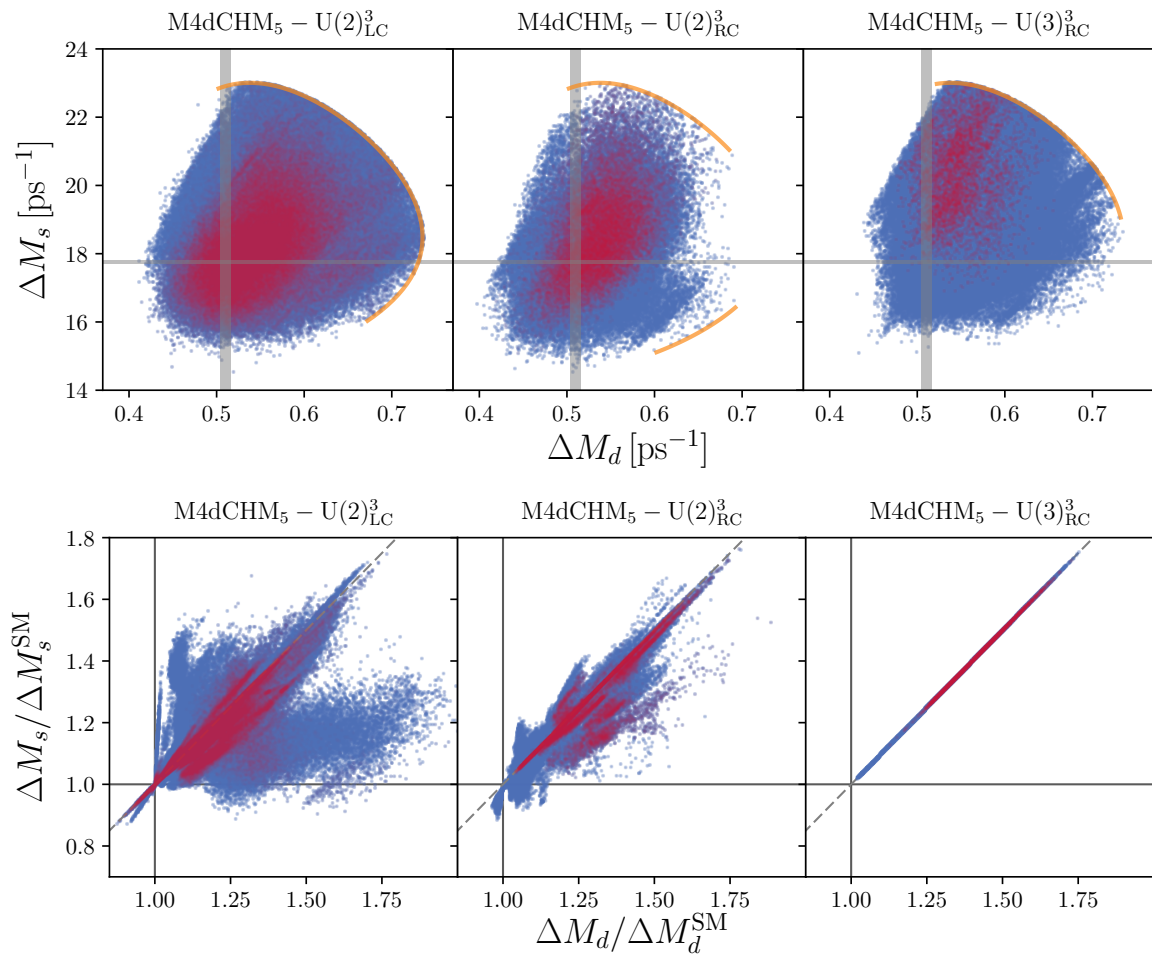


**Figure 4.13.:** Mass differences in the  $B_d$ - and  $B_s$ -systems. All viable parameter points are shown in blue while the red points mark  $\Delta_{\text{BG}} < 100$ . *Top row:* Absolute mass differences. The gray regions denote the  $2\sigma$  experimental results. To guide the eye orange lines are drawn where these constraints cut into the parameter space. *Bottom row:* Mass differences normalized to the SM values. The dashed line marks the MFV limit.

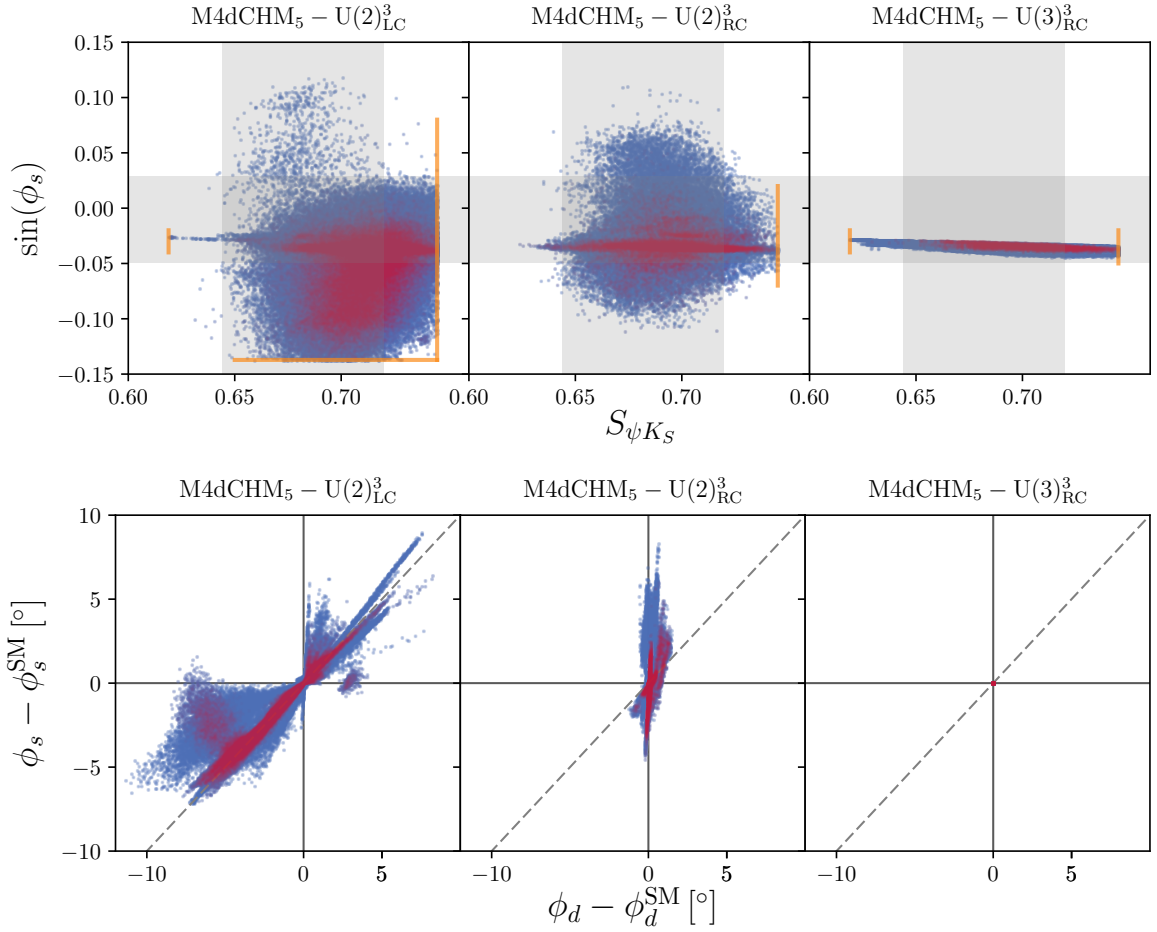


**Figure 4.14.:** Mixing phases in the  $B_d$ - and  $B_s$ -systems. All viable parameter points are shown in blue while the red points mark  $\Delta_{\text{BG}} < 100$ . *Top row:* Total phases. The gray regions denote the  $2\sigma$  experimental results. To guide the eye orange lines are drawn where these constraints cut into the parameter space. *Bottom row:* Corrections to the mixing phases induced by NP only. The dashed line marks the MFV limit.

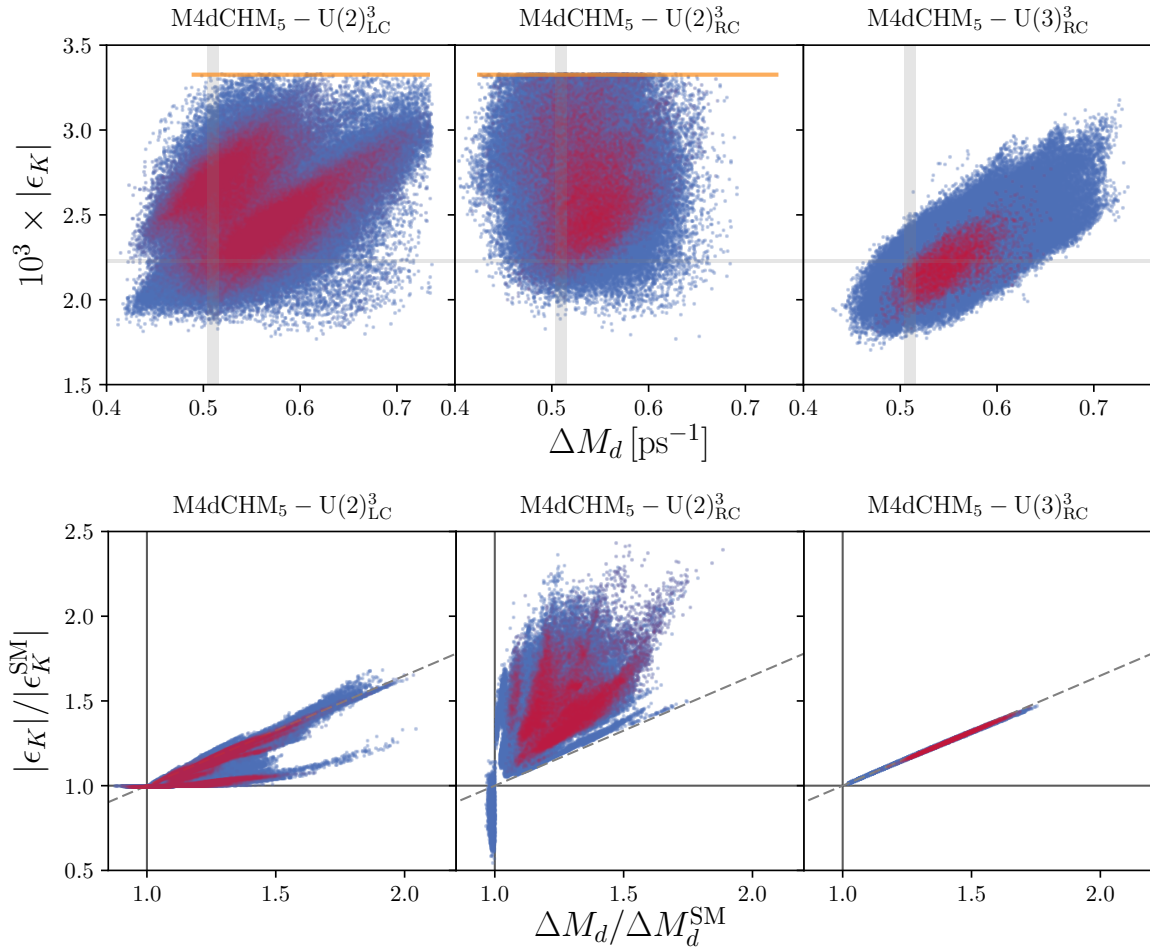


**Figure 4.15.:** Correlation between indirect  $CP$  violation in the Kaon system and particle-antiparticle mixing of  $B$  mesons. All viable parameter points are shown in blue while the red points mark  $\Delta_{BG} < 100$ . *Top row:* Total values. The gray regions denote the  $2\sigma$  experimental results. To guide the eye orange lines are drawn where these constraints cut into the parameter space. *Bottom row:* Correlations normalized to the SM values. The dashed line marks the MFV limit.

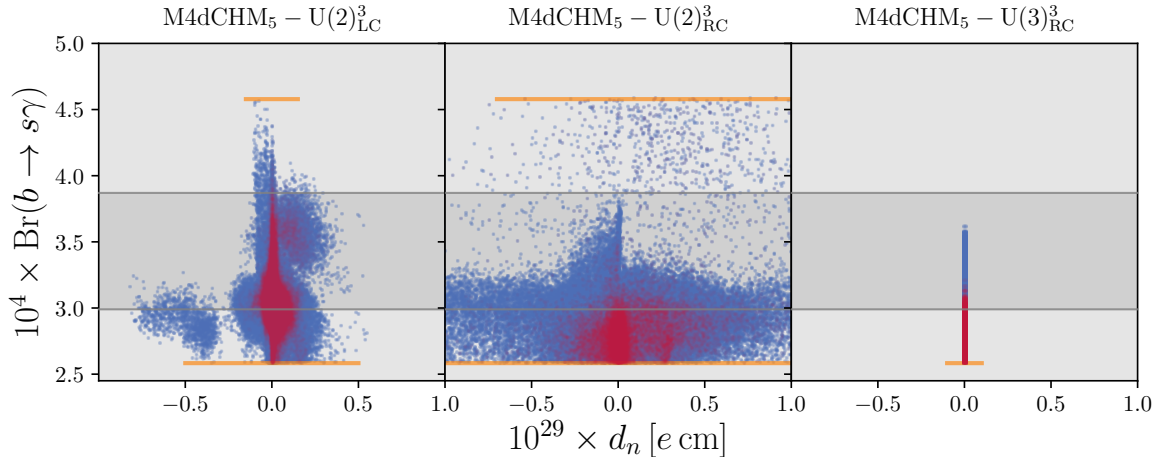


**Figure 4.16.:** Contributions to dipole transitions. In the heavy quark sector we show  $\text{Br}(b \rightarrow s\gamma)$  and for first generation quarks we present contributions to electric dipole moment of the neutron. All viable parameter points are shown in blue while the red points mark  $\Delta_{\text{BG}} < 100$ . The gray regions denote the  $2\sigma$  experimental results. To guide the eye orange lines are drawn where these constraints cut into the parameter space.

#### 4.7.2. Rare decays

In section 3.3.5 rare  $B$  meson decays were included in the analysis to constrain the semi-leptonic operators given in (3.62). The dipole operators  $\mathcal{O}_7^{(\prime)}$  and  $\mathcal{O}_8^{(\prime)}$  give rise to the inclusive decay  $B \rightarrow X_s \gamma$ . For light quarks analogous operators induce the electric dipole moment of the neutron. We present results on both dipole transitions in figure 4.16. For all three flavour structures one sees that the majority of the viable parameter points are scattered towards the lower end of the allowed region for  $b \rightarrow s\gamma$ , such that this gives a relevant bound on the parameters space. In the models with a  $U(2)$  flavour symmetry large enhancements are also possible, although only for a few fine-tuned points. Generally, we find that only small imaginary parts for these Wilson coefficients are generated, indicating that no large contributions to  $CP$  sensitive observables in dipole transitions are to be expected. This is also true for dipole operators involving first generation quarks. As figure 4.16 shows, although the allowed values for the electric dipole moment of the neutron vary over a large range, they are still several orders of magnitude below the experimental limit (3.75). Therefore, this constraint is not relevant at all.

Regarding the vector operators  $\mathcal{O}_9^{(\prime)}$  and  $\mathcal{O}_{10}^{(\prime)}$  in (3.62), we included the rare decay  $B_s \rightarrow \mu^+ \mu^-$  as a constraint, which is sensitive to the combination  $|C_{10} - C'_{10}|$  (see eq. 3.69). In figure 4.17 we present correlations between the decays  $B_d \rightarrow \mu^+ \mu^-$  and  $B_s \rightarrow \mu^+ \mu^-$ . In models with a  $U(2)$  flavour symmetry the relative contributions normalized to the SM have to be equal, as  $d$ - and  $s$ -quarks are part of the same flavour doublet. We find, however, that this relation is washed out by variations in the CKM parameters. For a  $U(2)_{\text{LC}}^3$  flavour symmetry the experimental upper bound on  $B_s \rightarrow \mu^+ \mu^-$  can be saturated, while also rather low values are possible. For right-compositeness on the other hand, we observe that generally only small modifications of the branching ratio are allowed. In all three models we find that for  $B_d \rightarrow \mu^+ \mu^-$  values at the lower end of the experimental  $2\sigma$  end are preferred.

We purposely did not include constraints on the operators  $\mathcal{O}_9^{(\prime)}$ . In light of recent anomalies in  $b \rightarrow s \ell^+ \ell^-$  data (which we will discuss in chapter 6) it is interesting to see which values are still allowed for their Wilson coefficients in CHMs, if we just include the constraints on  $\mathcal{O}_{10}^{(\prime)}$  coming from  $B_s \rightarrow \mu^+ \mu^-$ . In figure 4.18 the results on the vector operators are presented. In gray we further show the  $1\sigma$  and  $2\sigma$  regions preferred by a global fit to  $b \rightarrow s \mu^+ \mu^-$  data, which has been performed in [1] using `flavio` [147]. It is very interesting that for all three flavour structures we find viable parameter points inside the  $1\sigma$  region, showing that these models can potentially explain these anomalies. But we have to remark that for all cases these points do not have a good fine-tuning. We observe that all points with  $C_9^{\text{NP}} \lesssim -0.5$  have a relatively small composite coupling  $g_X$  in the range  $g_X = \mathcal{O}(1-2)$ . As a consequence, there will be a light neutral composite vector resonance in the spectrum. Furthermore, as the coupling  $g_X$  is small, this resonance will dominantly be  $X_\mu$ , since the admixtures of other neutral

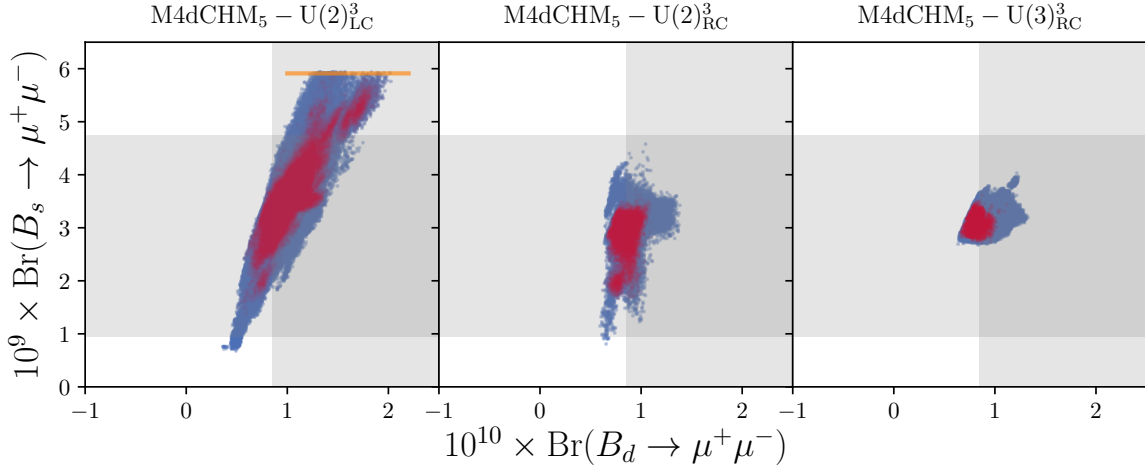


**Figure 4.17.:** Modifications of the branching ratios for  $B_d \rightarrow \mu^+\mu^-$  and  $B_s \rightarrow \mu^+\mu^-$ . In blue all viable parameter points are shown while the red points mark  $\Delta_{\text{BG}} < 100$ . The gray regions denote the  $2\sigma$  experimental results. To guide the eye orange lines are drawn where  $B_s \rightarrow \mu^+\mu^-$  cuts into the parameter space.

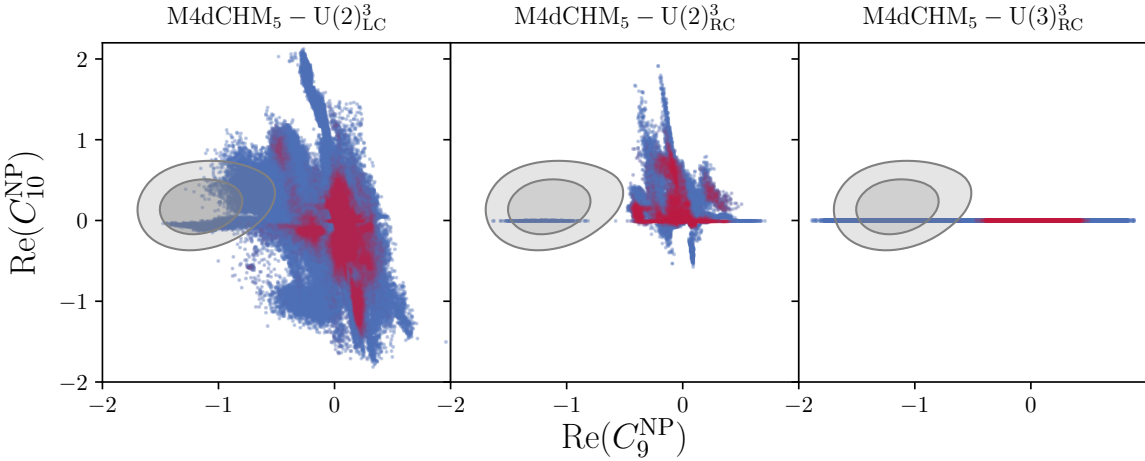


**Figure 4.18.:** Contributions to the Wilson coefficients  $C_9$  and  $C_{10}$ . In the heavy quark sector we show  $\text{Br}(b \rightarrow s\gamma)$  and for first generation quarks we present contributions to electric dipole moment of the neutron. In blue all viable parameter points are shown while the red points mark  $\Delta_{\text{BG}} < 100$ . The preferred region for the Wilson coefficients at  $1\sigma$  and  $2\sigma$  as obtained through a global fit to  $b \rightarrow s\mu^+\mu^-$  data (using the numerical results of [1]) are shown by gray ellipses. To guide the eye orange lines are drawn where these constraints cut into the parameter space.



resonances are  $g_X$ -suppressed<sup>5</sup>. Therefore, this resonance will only have non-chiral vector couplings to the fermions such that one can effectively consider it as a  $\gamma'$  resonance which only contributes to  $C_9^{\text{NP}}$ . Since we implemented the lepton sector as purely elementary in this work, the coupling of the  $\gamma'$  resonance to SM leptons has to go through mixing with elementary gauge bosons. These mixings are suppressed by  $g_X$ , but this suppression is lifted again by an enhancement due to the small  $\gamma'$  mass, such that effectively the Wilson coefficient gets corrections  $C_9^{\text{NP}} \sim (1/m_X^2) \times f_X^2 g_0 g_X \sim g_0/g_X$ , which need not be small. Hence, there can be large effects in  $C_9^{\text{NP}}$ , provided the flavour off-diagonal coupling to SM quarks is not too small. In some sense, the Markov chains have found a way to circumvent the arguments given in section 3.3.5. For these points we therefore predict the existence of a light vector resonance which could show up in direct searches. Furthermore, we find that this light  $\gamma'$  has the largest branching ratio into  $\bar{t}t$  pairs

Let us note here that CHMs possess also another mechanism for generating sufficient contributions to  $C_9$  and  $C_{10}$  to explain the anomalies in  $b \rightarrow s\ell\ell$  data which was investigated by us in [5]. If one extends the framework used in this analysis and introduces partially composite leptons then one can show that under certain circumstances (which are described below) effects in  $\mathcal{O}_9$  and  $\mathcal{O}_{10}$  can be generated in the right ballpark without getting into conflict with other measurements. The idea behind this is that a good agreement with the  $b \rightarrow s\ell\ell$  data can be achieved if NP enters via  $C_9^{\text{NP}} = -C_{10}^{\text{NP}}$  suggesting a NP contributions solely to left-handed neutral currents. This can be generated in CHMs if the left-handed muons are significantly composite. In this framework it is even possible to explain the recently hinted lepton flavour violation in  $B \rightarrow K\mu^+\mu^-$  and  $B \rightarrow K^*\mu^+\mu^-$  decays [190, 191] if muons and electrons are equipped with different degrees of compositeness. Note that the small muon mass can still be reproduced in this case if the right-handed muons are mostly elementary. Introducing composite muons immediately leads to large corrections of  $Z\mu_L\mu_L$  couplings if these are not protected by custodial symmetry analogous to section 2.2.1. It is remarkable that this requirement in the lepton sector uniquely determines the representation under  $\text{SO}(4) \times \text{U}(1)_X$ . The only possibility (if one neglects representations of dimension higher than 3 which would lead to states with exotic electrical charges greater than  $\pm 2$ ) allowed by the symmetries is  $(\mathbf{2}, \mathbf{2})_0 \oplus (\mathbf{1}, \mathbf{3})_0 \oplus (\mathbf{3}, \mathbf{1})_0$ , where  $\mu_L$  is embedded into the bidoublet and  $\mu_R$  is part of  $(\mathbf{1}, \mathbf{3})_0$ . In a pNGB model based on the coset  $\text{SO}(5)/\text{SO}(4)$  this corresponds to an embedding into the antisymmetric representation  $\mathbf{10}$  of  $\text{SO}(5)$ . The necessary contributions to the Wilson coefficients can be generated by a resonance exchange similar to figure 3.8b, but where the vector resonance directly couples to the compositeness of the leptons. In this case, Wilson coefficients are given as

$$\frac{C_9^{\text{NP}}}{\Lambda^2} = -\frac{C_{10}^{\text{NP}}}{\Lambda^2} \sim (c_{bs} g_\rho) \times \frac{1}{m_\rho^2} \times (c_{\mu\mu} s_{\mu_L}^2 g_\rho) \sim \frac{c_{bs} c_{\mu\mu} s_{\mu_L}^2}{f^2}, \quad (4.24)$$

where  $s_{\mu_L}$  denotes the muon degree of compositeness and  $c_{bs}$  and  $c_{\mu\mu}$  are model-dependent numerical factors. An upper bound on  $c_{bs}$  can be obtained from  $B_s$  mixing as for this the mass difference should go like  $\Delta M_s \sim c_{bs}^2$ . A large muon degree of compositeness affects the extraction of the Fermi constant  $G_\mu$  from muon decay. However, one can show that there exist regions in parameter space where this effect is not too large, but also sizable effects in the vector operators can be generated.

### Predictions in the kaon sector

We did not include rare kaon decays as constraints into the analysis, therefore we are able to give predictions. The rare decays  $K^+ \rightarrow \pi^+\bar{\nu}\nu$  and  $K_L \rightarrow \pi^0\bar{\nu}\nu$  will be highlights in flavour physics in the next 5-10 years [192, 193]. Being theoretically very clean these decays have the potential to probe the flavour sector to high accuracy [194]. Currently, the experimental situation for both decays is not overwhelming. The charged kaon mode  $K^+ \rightarrow \pi^+\bar{\nu}\nu$  has been measured by the E949 experiment at Brookhaven National Laboratory, but only with a 65% uncertainty [195],

$$\text{Br}(K^+ \rightarrow \pi^+\bar{\nu}\nu)_{\text{exp}} = (1.7 \pm 1.1) \cdot 10^{-10}. \quad (4.25)$$

For the neutral mode only an upper bound exists from the E391a experiment at KEK [196],

$$\text{Br}(K_L \rightarrow \pi^0\bar{\nu}\nu) < 2.6 \cdot 10^{-8} \text{ @ } 90\% \text{CL}, \quad (4.26)$$

<sup>5</sup>As this resonance is mainly  $X_\mu$  it does not contribute to the  $S$  parameter, such that the bound (3.34) is not applicable for it.

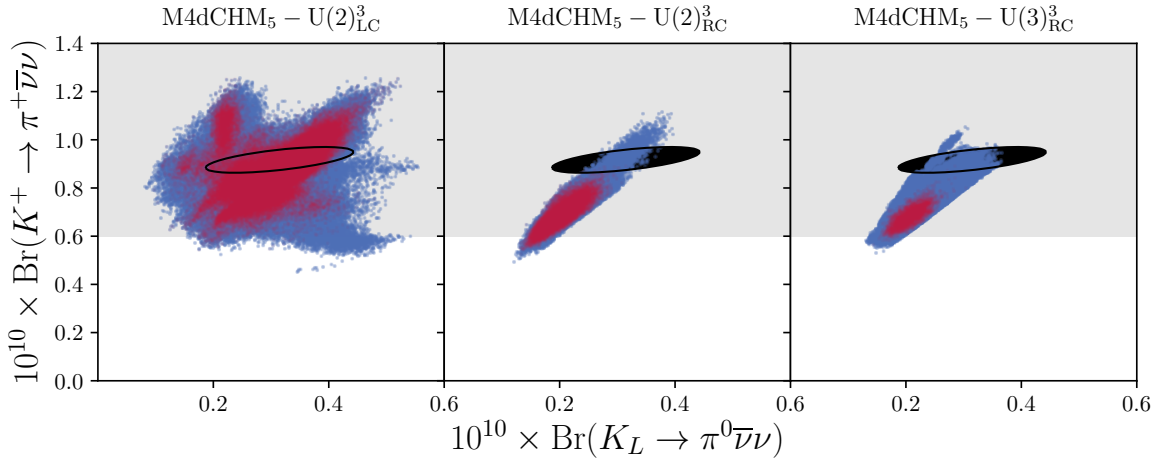


**Figure 4.19.:** Predictions for the rare kaon decays  $K^+ \rightarrow \pi^+ \bar{\nu} \nu$  and  $K_L \rightarrow \pi^0 \bar{\nu} \nu$ . All viable parameter points are shown in blue while the red points mark  $\Delta_{\text{BG}} < 100$ . The light gray band shows the experimental  $1\sigma$  region for  $K^+ \rightarrow \pi^+ \bar{\nu} \nu$ . We do not explicitly show the experimental upper bound  $\text{Br}(K_L \rightarrow \pi^0 \bar{\nu} \nu) < 2.6 \cdot 10^{-8}$  @ 90%CL [108] as this does not pose any bound. The black ellipses show the  $1\sigma$  SM values.

which is still more than three orders of magnitude above the SM prediction. The experimental prospects for these decays are very promising [192]. The NA62 experiment at CERN expects to measure  $\text{Br}(K^+ \rightarrow \pi^+ \bar{\nu} \nu)$  with an accuracy of 5% in the next couple of years. Also the KOTO experiment located at J-PARC expects to measure  $\text{Br}(K_L \rightarrow \pi^0 \bar{\nu} \nu)$  with SM sensitivity within the next 5 years.

We present the predictions for these rare decays in figure 4.19 and observe that no large corrections are to be expected. Although presently there is plenty of room for NP in  $K_L \rightarrow \pi^0 \bar{\nu} \nu$ , we only find SM-like values. In general, we find SM-like values for  $U(2)_{\text{LC}}^3$  and a moderate  $\sim 20\%$  suppression with respect to the SM value in right-compositeness for  $K^+ \rightarrow \pi^+ \bar{\nu} \nu$ . The majority of the points lie within in the current experimental  $1\sigma$  region. But with the expected future sensitivity at the 10% level these effects could become visible making this observable a promising one for the future.

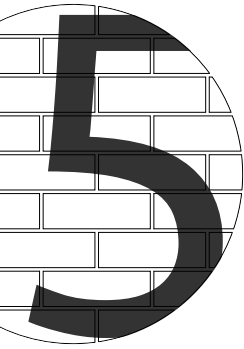
## 4.8. Summary

Generally, we find that CHMs are in a good shape when confronted with current experimental data. Our findings are the following:

- We do not find any viable parameter point supporting a  $U(3)_{\text{LC}}^3$  flavour symmetry.
- For all other flavour structures we find a significant fraction of points with better than percent-level tuning.
- Generally, we find a top mass which is about 10% too light. As expected, the main tension with fine-tuning is given by the large value of the top mass. But we also note that this is still within the uncertainties of our theoretical calculation for the top mass.
- Model-independently we find minima of the effective potential everywhere in the range  $s_h^* \sim 0.2 - 0.6$ , which corresponds to values of  $f$  in the range  $f \sim (500 - 1500)$  GeV.
- EWSB can be induced by top partners as well as by bottom partners. But the latter option is not favoured for  $U(2)_{\text{RC}}^3$ .
- The lightest fermion resonances always have masses below 2 TeV, but the lightest vector resonances are usually heavier than 1.5 TeV. Exceptions are light neutral  $Z'$  bosons that dominantly consist of  $X_\mu$ .
- In all models large corrections to EWPOs can occur.

- 
- For left-compositeness first-row CKM unitarity is the most significant bound. For right-compositeness dijet bounds and the CKM angle  $\gamma$  are most constraining.
  - In Higgs physics we find significant modifications of signal strengths which are, however, in most cases still compatible with current experimental data. Future estimations show that  $h \rightarrow \gamma\gamma$  and in particular  $h \rightarrow \bar{b}b$  will become relevant probes of CHMs in the not-so-distant future.
  - Large effects (up to saturating present experimental bounds) are possible in meson-antimeson mixing.
  - For most points expectations for  $\Delta F = 2$  observables as given in U(2) and U(3) flavour symmetries are satisfied, while also large violations of these conditions are possible.
  - Correlations between  $\Delta F = 2$  observables (in particular  $|\epsilon_K|/|\epsilon_K^{\text{SM}}|$  vs.  $\Delta M_d/\Delta M_d^{\text{SM}}$ ) allow to distinguish the flavour structure.
  - We find no obvious correlation between flavour observables and the effective potential. Points with an acceptable fine-tuning are mostly clustered around the experimental values.
  - Large effects in  $b \rightarrow s\gamma$  (mostly a suppression) are possible.
  - We find only tiny contributions to the electric dipole moment of the neutron.
  - For  $U(2)_{\text{LC}}^3$  the rare decay  $B_s \rightarrow \mu^+\mu^-$  is an important probe for the axial vector operator  $\mathcal{O}_{10}^{(\prime)}$ , but for right-handed compositeness we only find minor effects.
  - Generally, we find values at the lower end of the experimentally allowed region for the rare decay  $B_d \rightarrow \mu^+\mu^-$  and for right-compositeness the decay  $B_s \rightarrow \mu^+\mu^-$  is SM-like.
  - For all flavour structures we find parameter points that can explain the current anomalies in  $b \rightarrow s\ell\ell$  data, which however are plagued by a certain amount of fine-tuning. For these we predict the existence of a light neutral vector resonance with a significant branching ratio into top pairs.
  - We can make predictions for the rare kaon decays  $K \rightarrow \pi\nu\nu$ . Corrections of about 20% to the SM value are found which can become visible in the forthcoming generation of kaon experiments.





## SO(6)/SO(5) – the next-to-minimal model

For a CHM that is phenomenologically successful without being fine-tuned to a large degree the coset  $SO(5)/SO(4)$  is the minimal choice. Abandoning minimality there is plenty of room for model-building (for a recent review see e.g. [197]). In this chapter we want to deform the minimal scenario to the next-to-minimal coset  $SO(6)/SO(5)$ .

The main consequences of enlarging the coset structure is a larger NGB sector. For the next-to-minimal coset the scalar sector will, apart from the Higgs doublet, contain an additional scalar field  $\eta$  which is a singlet under the SM gauge symmetries. The presence of this scalar leads to profound modifications compared to the minimal coset. The effective scalar potential becomes a combined one for the singlet and the doublet. Consequently, the new scalar can possibly obtain a non-trivial vev giving interesting contributions to EWSB. Furthermore,  $\eta$  can be shown to be a pseudo-scalar field, such that the effective potential can act as a source of spontaneous  $CP$  violation through the  $\eta$  vev. In this case also a mixing between the singlet and doublet scalars will be allowed, leading to modifications in Higgs physics.

A further interesting motivation for this coset lies in the fact that it is isomorphic to  $SU(4)/Sp(4)$  which is in fact the minimal option admitting a purely fermionic 4d UV completion [198, 199, 200, 201, 202, 203, 204, 205]. Furthermore, it could give important contributions to baryogenesis in the early universe as the effective Higgs potential can give rise to a strongly first-order electroweak phase transition and new sources of  $CP$  violation [168]. If the coset is supplemented by a suitable  $\mathbb{Z}_2$  parity (such that the coset becomes  $O(6)/O(5)$ ), the additional scalar is stable and could serve as a dark matter candidate [206].

In the following we will modify the M4dCHM used in the previous chapter to the next-to-minimal coset and perform an analysis along the same lines as for the minimal model. After discussing the level of fine-tuning that can be obtained in this model we investigate the limit in which the next-to-minimal model reduces to the minimal one before we discuss novel features that the enlarged coset introduces.

### 5.1. The next-to-minimal 4d composite Higgs model

In this section we introduce the Next-to-Minimal 4d Composite Higgs Model (NM4dCHM) based on the coset  $SO(6)/SO(5)$ . The main difference with respect to the minimal model considered in chapter 4 is the existence of an enlarged scalar sector containing an additional SM singlet state [207, 51, 208, 209, 210, 211]. In the following we will discuss in detail the deformation of the minimal model to the next-to-minimal coset. We will again use the 4d Composite Higgs [99] as the basis for the model used in this analysis.

#### 5.1.1. Nambu-Goldstone bosons in $SO(6)/SO(5)$

The next-to-minimal coset is subject to an isomorphism  $SO(6)/SO(5) \cong SU(4)/Sp(4)$ . As a consequence the group theory of this coset can be described either by complex  $4 \times 4$  matrices or by  $6 \times 6$  orthogonal matrices. Both conventions have been used in the literature, see [51] for a work using the  $SU(4)/Sp(4)$  language and [212, 211] for related analyses in the  $SO(6)/SO(5)$  framework. We decided to perform the following analysis using the coset  $SO(6)/SO(5)$  as it has the advantage that the connection to the minimal coset will be clearer and one could easily write down a decomposition of  $SO(6)$  components into  $SO(4) \cong SU(2)_L \times SU(2)_R$  components, which is convenient considering

custodial symmetry and embeddings of SM fields. Going back to chapter 4, the generators of  $\text{SO}(5)$  are written as

$$\text{SO}(5) : \quad \mathbb{T}^A = \left( \underbrace{\mathbb{T}_L^a, \mathbb{T}_R^a}_{\text{SO}(4)}, \underbrace{\mathbb{T}_{(2,2)}^{\hat{a}}}_{\text{coset}} \right), \quad (5.1)$$

where  $\mathbb{T}_{L,R}^a$  are the generators of the  $\text{SU}(2)_{L,R}$  subgroups and the four generators  $\mathbb{T}_{(2,2)}^{\hat{a}}$  parametrize the coset. Going to the larger group  $\text{SO}(6) \supset \text{SO}(5)$ , 5 generators have to be added.<sup>1</sup> Under  $\text{SO}(5)$  the coset states form a **5**-plet which is why under  $\text{SO}(4)$  they can be written as a bidoublet and a singlet. Hence, the generators can be written as

$$\text{SO}(6) : \quad \mathbb{T}^A = \left( \underbrace{\mathbb{T}_L^a, \mathbb{T}_R^a, \mathbb{T}_{(2,2)}^{1,a}}_{\text{SO}(5)}, \underbrace{\mathbb{T}_{(2,2)}^{2,\hat{a}}, \mathbb{T}_S}_{\text{coset}} \right), \quad (5.2)$$

where now the unbroken subgroup contains a bidoublet  $\mathbb{T}_{(2,2)}^{1,a}$  and the coset consists of another bidoublet and a singlet.

The description of Nambu-Goldstone bosons in the next-to-minimal coset works in principle just the same as in the minimal one. Using the CCWZ formalism (see appendix II) we can implement them in terms of a NGB matrix that takes the usual form

$$\mathcal{U} = \exp \left[ i \frac{\sqrt{2}}{f} \Pi(x) \right] \quad \text{with } \Pi(x) = \pi_5 \mathbb{T}_S + \sum_i \pi^i \mathbb{T}_{(2,2)}^{2,i} \quad (5.3)$$

$$= \begin{pmatrix} 1 & 0 & 0 & 0 & 0 & 0 \\ 0 & 1 & 0 & 0 & 0 & 0 \\ 0 & 0 & 1 & 0 & 0 & 0 \\ 0 & 0 & 0 & \frac{\cos\left(\frac{\sqrt{\pi_4^2 + \pi_5^2}}{f}\right) \pi_4^2 + \pi_5^2}{\pi_4^2 + \pi_5^2} & \frac{\pi_4 \pi_5 \left(\cos\left(\frac{\sqrt{\pi_4^2 + \pi_5^2}}{f}\right) - 1\right)}{\pi_4^2 + \pi_5^2} & \frac{\pi_4 \sin\left(\frac{\sqrt{\pi_4^2 + \pi_5^2}}{f}\right)}{\sqrt{\pi_4^2 + \pi_5^2}} \\ 0 & 0 & 0 & \frac{\pi_4 \pi_5 \left(\cos\left(\frac{\sqrt{\pi_4^2 + \pi_5^2}}{f}\right) - 1\right)}{\pi_4^2 + \pi_5^2} & \frac{\pi_4^2 + \pi_5^2 \cos\left(\frac{\sqrt{\pi_4^2 + \pi_5^2}}{f}\right)}{\pi_4^2 + \pi_5^2} & \frac{\pi_5 \sin\left(\frac{\sqrt{\pi_4^2 + \pi_5^2}}{f}\right)}{\sqrt{\pi_4^2 + \pi_5^2}} \\ 0 & 0 & 0 & \frac{\pi_4 \sin\left(\frac{\sqrt{\pi_4^2 + \pi_5^2}}{f}\right)}{\sqrt{\pi_4^2 + \pi_5^2}} & \frac{\pi_5 \sin\left(\frac{\sqrt{\pi_4^2 + \pi_5^2}}{f}\right)}{\sqrt{\pi_4^2 + \pi_5^2}} & \cos\left(\frac{\sqrt{\pi_4^2 + \pi_5^2}}{f}\right) \end{pmatrix}, \quad (5.4)$$

where already SM unitary gauge was assumed to eliminate  $\pi^{1,2,3}$ , such that in the end a bidoublet field  $\pi^4$  and a singlet field  $\pi^5$  appear in the scalar sector. The above form is not very convenient as it contains square roots and trigonometric functions of the scalar fields.<sup>2</sup> To obtain a more useful form we can perform a non-linear field transformation [211] which replaces  $\pi^4, \pi^5$  by modulus ( $h$ ) and angle ( $\eta$ ) in the  $\pi^4 - \pi^5$  plane,

$$\pi_4 = h \cos\left(\frac{\eta}{f}\right), \quad \pi_5 = h \sin\left(\frac{\eta}{f}\right). \quad (5.5)$$

With this the NGB matrix greatly simplifies,

$$\begin{pmatrix} 1 & 0 & 0 & 0 & 0 & 0 \\ 0 & 1 & 0 & 0 & 0 & 0 \\ 0 & 0 & 1 & 0 & 0 & 0 \\ 0 & 0 & 0 & \cos\left(\frac{h}{f}\right) \cos^2\left(\frac{\eta}{f}\right) + \sin^2\left(\frac{\eta}{f}\right) & -\sin^2\left(\frac{h}{2f}\right) \sin\left(\frac{2\eta}{f}\right) & \cos\left(\frac{\eta}{f}\right) \sin\left(\frac{h}{f}\right) \\ 0 & 0 & 0 & -\sin^2\left(\frac{h}{2f}\right) \sin\left(\frac{2\eta}{f}\right) & \cos^2\left(\frac{\eta}{f}\right) + \cos\left(\frac{h}{f}\right) \sin^2\left(\frac{\eta}{f}\right) & \sin\left(\frac{h}{f}\right) \sin\left(\frac{\eta}{f}\right) \\ 0 & 0 & 0 & -\cos\left(\frac{\eta}{f}\right) \sin\left(\frac{h}{f}\right) & -\sin\left(\frac{h}{f}\right) \sin\left(\frac{\eta}{f}\right) & \cos\left(\frac{h}{f}\right) \end{pmatrix}. \quad (5.6)$$

<sup>1</sup>Remember that the group  $\text{SO}(n)$  has  $\frac{1}{2}n(n-1)$  generators, which is why the coset  $\text{SO}(6)/\text{SO}(5)$  contains  $\frac{1}{2} \cdot 6 \cdot 5 - \frac{1}{2} \cdot 5 \cdot 4 = 5$  generators.

<sup>2</sup>Also, as we will see later there are mixing terms between composite scalars and vectors appearing that are very hard to eliminate using the above parameterization of the NGB matrix.

Note that now all dependence on the NGB fields comes through trigonometric functions as in the case of the minimal coset.

A very important consequence of this coset is that the additional NGB  $\pi^5$  is a pseudoscalar [51]. The reason for this is that the generators of the coset  $\text{SO}(6)/\text{SO}(5)$  give rise to an automorphism which acts as a  $CP$  transformation and yields<sup>3</sup>

$$\pi^4 \rightarrow \pi^4, \quad \pi^5 \rightarrow -\pi^5. \quad (5.7)$$

Through the transformation (5.5), parities are assigned such that  $h$  is a scalar field while  $\eta$  is a pseudoscalar.

In this non-minimal coset a subtlety arises which is not present in the minimal model. Considering a 4d strongly interacting UV completion, there could be anomalies connected with technicolor-like gauge interactions. To reflect these onto the low-energy effective theory of composite resonances one has to add Wess-Zumino-Witten (WZW) terms [213, 214]. Such a case is allowed for the next-to-minimal coset [51], giving

$$\mathcal{L} \supset \frac{\eta}{16\pi^2} \left( n_B B_{\mu\nu} \tilde{B}^{\mu\nu} + n_W \text{tr} \left[ W_{\mu\nu} \tilde{W}^{\mu\nu} \right] + n_G \text{tr} \left[ G_{\mu\nu} \tilde{G}^{\mu\nu} \right] \right), \quad (5.8)$$

where the tildes denote dual field strengths tensors. The structure of these terms is determined by symmetry considerations of the coset while the numerical values of the coefficients  $n_B$ ,  $n_W$  and  $n_G$  are dictated by the anomaly structure of the concrete underlying UV theory. However, for the given coset one finds generally that  $n_B + n_W = 0$  [209], such that these terms do not give effective couplings of  $\eta$  to photons, but they lead to additional  $\eta ZZ$ ,  $\eta W^+ W^-$  and  $\eta GG$  couplings. As we do not specify a concrete UV completion, we would have to include these couplings as free parameters whose net effect would be to increase the constraints coming from direct searches. In our analysis we chose to ignore these terms for two reasons. Without a UV theory in mind we do not know the values of these couplings, therefore ignoring them is the most conservative option as we do not want to arbitrarily exclude a model that possibly predicts smaller couplings than the ones assumed by us. Further, we are actually not able to include these terms in our scanning procedure. As these terms only rescale the bounds coming from direct searches, the Markov chains would always have the tendency to tune the couplings to zero in order to decrease the tensions associated with them.

### 5.1.2. Bosonic Lagrangian

For the NM4dCHM with the coset  $\text{SO}(6)/\text{SO}(5)$  the Lagrangian has the same form as in the  $\text{SO}(5)/\text{SO}(4)$  case. It consists of a *gauge part* (which parametrizes the composite vector resonances) and a  *$\sigma$ -model part* (which includes the NGB fields),

$$\mathcal{L}_{\text{boson}} = \mathcal{L}_{\text{gauge}} + \mathcal{L}_{\text{NGB}}. \quad (5.9)$$

The gauge Lagrangian contains the kinetic terms of the composite and elementary vectors as well as the mixing terms between  $B$  and  $G$  resonances (which take the same form as in eq. (4.3) for the minimal coset),

$$\mathcal{L}_{\text{gauge}} = -\frac{1}{4} \text{tr} [\rho_{\mu\nu} \rho^{\mu\nu}] - \frac{1}{4} \text{tr} [A_{\mu\nu}^0 A_0^{\mu\nu}] + \mathcal{L}_{B,G\text{-mixing}}. \quad (5.10)$$

The composite vector resonances, being in adjoint representations of  $\text{SO}(6)$ , consist of 15 components,

$$\rho^\mu = \rho_A^\mu \Gamma^A = \underbrace{\rho_L^\mu + \rho_R^\mu + \mathfrak{a}_1^\mu}_{\text{SO}(5)} + \underbrace{\mathfrak{a}_2^\mu + \rho_S^\mu}_{\text{coset}}, \quad (5.11)$$

which correspond to the 15 generators given in (I.9). Compared to the case of the minimal coset (4.1) there is an additional bidoublet  $\mathfrak{a}_1^\mu$  which does not belong to the coset, as well as a singlet coset state  $\rho_S^\mu$ .

The  $\sigma$  model Lagrangian also has the same form as before since the symmetry breaking is analogous (only with larger groups). In the 2-site description there are two  $\sigma$ -model fields,  $\Omega_1$  and  $\Omega_2$ , transforming in the same way under the symmetries as in the  $\text{SO}(5)/\text{SO}(4)$  case (with the replacement

<sup>3</sup>Note that since the fundamental representation of  $\text{SO}(6)$  is a real one, this  $CP$  transformation does not involve a complex conjugation. We thank Andreas Trautner for pointing this out.

$\text{SO}(5) \rightarrow \text{SO}(6)$  and  $\text{SO}(4) \rightarrow \text{SO}(5)$ ). Thus, the Lagrangian<sup>4</sup> can be written as

$$\mathcal{L}_{\text{NGB}} = \frac{f_1^2}{4} \text{tr} \left[ (\mathcal{D}_\mu \Omega_1)^\dagger (\mathcal{D}^\mu \Omega_1) \right] + \frac{f_2^2}{2} \left[ (\mathcal{D}_\mu \Omega_2)^\dagger (\mathcal{D}^\mu \Omega_2) \right]_{66} \quad (5.12)$$

with the covariant derivatives

$$\mathcal{D}_\mu \Omega_1 = \partial_\mu \Omega_1 - i (g_0 W_\mu^0 \mathbf{T}_L^a + g'_0 B_\mu^0 \mathbf{T}_R^3) \Omega_1 + i g_\rho \Omega_1 \rho_\mu \quad (5.13)$$

$$\mathcal{D}_\mu \Omega_2 = \partial_\mu \Omega_2 - i g_\rho \rho_\mu \Omega_2. \quad (5.14)$$

Going to holographic gauge (2.132) we set<sup>5</sup>

$$\Omega_1 = \mathcal{U} \quad \text{and} \quad \Omega_2 = \mathbb{1}. \quad (5.15)$$

As in the  $\text{SO}(5)/\text{SO}(4)$  case, the holographic gauge leads to mixing terms between the NGBs and neutral components of the coset vector resonances. In particular, there are mixing matrices connecting  $\partial_\mu h$ ,  $\partial_\mu S$ ,  $\mathbf{a}_{1\mu}^4$ ,  $\mathbf{a}_{2\mu}^4$  and  $\rho_{S\mu}$ . In general, these terms are of the form

$$(\partial_\mu h) \mathbf{a}_{2\mu}^{4\mu} \times (1 + h + h^2 + \eta + \eta^2 + h\eta + \dots). \quad (5.16)$$

For the  $\text{SO}(5)/\text{SO}(4)$  case there was only the first term linear in the mixing, which could be eliminated by a simple shift (4.9) of the vector resonances. For the coset we are considering now, the situation is slightly different since we also find nonlinear terms for the mixing. After EWSB these lead to vev-dependent mixings of scalars and vectors.

Explicitly, these mixings take the form<sup>6</sup>

$$\left( \begin{array}{c|ccccc} & \partial_\mu h & \partial_\mu \eta & \mathbf{a}_{4\mu}^2 & \mathbf{a}_{4\mu}^1 & \rho_{S\mu} \\ \hline \partial_\mu h & \frac{1}{2} & 0 & \frac{f_1 g_\rho \cos\left(\frac{v_\eta}{f_1}\right)}{2\sqrt{2}} & 0 & \frac{f_1 g_\rho \sin\left(\frac{v_\eta}{f_1}\right)}{2\sqrt{2}} \\ \partial_\mu \eta & 0 & 2 \sin^2\left(\frac{v_h}{2f_1}\right) & -\frac{f_1 g_\rho \sin\left(\frac{v_h}{f_1}\right) \sin\left(\frac{v_\eta}{f_1}\right)}{2\sqrt{2}} & \frac{f_1 g_\rho \sin^2\left(\frac{v_h}{2f_1}\right)}{\sqrt{2}} & \frac{f_1 g_\rho \cos\left(\frac{v_\eta}{f_1}\right) \sin\left(\frac{v_h}{f_1}\right)}{2\sqrt{2}} \\ \mathbf{a}_{4\mu}^2 & \frac{f_1 g_\rho \cos\left(\frac{v_\eta}{f_1}\right)}{2\sqrt{2}} & -\frac{f_1 g_\rho \sin\left(\frac{v_h}{f_1}\right) \sin\left(\frac{v_\eta}{f_1}\right)}{2\sqrt{2}} & \frac{1}{4} (f_1^2 + f_2^2) g_\rho^2 & 0 & 0 \\ \mathbf{a}_{4\mu}^1 & 0 & \frac{f_1 g_\rho \sin^2\left(\frac{v_h}{2f_1}\right)}{\sqrt{2}} & 0 & \frac{f_1^2 g_\rho^2}{4} & 0 \\ \rho_{S\mu} & \frac{f_1 g_\rho \sin\left(\frac{v_\eta}{f_1}\right)}{2\sqrt{2}} & \frac{f_1 g_\rho \cos\left(\frac{v_\eta}{f_1}\right) \sin\left(\frac{v_h}{f_1}\right)}{2\sqrt{2}} & 0 & 0 & \frac{1}{4} (f_1^2 + f_2^2) g_\rho^2 \end{array} \right) \quad (5.17)$$

As described in [215]<sup>7</sup>, these mixings can be eliminated by suitable redefinitions of the vector resonances,

$$\text{vector}_\mu \rightarrow \text{vector}_\mu + \alpha(v_h, v_\eta) \partial_\mu \text{scalar}, \quad (5.18)$$

followed by a rescaling of the scalar fields. Here,  $\alpha(v_h, v_\eta)$  is just a number depending on the numerical values of the  $h$ - and  $\eta$ -vevs.

<sup>4</sup>One might be wondering whether this generalization of the  $\text{SO}(5)/\text{SO}(4)$  case is valid here. In particular the second term. In general, one would write these terms using the Maurer-Cartan symbol  $d_\mu^{\hat{a}} = -i \text{tr} \left[ \Omega_2^1 \mathcal{D}_\mu \Omega_2 \mathbf{T}^{\hat{a}} \right]$  as  $\mathcal{L} \supset \frac{f_2^2}{4} d_\mu^{\hat{a}} d^{\hat{a}\mu}$ . But in the  $\text{SO}(N+1)/\text{SO}(N)$  case this is the same as  $\mathcal{L} \supset \frac{f_2^2}{4} (\mathcal{D}_\mu \Phi_2)^\dagger (\mathcal{D}^\mu \Phi_2)$  where  $\Phi_2 = \Omega_2 \phi_0$  with  $\phi_0 = (0, 0, 0, 0, 1)$  [100].

<sup>5</sup>One has to remember that in this gauge one has to replace  $f \rightarrow f_1$  in (5.6).

<sup>6</sup>We extracted these expressions by expanding every term in the Lagrangian (5.12) around  $(h, \eta) = (v_h, v_\eta)$  and keeping only the 0-th order terms.

<sup>7</sup>In even more detail this is described in [216]



We can perform the following redefinitions:<sup>8</sup>

$$\mathbf{a}_{4\mu}^1 \rightarrow \mathbf{a}_{4\mu}^1 + \frac{\left(\sqrt{2} \cos\left(\frac{v_h}{f}\right) - \sqrt{2}\right)}{f_1 g_\rho} \partial_\mu \eta, \quad (5.19a)$$

$$\mathbf{a}_{4\mu}^2 \rightarrow \mathbf{a}_{4\mu}^2 + \frac{\sqrt{2}(f^2 - f_1^2) \cos\left(\frac{v_\eta}{f \sin\left(\frac{v_h}{f}\right)}\right)}{f_1^3 g_\rho} \partial_\mu h - \frac{\sqrt{2}(f^2 - f_1^2) \sin\left(\frac{v_h}{f}\right) \sin\left(\frac{v_\eta}{f \sin\left(\frac{v_h}{f}\right)}\right)}{f_1^3 g_\rho} \partial_\mu \eta, \quad (5.19b)$$

$$\rho_{S\mu} \rightarrow \rho_{S\mu} + \frac{\sqrt{2}(f^2 - f_1^2) \sin\left(\frac{v_\eta}{f \sin\left(\frac{v_h}{f}\right)}\right)}{f_1^3 g_\rho} \partial_\mu h + \frac{\sqrt{2}(f^2 - f_1^2) \sin\left(\frac{v_h}{f}\right) \cos\left(\frac{v_\eta}{f \sin\left(\frac{v_h}{f}\right)}\right)}{f_1^3 g_\rho} \partial_\mu \eta, \quad (5.19c)$$

$$h \rightarrow \frac{f_1}{f} h, \quad \eta \rightarrow \frac{f_1}{f \sin\left(\frac{v_h}{f}\right)} \eta. \quad (5.19d)$$

As a consequence, all unwanted mixing terms vanish, but due to the rescaling (5.19d), all dependence of the NGB fields will now come via

$$s_h = \sin\left(\frac{h}{f}\right), \quad \tilde{s}_\eta = \sin\left(\frac{\eta}{f \sin\left(\frac{v_h}{f}\right)}\right). \quad (5.20)$$

In particular, the effective potential will be a function of these entities,  $V_{\text{eff}}(s_h, \tilde{s}_\eta)$ .

This Lagrangian leads to mass mixing matrices for the vector resonances, that are presented in appendix III.2.1.

### 5.1.3. Fermion Lagrangian

Formally, including composite fermion resonances for the next-to-minimal coset is analogous to the case of the minimal one. One first has to specify the representation of the fermion under SO(4). Using the SU(4)/Sp(4) language the smallest representations have been investigated in [51]. It was found that the **4**- and **10**-dimensional representations (which are spinor representations of SO(6)) are phenomenologically not viable. The **4** = **(1, 2)**  $\oplus$  **(2, 1)** does not contain a bidoublet under the custodial symmetry and therefore  $Z b_L b_L$  vertices are not protected in this model (see section 2.2.1). The symmetric tensor **10** = **(2, 2)**  $\oplus$  **(3, 1)**  $\oplus$  **(1, 3)** does contain a custodial protection, but it gives rise to an electroweak-scale axion-like particle that would be in conflict with measurements. For the **6**-dimensional representation (which corresponds to the fundamental representation of SO(6)) the authors of [51] report no apparent tension with experimental data. The next smallest representations of SO(6) are the antisymmetric **15**-dimensional tensor and the symmetric **20**-dimensional tensor. For reasons of simplicity we choose the smallest possibility and assume the composite fermion resonances to belong to the fundamental **6**-dimensional representation of SO(6).

Under the SO(5) and SO(4) subgroups the fundamental representation decomposes as **6** = **5** + **1** = **(2, 2)** + **(1, 1)** + **(1, 1)**. This shows that the structure of the fermion representations is similar to the fundamentals of SO(5) (see (4.11)), but supplemented with an additional singlet component,

$$\Psi_{\mathbf{6}} = \left( \begin{array}{c} \left[ \begin{array}{cc} Q^{++} & Q^{+-} \\ Q^{-+} & Q^{--} \end{array} \right] \\ S_1^{00} \\ S_2^{00} \end{array} \right) = \frac{1}{\sqrt{2}} \left( \begin{array}{c} Q^{++} + Q^{--} \\ iQ^{++} - iQ^{--} \\ Q^{+-} - Q^{-+} \\ iQ^{+-} + iQ^{-+} \\ \sqrt{2} S_1^{00} \\ \sqrt{2} S_2^{00} \end{array} \right), \quad (5.21)$$

leading to an additional composite singlet resonances in the theory.

The embedding of left-handed elementary fields into SO(6) fundamentals proceeds along the same lines as for the case of SO(5), i.e. we can use eq. (4.12a) and simply add an additional 0 for the

<sup>8</sup>Note that after this shift also the kinetic mixing  $(\partial_\mu h)(\partial^\mu \eta)$  vanishes! This does not happen when using the expression (5.4) without the transformation (5.5) for the Goldstone matrix.

6th component. The embeddings of the right-handed elementary fermions, on the other hand, is ambiguous as there are two singlets in the fundamental (5.21). To be as general as possible, this means that two different embeddings have to be considered [51],

$$\xi_{q_R}^5 = \begin{pmatrix} 0 \\ 0 \\ 0 \\ 0 \\ q_R^0 \\ 0 \end{pmatrix}, \quad \xi_{q_R}^6 = \begin{pmatrix} 0 \\ 0 \\ 0 \\ 0 \\ 0 \\ q_R^0 \end{pmatrix}, \quad (5.22)$$

where  $q$  denotes either the elementary up- or down-quark.

The general form of the fermion Lagrangian looks is similar to the minimal coset,

$$\mathcal{L}_{\text{quark}} = \mathcal{L}_{\text{quark}}^{(\text{elem})} \quad (5.23a)$$

$$+ \bar{\Psi}_u (i\mathcal{D} - m_U) \Psi_u + \bar{\tilde{\Psi}}_u (i\mathcal{D} - m_{\tilde{U}}) \tilde{\Psi}_u \quad (5.23b)$$

$$- Y_u \bar{\Psi}_{uL} \phi_2^t \phi_2 \tilde{\Psi}_{uR} - m_{Y_u} \bar{\Psi}_{uL} \tilde{\Psi}_{uR} + \text{h.c.} \quad (5.23c)$$

$$+ \Delta_{uL} \bar{\xi}_{uL} \Omega_1 \Psi_{uR} + \Delta_{uR}^5 \bar{\xi}_{uR}^5 \Omega_1 \tilde{\Psi}_{uL} + \Delta_{uR}^6 \bar{\xi}_{uR}^6 \Omega_1 \tilde{\Psi}_{uL} + \text{h.c.} \quad (5.23d)$$

$$+ (u \leftrightarrow d), \quad (5.23e)$$

where the breaking  $\text{SO}(6) \rightarrow \text{SO}(5)$  is parametrized by  $\phi_2 = \Omega^* \cdot (0, 0, 0, 0, 0, 1)$ . Note that there are two different composite-elementary mixings for the right-handed elementary quarks, that in general can have independent couplings.

If we go to holographic gauge (eq. (5.15)) we can write the fermion Lagrangian as

$$\mathcal{L}_{\text{quark}} = \mathcal{L}_{\text{quark}}^{(\text{elem})} \quad (5.24a)$$

$$+ i\bar{\Psi}_u \mathcal{D} \Psi_u + i\bar{\tilde{\Psi}}_u \mathcal{D} \tilde{\Psi}_u \quad (5.24b)$$

$$- m_U (\bar{Q}_u Q_u + \bar{S}_{1u} S_{1u} + \bar{S}_{2u} S_{2u}) - \tilde{m}_U (\bar{\tilde{Q}}_u \tilde{Q}_u + \bar{\tilde{S}}_{1u} \tilde{S}_{1u} + \bar{\tilde{S}}_{2u} \tilde{S}_{2u}) \quad (5.24c)$$

$$- (m_{Y_u} + Y_u) \bar{S}_{2uL} \tilde{S}_{2uR} - m_{Y_u} (\bar{Q}_{uL} \tilde{Q}_{uR} + \bar{S}_{1uL} \tilde{S}_{1uR}) + \text{h.c.} \quad (5.24d)$$

$$+ \Delta_{uL} \bar{\xi}_{uL} \mathcal{U} \Psi_{uR} + \Delta_{uR}^5 \bar{\xi}_{uR}^5 \mathcal{U} \tilde{\Psi}_{uL} + \Delta_{uR}^6 \bar{\xi}_{uR}^6 \mathcal{U} \tilde{\Psi}_{uL} + \text{h.c.} \quad (5.24e)$$

$$+ (u \leftrightarrow d). \quad (5.24f)$$

Here we decomposed the fundamental  $\mathbf{6}$  into  $\text{SO}(5)$  representations,  $\Psi = (Q, S_1, S_2)$ . Note that this Lagrangian explicitly shows the remaining invariance under  $\text{SO}(5)$ , while there is a mass splitting between  $(Q, S_1)$  and  $S_2$  that demonstrates the explicit breaking of  $\text{SO}(6)$ .

The mass matrices which we find for the fermion sector of this model are given in appendix III.2.2.

#### 5.1.4. Flavour structure

For the flavour structure, one could in principle consider the same possibilities as in the case of the minimal coset, i.e.  $\text{U}(2)^2$  or  $\text{U}(3)^3$  flavour symmetries with either right- or left-compositeness. In this analysis, however, an investigation of the detailed aspects of flavour physics is not our main concern. Also, left-compositeness would bring additional complications due to the enlarged possibilities for right-handed embeddings. In particular, the theory does not lead to CKM-like flavour violation without additional ad hoc assumptions not motivated by flavour symmetries. Therefore, we consider only one possibility for the flavour structure that proved to be successful in the minimal model. Therefore, in the following analysis we will exclusively consider the  $\text{U}(2)_{\text{RC}}^3$  flavour structure.

The explicit form of the left-handed composite-elementary mixings is precisely the same as in the minimal case (see appendix IV). The right-handed mixings contain a subtlety. Counting the physical phases in these mixings one finds that the relative phases between the (flavour-diagonal)  $\Delta_{\text{R}}^{(5)}$  and  $\Delta_{\text{R}}^{(6)}$  cannot be absorbed, meaning that they are physical and have to be included as free parameters. We write them as complex phases for the  $\Delta_{\text{R}}^6$  mixing and use the following form for the composite-

elementary mixings

$$\Delta_{uL} = \begin{pmatrix} c_u \Delta_{u_1L} & -s_u \Delta_{u_2L} e^{i\alpha_u} & \epsilon_u \Delta_{u_3L} e^{i\phi_u} \\ s_u \Delta_{u_1L} e^{-i\alpha_u} & c_u \Delta_{u_2L} & \Delta_{u_3L} \end{pmatrix}, \quad (5.25a)$$

$$\Delta_{uR}^{5\dagger} = \begin{pmatrix} \Delta_{u_{12}R}^5 & & \\ & \Delta_{u_{12}R}^5 & \\ & & \Delta_{u_3R}^5 \end{pmatrix}, \quad \Delta_{uR}^{6\dagger} = \begin{pmatrix} \Delta_{u_{12}R}^6 e^{i\phi_{u_{12}R}^6} & & \\ & \Delta_{u_{12}R}^6 e^{i\phi_{u_{12}R}^6} & \\ & & \Delta_{u_3R}^6 e^{i\phi_{u_3R}^6} \end{pmatrix}, \quad (5.25b)$$

with analogous expressions for the down-type quark sector.

### 5.1.5. The effective potential and electroweak symmetry breaking

Let us discuss in this section the effective potential of the enlarged scalar sector. The main difference compared to the minimal model is the appearance of the additional scalar field  $\eta$ . As a consequence, there will be a combined potential for  $h$  and  $\eta$  such that, possibly, both can obtain a vev and all particle masses and couplings will depend on the values of both vevs. We have already seen in previous sections that the mass mixing matrices in this theory also depend on  $s_h$  and  $\tilde{s}_\eta$ , so the effective potential can be calculated by the usual methods laid out in section 2.2.2. A new feature that could appear in the next-to-minimal model are contributions to the effective potential induced by interactions between the NGB fields. However, as is well known NGBs only have derivative self-interactions [33]. Furthermore, loops contributing to the effective potential are evaluated at vanishing external momentum. We conclude that NGB self interactions do not contribute to the effective potential.

As we are still working in the framework of 4dCMHs, we benefit from the fact that the model is deconstructed from an extra-dimensional theory. In particular, this means that also for the next-to-minimal coset it is guaranteed that the Weinberg sum rules (2.52) are satisfied and the calculability of the effective potential at one loop level is ensured. This can be seen explicitly by inserting the mass matrices given in appendix III.2 into eq. (2.52).

EWSB is triggered by an explicit breaking of  $SO(5)$  that is generated by the interactions between the composite and the elementary sector. Analogously to the potential in the minimal model (see section 2.2.2), there are contributions coming from the boson and fermion sectors that have to work together to generate a potential that is in accordance with experiment. But due to the larger symmetry structure, new features arise that are interesting to investigate. The general structure of the effective potential in the next-to-minimal model has already been analyzed in great detail in [51] in the language of  $SU(4)/Sp(4)$ . At this point let us review the results and translate them into the  $SO(6)/SO(5)$  notation used in this work.

**Gauge contributions:** Contributions from vector bosons originate from the fact that the global symmetry is broken explicitly by gauging its SM-like subgroup. Although it was the case in the minimal coset that the global symmetry is then broken down completely to the gauged subgroup, this is not true in general. By gauging a subgroup, the global symmetry is only broken down to the largest subgroup that contains the gauged one as an ideal [51]. For  $SO(6)$ , this implies that by gauge interactions alone, the global symmetries are broken down to  $SU(2)_L \times U(1)_Y \times U(1)_S$ . There is an additional  $U(1)_S$  which is still a symmetry of the theory. It is generated by the generator  $T_S$  under which the NGB  $\pi^5$  in (5.3) shifts. As a consequence, gauge contributions alone do not generate a potential for  $\pi^5$  because it is still associated to an unbroken theory and therefore a true NGB. In this case the theory necessarily contains a massless scalar mode.

**Fermion contributions:** To prevent a massless scalar mode one also has to break the  $U(1)_S$  symmetry explicitly. This is possible in the fermion sector if the elementary fermion embeddings have a non-consistent  $U(1)_S$ -charge assignment. The composite resonances, being complete  $SO(6)$  multiplets, are invariant under  $U(1)_S$  by construction. For an elementary embedding  $\xi$  the action of  $U(1)_S$  is given as

$$\xi \rightarrow \xi' = \exp(iq_S \theta T_S) \xi \approx (\mathbb{1} + iq_S \theta T_S + \dots) \xi = \xi + \delta\xi + \dots \quad (5.26)$$

The  $U(1)_S$ -charge assignment is consistent only if  $\delta\xi \sim T_S \xi = q_S \xi$ , i.e. if the embedding is an eigenvector of the generator  $T_S$ . Out of the six eigenvectors of  $T_S$  we find four to have a

degenerate eigenvalue of 0, which correspond to the bidoublet in (5.21). This shows that the left-handed elementary embeddings are always neutral under  $U(1)_S$  and therefore cannot break it. The remaining two eigenvectors correspond to embeddings of the right-handed elementary fermions. These are:

$$\xi_{\text{R}}^+ \sim (0, 0, 0, 0, -i, 1) \quad \text{with } q_S = +\frac{1}{\sqrt{2}}, \quad (5.27a)$$

$$\xi_{\text{R}}^- \sim (0, 0, 0, 0, i, 1) \quad \text{with } q_S = -\frac{1}{\sqrt{2}}. \quad (5.27b)$$

Remembering that there are two right-handed embeddings to be included (see 5.22), this means that the global  $U(1)_S$  symmetry is preserved by the elementary fermion embeddings if

$$\Delta_{\text{R}}^5 = \pm i \Delta_{\text{R}}^6. \quad (5.28)$$

Phrasing this the other way around, this means that a potential for  $\pi^5$  is generated as long as (5.28) is not satisfied.

Using the matrices given in appendix III.2 the effective potential can be calculated just as in the case of the minimal coset via 2.53,

$$V_{\text{eff}}(s_h, \tilde{s}_\eta) = \sum \frac{c_i}{64\pi^2} m_i^4(s_h, \tilde{s}_\eta) \log [m_i^2(s_h, \tilde{s}_\eta)]. \quad (5.29)$$

From this we can calculate the scalar mass mixing matrix as given in (3.17),

$$M_S^2(s_h^*, \tilde{s}_\eta^*) = \left( \begin{array}{cc} \partial_h^2 V_{\text{eff}} & \partial_h \partial_\eta V_{\text{eff}} \\ \partial_h \partial_\eta V_{\text{eff}} & \partial_\eta^2 V_{\text{eff}} \end{array} \right) \Big|_{s_h^*, \tilde{s}_\eta^*}. \quad (5.30)$$

This matrix determines the masses of the scalar fields as well as their mixing. It is interesting to see that due to

$$\partial_\eta V_{\text{eff}} \Big|_{\tilde{s}_\eta^*} = \frac{d\tilde{s}_\eta}{d\eta} \partial_{\tilde{s}_\eta} V_{\text{eff}} \Big|_{\tilde{s}_\eta^*} = \frac{\tilde{c}_\eta^*}{f s_h^*} \partial_{\tilde{s}_\eta} V_{\text{eff}} \Big|_{\tilde{s}_\eta^*} \quad (5.31)$$

the theory contains a very light scalar field in the limit  $\tilde{s}_\eta^* \rightarrow 1$ . For the last equation in (5.31) we made use of (5.20).

## 5.2. The scan

As for the minimal model, a parameter scan along the lines of section 3.1 was performed for the next-to-minimal model. Computationally, the most significant change is the numerical minimization of the now two-dimensional effective scalar potential. This is notably slower than a minimization in only one direction. Together with other additions in the code (such as the numerical evaluation of second and third derivatives of the effective potential for calculating scalar masses and couplings) this led to an increase in computation time to around 1 s for the evaluation of the  $\chi^2$ -function for a single parameter point. Furthermore, due to additional parameters in the composite-elementary mixings of right-handed quarks the dimensionality of the parameter space increased to 52. In total, this made the generation of viable parameter points significantly less efficient compared to the minimal models. We started a total number of  $\mathcal{O}(32\,000)$  Markov chains that in the end resulted in 125 successful chains containing 66161 viable parameter points. The complete analysis consumed  $\mathcal{O}(250\,000)$  cpuh) on the C2PAP computational cluster.

As we will discuss later, it is interesting to consider the limit in which all  $\Delta_{\text{R}}^5$  are small. This is, however, difficult to find in a general parameter scan with Markov chains. Therefore, about one third of all scans were started where this condition was put in by hand for the starting point. By this, we obtain a good coverage of the parameter space also in this limit.

## 5.3. Fine-tuning

As a first result let us assess the amount of fine-tuning needed in the next-to-minimal model to generate the electroweak scale. Analogously to the case of the minimal coset in section 4.3.1 we calculated the

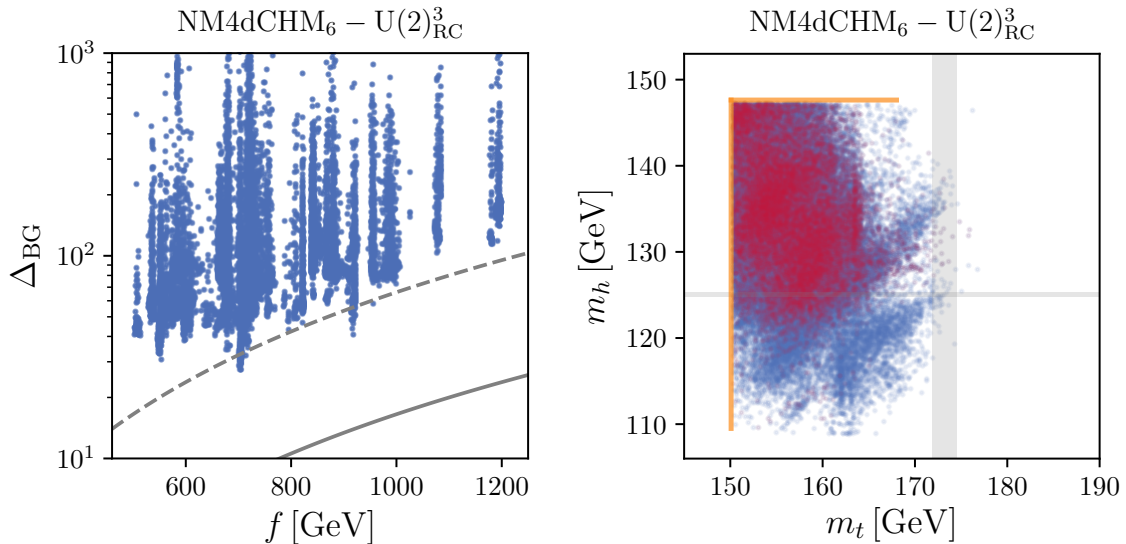


**Figure 5.1.:** Fine-tuning of the effective scalar potential. *Left:* Barbieri-Giudice measure  $\Delta_{\text{BG}}$  of fine-tuning for the found points and its correlation with  $f$ . The gray lines show naive expectations for the fine-tuning (see main text). Note that results are only shown for a relatively small fraction of all found points. This plot is meant to merely give an indication of the general size of fine-tuning. *Right:* Found masses for the top and the Higgs. The red points have  $\Delta_{\text{BG}} < 100$  and the gray band mark the experimental  $1\sigma$  measurements of the masses. To guide the eye orange lines are drawn where these constraints cut into the parameter space of the model.

Barbieri-Giudice measure of tuning (4.18) for the viable parameter points.<sup>9</sup> The results are shown in figure 5.1. We find a minimal fine-tuning  $\Delta_{\text{BG}}^{\text{min}} = 30$ . This is even slightly better than for the minimal model with the same flavour structure (see eq. (4.20))<sup>10</sup>. Hence, a better-than-percent level tuning is also achievable in the next-to-minimal model and a moderate tuning,  $\Delta_{\text{BG}} < 100$ , is possible for  $f \lesssim 1000$  GeV. In figure 5.1 we further show the naive expectation for the minimal fine-tuning,  $\Delta_{\text{min}} \sim f^2/v_{\text{SM}}^2$  displayed as a solid gray line. For the minimal CHM based on the coset  $\text{SO}(5)/\text{SO}(4)$  with fermions in the fundamental representation it is well known that the potential is subject to a so-called double-tuning [56],  $\Delta_{\text{min}} \sim 1/\epsilon^2 \times f^2/v_{\text{SM}}^2$ , meaning a parametrically larger tuning due to the particular structure of the potential (see the discussion in section 2.2.2). We expect this to be true also for the next-to-minimal coset with fermions in the fundamental representation. To guide the eye, we included the expectation for an exemplary value  $\epsilon = 0.5$  as the dashed line in figure 5.1, which shows that our data points are consistent with double-tuning.

Also in the next-to-minimal model moderate fine-tuning is achieved at the expense of having deviations in the top and Higgs mass as seen in the right plot in figure 5.1. For moderate amounts of fine-tuning we generally find a top mass that is 5 – 15% too small and a Higgs boson that is up to 15% too heavy. However, one has to keep in mind that these values are still within in large theory uncertainties of our calculation and that higher-order corrections can lift these tensions.

## 5.4. The $\text{SO}(5)/\text{SO}(4)$ limit

The NM4dCHM features a limit in which it effectively reduces to a theory similar to the M4dCHM. To see this, let us go back to the embeddings of the elementary fermions into  $\text{SO}(6)$  fundamentals. As shown in (5.22) there is an ambiguity for the embeddings of the right-handed quarks, which leads to the introduction of two independent composite-elementary couplings in (5.23). Intuitively, both couplings are on different qualitative grounds. Imagine for the time being that only the mixing  $\Delta_{\text{R}}^6$  is present and  $\Delta_{\text{R}}^5$  is set to zero. In this case  $\text{SO}(6)$  is explicitly broken by the right-handed embeddings

<sup>9</sup>As these calculation are numerically not trivial, we calculated the fine-tuning for around 40% of the viable parameter points. However, this number is enough for our purposes.

<sup>10</sup>In a recent analysis [217] the improved fine-tuning in the next-to-minimal coset was interpreted as being due to so-called “level repulsion”. This means that due to scalar mixing the Higgs mass gets further reduced such that less tuning is needed to obtain a realistic mass for the Higgs boson.

only to SO(5). If now also  $\Delta_{\text{R}}^5$  takes non-zero values then SO(6) is broken down to SO(4). In this sense, the case  $\Delta_{\text{R}}^5 \neq 0$  marks a more violent explicit breaking of the global symmetries than the case  $\Delta_{\text{R}}^5 = 0$ , especially as we are considering a flavour structure with right-compositeness. In this section we will consider the latter case of milder explicit breaking and show that this corresponds to a theory virtually indistinguishable from the minimal coset. The case of a non-vanishing  $\Delta_{\text{R}}^5$  will be discussed in the following section 5.5.

Since we are including the full flavour sector in this work, the composite-elementary mixings are matrix-valued in flavour space. This means that in the considered  $\text{U}(2)_{\text{RC}}^3$  flavour structure there are four different mixings  $\Delta_{\text{R}}^5 = \Delta_{u_{12}\text{R}}^5, \Delta_{u_3\text{R}}^5, \Delta_{d_{12}\text{R}}^5, \Delta_{d_3\text{R}}^5$  (see eq. (5.25)). The SO(5)/SO(4) limit corresponds to the case where all four mixings vanish. Therefore we introduce an order parameter

$$\max \frac{\Delta_{\text{R}}^5}{\Delta_{\text{R}}^6} = \max \left\{ \frac{\Delta_{u_{12}\text{R}}^5}{\Delta_{u_{12}\text{R}}^6}, \frac{\Delta_{u_3\text{R}}^5}{\Delta_{u_3\text{R}}^6}, \frac{\Delta_{d_{12}\text{R}}^5}{\Delta_{d_{12}\text{R}}^6}, \frac{\Delta_{d_3\text{R}}^5}{\Delta_{d_3\text{R}}^6} \right\} \quad (5.32)$$

and consider the limit  $\max \Delta_{\text{R}}^5 / \Delta_{\text{R}}^6 \rightarrow 0$ . To simplify the notation we will denote this limit simply by  $\Delta_{\text{R}}^5 \rightarrow 0$ , but imply the above. The effects of one (or more)  $\Delta_{\text{R}}^5 / \Delta_{\text{R}}^6 \gtrsim 1$  will be discussed in section 5.5.

To see why this limit effectively reduces the theory to SO(5)/SO(4), it is instructive to look at the effective potential in a different form than given in eq. (2.51). Using the methods used e.g. in [55] one can integrate out the heavy sector such that the Lagrangian of the elementary quarks in momentum space takes the form

$$\mathcal{L} \supset \Pi_{\text{L}}^{ij} \bar{q}_{\text{L}}^0 i \not{p} q_{\text{L}}^j + \Pi_{\text{R}}^{ij} \bar{q}_{\text{R}}^i \not{p} q_{\text{R}}^j - \left( \Pi_{\text{LR}}^{ij} \bar{q}_{\text{L}}^i q_{\text{R}}^j + \text{h.c.} \right), \quad (5.33)$$

where the effect of the heavy sector is parametrized in terms of form factors  $\Pi = \Pi(p^2, s_h, \tilde{s}_\eta)$  which depend on the momentum and the pNGBs. We show the derivation of the potential in appendix VI and show at this place only the final result for fermion contributions to the effective potential,

$$V_f(s_h, \tilde{s}_\eta) \sim \int \frac{d^4 p_{\text{E}}}{(2\pi)^4} \log \text{tr} \left[ p_{\text{E}}^2 \Pi_{\text{L}} \Pi_{\text{R}} + |\Pi_{\text{LR}}|^2 \right], \quad (5.34)$$

where the dependence on the pNGBs and the composite-elementary mixings is given through

$$\Pi_{\text{L}}(p^2, s_h, \tilde{s}_\eta) = \left[ 1 - \Delta_{u\text{L}} \pi_u(p^2) \Delta_{u\text{L}}^\dagger - \Delta_{d\text{L}} \pi_d(p^2) \Delta_{d\text{L}}^\dagger \right] - \frac{1}{2} s_h^2 \tilde{c}_\eta^2 \Delta_{u\text{L}} (\pi_{Su}(p^2) - \pi_u(p^2)) \Delta_{u\text{L}}^\dagger, \quad (5.35\text{a})$$

$$\begin{aligned} \Pi_{\text{R}}(p^2, s_h, \tilde{s}_\eta) &= \left[ 1 - \Delta_{u\text{R}}^5 \pi_{Su}(p^2) \Delta_{u\text{R}}^{5\dagger} - \Delta_{u\text{R}}^6 \pi_{Su}(p^2) \Delta_{u\text{R}}^{6\dagger} \right] + \tilde{c}_\eta^2 \Delta_{u\text{R}}^5 (\pi_{Su}(p^2) - \pi_u(p^2)) \Delta_{u\text{R}}^{5\dagger} \\ &+ (c_h \tilde{s}_\eta \Delta_{u\text{R}}^5 - s_h \Delta_{u\text{R}}^6) (\pi_{Su}(p^2) - \pi_u(p^2)) (c_h \tilde{s}_\eta \Delta_{u\text{R}}^{5\dagger} - s_h \Delta_{u\text{R}}^{6\dagger}), \end{aligned} \quad (5.35\text{b})$$

$$\Pi_{\text{LR}}(p^2, s_h, \tilde{s}_\eta) = i s_h \tilde{c}_\eta \Delta_{u\text{L}} \pi_{\text{LR}}(p^2) (s_h \tilde{s}_\eta \Delta_{u\text{R}}^{5\dagger} + c_h \Delta_{u\text{R}}^{6\dagger}). \quad (5.35\text{c})$$

Here we only wrote down the contribution from up-type quarks; the down-type contributions have to be added and are obtained by replacing  $u \leftrightarrow d$ . The explicit forms of the form factor functions  $\pi_q(p^2)$  and  $\pi_{\text{LR}}(p^2)$  are not important in this discussion but they are given in appendix VI.

If we now go to the limit  $\Delta_{\text{R}}^5 \rightarrow 0$ , we see that the potential depends on  $\eta$  only through  $\tilde{c}_\eta^2$  and the potential effectively reduces to the much simpler expression

$$V_f(s_h, \tilde{s}_\eta) \sim \int \frac{d^4 p_{\text{E}}}{(2\pi)^4} \log \text{tr} \left[ \Pi^{(0)}(p_{\text{E}}^2, s_h) + \tilde{c}_\eta^2 \Pi^{(2)}(p_{\text{E}}^2, s_h) \right], \quad (5.36)$$

where the form factors used are combinations of the above form factors. This general dependence on  $\tilde{c}_\eta^2$  is enough to draw some general conclusions about the theory in this limit. The minimum of the potential is obviously given by the values of  $(s_h^*, \tilde{s}_\eta^*)$  at which the derivatives vanish,

$$\partial_{s_h} V_f(s_h, \tilde{s}_\eta) \Big|_{s_h^*, \tilde{s}_\eta^*} = 0, \quad \partial_{\tilde{s}_\eta} V_f(s_h, \tilde{s}_\eta) \Big|_{s_h^*, \tilde{s}_\eta^*} = 0. \quad (5.37)$$

Calculating the derivative in the  $\tilde{s}_\eta$ -direction one easily finds

$$\partial_{\tilde{s}_\eta} V_f(s_h, \tilde{s}_\eta) \sim \int \frac{d^4 p_{\text{E}}}{(2\pi)^4} \frac{\tilde{s}_\eta \text{tr} [\Pi^{(2)}(p_{\text{E}}^2, s_h)]}{\text{tr} [\Pi^{(0)}(p_{\text{E}}^2, s_h) + \tilde{c}_\eta^2 \Pi^{(2)}(p_{\text{E}}^2, s_h)]}, \quad (5.38)$$

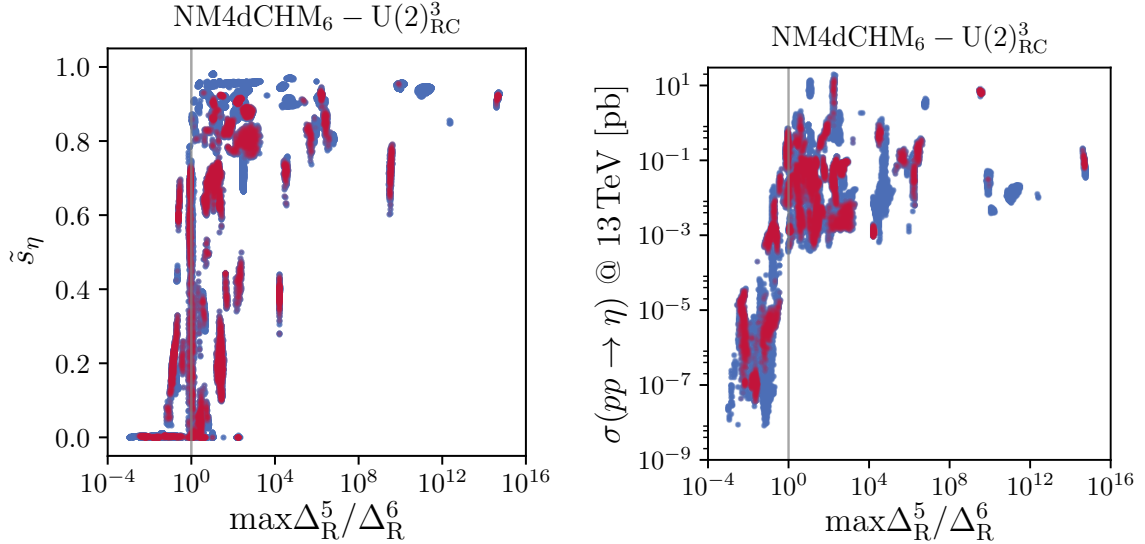


**Figure 5.2.:** Impact of the  $SO(5)/SO(4)$  limit on the phenomenology of  $\eta$ . The results including all viable parameter points are shown in blue while red shows the same but only including parameter points with  $\Delta_{BG} < 100$ . *Left:* Dependence of the  $\eta$ -vev on the order parameter  $\max\Delta_R^5/\Delta_R^6$ . *Right:* Production cross section at a 13 TeV proton-proton collider. In this, gluon fusion, quark-antiquark annihilation and vector boson fusion are included.

which shows that in the limit  $\Delta_R^5 \rightarrow 0$  there is always a minimum in the  $\tilde{s}_\eta$ -direction realized for  $\tilde{s}_\eta^* = 0$ . In this case the potential in the  $s_h$ -direction reduces to the one for the  $SO(5)/SO(4)$  coset<sup>11</sup>. This is shown in the left plot of figure 5.2. One can further observe a form of factorization, namely, as (5.38) shows, acting additionally with a derivative  $\partial_{s_h}$  in the  $s_h$ -direction to calculate the mixing term  $\partial_h \partial_\eta V_{\text{eff}}$  in the scalar mass matrix (3.17) will always give  $\partial_h \partial_\eta V_f = 0$  when evaluated at the minimum of the potential. This shows that in the limit  $\Delta_R^5 \rightarrow 0$  there will be no mixing between the doublet state  $h$  and the singlet  $\eta$ . This picture still remains valid when including gauge contributions into the effective potential.

Looking at the explicit form of the form factors for the effective potential given in (5.35a), we can insert the limit  $\Delta_R^5 \rightarrow 0, \tilde{s}_\eta \rightarrow 0$ . In this case we observe that the potential reduces to the expression given in [55] for the potential in the  $SO(5)/SO(4)$  coset. Therefore, all conclusions on the effective potential obtained in chapter 4 hold for the next-to-minimal potential in this limit. In particular, the allowed values for  $s_h^*$  and  $f$  coincide with the values given in the analysis of the minimal model.

As (5.35c) further shows, there is no linear  $\eta$ -coupling to SM quarks in the limit  $\Delta_R^5 \rightarrow 0$ . Therefore,  $\eta$  is not singly produced at a hadron collider (neither at tree level directly from quarks nor at the loop level via gluon fusion), making it invisible in a classical ‘bump hunt’ of the form  $pp \rightarrow \eta \rightarrow \text{SM}$ . This is shown in the right plot of figure 5.2. Furthermore, couplings to SM gauge bosons are also absent or at least highly suppressed as the singlet  $\eta$  does not mix with the Higgs-like doublet component  $h$ .

In the next-to-minimal coset there are additional vector resonances (a bidoublet  $\mathbf{a}_{1\mu}$  and a singlet  $\rho_{S\mu}$ , see eq. (5.11)) and fermion resonances (singlet fields  $S_{u,d}^1$  and  $\tilde{S}_{u,d}^1$ , see eq. (5.21)) as compared to the minimal case. From the mass matrices given in appendix III.2 one can observe that these additional fields decouple from the theory in the limit  $\Delta_R^5 \rightarrow 0, \tilde{s}_\eta \rightarrow 0$ . Consequently, these fields will impact neither direct nor indirect constraints on the model. Furthermore, the mass matrices of the remaining fields reduce to the expressions in the minimal coset  $SO(5)/SO(4)$  (see appendix III.1), making all effects indistinguishable from the results presented in chapter 4.

Although the pNGB  $\eta$  effectively decouples from the theory, it still receives a mass from the effective potential. Going to the limit  $\Delta_R^5 \rightarrow 0$ , we see that eq. (5.28) cannot be satisfied as long as  $\Delta_R^6 \neq 0$  (which is necessary in order to couple the SM quarks to the Higgs). Therefore, the global  $U(1)_S$  is necessarily broken such that  $\eta$  receives a massless and there is no mass scalar fields in the spectrum.

<sup>11</sup>Formally, there seems to be also the possibility of another extremum connected to the  $\tilde{c}_\eta^2$  in (5.38). But as  $\tilde{c}_\eta^2$  only appears in the denominator we do not think that such an extremum can be realized for physical values of  $\tilde{s}_\eta$ . Also, the numerical results show no indication for the existence of such a solution.

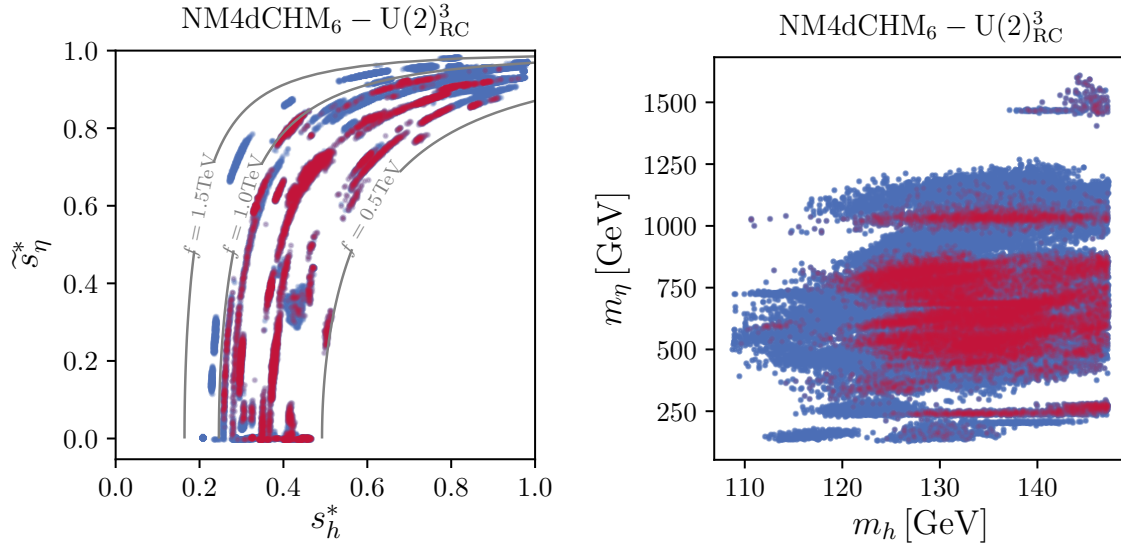


**Figure 5.3.:** Characteristics of the effective scalar potential in the next-to-minimal coset. Results including all viable parameter points are shown in blue, while red denotes parameter points with a moderate fine-tuning,  $\Delta_{\text{BG}} < 100$ . *Left:* Location of the found minima in the  $(s_h^*, \tilde{s}_\eta^*)$ -plane. In gray we show lines of constant  $f$  that reproduce the correct value of  $v_{\text{SM}}$  via (5.39). *Right:* Found masses for  $h$  and  $\eta$ . This directly corresponds to the curvature of the potential at the minimum.

Summarizing, we find that in the limit  $\Delta_{\text{R}}^5 \rightarrow 0$ , the pseudoscalar  $\eta$  does not develop a vev, i.e.  $\tilde{s}_\eta^* = 0$ . Consequently, the effective potential does not act as a source of spontaneous  $CP$  violation. Furthermore,  $\eta$  does not mix with the Higgs-like scalar  $h$ , decouples from SM fields and is not produced at collider experiments. Furthermore, additional vector and fermion resonances decouple from the other fields such that effectively the theory becomes indistinguishable from the M4dCHM. However, the scalar  $\eta$  obtains a mass. Whether in this limit  $\eta$  acts as a possible candidate for dark matter is beyond the scope of this work.

## 5.5. Novel features

In the last section we have seen that the next-to-minimal model exhibits a limit in which it effectively reduces to a model very similar to the minimal one. In this section we want to address the question of what changes if we deviate from this limit. To be concrete, we are considering the case in which at least one of the ratios  $\Delta_{\text{R}}^5/\Delta_{\text{R}}^6$  (see eq. (5.32)) is not small. This marks the general case in which the pseudoscalar  $\eta$  is allowed to obtain a vev (but it does not have to), such that it mixes with the Higgs-like doublet  $h$  and  $CP$  can be broken spontaneously. In this case it is interesting to see what the experimental signatures are that allow to differentiate the next-to-minimal model from the minimal one.

### 5.5.1. Potential

An important novel feature of the NM4dCHM away from the  $\text{SO}(5)/\text{SO}(4)$  limit is the fact that also the pseudoscalar  $\eta$  can obtain a vev such that  $\tilde{s}_\eta^* \neq 0$ . As the mass matrices in appendix III.2 show, there are, in this case, additional mixings between elementary and composite fermion and vector states, which has an impact on all observables. In particular, the value of the SM Higgs vev as defined through the  $W$  mass gets contributions from  $\tilde{s}_\eta^*$ ,<sup>12</sup>

$$v_{\text{SM}} = s_h^* \tilde{c}_\eta^* f, \quad (5.39)$$

where  $\tilde{c}_\eta^{*2} = 1 - \tilde{s}_\eta^{*2}$ . In the limit  $\tilde{s}_\eta^* \ll 1$  this reduces to the expression in the  $\text{SO}(5)/\text{SO}(4)$  case, but away from this limit the  $\eta$ -contribution becomes important and allows  $s_h^*$  to take large values up to

<sup>12</sup>This can be calculated by an expansion of the eigenvectors of the charged vector boson mass matrix in terms of  $s_h^*$  and  $\tilde{s}_\eta^*$ . For this one can use techniques from time-independent perturbation theory.



$s_h^* \sim 1$  without the need to introduce light vector resonances as it would be the case in a model based on the minimal coset.

Electroweak symmetry breaking is characterized by the location  $(s_h^*, \tilde{s}_\eta^*)$  of the minimum of the effective scalar potential. In principle, the minimum is allowed to take any value on the unit square  $[0, 1] \times [0, 1]$ , but demanding the correct SM Higgs vev  $v_{\text{SM}} = 246 \text{ GeV}$  (cf. eq. (5.39)) restricts the allowed region for reasonable values of  $f$ . In our scans we found values for  $f$  roughly in the range 500 – 1500 GeV.

In the left plot of figure 5.3, we show predictions for the minimum of the effective potential. We find viable parameter points for all reasonable values of  $s_h^*$  and  $\tilde{s}_\eta^*$ . Generically, the scan has the tendency to yield minima with large  $s_h^*$  and  $\tilde{s}_\eta^*$ . However, points with  $\tilde{s}_\eta^* \approx 1$  are excluded as they imply a very small  $m_\eta$  (see eq. (5.31)). The region of  $\tilde{s}_\eta^* \approx 0$  is more tuned in the sense that it corresponds to the case of  $\Delta_R^5 \rightarrow 0$  which is hard to find in a general scan. Therefore, we started dedicated scans with a preference for these values of parameters to have a good coverage of the small  $\tilde{s}_\eta^*$  region (cf. section 5.2). One finds that for this case the found range of  $s_h^*$  is comparable to the one found in chapter 4. Only in the region of intermediate  $\tilde{s}_\eta^*$  the coverage is comparably low.

In the left plot of figure 5.3, one can also identify the individual Markov chains as different clouds with constant  $f$ . This is easy to understand from the fact that fermion and gauge boson contributions to the potential have to cancel each other to a rather large extent to guarantee the lightness of the Higgs [55, 56]. While the size of the gauge boson contributions is mainly driven by the parameter  $f$ , the fermion contributions depend on a large number of independent parameters, such as composite masses and composite-elementary mixings. Thus, a change in  $f$  would require a coordinated and collective change in many fermion parameters, which is again difficult to realize in a Markov Chain scan.

Further, in the left plot of figure 5.3 we also indicate the position of points with  $\Delta_{\text{BG}} < 100$  in the  $s_h^* - \tilde{s}_\eta^*$  plane. This shows that a moderate fine-tuning can be achieved for all values of the vevs that allow for a not too large scale  $f$ .

In the right plot of figure 5.3 we present the found values for the scalar masses. As in figure 5.1, the tendency to predict a large Higgs mass is obvious. For the pseudoscalar  $\eta$  we generally find larger masses. The lower bound is given by the Higgs mass, as we explicitly demand  $\eta$  to be heavier than the Higgs. We find maximal values in the region of around 1.5 TeV, but most of the points are clustered in the region 500 – 1000 GeV.

## 5.5.2. Higgs physics

For the CHM with minimal coset the couplings of the Higgs to SM states get corrections due to the non-linearly realized nature of the pNGB Higgs. In models with an enlarged scalar sector there are additional corrections if the Higgs mixes with the additional scalar states. In the setup considered in this work, this is the case when  $\eta$  gets a non-vanishing vev from the effective potential.

Analogously to section 4.6 we consider modifications of the Higgs signal strengths as a probe of the Higgs sector. Then, it is interesting to see how much the presence of the additional scalar  $\eta$  changes the Higgs couplings as compared to the minimal coset. We present our results on the Higgs signal strengths in figure 5.4. Comparing them with figure 4.12 we observe that the same rough overall dependence on the symmetry breaking scale  $f$  as in the minimal coset is valid also in the non-minimal one. However, one also sees that especially the signal strengths of the Higgs into vector bosons are rather “washed out” which shows that there are significant contributions from the mixing between the scalars. These additional contributions are not enough to bring the model in conflict with current Higgs coupling measurements. But using the estimates for future Higgs signal strength measurements discussed in section 4.6,  $h \rightarrow \bar{b}b$  in particular will become a relevant constraint for this model in the coming LHC runs.

## 5.5.3. Flavour physics

$\Delta F = 2$  observables were shown in have section 4.7.1 to be important constraints on the compositeness of third generation quarks. However, we also found that for the minimal coset there was no general correlation between the effective potential and flavour observables, meaning that flavour observables are dominantly determined by the flavour structure. We find this picture confirmed in the case of the next-to-minimal coset. In figure 5.5 we show the results on  $\Delta F = 2$  observables that correspond to figures 4.13, 4.14 and 4.15 for the minimal model. We find that in all observables the effects

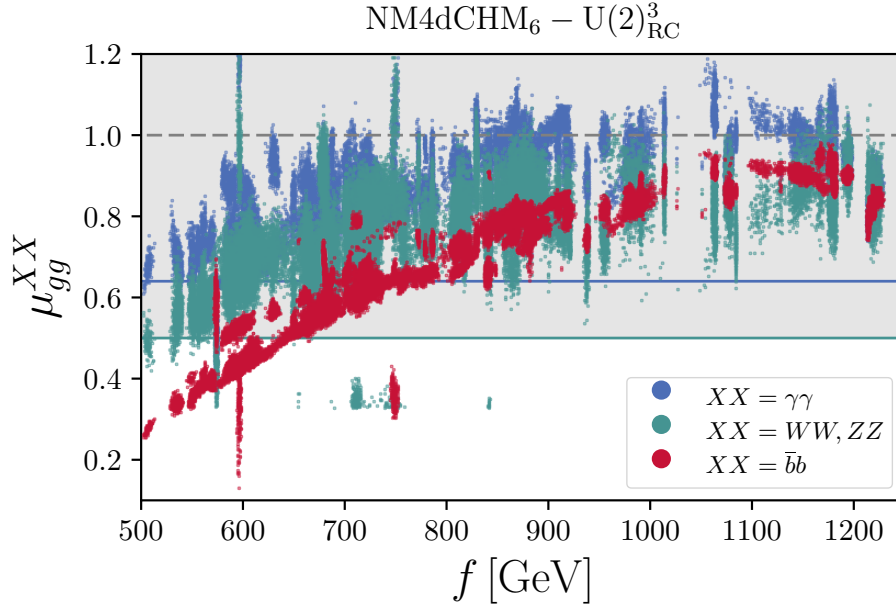


**Figure 5.4.:** Higgs signal strengths (3.40) in the channels  $h \rightarrow WW, ZZ$  (both are the same due to custodial symmetry),  $h \rightarrow \gamma\gamma$  and  $h \rightarrow \bar{b}b$  as functions of the symmetry breaking scale  $f$ . The gray bands and colored horizontal lines mark the  $2\sigma$  experimental limits. We refrained from showing results for  $h \rightarrow \tau^+\tau^-$  as due to the large experimental uncertainties this does not pose any constraint at the moment.

are virtually identical to the M4dCHM with a  $U(2)_{\text{RC}}^3$  flavour structure. Furthermore, we analyzed whether parameter points outside of the  $\text{SO}(5)/\text{SO}(4)$  limit,  $\max\Delta_{\text{R}}^5/\Delta_{\text{R}}^6 \ll 1$ , prefer certain values of  $\Delta F = 2$  observables and found that these points follow the same distributions as the remaining points. Therefore, we conclude that the effects of the enlarged pNGB sector and of the additional composite resonances are not important in flavour observables making this sector essentially blind to the different cosets.

One point worth mentioning (but already touched upon in section 3.3.5) is the impact of updated bag parameters in  $B$  meson mixing compared to the analysis of the minimal coset in section 4.7. Compared to the results shown in figure 4.13, one can see that with the updated bag parameters only a much smaller region is allowed. Furthermore, we observe that the points with moderate fine-tuning  $\Delta_{\text{BG}} < 100$  tend to predict slightly enhanced values for the mass differences.

#### 5.5.4. $CP$ violation

CHMs necessarily contain a certain amount of direct  $CP$  violation through complex valued composite-elementary mixings. This has to be large enough to reproduce the  $CP$  violation already present in the SM. An observable sensitive to this is the electric dipole moment of the neutron (see section 3.3.6). As we found in section 4.7.2, the amount of  $CP$  violation introduced in the M4dCHM is not sufficient to generate a measurable effect in this observable. In the NM4dCHM, however, an additional source of  $CP$  breaking is present. If the pseudoscalar  $\eta$  obtains a non-vanishing vev the effective potential acts as a source of spontaneous  $CP$  violation. We present predictions for the electric dipole moment of the neutron in figure 5.6. As expected, we find that in the limit  $\max\Delta_{\text{R}}^5/\Delta_{\text{R}}^6 \ll 1$  there are only tiny contributions, many orders of magnitude below the current experimental upper bound. If one, however, deviates from this limit such that at least one of the ratios  $\Delta_{\text{R}}^5/\Delta_{\text{R}}^6$  does not need to be small, we observe that the neutron electric dipole moment can take large values up to saturating the experimental upper limit. This indicates that additional  $CP$  violation can be a clear discriminator between the minimal and the next-to-minimal model.

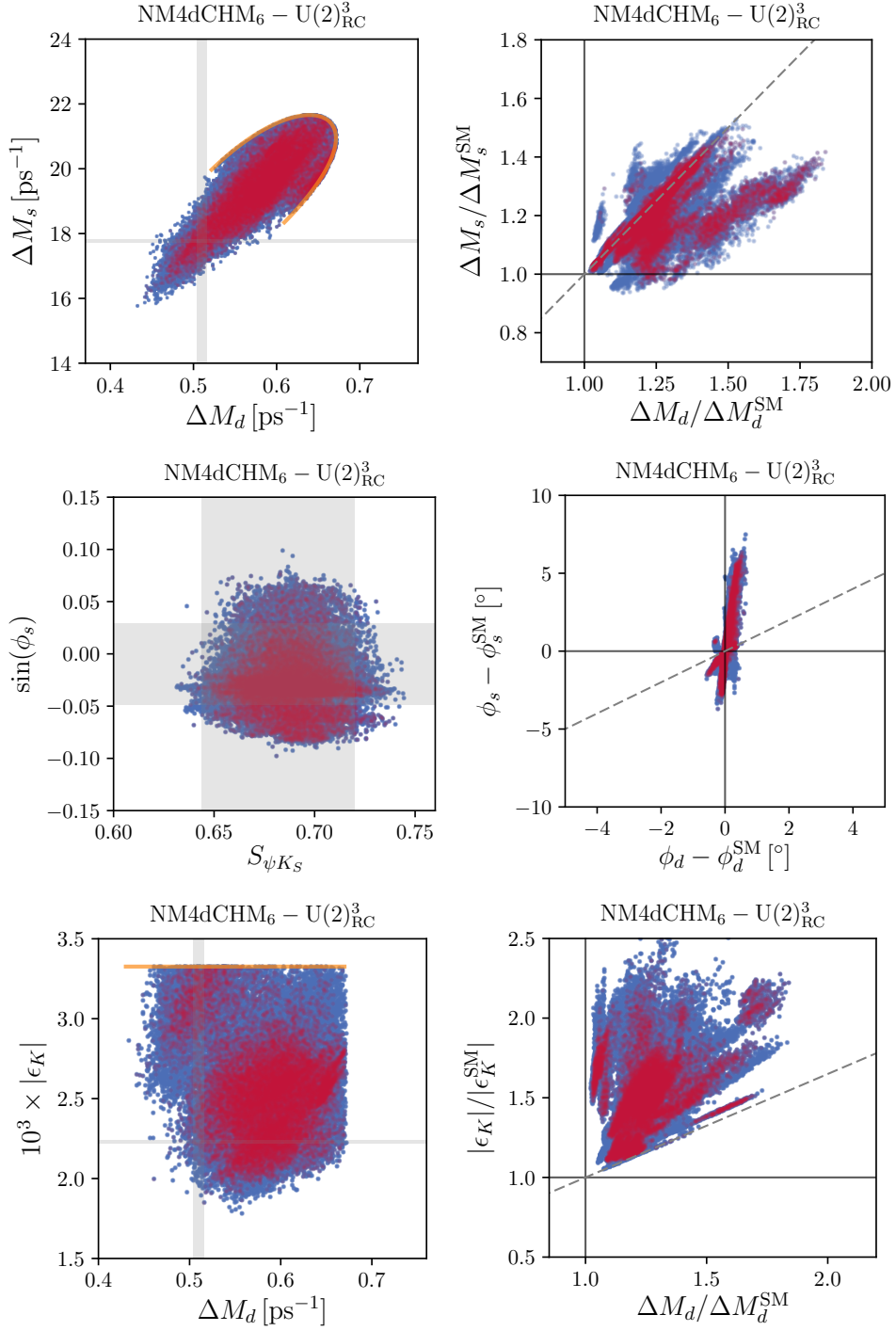


**Figure 5.5.:** Results on  $\Delta F = 2$  observables in the NM4dCHM. These plots are the analogue to figures 4.13, 4.14 and 4.15 for the M4dCHM.

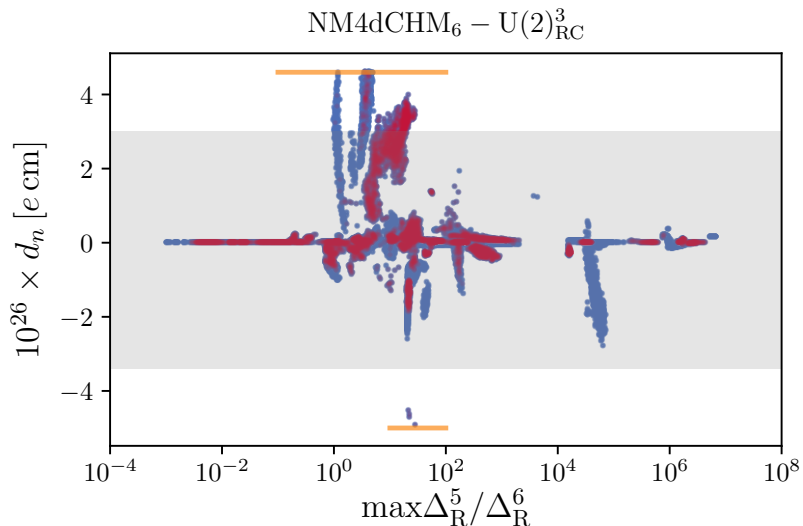


**Figure 5.6.:** Electric dipole moment of the neutron. Scatter plot including all viable points (blue). In red we mark all points with  $\Delta_{\text{BG}} < 100$ . The gray band is the experimental  $2\sigma$  constraint. One can see that in the  $\text{SO}(5)/\text{SO}(4)$  limit,  $\max\Delta_{\text{R}}^5/\Delta_{\text{R}}^6 \ll 1$  only negligible contributions are generated, but away from this limit the  $d_n$  can take large values indicating large amounts of  $CP$  violation.

### 5.5.5. Collider phenomenology of $\eta$

In section 5.4 we found that in the  $\text{SO}(5)/\text{SO}(4)$  limit,  $\max\Delta_{\text{R}}^5/\Delta_{\text{R}}^6 \ll 1$ , the composite scalar  $\eta$  decouples from the theory. In fact, as the right plot in figure 5.2 shows the production cross section is significantly suppressed in this limit. But away from this limit  $\eta$  can be produced at rates that are very well in the reach of present and future collider experiments.

As in the case of the minimal coset we do not want to discuss the collider signatures of the next-to-minimal model in detail and refer to [28] for an extensive analysis. At this point we just give a short overview of the collider phenomenology of the new scalar  $\eta$  as this is one of the major differences between the minimal and the next-to-minimal model. In figure 5.7 we show results on production and decay of  $\eta$ .

We find that for nearly all points  $\eta$  is almost exclusively produced via gluon fusion, similar to the Higgs. Other production channels are direct production from heavy quarks (which is suppressed by the small parton distribution functions) and vector boson fusion.

As a dominant decay mode of  $\eta$  we can identify the decay into a pair of Higgs bosons, but also the decay into a top pair as well as pairs of electroweak vector bosons can have a sizable branching ratio. Decays into light quarks as well as photons are always strongly suppressed. We note that the decay into composite resonances is usually kinematically not open. These findings are contrary to what one might expect from the Goldstone boson equivalence theorem. The reason for this is the mixings of the scalar fields. As the pseudoscalar  $\eta$  mixes with the doublet component  $h$  but not with NGBs that yield the longitudinal polarizations of the  $W$  and  $Z$  bosons the  $\eta hh$  coupling gets enhanced compared to the  $\eta WW$  and  $\eta ZZ$  couplings.

## 5.6. Summary

Generally, we find that the 4dCHM based on the next-to-minimal coset  $\text{SO}(6)/\text{SO}(5)$  is in a comparably good shape when confronted with experimental data as the minimal model. The main results of this analysis are:

- $\text{SO}(6)/\text{SO}(5)$  is the next-to-minimal coset.
- The enlarged coset gives rise to an additional pseudoscalar field  $\eta$ . Therefore, the effective potential becomes two-dimensional. If the pseudoscalar  $\eta$  receives a vev then the potential acts as a source of spontaneous  $CP$  violation.

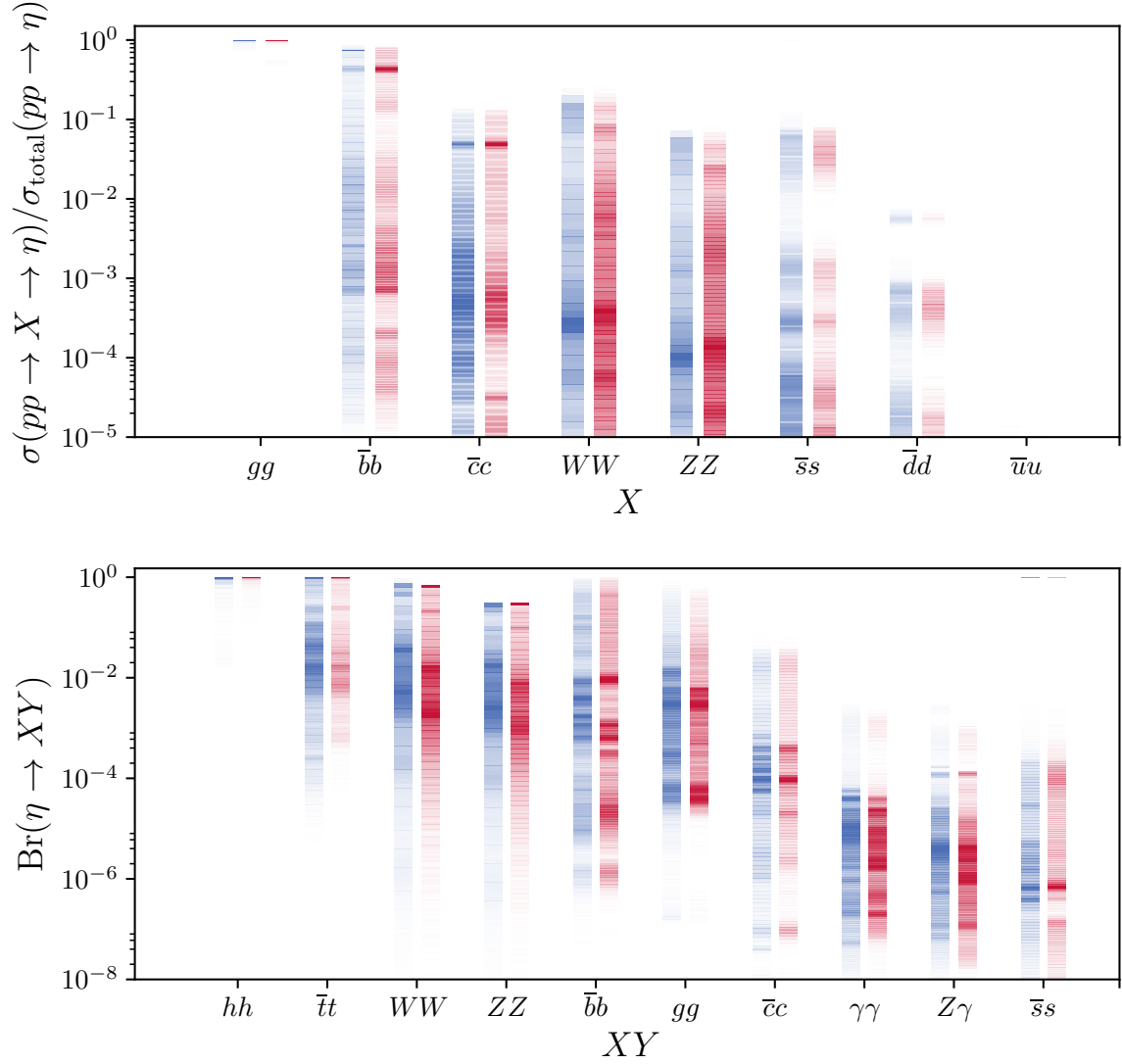
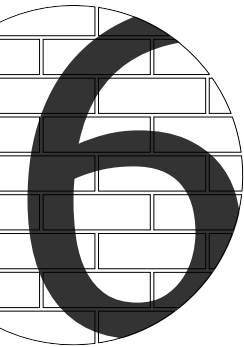


**Figure 5.7.:** Collider phenomenology of the composite scalar  $\eta$ . In blue we show the distribution including all viable parameter points. In red we show points with  $\Delta_{\text{BG}} < 100$ . *Top:* Production channels normalized to the total production cross section. *Bottom:* Decay channels into specific final states.

- The number of heavy resonances also increases as one has to consider larger representations under the global symmetries. In the vector sector there is an additional bidoublet field as well as an extra singlet field. In the fermion sector one finds an additional singlet field.
- There is an ambiguity in the choice of embeddings of right-handed elementary quarks into  $\text{SO}(6)$  fundamentals. This leads to additional composite-elementary couplings which can carry complex phases.
- We find a minimal fine-tuning of about  $\Delta_{\text{BG}}^{\text{min}} = 30$ . This is even slightly better than for the minimal coset with the same flavour structure. A tuning better than percent-level is achievable for  $f < 1 \text{ TeV}$ .
- This model possesses a limit,  $\max \Delta_{\text{R}}^5 / \Delta_{\text{R}}^6 \rightarrow 0$ , in which it becomes indistinguishable from the minimal coset. In this limit the additional fields decouple, the couplings of  $\eta$  to SM fermions vanish and no spontaneous  $CP$  violation through the potential occurs since  $\eta$  does not obtain a non-trivial vev.
- Away from this limit  $s_h^*$  can be large if this is balanced by an also large  $\tilde{s}_\eta^*$ . This stands in contrast to the situation in the minimal model and can be one reason for the smaller fine-tuning. We find values for  $s_h^*$  and  $\tilde{s}_\eta^*$  in all theoretical allowed regions. We see no preference of a value due to fine-tuning.
- We find values  $500 \text{ GeV} \leq f \leq 1500 \text{ GeV}$  for the symmetry breaking scale  $f$ .
- For  $\eta$  we find masses as low as nearly the Higgs mass all the way up to around  $1.5 \text{ TeV}$ , but most points are clustered in the region  $500 - 1000 \text{ GeV}$ .
- In Higgs physics large deviations are possible stemming from Higgs non-linearities and mixings of the Higgs and  $\eta$ .
- Flavour physics is dominated by the flavour structure. We find no qualitatively new features in this model.
- Due to spontaneous  $CP$  violation through the potential large effects in the neutron electric dipole moment are possible up to saturating present experimental bounds.
- Regarding collider phenomenology we find that  $\eta$  is almost exclusively produced through gluon fusion. It decays mostly into Higgs bosons, top pairs or electroweak vector bosons. Decays via the diphoton mode or to light quarks are suppressed.



## Leptoquarks in $b \rightarrow s$ transitions

In the last chapter of this work we will jump to a different class of NP scenarios. The previous chapters always investigated thorough, fully-fledged BSM theories that tried to solve the ‘big problems’ of particle physics, such as the fine-tuning problem or the generation of flavour hierarchies. Especially in the last decade the trend in high energy physics has shifted to be in some sense more data-driven. As the experimental results of the last years have not shown any torch-like signal such as supersymmetric partners or composite resonances that would be expected in a complete theory, it might be well-motivated to add only small pieces of NP to the SM. Then, it is not of immediate interest how and whether these pieces can be implemented in a more fundamental theory, but one wants to see if the general idea of such NP makes sense. This is always done under the assumption that for the processes under consideration the added NP pieces give the dominant contributions. For the remainder of this work we now want to continue this road of simplified models and consider the possibility that beyond the SM there exist leptoquarks (LQ), i.e. spin-0 or spin-1 bosons that couple to a quark-lepton current. A recent review on the phenomenology of LQs is given in [218]

In recent years LQs have been subject to a large amount of interest, especially in connection with the  $bs\ell\ell$  anomalies. The reason for this is that LQs can naturally generate the patterns of effective semi-leptonic operators that are needed to explain these anomalies. In the following we want to investigate LQ models in the light of these anomalies while considering the related modes  $B \rightarrow K^{(*)}\bar{\nu}\nu$  and  $B_s \rightarrow \mu^+\mu^-$ . The main goal will be to see whether these modes can be used to extract additional information about NP through LQ models.

### 6.1. $b \rightarrow s$ transitions

Generally,  $b \rightarrow s$  transitions are powerful probes of NP [159]. In recent years a lot of interest in these transitions was triggered by several tensions observed between experimental measurements and SM predictions in particular in  $b \rightarrow s\ell^+\ell^-$  decays. In principle, these tensions are independent of each other, but as was soon found, they all consistently fit together into a single hypothesis of NP. These tensions are:

- In 2013 LHCb conducted an angular analysis of the  $B \rightarrow K^{(*)}\mu^+\mu^-$  decay and reported a tension in the angular observable  $P'_5$  at the level of three standard deviations [219, 220], which was confirmed in 2015 by LHCb using the complete Run-1 dataset [221]. Recently also ATLAS and CMS presented analyses [222, 223].
- An independent tension was presented in 2014 by the LHCb collaboration in the ratio [190]

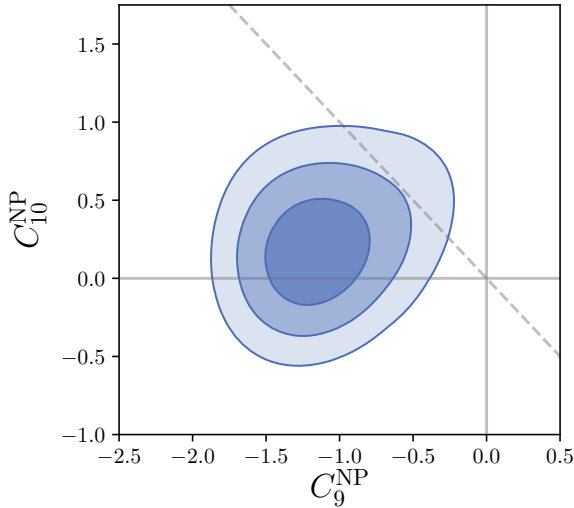
$$R_K = \frac{\text{Br}(B^+ \rightarrow K^+\mu^+\mu^-)_{[1,6] \text{ GeV}^2}}{\text{Br}(B^+ \rightarrow K^+e^+e^-)_{[1,6] \text{ GeV}^2}} = 0.745^{+0.090}_{-0.074} \pm 0.036 \quad (6.1)$$

which shows a  $2.6\sigma$  tension with the SM that predicts  $R_K = 1$  to an excellence precision [224]. This measurement therefore presents a hint for a possible violation of lepton flavour universality (LFU) which is predicted by the SM. Very recently this hint was strengthened by the observation of a similar anomaly in the related mode [191]

$$R_{K^{*0}} = \frac{\text{Br}(B^0 \rightarrow K^{*0}\mu^+\mu^-)_{[1,6] \text{ GeV}^2}}{\text{Br}(B^0 \rightarrow K^{*0}e^+e^-)_{[1,6] \text{ GeV}^2}} = 0.685^{+0.113}_{-0.069} \pm 0.047. \quad (6.2)$$

This value is very well compatible with predictions made by us [1] assuming the experimental data on  $bsll$  prior to the announcement of  $R_{K^{*0}}$ . As a caveat one however has to note that LHCb also sees a similar excess in the low- $q^2$  bin  $[0.045, 1.1] \text{ GeV}^2$  in which no effect due to NP was expected.

- Further tensions were found in branching ratio measurements of  $B \rightarrow K\mu^+\mu^-$  and  $B_s \rightarrow \phi\mu^+\mu^-$  [225, 190, 226].



WC scenario	best fit	$1\sigma$
$C_9^{\text{NP}}$	-1.19	[-1.41, -0.97]
$C'_9$	+0.13	[-0.08, +0.34]
$C_{10}^{\text{NP}}$	+0.64	[+0.41, +0.90]
$C'_{10}$	-0.05	[-0.22, +0.11]
$C_9^{\text{NP}} = +C_{10}^{\text{NP}}$	-0.33	[-0.53, -0.12]
$C_9^{\text{NP}} = -C_{10}^{\text{NP}}$	-0.61	[-0.74, -0.45]
$C'_9 = +C'_{10}$	+0.07	[-0.18, +0.32]
$C'_9 = -C'_{10}$	+0.05	[-0.05, +0.15]

**Figure 6.1 & Table 6.1:** Preferred ranges for Wilson coefficients obtained by a global fit to  $bsll$  data. *Left:* Contours in the two-dimensional  $C_9^{\text{NP}} - C_{10}^{\text{NP}}$  plane. *Right:* Best fit values and  $1\sigma$  ranges for the case that only one Wilson coefficient or a certain combination is non-vanishing. These results use the numerical data obtained in [1].

Several theory groups [227, 163, 228, 229] conducted independent global fits of the effective Hamiltonian (3.62) to these experimental data in order to assess the potential of NP showing up through these tensions. In a recent update [1] we incorporated the most recent theoretical and experimental data into this fit. The consensus is that all these tensions can be explained together in a consistent way by NP in the Wilson coefficient  $C_9^{\mu\mu}$  which interferes destructively with the SM (see figure 6.1). A similarly good fit is found if NP also affects the Wilson coefficient  $C_{10}$  such that  $C_9^{\text{NP}} = -C_{10}^{\text{NP}}$ , which is a very convenient option for model building as it indicates NP connected with left-handed muons. The tensions in  $R_{K^{(*)}}$  are explained if NP only enters the second lepton generation, while the interactions of electrons remain SM-like.

A caveat is that  $b \rightarrow s\ell^+\ell^-$  transitions are plagued by hadronic uncertainties such as form factors or non-factorizable hadronic effects due to the presence of charmonium resonances. It has been argued that underestimated hadronic effects could mimic a NP contribution to  $C_9$  [230, 231, 232]. This, however, does not apply to the LFU observable  $R_K$  since hadronic effects mostly cancel in this ratio [224]. We therefore adopt the following standpoint for this work: neglecting the possibility of a hadronic effect we assume that the anomalies in  $b \rightarrow s\ell^+\ell^-$  transitions are in fact due to NP effects.

## 6.2. Leptoquark basics

LQs are particles that carry lepton- as well as baryon-number such that they couple leptons and quarks into one vertex. For this, they necessarily have to be bosons, where scalar and vector LQs are the simplest options. Generally, LQs appear naturally in many different NP scenarios. The first examples where LQs appeared were models for gauge coupling unification such as e.g. Pati-Salam models [233] or  $SU(5)$  grand unification theories (GUTs) [234]. In these models quarks and leptons are usually embedded into the same multiplet of the GUT symmetry. Therefore, LQs can appear as gauge bosons of this theory or as scalar fields that obtain a vev in order to break the GUT symmetry. Supersymmetric theories also offer the possibility of LQs. The scalar superpartners of the SM quarks,



Scenario	Spin	$G_{\text{SM}}$	$\mathcal{L}_{\text{int}}$
$S_1$	0	$(\bar{\mathbf{3}}, \mathbf{1})_{\frac{1}{3}}$	$\hat{\lambda}_L (\bar{q}_L^c \cdot \epsilon \cdot l_L) \phi + \hat{\lambda}_R \bar{u}_R^c \ell_R \phi + \hat{\lambda}_{qq}^1 (\bar{q}_L \cdot \epsilon \cdot q_L^c) \phi + \hat{\lambda}_{qq}^2 \bar{d}_R u_R^c \phi$
$\tilde{S}_1$	0	$(\bar{\mathbf{3}}, \mathbf{1})_{\frac{4}{3}}$	$\hat{\lambda}_R \bar{d}_R^c \ell_R \phi + \hat{\lambda}_{qq} \bar{u}_R u_R^c \phi$
$R_2$	0	$(\mathbf{3}, \mathbf{2})_{\frac{7}{6}}$	$\hat{\lambda}_L (\bar{q}_L \cdot \phi) \ell_R + \hat{\lambda}_R \bar{u}_R (l_L \cdot \epsilon \cdot \phi)$
$\tilde{R}_2$	0	$(\mathbf{3}, \mathbf{2})_{\frac{1}{6}}$	$\hat{\lambda}_R \bar{d}_R (l_L \cdot \epsilon \cdot \phi)$
$S_3$	0	$(\bar{\mathbf{3}}, \mathbf{3})_{\frac{1}{3}}$	$\hat{\lambda}_L (\bar{q}_L^c \cdot \epsilon \cdot \tau^a \cdot l_L) \phi^a + \hat{\lambda}_{qq} (\bar{q}_L \cdot \epsilon \cdot \tau^a \cdot q_L^c) \phi^a$
$U_1$	1	$(\mathbf{3}, \mathbf{1})_{\frac{2}{3}}$	$\hat{\lambda}_L (\bar{q}_L \gamma^\mu l_L) \phi_\mu + \hat{\lambda}_R \bar{d}_R \gamma^\mu \ell_R \phi_\mu$
$\tilde{U}_1$	1	$(\mathbf{3}, \mathbf{1})_{\frac{5}{3}}$	$\hat{\lambda}_R \bar{u}_R \gamma^\mu \ell_R \phi_\mu$
$V_2$	1	$(\bar{\mathbf{3}}, \mathbf{2})_{\frac{5}{6}}$	$\hat{\lambda}_L (\bar{q}_L^c \cdot \epsilon \cdot \phi_\mu) \gamma^\mu \ell_R + \hat{\lambda}_R \bar{d}_R^c \gamma^\mu (l_L \cdot \epsilon \cdot \phi_\mu) + \hat{\lambda}_{qq} \bar{u}_R \gamma^\mu (q_L^c \cdot \phi_\mu)$
$\tilde{V}_2$	1	$(\bar{\mathbf{3}}, \mathbf{2})_{-\frac{1}{6}}$	$\hat{\lambda}_R \bar{u}_R^c \gamma^\mu (l_L \cdot \epsilon \cdot \phi_\mu) + \hat{\lambda}_{qq} (\bar{q}_L \cdot \phi_\mu) \gamma^\mu d_R^c$
$U_3$	1	$(\mathbf{3}, \mathbf{3})_{\frac{2}{3}}$	$\hat{\lambda}_L (\bar{q}_L \cdot \tau^a \cdot \gamma^\mu l_L) \phi_\mu^a$

**Table 6.2.:** Possible representations for leptoquarks  $\phi$ . In the last column we show the interaction terms with SM fermions. With  $\epsilon$  we denote the 2-dimensional Levi-Cevita symbol and  $\tau^a$  are the generators of  $\text{SU}(2)_L$

the squarks, carry the correct quantum numbers to act as LQs. But for this a certain amount of  $R$ -parity violation has to be present, such that vertices with two SM fields and only one superpartner are allowed [235]. Another class of NP models where, admittedly, LQs are not predicted but they come in handy, are models in which neutrino masses are generated at the (multi-)loop level (see e.g. [236]). Finally, let us note that LQs also appear in CHMs if larger GUT-like cosets are assumed. In [237] scalar LQs are implemented as pNGBs of a coset  $[\text{SO}(9) \times \text{SO}(5)] / [\text{SU}(4) \times \text{SU}(2)_\Pi \times \text{SU}(2)_\text{H} \times \text{SU}(2)_\text{R}]$ . Under a coset based on the Pati-Salam-like global symmetries  $\text{SU}(4)_c \times \text{SO}(5) \times \text{U}(1)_X$  (as compared to (2.7)) vector LQs can emerge as composite vector resonances [31].

Although LQs can appear in many concrete models, the standard treatment is usually model-independent. Therefore, one can work in a simplified model that assumes SM gauge invariance. Then, the LQ has to carry defined quantum numbers under the SM gauge group and one can classify all possible representations such that LQ interactions are gauge invariant. Assuming no larger representations than triplets under  $\text{SU}(3)_c$  and  $\text{SU}(2)_L$  and neglecting also right-handed neutrinos, there are 5 possible representations for scalar LQs and also 5 representations for vector leptoquarks [238]. These are shown in table 6.2. All LQs have to carry colour charge in order to be able to couple quarks to leptons. As a consequence no couplings of LQs to two leptons are allowed. In the last column of table 6.2 the possible interaction terms with SM fermions are shown. Dictated by the symmetries, every LQ representation has unique coupling patterns to SM fields leading to a rather distinct phenomenology for each scenario.

The interaction terms in table 6.2 are written in the gauge basis prior to EWSB. In general, the SM fields carry a flavour index, which is why the LQ couplings also have to be equipped with two flavour indices; one carries quark flavour the other lepton flavour. A priori, there is no structure for these couplings such that they are general matrices in flavour space. When matching these operators to a Hamiltonian relevant for low energy phenomenology, the quark fields have to be rotated into the physical mass basis using rotation matrices defined by the SM Yukawa interactions. This then means that effectively also the LQ couplings have to be rotated into the mass basis.

To see this explicitly, we find it instructive to conduct a short exemplary calculation at this point. Let us consider the LQ representation  $U_1$  with the interaction term (see table 6.2 and for the moment

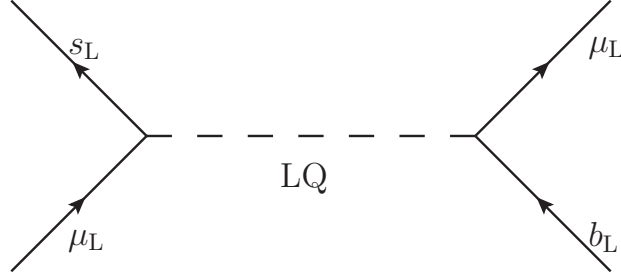


**Figure 6.2.:** Example of a tree-level contribution to a semi-leptonic  $bs\mu\mu$ -operator by LQ exchange.

we are only interested in the interaction of left-handed quarks)

$$\mathcal{H}_{\text{int}} \supset [\hat{\lambda}_L]^{ij} \left( \bar{q}_L^i \gamma^\mu \ell_L^j \right) \phi_\mu + \text{h.c.} \quad (6.3a)$$

$$= [\hat{\lambda}_L]^{ij} \left( \bar{u}_L^i \gamma^\mu \nu_L^j \right) \phi_\mu + [\hat{\lambda}_L]^{ij} \left( \bar{d}_L^i \gamma^\mu \ell_L^j \right) \phi_\mu + \text{h.c.} \quad (6.3b)$$

We further pretend for the time being that we are only interested in  $b - \mu$  and  $s - \mu$  interactions. Then we can rotate the above operators into the mass basis yielding

$$\mathcal{H}_{\text{int}} \subset \lambda_L^{b\mu} (\bar{b}_L \gamma^\mu \mu_L) + \lambda_L^{s\mu} (\bar{s}_L \gamma^\mu \mu_L) + \text{h.c.}, \quad (6.4)$$

where the mass basis couplings are given as

$$\lambda_L^{s\mu} = [V_{dL}^\dagger]_{2i} [\hat{\lambda}_L]^{i2}, \quad \lambda_L^{b\mu} = [V_{dL}^\dagger]_{3i} [\hat{\lambda}_L]^{i2} \quad (6.5)$$

and  $V_{dL}$  rotate the left-handed down-type quarks into the mass basis. In this basis it is now possible to calculate semi-leptonic effective operators by integrating out the LQ in diagrams like the one shown in figure 6.2,

$$\begin{aligned} \text{diagram} &= (\bar{s}_L \gamma^\mu \mu_L) \times (-i\lambda_L^{s\mu}) \times \left( \frac{i\eta_{\mu\nu}}{m_{LQ}^2} \right) \times (-i\lambda_L^{b\mu*}) \times (\bar{\mu}_L \gamma^\nu b_L) \\ &= -i \frac{\lambda_L^{s\mu} \lambda_L^{b\mu*}}{m_{LQ}^2} (\bar{s}_L \gamma^\mu \mu_L) (\bar{\mu}_L \gamma_\mu b_L) \\ &= \frac{\lambda_L^{s\mu} \lambda_L^{b\mu*}}{m_{LQ}^2} (\bar{s}_L \gamma^\mu b_L) (\bar{\mu}_L \gamma_\mu \mu_L) \\ &= \frac{\lambda_L^{s\mu} \lambda_L^{b\mu*}}{2m_{LQ}^2} (\bar{s}_L \gamma^\mu b_L) (\bar{\mu} \gamma_\mu \mu) - \frac{\lambda_L^{s\mu} \lambda_L^{b\mu*}}{2m_{LQ}^2} (\bar{s}_L \gamma^\mu b_L) (\bar{\mu} \gamma_\mu \gamma_5 \mu), \end{aligned}$$

where we made use of a Fierz transformation. Then, we can match the LQ theory onto the effective Hamiltonian (3.61) and we find the following relation for the Wilson coefficients:

$$C_9^{\text{NP}} = -C_{10}^{\text{NP}} = -\frac{1}{2} \mathcal{N}(m_{LQ}) \lambda_L^{s\mu} \lambda_L^{b\mu*}, \quad (6.6)$$

introducing the normalization factor

$$\mathcal{N}(m_{LQ}) = -\frac{2\pi}{\alpha_{\text{em}}} \frac{v_{\text{SM}}^2}{V_{tb} V_{ts}^* m_{LQ}^2} \approx -1176 \left( \frac{1 \text{ TeV}}{m_{LQ}} \right)^2. \quad (6.7)$$

This shows that LQs are able to explain the recent LHCb anomalies in  $bs\ell\ell$  data through a NP contribution to the Wilson coefficients  $C_9^{\text{NP}} = -C_{10}^{\text{NP}}$  is one of the preferred scenarios obtained by global fits for explaining these anomalies [1]. The assumption that the LQs only couple to 2nd generation leptons can also serve as a natural explanation for the experimental hints for lepton flavour non-universality seen in  $B \rightarrow K^{(*)} \mu^+ \mu^-$  decays. The LQ  $S_3$  was considered in [239] as a promising

possibility for this. The authors of [240] investigated the representation  $S_1$  in which the anomaly in the charged current process  $B \rightarrow D^{(*)} \ell \nu$  [241, 242, 243] can be explained by a tree-level exchange while the neutral current anomalies in  $bs\ell\ell$  are solved at the loop level, such that naturally a hierarchy is given between both effects. The vector LQs  $U_1$  and  $U_3$  have been considered in [244, 245]. The LQ  $R_2$  can generate the relation  $C_9^{\text{NP}} = -C_{10}^{\text{NP}}$  at one-loop level [246], if one assumes that the coupling  $\hat{\lambda}_L$  such that the Wilson coefficients do not get a tree-level contribution.

At first sight the assumption that the considered LQ only couples to one generation of leptons seems a bit ad hoc. Relaxing this assumption, however, inevitably leads to lepton flavour violating processes. In [247] an attempt was made to generate such a flavour pattern from a slightly broken  $U(2)$  flavour symmetry.

### 6.3. Leptoquarks and $b \rightarrow s\bar{\nu}\nu$

The rare decays  $B \rightarrow K^{(*)} \bar{\nu}\nu$  are important for constraining NP scenarios for several reasons. Theoretically they are very clean as they do not suffer from hadronic uncertainties beyond the ones associated to hadronic form factors. Since the final state leptons are not charged under QED, these decays do not suffer from non-factorizable corrections due to photon exchange. Another important point is that the decay in the dineutrino channel can be related to the decays  $B \rightarrow K^{(*)} \mu^+ \mu^-$  as neutrinos and charged leptons are components of the same  $SU(2)_L$  doublet. This allows the use of experimental data on the mode with charged leptons to obtain information about the dineutrino mode.

In this section we will pursue this road and assess the possible NP effects in  $b \rightarrow s\nu\nu$  while using the charged lepton channel as input.

#### Effective Hamiltonian and current status

The theory of  $b \rightarrow s\bar{\nu}\nu$  transitions has been investigated in [248, 249, 250]. Assuming no right-handed neutrinos, the effective Hamiltonian at the scale  $m_b$  contains only two effective operators and is given by

$$\mathcal{H}_{\text{eff}} = -\frac{4G_F}{\sqrt{2}} V_{tb} V_{ts}^* (C_L \mathcal{O}_L + C_R \mathcal{O}_R) + \text{h.c.}, \quad (6.8)$$

with

$$\mathcal{O}_L = \frac{e^2}{16\pi^2} (\bar{s}\gamma^\mu P_L b) (\bar{\nu}\gamma_\mu (\mathbb{1} - \gamma_5) \nu), \quad \mathcal{O}_R = \frac{e^2}{16\pi^2} (\bar{s}\gamma^\mu P_R b) (\bar{\nu}\gamma_\mu (\mathbb{1} - \gamma_5) \nu). \quad (6.9)$$

In the SM such operators are only generated at the loop-level through diagrams involving  $W$ -bosons; which is why  $C_R^{\text{SM}}$  vanishes. The Wilson coefficient  $C_L^{\text{SM}}$  is known to a high precision including NLO QCD corrections [251, 252, 253] and two-loop electroweak contributions [254]. The SM values are given by

$$C_L^{\text{SM}} = -X_t/s_W^2, \quad C_R^{\text{SM}} = 0 \quad \text{with} \quad X_t = 1.469 \pm 0.017. \quad (6.10)$$

Using this effective Hamiltonian, the dineutrino invariant mass distribution for  $B \rightarrow K\bar{\nu}\nu$  can be written as [255]

$$\frac{d\Gamma(B \rightarrow K\bar{\nu}\nu)}{ds_B} = \frac{G_F^2 \alpha^2}{256\pi^5} |V_{tb} V_{ts}^*|^2 m_B^5 \lambda^{\frac{3}{2}}(s_B, \frac{m_K}{m_B}, 1) [f_+^K(s_B)]^2 |C_L + C_R|^2, \quad (6.11)$$

where  $s_B = q^2/m_B^2$  ranges in  $0 \leq s_B \leq (1 - m_K/m_B)^2$  and  $\lambda(a, b, c) = a^2 + b^2 + c^2 - 2(ab + bc + ac)$  is a kinematical factor.

Since the  $K^*$  is a vector particle, the decay mode  $B \rightarrow K^*(\rightarrow K\pi)\bar{\nu}\nu$  is richer as it contains angular information. Because of this, the dineutrino mass distribution is written in terms of helicity amplitudes [255],

$$\frac{d\Gamma(B \rightarrow K^*\bar{\nu}\nu)}{ds_B} \propto |\mathcal{A}_\perp|^2 + |\mathcal{A}_\parallel|^2 + |\mathcal{A}_0|^2, \quad (6.12)$$

where we did not write down kinematical factors and the amplitudes are schematically given by

$$\mathcal{A}_\perp(s_B) \propto (C_L + C_R) V(s_B), \quad (6.13a)$$

$$\mathcal{A}_\parallel(s_B) \propto (C_L - C_R) A_1(s_B), \quad (6.13b)$$

$$\mathcal{A}_0(s_B) \propto (C_L - C_R) A_{12}(s_B). \quad (6.13c)$$

Here we again did not show explicitly kinematic factors but rather showed the general dependence on the Wilson coefficients and the form factors. Both decay channels intimately depend on the form factors  $f_+^K$  as well as  $V, A_1, A_{12}$  that parametrize the hadronic matrix elements  $\langle K^{(*)} | \mathcal{O}_{L,R} | B \rangle$ . Being QCD objects these are hard to calculate from first principles. At low recoils,  $q^2 \lesssim (m_B - m_K)^2$ , the matrix elements can be evaluated via lattice QCD [256, 257], whereas for  $q^2 \approx 0$  the form factors can be calculated via lightcone sum rules (LCSR) [258, 259]. In [260] the results from lattice QCD and LCSR were fitted together to obtain a reliable description of the form factors over the whole kinematic range. These results are essential for the considered decays as the branching ratios are calculated as  $q^2$ -integrals over the form factors. The fitted form factors for  $B \rightarrow K^*$  as well as lattice calculations for  $B \rightarrow K$  form factors [261] are implemented in `flavio` [147] which we use in this analysis.

Although the neutrinos escape the detector without being observed, there is still a third observable in these decays besides the branching ratios. Angular information can be obtained through the  $K^*$  longitudinal polarization fraction

$$F_L = \frac{\Gamma_0}{\Gamma} = \frac{\int ds_B |A_0(s_B)|^2}{\int ds_B \left( |A_\perp(s_B)|^2 + |A_\parallel(s_B)|^2 + |A_0(s_B)|^2 \right)}, \quad (6.14)$$

By construction most of the hadronic uncertainties drop out in the ratio making it a clean observable. Furthermore, in the absence of right-handed currents, i.e. for  $C_R = 0$ , all dependence on the Wilson coefficients drops out such that measuring a non-SM value would be a direct signal for NP with right-handed currents.

The physics of  $b \rightarrow s\bar{\nu}\nu$  is described by two complex numbers: the Wilson coefficients  $C_L$  and  $C_R$ . It has proven useful to parametrize the NP contributions by other coefficients [249, 250],

$$\epsilon = \frac{\sqrt{|C_L|^2 + |C_R|^2}}{|C_L^{\text{SM}}|}, \quad \eta = \frac{-\text{Re}(C_L C_R^*)}{|C_L|^2 + |C_R|^2}, \quad (6.15)$$

which are real numbers. In terms of these one can express the three observables in  $b \rightarrow s\bar{\nu}\nu$  decays normalized to their SM values as

$$\mathcal{R}_K := \frac{\text{Br}(B \rightarrow K\bar{\nu}\nu)}{\text{Br}(B \rightarrow K\bar{\nu}\nu)^{\text{SM}}} = (1 - 2\eta)\epsilon^2, \quad (6.16a)$$

$$\mathcal{R}_{K^*} := \frac{\text{Br}(B \rightarrow K^*\bar{\nu}\nu)}{\text{Br}(B \rightarrow K^*\bar{\nu}\nu)^{\text{SM}}} = (1 + \kappa_\eta\eta)\epsilon^2, \quad (6.16b)$$

$$\mathcal{R}_{F_L} := \frac{F_L}{F_L^{\text{SM}}} = \frac{1 + 2\eta}{1 + \kappa_\eta\eta}. \quad (6.16c)$$

Here,  $\kappa_\eta = 1.33$  is a numerical factor that depends on the integrated hadronic form factors. In the SM the two parameters take the values  $(\epsilon, \eta)_{\text{SM}} = (1, 0)$ . The advantage of this parametrization is that in the absence of right-handed currents ( $C_R = 0$ ) one always has  $\eta = 0$  such that  $\mathcal{R}_K = \mathcal{R}_{K^*}$ . Consequently, a measurement of a different relative modification of the two decay modes,  $\mathcal{R}_K \neq \mathcal{R}_{K^*}$  would be a direct signal of NP with right-handed couplings. Furthermore, there are two parameters to describe three observables such that the system is over-determined. A measurement of  $F_L$  has to be consistent with the determination of the branching ratios according to (6.16). Otherwise, that would be a direct signal for invisible particles in the final state other than neutrinos.

The SM predictions for the observables can be calculated using `flavio` [147] which yields

$$\text{Br}(B^+ \rightarrow K^+\bar{\nu}\nu)_{\text{SM}} = (4.59 \pm 0.55) \times 10^{-6}, \quad (6.17a)$$

$$\text{Br}(B^0 \rightarrow K^{*0}\bar{\nu}\nu)_{\text{SM}} = (9.59 \pm 1.00) \times 10^{-6}. \quad (6.17b)$$

Experimentally these decays have not been observed yet, but the current experimental bounds are given by the Belle collaboration [262] at the 90% CL as

$$\text{Br}(B \rightarrow K\bar{\nu}\nu) < 1.6 \times 10^{-5} \quad \text{such that} \quad \mathcal{R}_K < 3.5, \quad (6.18a)$$

$$\text{Br}(B \rightarrow K^*\bar{\nu}\nu) < 2.7 \times 10^{-5} \quad \text{such that} \quad \mathcal{R}_{K^*} < 2.8. \quad (6.18b)$$

The future prospects are very promising. The upcoming Belle II experiment will be well-equipped for investigating these decays with a missing energy signature. The current luminosity projection is to

collect an integrated luminosity of  $50 \text{ ab}^{-1}$  by the year 2024 [263]. With this amount of statistics the expected sensitivities are at the level of 22% for  $B^+ \rightarrow K^+ \bar{\nu} \nu$  and even 17% for  $B \rightarrow K^* \bar{\nu} \nu$  [264, 265] assuming SM values. Therefore, strong evidence for these decay will definitely be possible within the next decade. In many NP scenarios the decay rates can be significantly enhanced such that signs for NP could show up much earlier.

### Departing from lepton flavour universality

In the above formulae (especially in (6.16)) it was implicitly assumed that NP couples to all lepton generations in the same way. At the experiments the detectors do not differentiate between the neutrino flavours. Therefore, the assumption of lepton flavour universality (LFU) effectively gives a factor of 3 in the branching ratio. In the case of LQs, however, it is difficult to implement LFU since this would automatically generate lepton flavour violation (LFV), e.g. in the decays  $B \rightarrow K^{(*)} \mu e$ . Therefore, a frequent assumption in LQ scenarios is that the LQ couples exclusively to one generation of leptons. In such a case there will be contributions to e.g.  $C_L^{bs\mu\mu}$  but none to  $C_L^{bsee}$  and  $C_L^{bs\tau\tau}$ . Including generation-dependent couplings to leptons adds a flavour index  $\ell$  to the Wilson coefficients  $C_L^\ell$  and  $C_R^\ell$  contributing to  $b \rightarrow s \bar{\nu}_\ell \nu_\ell$  transitions. Then, the parameters  $\epsilon$  and  $\eta$  become also flavour dependent and eqs. (6.16) have to be modified to

$$\mathcal{R}_K = \frac{1}{3} \sum_\ell (1 - 2\eta_\ell) \epsilon_\ell^2, \quad (6.19a)$$

$$\mathcal{R}_{K^*} = \frac{1}{3} \sum_\ell (1 + \kappa_\eta \eta_\ell) \epsilon_\ell^2, \quad (6.19b)$$

$$\mathcal{R}_{FL} = \frac{1}{3} \sum_\ell \frac{1 + 2\eta_\ell}{1 + \kappa_\eta \eta_\ell}. \quad (6.19c)$$

### Consequences of SM gauge invariance

By construction LQs come in representations of the SM gauge group such that the theory is SM gauge invariant. Further, along the lines discussed at the beginning of this chapter, we assume other NP to be heavier than the LQ fields. Under the assumption that the NP scale is much larger than  $v_{\text{SM}}$ , the SM gauge symmetries are respected to a high degree at low energies and it is convenient to parametrize the NP effects at low energies in a  $G_{\text{SM}}$  invariant way, which is done in the so-called SMEFT [266, 68]. As we will see in the following, in LQ models only a subset of all possible NP operators is generated, such that the SMEFT formulation leads to strong correlations between the dineutrino mode and the decay into charged leptons. Therefore, the wealth of experimental data on  $B \rightarrow K^{(*)} \ell^+ \ell^-$  can be used to give predictions for the neutrino mode.

Using an effective Lagrangian for dimension-6 operators,

$$\mathcal{L}^{(6)} = \sum_i \frac{c_i}{\Lambda_{\text{NP}}^2} \mathcal{O}_i, \quad (6.20)$$

let us first write down the basis of effective operators relevant for  $b \rightarrow s \ell \ell$  and  $b \rightarrow s \bar{\nu} \nu$  transitions that is invariant under the SM gauge symmetry [68] (omitting flavour indices),

$$\mathcal{O}_{Hq}^{(1)} = i(\bar{q}_L \gamma_\mu q_L) H^\dagger D^\mu H, \quad \mathcal{O}_{qL}^{(1)} = (\bar{q}_L \gamma_\mu q_L)(\bar{l}_L \gamma^\mu l_L), \quad (6.21a)$$

$$\mathcal{O}_{Hq}^{(3)} = i(\bar{q}_L \gamma_\mu \tau^a q_L) H^\dagger D^\mu \tau_a H, \quad \mathcal{O}_{qL}^{(3)} = (\bar{q}_L \gamma_\mu \tau^a q_L)(\bar{l}_L \gamma^\mu \tau_a l_L), \quad (6.21b)$$

$$\mathcal{O}_{Hd} = i(\bar{d}_R \gamma_\mu d_R) H^\dagger D^\mu H, \quad \mathcal{O}_{dL} = (\bar{d}_R \gamma_\mu d_R)(\bar{l}_L \gamma^\mu l_L), \quad (6.21c)$$

$$\mathcal{O}_{de} = (\bar{d}_R \gamma_\mu d_R)(\bar{\ell}_R \gamma^\mu \ell_R), \quad \mathcal{O}_{qe} = (\bar{q}_L \gamma_\mu q_L)(\bar{\ell}_R \gamma^\mu \ell_R). \quad (6.21d)$$

For simplicity, we have omitted dipole operators, that are only relevant in semi-leptonic  $b \rightarrow s \ell^+ \ell^-$  processes at low dilepton invariant mass and in radiative decays, as well as scalar operators, that are relevant in the  $B_s \rightarrow \mu^+ \mu^-$  decay (see 6.5).

The NP contributions to rare  $B$  decays are described at low energies (and after EWSB) by the effective operators  $\mathcal{O}_9^{(\prime)}$  and  $\mathcal{O}_{10}^{(\prime)}$  (see eq. 3.62) for  $b \rightarrow s \ell^+ \ell^-$  as well as by  $\mathcal{O}_L$  and  $\mathcal{O}_R$  for  $b \rightarrow s \bar{\nu} \nu$

	Spin	$G_{\text{SM}}$	interaction term	generated Wilson coefficients
$S_1$	0	$(\bar{\mathbf{3}}, \mathbf{1})_{\frac{1}{3}}$	$\hat{\lambda}_L^{ij} (\bar{q}_{Li}^c \cdot \epsilon \cdot l_{Lj}) \phi$	$\frac{[c_{ql}^{(1)}]_{ij;kl}}{\Lambda_{\text{NP}}^2} = -\frac{[c_{ql}^{(3)}]_{ij;kl}}{\Lambda_{\text{NP}}^2} = -\frac{1}{4} \frac{\hat{\lambda}_L^{jl} \hat{\lambda}_L^{ik*}}{m_{LQ}^2}$
$S_3$	0	$(\bar{\mathbf{3}}, \mathbf{3})_{\frac{1}{3}}$	$\hat{\lambda}_L^{ij} (\bar{q}_{Li}^c \cdot \epsilon \cdot \tau^a \cdot l_{Lj}) \phi^a$	$\frac{[c_{ql}^{(1)}]_{ij;kl}}{\Lambda_{\text{NP}}^2} = 3 \frac{[c_{ql}^{(3)}]_{ij;kl}}{\Lambda_{\text{NP}}^2} = \frac{3}{4} \frac{\hat{\lambda}_L^{jl} \hat{\lambda}_L^{ik*}}{m_{LQ}^2}$
$\tilde{R}_2$	0	$(\mathbf{3}, \mathbf{2})_{\frac{1}{6}}$	$\hat{\lambda}_R^{ij} \bar{d}_{Ri} (l_{Lj} \cdot \epsilon \cdot \phi)$	$\frac{[c_{dl}]_{ij;kl}}{\Lambda_{\text{NP}}^2} = -\frac{1}{2} \frac{\hat{\lambda}_R^{il} \hat{\lambda}_R^{jk*}}{m_{LQ}^2}$
$U_1$	1	$(\mathbf{3}, \mathbf{1})_{\frac{2}{3}}$	$\hat{\lambda}_L^{ij} (\bar{q}_{Li} \gamma^\mu l_{Lj}) \phi_\mu$	$\frac{[c_{ql}^{(1)}]_{ij;kl}}{\Lambda_{\text{NP}}^2} = \frac{[c_{ql}^{(3)}]_{ij;kl}}{\Lambda_{\text{NP}}^2} = \frac{1}{2} \frac{\hat{\lambda}_L^{il} \hat{\lambda}_L^{jk*}}{m_{LQ}^2}$
$U_3$	1	$(\mathbf{3}, \mathbf{3})_{\frac{2}{3}}$	$\hat{\lambda}_L^{ij} (\bar{q}_{Li} \gamma^\mu \tau^a l_{Lj}) \phi_\mu^a$	$\frac{[c_{ql}^{(1)}]_{ij;kl}}{\Lambda_{\text{NP}}^2} = -3 \frac{[c_{ql}^{(3)}]_{ij;kl}}{\Lambda_{\text{NP}}^2} = -\frac{3}{2} \frac{\hat{\lambda}_L^{il} \hat{\lambda}_L^{jk*}}{m_{LQ}^2}$
$V_2$	1	$(\bar{\mathbf{3}}, \mathbf{2})_{\frac{5}{6}}$	$\hat{\lambda}_R^{ij} \bar{d}_{Ri}^c \gamma^\mu (l_{Lj} \cdot \epsilon \cdot \phi_\mu)$	$\frac{[c_{dl}]_{ij;kl}}{\Lambda_{\text{NP}}^2} = \frac{\hat{\lambda}_R^{il} \hat{\lambda}_R^{jk*}}{m_{LQ}^2}$

**Table 6.3.:** Possible leptoquark scenarios relevant for  $b \rightarrow s\nu\bar{\nu}$  decays. In the first columns, the spin and gauge quantum numbers are given as well as the relevant interaction term. In the last column, we give expressions for the Wilson coefficients of the generated four-fermion operators. The SM left-handed quark and lepton doublets are denoted by  $Q_L$  and  $L_L$ , respectively, while the leptoquark is written as  $\phi_{(\mu)}$ . We explicitly showed the flavour indices here.

(see eq. (6.9)). The effective operators (6.21) can be mapped onto the weak effective Hamiltonian (3.61) yielding the dictionary<sup>1</sup>

$$C_L = C_L^{\text{SM}} + \tilde{c}_{ql}^{(1)} - \tilde{c}_{ql}^{(3)} + \tilde{c}_Z, \quad C_R = \tilde{c}_{dl} + \tilde{c}'_Z, \quad (6.22a)$$

$$C_9 = C_9^{\text{SM}} + \tilde{c}_{qe} + \tilde{c}_{ql}^{(1)} + \tilde{c}_{ql}^{(3)} - \zeta \tilde{c}_Z, \quad C'_9 = \tilde{c}_{de} + \tilde{c}_{dl} - \zeta \tilde{c}'_Z, \quad (6.22b)$$

$$C_{10} = C_{10}^{\text{SM}} + \tilde{c}_{qe} - \tilde{c}_{ql}^{(1)} - \tilde{c}_{ql}^{(3)} + \tilde{c}_Z, \quad C'_{10} = \tilde{c}_{de} - \tilde{c}_{dl} + \tilde{c}'_Z, \quad (6.22c)$$

where

$$\tilde{c}_Z = \frac{1}{2}(\tilde{c}_{Hq}^{(1)} + \tilde{c}_{Hq}^{(3)}), \quad \tilde{c}'_Z = \frac{1}{2}\tilde{c}_{Hd} \quad \text{and} \quad \zeta = 1 - 4s_w^2 \approx 0.08 \quad (6.23)$$

To match the normalizations of the effective operators the notation

$$\tilde{c}_k = \frac{(c_k)_{23}}{\Lambda^2} \frac{\pi}{\sqrt{2}G_F\alpha V_{tb}V_{ts}^*} \approx \frac{(c_k)_{23}}{V_{tb}V_{ts}^*} \left( \frac{5 \text{ TeV}}{\Lambda_{\text{NP}}} \right)^2, \quad (6.24)$$

was introduced where we restored flavour indices and worked in a basis where the down-type quark mass matrix is diagonal. The dictionary (6.22) now reveals the correlations between the Wilson coefficients induced by the SM gauge symmetry.

In LQ models we find that only a few of the operators (6.21) are actually generated and that they are directly correlated such that for all scenarios there is effectively only one free parameter. Exceptions are the scenarios  $\tilde{S}_1$ ,  $R_2$ ,  $\tilde{U}_1$  and  $\tilde{V}_2$  as they do not generate any effects in  $b \rightarrow s\bar{\nu}\nu$ . The LQs  $\tilde{U}_1$  and  $\tilde{V}_2$  only contribute to weak decays of up-type quarks while the LQs  $\tilde{S}_1$  and  $R_2$  can give effects in down-type  $\Delta F = 1$  processes but then it necessarily involves only charged leptons. The results for the viable options are shown in table 6.3. In models in which the LQ is an  $\text{SU}(2)_L$  singlet or triplet only the operators  $\mathcal{O}_{ql}^{(1)}$  and  $\mathcal{O}_{ql}^{(3)}$  are generated, but are predicted to obey the relation

$$\tilde{c}_{ql}^{(1)} = n \cdot \tilde{c}_{ql}^{(3)}, \quad (6.25)$$

where  $n$  is a model-dependent real constant. From (6.22) we then find that, for a given  $n$ , the

<sup>1</sup>The correct treatment would be to perform the matching at the high scale and then use RG evolution to obtain the effective operators at the low scale  $m_b$ . However, for the considered operators the RGE effects are small such that we neglect their impact.

	$C_9^{\text{NP}}$	$C_{10}^{\text{NP}}$	$C'_9$	$C'_{10}$	$C_S$	$C_P$	$C'_S$	$C'_P$	$C_L^{\text{NP}}$	$C_R$
$S_1$	—	—	—	—	—	—	—	—	$-\frac{1}{4}\lambda_L^{bl}\lambda_L^{sl*}$	—
$\tilde{S}_1$	—	—	$-\frac{1}{2}\lambda_R^{bl}\lambda_R^{sl*}$	$+C'_9$	—	—	—	—	—	—
$R_2$	$\frac{1}{2}\lambda_L^{sl}\lambda_L^{bl*}$	$+C_9^{\text{NP}}$	—	—	—	—	—	—	—	—
$\tilde{R}_2$	—	—	$-\frac{1}{2}\lambda_R^{sl}\lambda_R^{bl*}$	$-C'_9$	—	—	—	—	—	$+C'_9$
$S_3$	$\frac{3}{4}\lambda_L^{bl}\lambda_L^{sl*}$	$-C_9^{\text{NP}}$	—	—	—	—	—	—	$+\frac{1}{2}C_9^{\text{NP}}$	—
$U_1$	$-\frac{1}{2}\lambda_L^{sl}\lambda_L^{bl*}$	$-C_9^{\text{NP}}$	$-\frac{1}{2}\lambda_R^{sl}\lambda_R^{bl*}$	$+C'_9$	$\lambda_L^{sl}\lambda_R^{bl*}m_b^{-1}$	$-C_S$	$-\lambda_R^{sl}\lambda_L^{bl*}m_b^{-1}$	$+C'_S$	—	—
$\tilde{U}_1$	—	—	—	—	—	—	—	—	—	—
$V_2$	$-\frac{1}{2}\lambda_L^{bl}\lambda_L^{sl*}$	$+C_9^{\text{NP}}$	$\frac{1}{2}\lambda_R^{bl}\lambda_R^{sl*}$	$-C'_9$	$\lambda_L^{bl}\lambda_R^{sl*}m_b^{-1}$	$-C_S$	$-\lambda_R^{bl}\lambda_L^{sl*}m_b^{-1}$	$+C'_S$	—	$+C'_9$
$\tilde{V}_2$	—	—	—	—	—	—	—	—	—	—
$U_3$	$-\frac{3}{2}\lambda_L^{bl}\lambda_L^{sl*}$	$-C_9^{\text{NP}}$	—	—	—	—	—	—	$+2C_9^{\text{NP}}$	—

**Table 6.4.:** Correlations between Wilson coefficients of  $b \rightarrow s\ell^+\ell^-$  as  $b \rightarrow s\bar{\nu}\nu$  transitions. It has to be understood that the LQs have to be multiplied by the normalization factor (6.7) as shown e.g. in (6.6). We do not include dipole or tensor operators as these would be generated only at loop-level so we assume that they are sub-leading.

low-energy Wilson coefficients only depend on one parameter,

$$C_L^{\text{NP}} = \tilde{c}_{qt}^{(1)} - \tilde{c}_{qt}^{(3)} = (n-1)\tilde{c}_{qt}^{(3)}, \quad (6.26a)$$

$$C_9^{\text{NP}} = -C_{10}^{\text{NP}} = \tilde{c}_{qt}^{(1)} + \tilde{c}_{qt}^{(3)} = (n+1)\tilde{c}_{qt}^{(3)}, \quad (6.26b)$$

$$C_R = C'_9 = C'_{10} = 0. \quad (6.26c)$$

Hence, we can write the corrections to the  $b \rightarrow s\bar{\nu}\nu$  branching ratios in the following way,

$$\mathcal{R}_{F_L} = 1, \quad \mathcal{R}_K = \mathcal{R}_{K^*} = \frac{2}{3} + \frac{1}{3} \frac{\left| C_L^{\text{SM}} + (n-1) [\tilde{c}_{qt}^{(3)}]_\ell \right|^2}{|C_L^{\text{SM}}|^2}. \quad (6.27)$$

In the case of a doublet LQ, only  $\mathcal{O}_{dl}$  is present. So again, we expect only a dependence on one parameter,

$$C_L^{\text{NP}} = C_9^{\text{NP}} = C_{10}^{\text{NP}} = 0, \quad (6.28a)$$

$$C_R = C'_9 = -C'_{10} = \tilde{c}_{dl}. \quad (6.28b)$$

In this case, we find a contribution to  $\eta \neq 0$  such that also  $\mathcal{R}_K \neq \mathcal{R}_{K^*}$ ,

$$\mathcal{R}_K = \frac{2}{3} + \frac{1}{3} \left( 1 + 2 \frac{C_L^{\text{SM}} \text{Re}([\tilde{c}_{dl}]_\ell)}{|C_L^{\text{SM}}|^2 + |[\tilde{c}_{dl}]_\ell|^2} \right) \left( 1 + \frac{|[\tilde{c}_{dl}]_\ell|^2}{|C_L^{\text{SM}}|^2} \right), \quad (6.29a)$$

$$\mathcal{R}_{K^*} = \frac{2}{3} + \frac{1}{3} \left( 1 - \kappa_\eta \frac{C_L^{\text{SM}} \text{Re}([\tilde{c}_{dl}]_\ell)}{|C_L^{\text{SM}}|^2 + |[\tilde{c}_{dl}]_\ell|^2} \right) \left( 1 + \frac{|[\tilde{c}_{dl}]_\ell|^2}{|C_L^{\text{SM}}|^2} \right). \quad (6.29b)$$

From table 6.3, we can already see two special cases. In the scenario  $U_1$  there is  $n = 1$  which implies that all contributions to  $\mathcal{R}_K = \mathcal{R}_{K^*}$  vanish such that we do not expect any deviation from the SM values in this model. For  $S_1$  we find  $n = -1$ , which means that this scenario does not give any contribution to the decay into charged leptons. Hence, the effects in  $\mathcal{R}_K$  and  $\mathcal{R}_{K^*}$  are unconstrained from these decays. Since we have connected  $b \rightarrow s\bar{\nu}\nu$  transitions to  $b \rightarrow s\ell^+\ell^-$  transitions it is now possible to use the wealth of experimental results regarding the latter to give predictions for possible modifications of the former. The experimental data on  $b \rightarrow s\ell^+\ell^-$  transitions show a significant tension

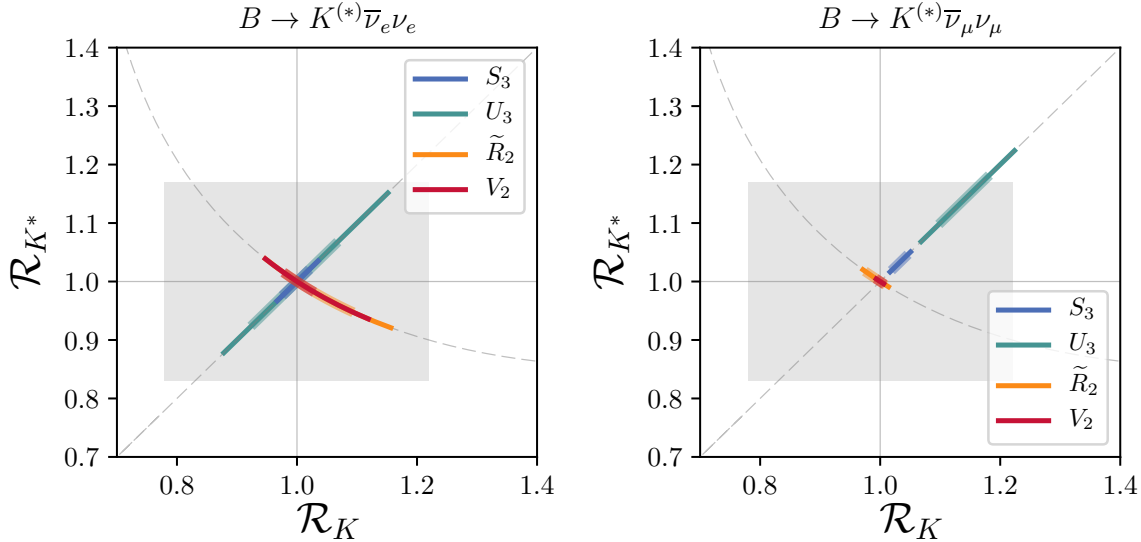


**Figure 6.3.:** Allowed ranges for  $\mathcal{R}_K$  and  $\mathcal{R}_{K^*}$  obtained by using correlations with  $b \rightarrow s\ell^+\ell^-$  transitions: *Left:* The case that LQs only couple to first-generation leptons. *Right:* LQs only couple to second-generation leptons. The  $1\sigma$  (transparent thick lines) and  $2\sigma$  ranges are shown. The dashed lines denote the expectations if only  $C_L$  (diagonal) or  $C_R$  (curved line) get contributions. The gray box shows the expected experimental precision assuming a measurement of a SM-like value. We did not show results for  $S_1$  as this is unconstrained by  $G_{\text{SM}}$  correlations and so it can extend over the diagonal dashed line as long as (6.18a) is satisfied.

with the SM predictions, which could be due to either NP or underestimated hadronic uncertainties. In this work we take the most optimistic standpoint and assume that the whole tension is in fact due to NP. Then, by the above relations, these tensions can be related to possible NP effects in the dineutrino mode to estimate how large NP effects can possibly become. This effectively acts as an upper bound on NP. If the  $bs\ell\ell$  anomaly is in fact due to hadronic physics then NP contributions will be small, such that one cannot expect large NP effects in  $b \rightarrow s\bar{\nu}\nu$  transitions.

For all LQ representations, we show in table 6.4 the correlations between the effective operators relevant for semi-leptonic  $b \rightarrow s$  transitions. Because of SM gauge invariance, there are either no or several operators that are relevant for  $b \rightarrow s\ell^+\ell^-$  transitions. The Wilson coefficients of these operators are directly linked to  $C_L$  or  $C_R$ . In the  $\text{SU}(2)_L$ -triplet scenarios only left-handed vector operators are generated that obey the relation  $C_9^{\text{NP}} = -C_{10}^{\text{NP}}$ , which is one of the preferred scenarios for the  $bs\ell\ell$  anomaly. For models in which the LQ is either an  $\text{SU}(2)_L$  singlet or a doublet the generated patterns of Wilson coefficients are qualitatively different depending on whether the LQ is spin-0 or spin-1. In the case of scalar LQs either left-handed or right-handed vector operators are generated whose Wilson coefficients can have either relative sign. For vector LQs  $U_1$  and  $V_2$  all vector and scalar operators involving charged leptons are generated, but their Wilson coefficients are tightly correlated. For the scalar singlet LQ  $S_1$  there are no contributions involving charged leptons at all. Therefore, the dineutrino channel is unbounded by  $G_{\text{SM}}$  relations and is allowed to saturate the experimental constraints (6.18a). The vector LQ  $U_1$  does not give any contributions to the dineutrino channel. We also note that the cases  $\tilde{U}_1$  and  $\tilde{V}_2$  cannot be probed by  $b \rightarrow s$  transitions at all.

For the time being let us concentrate on the case where the LQs couple only to one generation of leptons such that there are no LFV processes. The different leptons in the final states imply rather different experimental bounds. Therefore we will discuss the three different cases separately.

- $\ell = e$

Assuming that the LQs only couple to leptons of the first generation one can put constraints on  $b \rightarrow s\bar{\nu}_e\nu_e$  via the decay mode into charged leptons  $b \rightarrow se^+e^-$ . For these there exist measurements of the branching ratio  $\text{Br}(B^+ \rightarrow K^+e^+e^-)$  from LHCb [190] as well as measurements of the inclusive rate  $B \rightarrow X_s ee$  by BaBar [267]. Relevant for the LQ  $V_2$ , which also generates scalar operators, is further an upper bound on  $\text{Br}(B_s \rightarrow e^+e^-)$  given by CDF [268]. We have



performed a global fit to this data using `flavio` [147], which gives the following  $1\sigma$  ranges,

$$S_1 \quad C_L^{\text{NP}} \text{ unbounded} \quad (6.30a)$$

$$\tilde{R}_2 \quad C'_9 = -C'_{10} \in [-0.78, 0.15] \quad C_R \in [-0.78, 0.15] \quad (6.30b)$$

$$S_3 \quad C_9^{\text{NP}} = -C_{10}^{\text{NP}} \in [-0.28, 0.36] \quad C_L^{\text{NP}} \in [-0.11, 0.15] \quad (6.30c)$$

$$V_2 \quad C_R \in [-0.21, 0.16] \quad (6.30d)$$

$$U_3 \quad C_9^{\text{NP}} = -C_{10}^{\text{NP}} \in [-0.28, 0.36] \quad C_L^{\text{NP}} \in [-1.13, 1.45] \quad (6.30e)$$

where we used the relations (6.26) and (6.28) to calculate the allowed ranges for  $C_L^{\text{NP}}$  and  $C_R$ . For the LQ  $V_2$  we performed a dedicated Bayesian fit taking into account all effective operators that are present in this scenario (see table 6.4). The results are shown in the left plot of figure 6.3. Generally, we find that for both modes a suppression as well as an enhancement are possible. The corrections in the case  $S_3$  are small and will probably not be measurable given the expected experimental precision. For the cases  $S_3$ ,  $\tilde{R}_2$  and  $V_2$  the corrections are more sizable ranging about  $\pm 10\%$  or larger which, however, are probably also too small to be visible.

- $\ell = \mu$

In case the final state consists of muon neutrinos, the  $b \rightarrow s\bar{\nu}\nu$  transition is constrained by measurements of the decays  $b \rightarrow s\mu^+\mu^-$ . The allowed ranges for the Wilson coefficients  $C_{9,10}^{(\prime)}$  have recently been determined in a global fit to  $bs\mu^+\mu^-$  data [1] (see section 6.1). Using the results of table 6.4 we can now use the fit results given in table 6.1 to translate them into bounds on the dineutrino operators  $C_L$  and  $C_R$ . Concentrating on the relevant cases for  $b \rightarrow s\bar{\nu}\nu$  transitions the allowed  $1\sigma$  ranges translate as follows

$$S_1 \quad C_L^{\text{NP}} \text{ unbounded} \quad (6.31a)$$

$$\tilde{R}_2 \quad C'_9 = -C'_{10} \in [-0.02, +0.18] \quad C_R \in [-0.02, +0.18] \quad (6.31b)$$

$$S_3 \quad C_9^{\text{NP}} = -C_{10}^{\text{NP}} \in [-0.75, -0.46] \quad C_L^{\text{NP}} \in [-0.30, -0.18] \quad (6.31c)$$

$$U_3 \quad C_9^{\text{NP}} = -C_{10}^{\text{NP}} \in [-0.75, -0.46] \quad C_L^{\text{NP}} \in [-3.00, -1.84] \quad (6.31d)$$

A special case is the LQ  $V_2$  as it generates not only vector but also scalar operators. These operators are probed by the rare decay  $B_s \rightarrow \mu^+\mu^-$  (see section 6.5). This decay, however, has not been included into the analysis performed in [1] as in that analysis the focus was on vector operators. Therefore, we performed a dedicated Bayesian fit taking into account the correlated Wilson coefficients of the LQ  $V_2$  (see table 6.4) using `flavio` [147]. We included the same data as in [1] but additionally the branching ratio of  $B_s \rightarrow \mu^+\mu^-$  as measured<sup>2</sup> by CMS [269] and LHCb [270]. This results in

$$V_2 \quad C_R \in [-0.004, +0.006]. \quad (6.31e)$$

Taking into account these allowed ranges for the Wilson coefficients the preferred values in the  $\mathcal{R}_K - \mathcal{R}_{K^*}$  plane are shown in figure 6.3. For the scenarios  $S_3$ ,  $\tilde{R}_2$  and  $V_2$  only small modifications of the branching ratios of the order of a few percent are possible which, unfortunately, will not be resolvable in the foreseeable future. For the LQ  $U_3$  larger corrections of up to 25% are possible and, furthermore, accepting the  $B \rightarrow K^{(*)}\mu^+\mu^-$  anomalies as given through NP one would definitely expect an enhancement of  $\mathcal{R}_K = \mathcal{R}_{K^*}$  which could be detectable within the next decade, although this might be hard. This is interesting since both LQs  $S_3$  and  $U_3$  can potentially explain the  $B \rightarrow K^*\mu^+\mu^-$  anomaly. If this anomaly prevails the decays  $B \rightarrow K^{(*)}\bar{\nu}\nu$  could act as a discriminator between both LQ scenarios.

- $\ell = \tau$

If the LQ only couples to 3rd generation leptons then its couplings are effectively unbounded by  $G_{\text{SM}}$  relations. There exist upper bounds on the branching ratios  $\text{Br}(B_s \rightarrow \tau^+\tau^-)$  [271] by LHCb and  $\text{BR}(B^+ \rightarrow K^+\tau^+\tau^-)$  [272] by the BaBar collaboration, but these are several orders of magnitude above the SM predictions. Therefore, by far the strongest bounds are given by the searches for the dineutrino modes (6.18a).

<sup>2</sup>The experiments give these results as a correlated likelihood for  $B_s \rightarrow \mu^+\mu^-$  and  $B_d \rightarrow \mu^+\mu^-$ . In this fit we assumed no NP in  $b \rightarrow d$  transitions which is justified as the experimental likelihood only shows a weak correlation.

If the LQs couple to more than one generation of leptons then one inevitably also gets LFV processes like  $B \rightarrow K^{(*)} \bar{\nu}_e \nu_\mu$  or the corresponding charged lepton mode. Experimentally, upper bounds on such processes have been obtained,<sup>3</sup>

$$\begin{aligned} \text{Br}(B^+ \rightarrow K^+ e \mu) &< \mathcal{O}(10^{-7}) && \text{BaBar [273],} \\ \text{Br}(B \rightarrow K^* e \mu) &< \mathcal{O}(10^{-6}) && \text{BaBar [273],} \\ \text{Br}(B_s \rightarrow e \mu) &< \mathcal{O}(10^{-8}) && \text{LHCb [274],} \\ \text{Br}(B^+ \rightarrow K^+ e \tau) &< \mathcal{O}(10^{-5}) && \text{BaBar [275],} \\ \text{Br}(B^+ \rightarrow K^+ \mu \tau) &< \mathcal{O}(10^{-5}) && \text{BaBar [275].} \end{aligned}$$

Generally, LFV involving taus is only loosely constrained. If only the first two lepton generations are involved then the bounds are stronger but still one order of magnitude weaker than in the lepton flavour conserving case.

Denoting the Wilson coefficients contributing to  $b \rightarrow s \ell^i \ell^j$  generically by  $C_{sb;ij}$  we can relate the lepton flavour violating coefficients to the lepton flavour conserving ones (where we restrict ourselves to the first two lepton generations),<sup>4</sup>

$$C_{sb;ee} C_{sb;\mu\mu} = C_{sb;e\mu} C_{sb;\mu e}. \quad (6.32)$$

Therefore, as long as one is refraining from going to fine-tuned corners of parameter space in which one coupling is anomalously large while others are very small, the LFV effects cannot be too large given the current data on lepton flavour conserving processes. On the other hand, if in the future a non-zero NP contribution to both the electron and the muon mode will be established, then it is predicted that in the LQ models considered also a signal in the LFV modes should appear.

## 6.4. Direct bounds on leptoquarks

In this section we want to discuss direct constraints on LQs at  $pp$  colliders like the LHC. Since LQs carry colour, they are expected to be produced copiously at hadron colliders. Therefore direct searches put important constraints that are complementary to indirect bounds.

Before diving into the details of collider searches let us first discuss another bound that is very relevant for LQs. As LQs carry baryon number a breaking of this quantum number is induced if they couple to quark-antiquark pairs (these are the  $\hat{\lambda}_{qq}$  couplings in table 6.2) such that proton decay can be generated. This usually puts strong constraints on the theory making very high LQ masses inevitable. This is particularly relevant when considering concrete models. As an example, in GUT models the coupling  $\hat{\lambda}_{qq}$  is connected to gauge couplings. We, however, are considering a simplified approach in which the couplings are free parameters and have to be chosen to fulfill experimental constraints. Therefore, we set  $\hat{\lambda}_{qq} = 0$  in the following analysis to satisfy bounds from proton decay. Furthermore, regarding direct searches this marks a conservative choice of parameters as non-vanishing  $\hat{\lambda}_{qq}$  couplings would decrease the branching ratios of interesting decay channels such that direct constraints are effectively loosened.

### Leptoquark production

At hadron colliders LQs can be produced singly or in pairs at tree level [276]. Most experimental searches focus on pair production. The reason is that single production is strongly model-dependent since the production cross section depends on the detailed LQ couplings. Pair production is instead determined by the strong coupling constant.<sup>5</sup> Hence, the pair production cross section is a function of the LQ mass alone for all representations. In the following we will focus solely on pair production. We note that the experimental bounds on LQs can be significantly improved by including single production [277], but this is beyond the scope of this work.

The coupling of a scalar LQ  $S$  to gluons is uniquely determined by the kinetic Lagrangian,

$$\mathcal{L} = (\mathcal{D}_\mu S)^\dagger (\mathcal{D}^\mu S) - m_S^2 S^\dagger S, \quad (6.33)$$

<sup>3</sup>Here, we do not show the exact numbers as only the orders of magnitude are important.

<sup>4</sup>Note that generally the processes  $B \rightarrow K^{(*)} \mu^+ e^-$  and  $B \rightarrow K^{(*)} e^+ \mu^-$  have to be considered as different decays.

<sup>5</sup>There are also contributions from a  $t$ -channel lepton exchange, but this should be suppressed by a ratio  $\lambda^2/g_s^2$ .

where the gauge covariant derivative is given by  $\mathcal{D}_\mu = \partial_\mu - ig_s G_\mu^a \mathbb{T}^a$ . Then the partonic cross section is given by [278, 279]

$$\hat{\sigma}(pp \rightarrow SS) = \hat{\sigma}(pp \rightarrow gg \rightarrow SS) + \sum_q \hat{\sigma}(pp \rightarrow \bar{q}q \rightarrow SS), \quad (6.34)$$

where the cross sections for production from gluons or quark-antiquark pairs read

$$\hat{\sigma}(pp \rightarrow gg \rightarrow SS) = \frac{\pi\alpha_s^2}{96\hat{s}} \left\{ \beta (41 - 31\beta^2) - (17 - 18\beta^2 + \beta^4) \log \frac{|1 + \beta|}{|1 - \beta|} \right\}, \quad (6.35a)$$

$$\hat{\sigma}(pp \rightarrow \bar{q}q \rightarrow SS) = \frac{2\pi\alpha_s^2}{27\hat{s}} \beta^3. \quad (6.35b)$$

Here,  $\beta = \sqrt{1 - 4m_S^2/\hat{s}}$  contains the dependence on the LQ mass and  $\hat{s}$  is the partonic center-of-mass energy.

The production cross section of vector LQs is more involved. Here, gauge invariance allows for modifications of the couplings to gluons that are model-dependent. The most general Lagrangian describing the interactions of vector LQs  $V_\mu$  with gluons is given by [278]<sup>6</sup>

$$\mathcal{L} \supset -\frac{1}{2} \mathcal{V}_{\mu\nu}^\dagger \mathcal{V}^{\mu\nu} + M_V^2 V_\mu^\dagger V^\mu - ig_s(1 - \kappa) V_\mu^\dagger G^{\mu\nu} V_\nu, \quad (6.36)$$

where the LQ field strength tensor is written as  $\mathcal{V}_{\mu\nu} = \mathcal{D}_\mu V_\nu - \mathcal{D}_\nu V_\mu$  with the gauge covariant derivative stated below eq. (6.33). The value of  $\kappa$  is model-dependent. If the vector LQ  $V_\mu$  is part of a Yang-Mills gauge field, as would be the case for a GUT-like UV completion, one has  $\kappa = 0$ . In our general approach there are however no restrictions on  $\kappa$ . Therefore, we will consider two different scenarios for vector LQ production

**Yang-Mills:** We assume  $\kappa = 0$ .

**Minimal production:**  $\kappa$  is chosen such that the production cross section is minimized. This marks the most conservative option.

The expressions for the production cross sections with full  $\kappa$  dependence are given in ([278]).

To obtain the total production cross section the partonic ones have to be convoluted with parton distribution functions

$$\sigma_{\text{tot}}(pp \rightarrow \text{LQLQ}) = \sum_X \int dx_1 dx_2 f_X(x_1) f_X(x_2) \hat{\sigma}(pp \rightarrow X \rightarrow \text{LQLQ}), \quad (6.37)$$

where  $X$  denotes production from gluon and quark-antiquark pairs. For this we implemented CT14 NNLO parton distribution functions [280] using LHAPDF6 [281].

### Leptoquark decay

Pair produced leptoquarks decay into two leptons and two quarks (see figure 6.4). Therefore the experimental signature is either  $2j + \ell^+ \ell^-$ ,  $2j + \cancel{E}$  or  $2j + \ell^\pm + \cancel{E}$  where the missing energy indicates neutrinos in the final state. Experimental searches typically assume that the LQs only couple to one generation of quarks and leptons, but as long as there is no flavour tagging for the jets this is not a problem for inter-generational couplings such as e.g.  $b - \mu - \text{LQ}$ .

In the following we will assume that only those LQ couplings are non-vanishing which are sufficient for generating effects in  $b \rightarrow s \mu^+ \mu^-$  transitions. In particular, we assume that the LQs will only couple to second generation leptons and not to quarks of the first generation. Due to  $G_{\text{SM}}$  invariance this will lead to correlations with other decay channels involving e.g. top quarks. The experimental searches that are included in the following analysis are:

- $jj\nu\nu$ ,  $bb\nu\nu$ ,  $tt\nu\nu$  from ATLAS at 8 TeV [282],

<sup>6</sup>Note that there is also the possibility of a term  $V_\mu^\dagger \tilde{G}^{\mu\nu} V_\nu$  where  $\tilde{G}^{\mu\nu}$  is the dual gluonic field strength tensor. Therefore, this terms would violate  $CP$ . We will assume  $CP$  invariance and neglect this term. Furthermore, on the non-renormalizable level a dimension-6 operator of the form  $\mathcal{V}_{\sigma\mu} G^{\mu\nu} \mathcal{V}_\nu^\sigma$  could be present. Such an operator, however, would have to be suppressed by a UV-scale  $\Lambda_{\text{UV}} > m_{\text{LQ}}$ , such that we expect the effects of such an operator to be negligible.

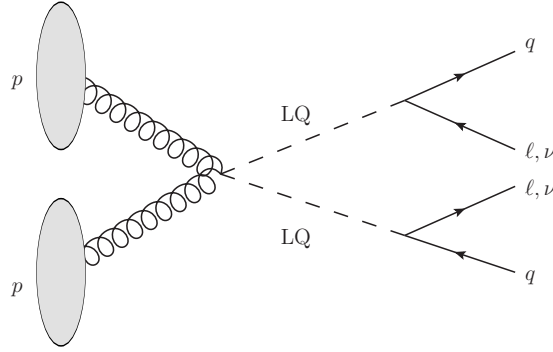


**Figure 6.4.:** Experimental signature of decaying pair produced LQs.

- $jj\nu\nu$  from ATLAS at 13 TeV [283],
- $jj\mu\mu, jj\nu\nu$  from CMS at 8 TeV [284],
- $jj\mu\mu$  from CMS at 13 TeV [285],

and the relevant decay patterns for the LQ models, which follow from the interaction terms shown in table 6.2, are given in table 6.5. We will further take the anomalies in  $b \rightarrow s\ell^+\ell^-$  seriously and assume that for each LQ, the Wilson coefficients take values given by the best fit points obtained in a global analysis to  $b \rightarrow s\ell^+\ell^-$  data [1]. To be concrete, each LQ scenario predicts correlations amongst the Wilson coefficients  $C_{9,10}^{(\prime)}$  which are given in table 6.4. Except for the representations<sup>7</sup>  $U_1$  and  $V_2$  these Wilson coefficients depend on two LQ couplings,  $\lambda^{s\mu}$  and  $\lambda^{b\mu}$ . For each coupling  $\lambda^{s\mu}$  we fix the other coupling,  $\lambda^{b\mu}$ , in such a way that the best fit values of table 6.1 are reproduced. This allows us to draw exclusion plots in the mass-coupling plane which are shown in figure 6.5. Fixing the one LQ coupling via  $\lambda^{s\mu}\lambda^{b\mu} = \text{const.}$  has the advantage that the exclusion plots contain both limiting cases  $\lambda^{s\mu} \gg \lambda^{b\mu}$  and  $\lambda^{s\mu} \ll \lambda^{b\mu}$ . We make the following observations:

- As the LQs  $\tilde{S}_1$  and  $R_2$  each generate only the relevant decay channel  $\text{LQ} \rightarrow j\mu$ , the exclusions are independent of the couplings and only depend on the production rate, which is the same for both LQ representations. In this case we find that LQ masses below around 900 GeV are excluded.
- For the LQ  $\tilde{R}_2$  we find that LQ masses below roughly 1250 GeV are excluded if  $\lambda_R^{s\mu} \gg \lambda_R^{b\mu}$ . In the opposite case,  $\lambda_R^{b\mu} \gg \lambda_R^{s\mu}$ , we find a significantly weaker bound of only 500 GeV.
- The LQ representation  $S_3$  is generally only weakly constrained. For  $\lambda_L^{s\mu} \gg \lambda_L^{b\mu}$  we find a bound of 500 GeV and for  $\lambda_L^{b\mu} \gg \lambda_L^{s\mu}$  we find roughly 600 GeV.
- For the vector LQ  $U_3$  we have to differentiate between minimal production and YM-like production. In the case of minimal production we find bounds of 700 GeV (for  $\lambda_L^{b\mu} \gg \lambda_L^{s\mu}$ ) and roughly 1200 GeV (for  $\lambda_L^{s\mu} \gg \lambda_L^{b\mu}$ ). In the case of YM-like production the bounds are stronger by roughly 200 GeV. We note that if both LQ couplings are of comparable size then the bounds are weaker.

We want to stress again that these bounds are only valid under the assumption that only the couplings needed for  $b \rightarrow s\mu^+\mu^-$  transitions are non-vanishing. If one also allows for other couplings then the bounds can be significantly weaker.

## 6.5. Leptoquarks and $B_s \rightarrow \mu\mu$

Until now we investigated the impact of LQs on  $b \rightarrow s$  transitions induced by vector operators. However, as table 6.4 shows, there are two LQs that give rise also to scalar operators. These are the spin-1 representations  $U_1$  and  $V_2$ . The first case is of particular interest as it predicts  $C_9^{\text{NP}} = -C_{19}^{\text{NP}}$

<sup>7</sup>We delay the discussion of direct bounds on the LQs  $U_1$  and  $V_2$  until section 6.5.

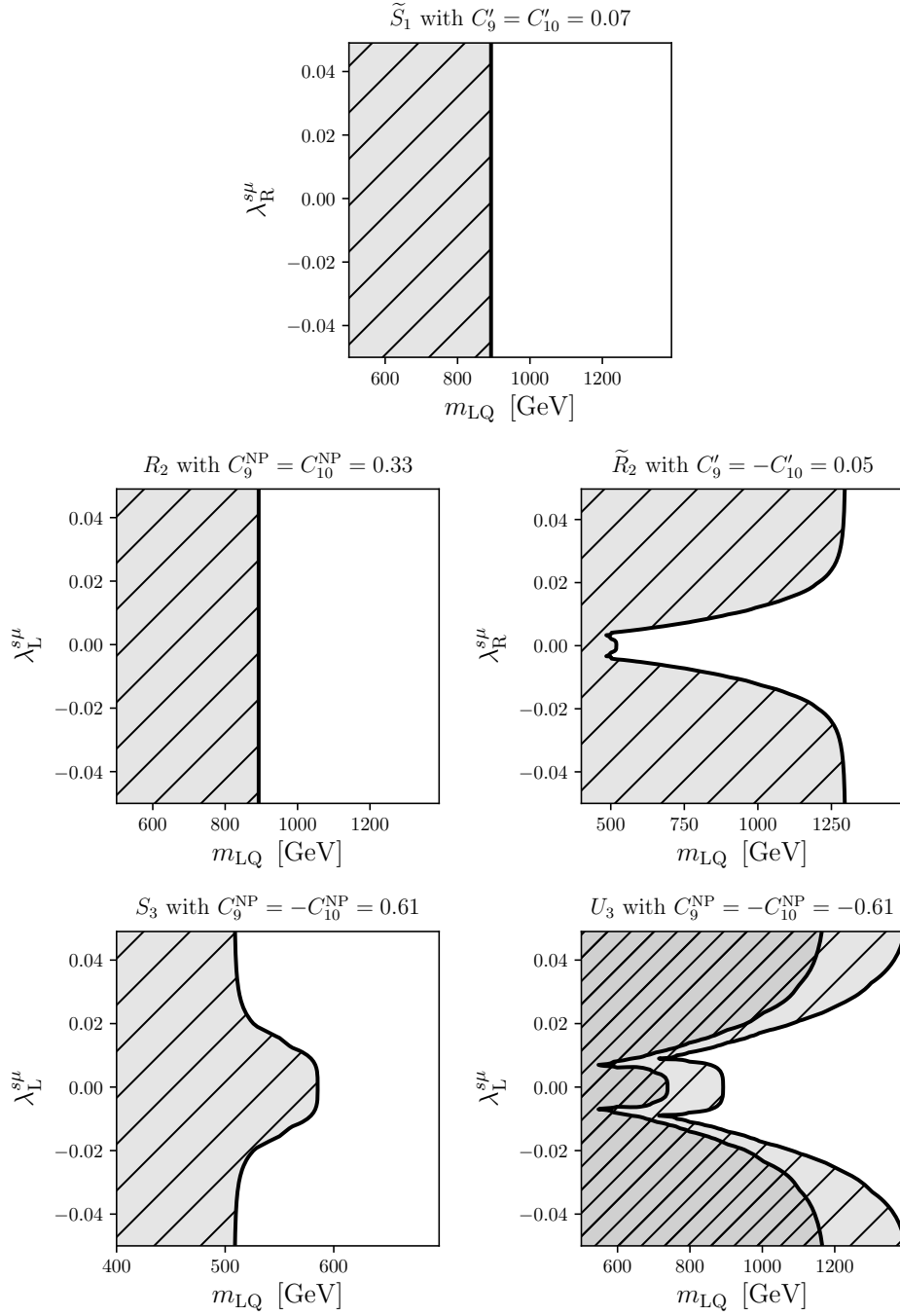


**Figure 6.5.:** Excluded parameter regions at 95% CL for LQs by direct searches at the LHC assuming that all LQ components are mass degenerate. The LQ couplings are fixed in such a way that the generated Wilson coefficients coincide with the best fits to  $bs\ell\ell$  data. For the vector LQ  $U_3$  we show exclusions for YM-like production as well as minimal production (doubly hatched).

Scenario	relevant decay channels	Scenario	relevant decay channels
$\tilde{S}_1$	$\tilde{S}_1 \rightarrow j\mu$	$U_1$	$U_1 \rightarrow \{j\mu, t\nu, j\nu\}$
$R_2$	$R_2^{\frac{2}{3}} \rightarrow j\mu$ $R_2^{\frac{5}{3}} \rightarrow \{j\mu, t\mu\}$	$V_2$	$V_2^{\frac{1}{3}} \rightarrow \{j\mu, j\nu\}$ $V_2^{\frac{4}{3}} \rightarrow j\mu$
$\tilde{R}_2$	$\tilde{R}_2^{-\frac{1}{3}} \rightarrow \{j\nu, b\nu\}$ $\tilde{R}_2^{\frac{2}{3}} \rightarrow j\mu$	$U_3$	$U_3^{-\frac{1}{3}} \rightarrow \{j\nu, b\nu\}$ $U_3^{\frac{2}{3}} \rightarrow \{j\mu, j\nu, t\nu\}$ $U_3^{\frac{5}{3}} \rightarrow \{j\mu, t\mu\}$
$S_3$	$S_3^{-\frac{2}{3}} \rightarrow \{j\mu, j\nu, b\nu, t\mu\}$ $S_3^{\frac{1}{3}} \rightarrow \{j\mu, j\nu, t\nu\}$ $S_3^{\frac{4}{3}} \rightarrow \{j\mu, j\nu, t\nu\}$		

**Table 6.5.:** Relevant decay channels for experimental searches. *Left:* Scalar LQs, *Right:* vector LQs. With  $j$  we denote jets possibly coming from all quarks but the top.

and therefore has the potential to explain the  $B \rightarrow K^{(*)}\ell^+\ell^-$  anomalies. As we shall see, although the constraints imposed in the last sections are already quite restraining there is still significant room for NP in scalar operators that is not probed by the above processes. Generally, there are not many observables that are sensitive to NP contributions to scalar operators. The most prominent one is the decay  $B_s \rightarrow \mu^+\mu^-$ . In the SM this is loop-, GIM- and helicity-suppressed making it a very rare decay. All three suppression mechanisms do not have to be at work for NP contributions and so large corrections could be generated. Furthermore, this decay is very clean theoretically as it does not suffer from any hadronic uncertainty except for the  $B_s$  decay constant which is determined from lattice QCD with an uncertainty of 2% (see e.g.

[286, 287]). Another observable sensitive to scalar NP is the “flat term”  $F_H$  in  $B \rightarrow K\mu^+\mu^-$ , but in accordance with [288] we find that this is not competitive with  $B_s \rightarrow \mu^+\mu^-$ .

In this section we will investigate the impact of the process  $B_s \rightarrow \mu^+\mu^-$  on LQ models and, in particular, highlight benefits of the mass-eigenstate rate asymmetry  $\mathcal{A}_{\Delta\Gamma}$  as it allows to lift degeneracies in the scalar couplings that cannot be resolved by a measurement of the branching ratio alone.

### Leptoquarks and scalar operators

As table 6.4 shows, there are only two LQ representations that can generate the scalar operators  $C_{S,P}^{(\prime)}$  at tree-level. These are the spin-1  $SU(2)_L$  singlet  $U_1$  and the spin-1  $SU(2)_L$  doublet  $V_2$ . It can be understood that these are the only possibilities by considering the interaction terms given in table 6.2. By their chiral structure scalar operators enforce that the LQ couples to four different fields, left- and right-handed leptons as well as left- and right-handed quarks. Therefore, scalar operators can only be generated if the LQ has left-handed  $\hat{\lambda}_L$  as well as right-handed couplings  $\hat{\lambda}_R$ . Due to their quantum numbers this is only allowed for the two vector LQs  $U_1$  and  $V_2$ .

An interesting question is whether scalar operators can be generated at the one-loop level via box diagrams. For LQ representations that only allow for one interaction term, box diagrams involving two LQs can only generate vector operators as only two different fields (modulo flavour indices) can appear as external states.<sup>8</sup> By a similar argument one sees that if a second interaction term exists which contains up-type quarks one cannot generate the correct semi-leptonic operators. To obtain the needed number of external fields one would have to include a  $W$  boson or Higgs in the loop, as these can change singlet to doublet or up-type to down-type. A  $W$  boson exchange necessarily leads to a neutrino inside the loop such that the needed helicity flip for a scalar operator cannot be generated. As a last possibility there are box diagrams involving one LQ and one Higgs exchange. These are, however, strongly suppressed by the small Yukawa couplings of the leptons. An explicit calculation shows that contributions are indeed numerically completely negligible. Hence, we conclude that the

<sup>8</sup>As an example consider the LQ  $\tilde{R}_2$  that couples  $d_R$  to  $\mu_L$ . The only semi-leptonic operator that can be written down is  $(\bar{d}_L\gamma^\mu d_L)(\bar{\mu}_L\gamma_\mu\mu_L)$  which due to its chiral structure has to have a vector interaction.

	$U_1$	$V_2$
$C_9^{\text{NP}}$	$-\frac{1}{2}\mathcal{N}\lambda_L^{s\mu}\lambda_L^{b\mu*}$	$\frac{1}{2}\mathcal{N}\lambda_L^{b\mu}\lambda_L^{s\mu*}$
$C_9'$	$-\frac{1}{2}\mathcal{N}\lambda_R^{s\mu}\lambda_R^{b\mu*}$	$\frac{1}{2}\mathcal{N}\lambda_R^{b\mu}\lambda_R^{s\mu*}$
$C_{10}^{\text{NP}}$	$\frac{1}{2}\mathcal{N}\lambda_L^{s\mu}\lambda_L^{b\mu*}$	$\frac{1}{2}\mathcal{N}\lambda_L^{b\mu}\lambda_L^{s\mu*}$
$C_{10}'$	$-\frac{1}{2}\mathcal{N}\lambda_R^{s\mu}\lambda_R^{b\mu*}$	$-\frac{1}{2}\mathcal{N}\lambda_R^{b\mu}\lambda_R^{s\mu*}$
$C_S = -C_P$	$\mathcal{N}\lambda_L^{s\mu}\lambda_R^{b\mu*}m_b^{-1}$	$\mathcal{N}\lambda_R^{b\mu}\lambda_L^{s\mu*}m_b^{-1}$
$C_S' = C_P'$	$\mathcal{N}\lambda_R^{s\mu}\lambda_L^{b\mu*}m_b^{-1}$	$\mathcal{N}\lambda_L^{b\mu}\lambda_R^{s\mu*}m_b^{-1}$

**Table 6.6.:** The  $bs\mu\mu$  Wilson coefficients in the two LQ models in terms of mass-basis couplings. The superscript “NP” denotes the new physics contribution. The normalization factor  $\mathcal{N}$  is defined in (6.7).

relevant scalar operators cannot be generated at one-loop level such that it suffices to consider only the cases  $U_1$  and  $V_2$ .

Using the SMEFT fixes correlations between the scalar operators of the form [289]<sup>9</sup>

$$C_S = -C_P, \quad \text{and} \quad C_S' = +C_P'. \quad (6.38)$$

Summarizing table 6.4, the results on the  $bs\mu\mu$  Wilson coefficients for the two relevant LQ representations are shown in table 6.6. An important result is that in both scenarios the Wilson coefficients are correlated via

$$m_b^2 C_S C_S' = -4 C_{10}^{\text{NP}} C_{10}' = -4 C_9^{\text{NP}} C_9'. \quad (6.39)$$

Fits to  $B \rightarrow K^{(*)}\mu^+\mu^-$  decays only constrain vector Wilson coefficients, i.e. effectively the products  $\lambda_L^{s\mu}\lambda_L^{b\mu*}$  and  $\lambda_R^{s\mu}\lambda_R^{b\mu*}$  whereas the ratios of these couplings are unconstrained. Then, one could for example consider a scenario in which the coupling  $\lambda_R^{b\mu}$  vanishes such that the left-handed couplings are chosen to fulfill the  $B \rightarrow K^{(*)}\mu^+\mu^-$  constraint and  $\lambda_R^{s\mu}$  effectively controls an arbitrary amount of NP in  $C_S = -C_P$ .

### The decay $B_s \rightarrow \mu^+\mu^-$

The rare decay  $B_s \rightarrow \mu^+\mu^-$  is a key observable for constraining scalar operators since contributions from vector NP are helicity suppressed. Another feature is the sizable width difference of the  $B_s$  system [149],

$$y_s = \frac{\Delta\Gamma_s}{2\Gamma_s} = 0.065 \pm 0.005, \quad (6.40)$$

which makes the effects of meson-antimeson mixing significant. Consequently, the time dependence of this decay becomes measurable allowing for a larger number of observables to disentangle NP contributions.

In this section we briefly review the observables accessible in the  $B_s \rightarrow \mu^+\mu^-$  decay. For a more detailed discussion we refer e.g. to [141, 290]. Since it cannot be expected to measure the helicity of the muons in the foreseeable future, one considers the helicity-averaged decay rate [290],

$$\begin{aligned} \Gamma(B_s(t) \rightarrow \mu^+\mu^-) &= \Gamma(B_s(t) \rightarrow \mu_L^+\mu_L^-) + \Gamma(B_s(t) \rightarrow \mu_R^+\mu_R^-) \\ &\propto \left[ \cosh\left(\frac{y_s t}{\tau_{B_s}}\right) + \mathcal{S}_{\mu\mu} \sin(\Delta M t) + \mathcal{A}_{\Delta\Gamma} \sinh\left(\frac{y_s t}{\tau_{B_s}}\right) \right] \times e^{-t/\tau_{B_s}}. \end{aligned} \quad (6.41)$$

Depending on whether a determination of the initial flavour of the  $B_s$  meson can be determined (tagged), one can then measure the *untagged* ( $CP$ -averaged) time-dependent rate

$$\Gamma(B_s(t) \rightarrow \mu^+\mu^-) + \Gamma(\bar{B}_s(t) \rightarrow \mu^+\mu^-) \propto \left[ \cosh\left(\frac{y_s t}{\tau_{B_s}}\right) + \mathcal{A}_{\Delta\Gamma} \sinh\left(\frac{y_s t}{\tau_{B_s}}\right) \right] \times e^{-t/\tau_{B_s}}, \quad (6.42)$$

<sup>9</sup>This can be understood in a simple way by the fact that all four operators are generated in the SMEFT by a single operators  $\mathcal{O}_{ledq} = (\bar{d}_R q_L)(\bar{l}_L \ell_R)$  which can have a flavour dependent Wilson coefficient.

or the  $CP$  asymmetry in the decay rate,

$$\frac{\Gamma(B_s(t) \rightarrow \mu^+\mu^-) - \Gamma(\bar{B}_s(t) \rightarrow \mu^+\mu^-)}{\Gamma(B_s(t) \rightarrow \mu^+\mu^-) + \Gamma(\bar{B}_s(t) \rightarrow \mu^+\mu^-)} = \frac{\mathcal{S}_{\mu\mu} \sin(\Delta Mt)}{\cosh\left(\frac{y_s t}{\tau_{B_s}}\right) + \mathcal{A}_{\Delta\Gamma} \sinh\left(\frac{y_s t}{\tau_{B_s}}\right)}. \quad (6.43)$$

Since the width difference in the  $B_s$  system is sizable the decay is characterized by three observables:

- The mass-eigenstate rate asymmetry

$$\mathcal{A}_{\Delta\Gamma} = \frac{\Gamma(B_s^H \rightarrow \mu^+\mu^-) - \Gamma(B_s^L \rightarrow \mu^+\mu^-)}{\Gamma(B_s^H \rightarrow \mu^+\mu^-) + \Gamma(B_s^L \rightarrow \mu^+\mu^-)}, \quad (6.44)$$

where  $B_s^H$  and  $B_s^L$  denote the heavy and light mass eigenstates of the  $B_s$  system. This asymmetry can be extracted from the untagged rate and it is of primary interest in the following. For poor statistics, an experimental extraction of this observable is easier via an *effective lifetime* [161],

$$\tau_{\mu\mu} = \frac{\int_0^\infty dt t \langle \Gamma(B_s(t) \rightarrow \mu^+\mu^-) \rangle}{\int_0^\infty dt \langle \Gamma(B_s(t) \rightarrow \mu^+\mu^-) \rangle}, \quad (6.45)$$

where  $\langle \Gamma(B_s(t) \rightarrow \mu^+\mu^-) \rangle = \Gamma(B_s(t) \rightarrow \mu^+\mu^-) + \Gamma(\bar{B}_s(t) \rightarrow \mu^+\mu^-)$  is the untagged rate. The effective lifetime is connected to  $\mathcal{A}_{\Delta\Gamma}$  via

$$\mathcal{A}_{\Delta\Gamma} = \frac{1}{y_s} \frac{(1 - y_s^2)\tau_{\mu\mu} - (1 + y_s^2)\tau_{B_s}}{2\tau_{B_s} - (1 - y_s^2)\tau_{\mu\mu}}. \quad (6.46)$$

The SM predictions for these observables are:

$$\mathcal{A}_{\Delta\Gamma}^{\text{SM}} = +1, \quad \tau_{\mu\mu}^{\text{SM}} = \frac{1}{1 - y_s} \tau_{B_s} = (1.615 \pm 0.010) \text{ ps}. \quad (6.47)$$

In general,  $\mathcal{A}_{\Delta\Gamma}$  can take values only between  $-1$  and  $+1$ .

- The time-integrated (and  $CP$ -averaged) branching ratio  $\overline{\text{Br}}(B_s \rightarrow \mu^+\mu^-)$ . It is related to the “prompt” branching ratio, i.e. the branching ratio in the absence of  $B_s$ - $\bar{B}_s$  mixing, as [161]

$$\begin{aligned} \overline{\text{Br}}(B_s \rightarrow \mu^+\mu^-) &= \frac{1}{2} \int_0^\infty dt \langle \Gamma(B_s(t) \rightarrow \mu^+\mu^-) \rangle \\ &= \frac{1 + \mathcal{A}_{\Delta\Gamma} y_s}{1 - y_s^2} \text{Br}(B_s \rightarrow \mu^+\mu^-)_{\text{prompt}}. \end{aligned} \quad (6.48)$$

The SM expectation can be obtained from **flavio** [147] and is

$$\overline{\text{Br}}(B_s \rightarrow \mu^+\mu^-)_{\text{SM}} = (3.60 \pm 0.18) \times 10^{-9}. \quad (6.49)$$

- The mixing-induced  $CP$  asymmetry  $\mathcal{S}_{\mu\mu}$ . The measurement of  $\mathcal{S}_{\mu\mu}$  requires flavour tagging, therefore large amounts of data are needed such that small tagging efficiencies at LHC can be overcome. In the SM one has  $\mathcal{S}_{\mu\mu}^{\text{SM}} = 0$ . We will not consider  $\mathcal{S}_{\mu\mu}$  in the following.

The NP contributions to this decay are described by the weak Hamiltonian (3.61) where the only relevant operators are  $\mathcal{O}_{10}^{(i)}$ ,  $\mathcal{O}_S^{(i)}$  and  $\mathcal{O}_P^{(i)}$ . In the absence of scalar NP this decay is only sensitive to the difference  $C_{10} - C'_{10}$ . The prompt branching ratio (as used in (6.48)) and  $\mathcal{A}_{\Delta\Gamma}$  are given in terms of the Wilson coefficients as

$$\text{BR}(B_s \rightarrow \mu^+\mu^-)_{\text{prompt}} = \frac{G_F^2 \alpha^2}{16\pi^3} |V_{ts} V_{tb}^*|^2 f_{B_s}^2 \tau_{B_s} m_{B_s} m_\mu^2 \sqrt{1 - 4 \frac{m_\mu^2}{m_{B_s}^2}} |C_{10}^{\text{SM}}|^2 (|P|^2 + |S|^2), \quad (6.50a)$$

$$\mathcal{A}_{\Delta\Gamma} = \frac{|P|^2 \cos(2\phi_P - \phi_s^{\text{NP}}) - |S|^2 \cos(2\phi_S - \phi_s^{\text{NP}})}{|P|^2 + |S|^2}, \quad (6.50b)$$



where the Wilson coefficients appear through the combinations

$$P = \frac{C_{10} - C'_{10}}{C_{10}^{\text{SM}}} + \frac{M_{B_s}^2}{2m_\mu} \frac{m_b}{m_b + m_s} \left( \frac{C_P - C'_P}{C_{10}^{\text{SM}}} \right), \quad S = \sqrt{1 - 4 \frac{m_\mu^2}{M_{B_s}^2} \frac{M_{B_s}^2}{2m_\mu} \frac{m_b}{m_b + m_s} \left( \frac{C_S - C'_S}{C_{10}^{\text{SM}}} \right)}, \quad (6.51)$$

with  $S = |S| \exp(i\phi_S)$ ,  $P = |P| \exp(i\phi_P)$ , and  $\phi_s^{\text{NP}}$  is a NP contribution to the  $B_s^0 - \bar{B}_s^0$  mixing phase which is strongly constrained (see eq. (3.56b)). In the SM one has  $S = 0$  and  $P = 1$ . Eq. (6.50a) shows the helicity suppression of the branching ratio by the fact that it is proportional to the square of the small muon mass. For the scalar operators this is again canceled in eq. (6.51), such that the bounds on the scalar operators will effectively be much stronger than for the vector operators.

First experimental evidence for  $B_s \rightarrow \mu^+ \mu^-$  has been found by the LHCb [291] and CMS [269] experiments individually in 2013, who subsequently combined their measurements of  $B_s \rightarrow \mu^+ \mu^-$  and their searches for  $B^0 \rightarrow \mu^+ \mu^-$  from LHC Run 1 data [164]. Recently, the LHCb collaboration presented a measurement including Run 2 data [270], which is the first single-experiment observation of the decay. For  $B_s \rightarrow \mu^+ \mu^-$ , the results of the two experiments have recently been combined yielding [2]

$$\overline{\text{Br}}(B_s \rightarrow \mu^+ \mu^-)_{\text{CMS+LHCb 2017}} = (3.00_{-0.54}^{+0.55}) \times 10^{-9}, \quad (6.52)$$

which is in reasonable agreement with the SM expectation (6.49). In the same measurement the LHCb collaboration presented a first measurement of the effective lifetime [270], albeit still with sizable uncertainties,

$$\tau_{\mu\mu}^{\text{LHCb}} = (2.04 \pm 0.44) \text{ ps}. \quad (6.53)$$

A naive use of (6.46) allows to estimate  $\mathcal{A}_{\Delta\Gamma}^{\text{LHCb}} = 8_{-7}^{+19}$  which is still far outside the physical range  $-1 \leq \mathcal{A}_{\Delta\Gamma} \leq +1$ , but is compatible with the  $\mathcal{A}_{\Delta\Gamma} = +1$  or  $\mathcal{A}_{\Delta\Gamma} = -1$  hypothesis at the  $1.0\sigma$  or  $1.4\sigma$  level, respectively.

At the moment the experimental uncertainty on the  $B_s \rightarrow \mu^+ \mu^-$  branching ratio is dominated by statistics and therefore can improve substantially with more data. For LHC Run 4 the LHCb collaboration expects to accumulate an integrated luminosity of  $50 \text{ fb}^{-1}$ . For this amount of data a statistical precision of  $0.19 \times 10^{-9}$  on the branching ratio is expected [292]. After a high-luminosity phase at LHC Run 5, LHCb would be able to collect an integrated luminosity of  $300 \text{ fb}^{-1}$ . Naive scaling then suggests a statistical uncertainty of  $0.08 \times 10^{-9}$ , which means a 2% uncertainty on the SM central value. At CMS it is expected to collect an integrated luminosity of  $3000 \text{ fb}^{-1}$  in the same time, corresponding to a precision of  $0.4 \times 10^{-9}$  [293]. To estimate the sensitivity for  $\mathcal{A}_{\Delta\Gamma}$  we assume comparable uncertainties for the time-dependent decay rate, such that a 5% (2%) uncertainty translates into an error of  $\pm 0.8$  ( $\pm 0.3$ ) on  $\mathcal{A}_{\Delta\Gamma}$  for Run 4 (Run 5). Therefore, we will consider the following scenarios

$$\sigma_{\text{exp}}(B_s \rightarrow \mu^+ \mu^-) = 0.19, \quad \sigma_{\text{exp}}(\mathcal{A}_{\Delta\Gamma}) = 0.8, \quad \text{for } 50 \text{ fb}^{-1} \quad (\text{“Run 4”}), \quad (6.54a)$$

$$\sigma_{\text{exp}}(B_s \rightarrow \mu^+ \mu^-) = 0.08, \quad \sigma_{\text{exp}}(\mathcal{A}_{\Delta\Gamma}) = 0.3, \quad \text{for } 300 \text{ fb}^{-1} \quad (\text{“Run 5”}). \quad (6.54b)$$

In figure 6.6 we show the current constraints on the scalar operators imposed by  $B_s \rightarrow \mu^+ \mu^-$  observables. The measurement of the branching ratio (6.52) is shown by the red ring. This demonstrates that there is a degeneracy, the position on the ring, that cannot be resolved no matter to what accuracy the branching ratio will be measured. This stays true even if  $C_S = 0$  or  $C'_S = 0$ , such that in these cases there are always two solutions that cannot be discriminated by a measurement of the branching ratio alone. As the color shading in the same figure suggests these degeneracies can be lifted by a measurement of  $\mathcal{A}_{\Delta\Gamma}$ . In the following we will illustrate in detail the potential of  $\mathcal{A}_{\Delta\Gamma}$  in discriminating degenerate solutions in scalar operators.

### Leptoquarks and $B_s \rightarrow \mu^+ \mu^-$

The LQ scenario  $U_1$  can explain present anomalies in semi-leptonic  $b \rightarrow s \mu \mu$  transitions [247] if  $C_9^{\text{NP}} = -C_{10}^{\text{NP}} \approx -0.61$  and  $C'_9 = C'_{10} \approx 0$  [1]. In the following we will focus on this case. We fix the left-handed couplings such that  $C_9^{\text{NP}}$  and  $C_{10}^{\text{NP}}$  take the above value and keep the right-handed

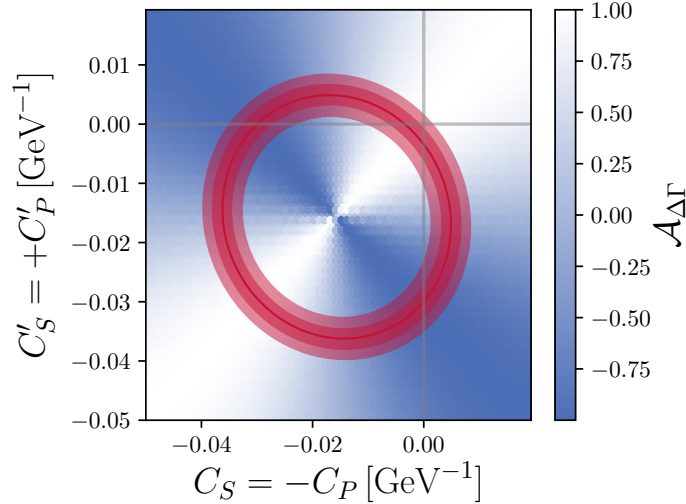


**Figure 6.6.:** Constraints on scalar operators from  $B_s \rightarrow \mu^+ \mu^-$  measurements. In red  $1\sigma$  and  $2\sigma$  contours are shown that mark the constraints coming from the measurement of the branching ratio. The green color shading specifies the values of  $\mathcal{A}_{\Delta\Gamma}$ , where white corresponds to a SM-like value. Due to SM gauge invariance the Wilson coefficients are correlated via  $C_S = -C_P$  and  $C'_S = +C'_P$  (see eq.(6.38)).

couplings as free parameters. By (6.39) we are then forced to set either the unprimed or primed scalar operator to zero. We consider the following benchmark scenario:<sup>10</sup>

$$U_1 : \quad \lambda_L^{s\mu} = \lambda_L^{b\mu} = +\sqrt{\frac{-\frac{1}{2} \times (-0.61)}{\mathcal{N}(m_{\text{LQ}})}}, \quad \lambda_R^{s\mu} = 0, \quad \lambda_R^{b\mu} \text{ free}, \quad (6.55)$$

which results in  $C_9^{\text{NP}} = -C_{10}^{\text{NP}} = -0.61$ ,  $C'_9 = C'_{10} = 0$ ,  $C_S = -C_P$  (free),  $C'_S = C'_P = 0$ .

The LQ  $V_2$  predicts  $C_9^{\text{NP}} = +C_{10}^{\text{NP}}$  and therefore cannot explain the  $b \rightarrow s\mu\mu$  anomalies. We assume degenerate masses for the two components with charges  $\frac{1}{4}$  and  $\frac{2}{3}$ , and consider the following scenario:

$$V_2 : \quad \lambda_L^{s\mu} = \lambda_L^{b\mu} = \sqrt{\frac{2 \times 0.1}{\mathcal{N}(m_{\text{LQ}})}}, \quad \lambda_R^{s\mu} = 0, \quad \lambda_R^{b\mu} \text{ free}. \quad (6.56)$$

This setup corresponds to a rather small value of  $C_9^{\text{NP}} = +C_{10} = 0.1$ , vanishing primed Wilson coefficients, and free  $C_S = -C_P$ .

In figure 6.7 we show the presently allowed parameter regions for both scenarios in the mass-coupling plane. In the parameter space still allowed by experimental searches, one finds two solutions that reproduce the current measurement of the branching ratio. One is SM-like while the other corresponds to large NP effects.

Projecting into the future, a measurement of  $\mathcal{A}_{\Delta\Gamma}$  will be able to disentangle this situation. We find that the NP solution gives rise to a large negative  $\mathcal{A}_{\Delta\Gamma}$ , such that already an estimation of its sign can rule out this scenario. In figure 6.8 we present future projections for the mass vs. coupling plane. We consider run 4 and run 5 of the LHC. We estimate the direct constraints by rescaling the present exclusion limits by the square root of the luminosity ratio,  $\sqrt{\mathcal{L}_{\text{today}}/\mathcal{L}_{\text{future}}}$ , where  $\mathcal{L}_{\text{future}} = 300 \text{ fb}^{-1}$ ,  $3000 \text{ fb}^{-1}$  for Run 4 and Run 5, respectively. In high mass ranges, for which presently there are no direct constraints, we conservatively extrapolate the current exclusion limits as constants. For the branching ratio we assume the current SM value (6.49) with uncertainties (6.54). These projections clearly show the power of an  $\mathcal{A}_{\Delta\Gamma}$  measurement in eliminating a degenerate solution as well as the general impact of  $B_s \rightarrow \mu^+ \mu^-$  on the LQ parameter space.

In figure 6.8 one further sees the complementarity of indirect constraints and bounds obtained from direct searches for these states at hadron colliders. Direct searches put a lower bound on LQ masses

<sup>10</sup>Note that the requirement of  $C_9^{\text{NP}} = -C_{10}^{\text{NP}} = -0.61$  does not uniquely determine the values of the left-handed couplings. Only the product of  $\lambda_L^{s\mu}$  and  $\lambda_L^{b\mu}$  is fixed, but not their ratio. We assume that both are of the same order.

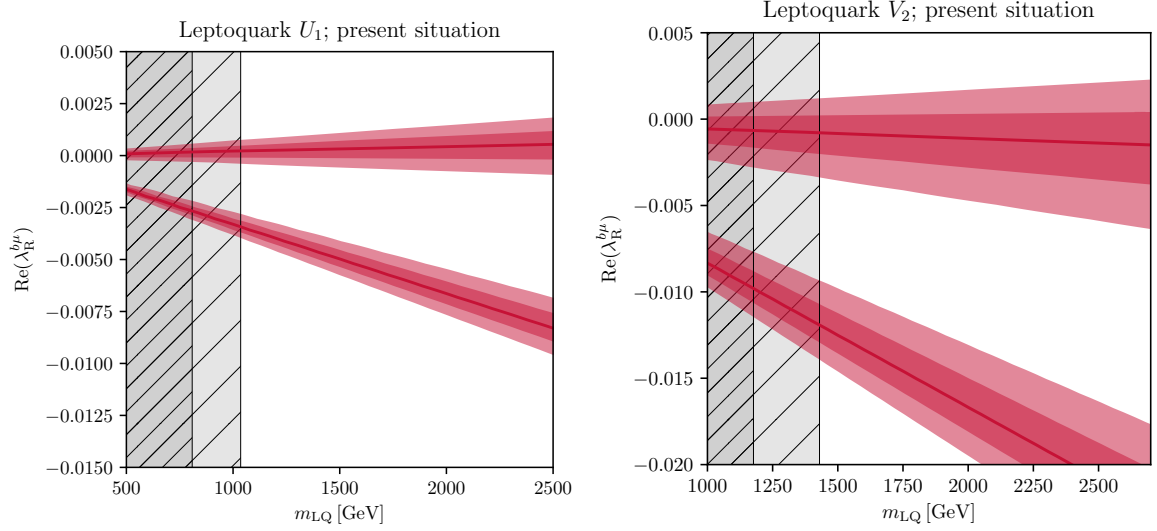


**Figure 6.7.:** The currently allowed parameter regions in the mass vs. coupling plane for the LQs  $U_1$  (left) and  $V_2$  (right) in the scenarios (6.55) and (6.56). Inside the dark and light green bands, the present value of the experimental branching ratio (6.52) is reproduced at  $1$  and  $2\sigma$ , respectively. The black //hatched regions show the exclusions from present direct searches. The more densely hatched region corresponds to minimal LQ production, while the more coarsely hatched region is for YM-like production.

but cannot put significant limits on LQ couplings. Indirect observables like  $\mathcal{A}_{\Delta F}$  are sensitive to the ratio of LQ couplings and masses. For the above scenarios we find that currently the direct bounds on LQ masses are in the region of 1 TeV for  $U_1$  and 1.3 TeV for  $V_2$ . If no signal will be found, these can go up to around 1.5 TeV for  $U_1$  and 1.8 TeV for  $V_2$  after LHC Run 5. This still leaves much room for NP.

Using the results of table 6.4 it is possible to give correlations between the decays  $B_s \rightarrow \mu^+\mu^-$  and  $B \rightarrow K^{(*)}\bar{\nu}\nu$  which are shown in figure 6.9. For the triplet LQs  $U_3$  and  $S_3$  one generally finds  $\mathcal{R}_K = \mathcal{R}_{K^*}$  such that the correlations of  $B_s \rightarrow \mu^+\mu^-$  with  $B \rightarrow K\bar{\nu}\nu$  and  $B \rightarrow K^*\bar{\nu}\nu$  are identical and one expects an enhancement of  $\mathcal{R}_K = \mathcal{R}_{K^*}$  while there is a slight suppression of the  $B_s \rightarrow \mu^+\mu^-$  rate. For the LQ  $\tilde{R}_2$  we find that  $B_s \rightarrow \mu^+\mu^-$  is correlated positively with  $B \rightarrow K\bar{\nu}\nu$  but negatively with  $B \rightarrow K^*\bar{\nu}\nu$ . However, we also expect these effects to be too small to be detectable. In the case of the LQ representation  $V_2$  we observe that  $B_s \rightarrow \mu^+\mu^-$  is correlated to the  $b \rightarrow s\nu\nu$  transition via  $m_{\frac{2}{3}}^2 C_R = m_{\frac{2}{3}}^2 C'_9 = -m_{\frac{2}{3}}^2 C'_{10}$ . As NP contributions to  $C'_9 = -C'_{10}$  are strongly constrained, one cannot expect large contributions to  $B \rightarrow K^{(*)}\nu\nu$ . Taking a benchmark value of  $C'_9 = -C'_{10} = 0.25$  (which corresponds to the maximally allowed value at the  $2\sigma$ -level found in [1]) and assuming degenerate masses for the two LQ components, we only find a modification of about 2% relative to the SM expectation. This, however, is only true if the LQ solely couples to muons. If couplings to other lepton generations are allowed, then the effects can be much larger.

## 6.6. Summary

In this chapter we investigated the impact of recent measurements of  $b \rightarrow s\ell^+\ell^-$  decays on parameter spaces of LQ models. We make the following observations:

- For all LQ scenarios there are tight correlations between the generated semi-leptonic four-fermion operators as shown in table 6.4. The LQ representations  $S_3$ ,  $U_1$  and  $U_3$  generate  $C_9^{\text{NP}} = -C_{10}^{\text{NP}}$  which is the favored option for explaining the  $b \rightarrow s\mu^+\mu^-$  anomalies. Possible hints for LFNU as measured through  $R_K$  can also be explained if the LQs dominantly couple to second generation leptons.
- SM gauge invariance can be used to correlate  $b \rightarrow s\mu^+\mu^-$  and  $b \rightarrow s\bar{\nu}\nu$  transitions. Generally, we predict modifications of  $b \rightarrow s\bar{\nu}\nu$  observables of a size that is unfortunately within the expected

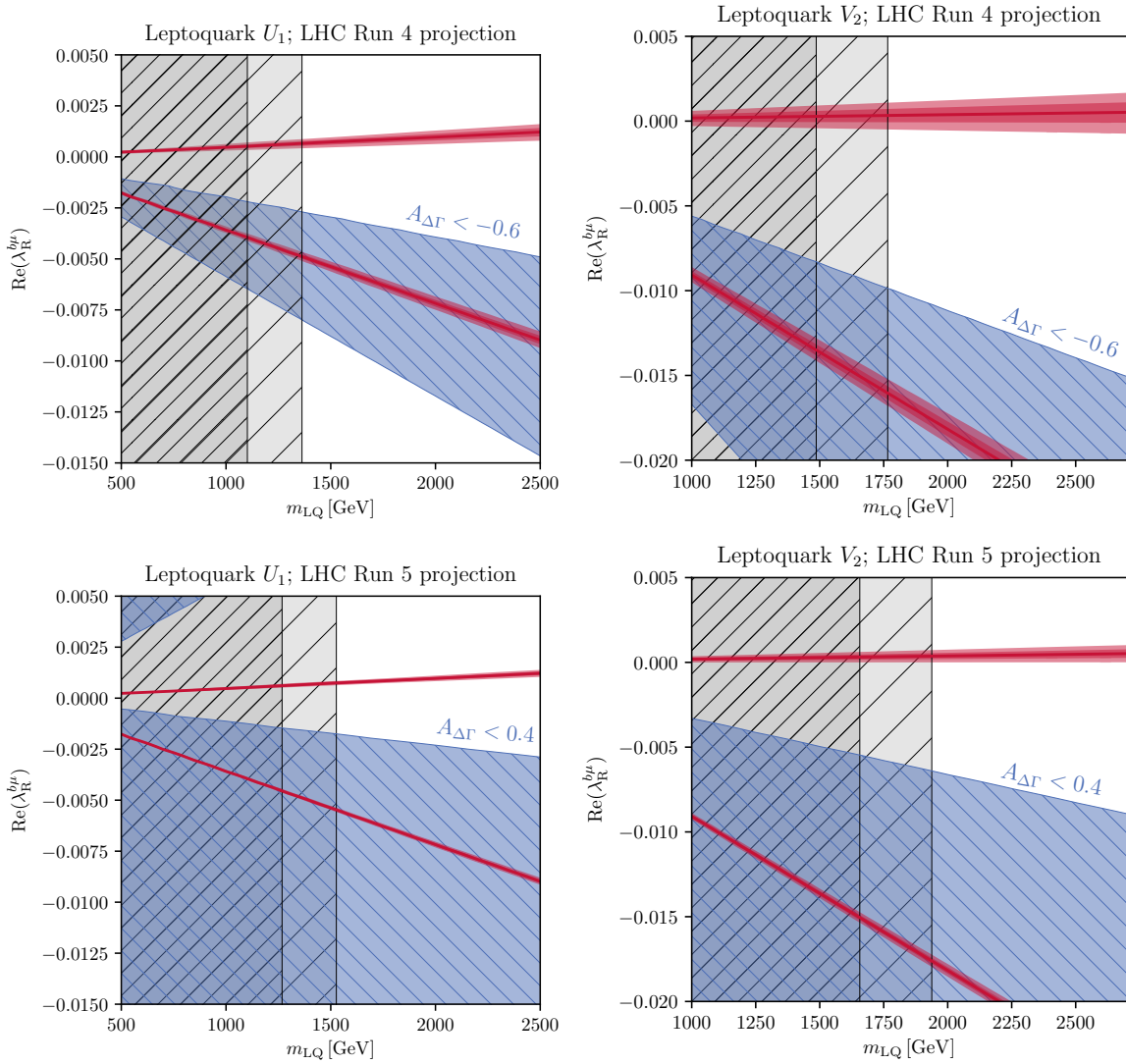


**Figure 6.8.:** Future constraints in the mass vs. coupling planes for the LQs  $U_1$  (left) and  $V_2$  (right) in the scenarios (6.55) and (6.56). The first row is for the “Run 4” scenario while the second row marks “Run 5”. The green  $1\sigma$ - and  $2\sigma$ -regions correspond to the anticipated future experimental sensitivity of the branching ratio, assuming the SM central value (6.49). The black // -hatched regions show the extrapolated exclusions from direct searches. The more densely hatched region corresponds to minimal LQ production, while the more coarsely hatched region is for YM-like production. The blue \\\ -hatched region would be excluded at the  $2\sigma$  level by a measurement of  $\mathcal{A}_{\Delta\Gamma}$  with SM-like central value.

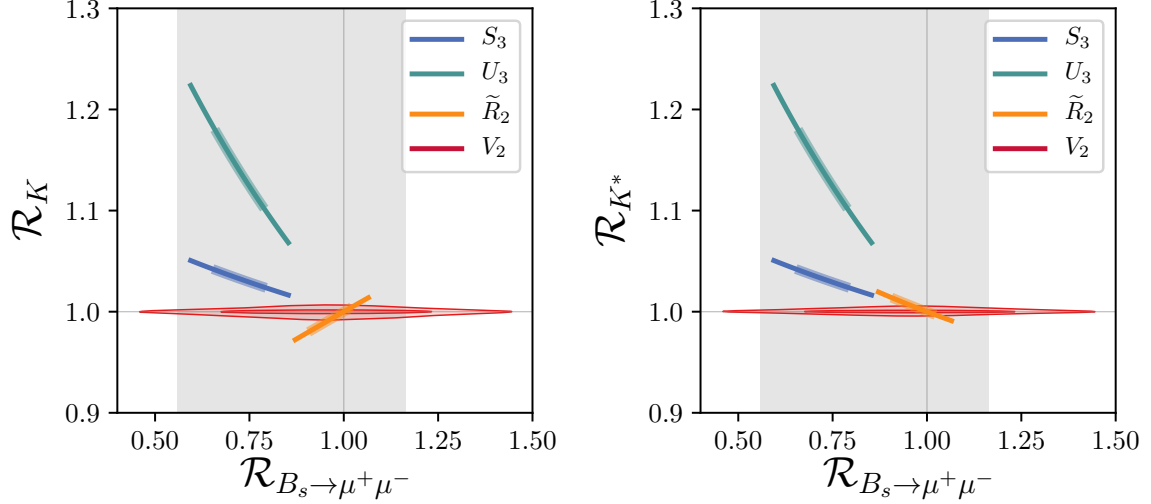
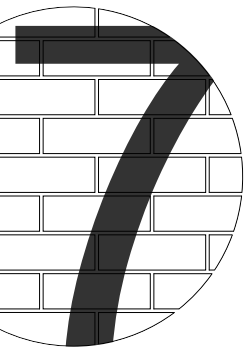


**Figure 6.9.:** Correlations between  $B_s \rightarrow \mu^+\mu^-$  and  $B \rightarrow K^{(*)}\bar{\nu}\nu$ . *Left:*  $B_s \rightarrow \mu^+\mu^-$  vs.  $B \rightarrow K\bar{\nu}\nu$ . *Right:*  $B_s \rightarrow \mu^+\mu^-$  vs.  $B \rightarrow K^*\bar{\nu}\nu$ . The  $1\sigma$  (transparent thick lines) and  $2\sigma$  ranges are shown.

future experimental uncertainty for these decays. Only the LQ  $U_3$  can possibly give a measurable effect.

- Currently, LFV in  $b \rightarrow s\ell\ell'$  transitions is only weakly constrained. In the LQ case it is possible to bound the LFV decays with lepton flavour conserving ones.
- If the LQs couple to  $\tau$ 's then the experimental bounds are very weak such that large effects in  $B \rightarrow K^{(*)}\bar{\nu}\nu$  are possible.
- Direct constraints on LQs vary strongly between the different representations. We find particularly strong bounds for vector LQs. The scalar LQ  $S_3$  is however only weakly constrained by direct searches at the moment.
- The LQs  $U_1$  and  $V_2$  generate scalar Wilson coefficients. These can be constrained by the decay  $B_s \rightarrow \mu^+\mu^-$ , but a measurement of the branching ratio alone cannot lift all degeneracies in the LQ couplings. The observable  $\mathcal{A}_{\Delta\Gamma}$  however is a powerful tool for eliminating degenerate solutions.





## Conclusion

Although the SM is extremely successful in describing the physics at energies as high as the ones at the LHC there is good reason to believe that it is not the end of the story. Lacking concrete experimental evidence for physics beyond the SM, the strongest motivations are theory-driven and regard the origin of EWSB and flavour and the stability of the electroweak scale. In particular the last point has pushed model building for the last decades. In recent years, experiments observed hints for possible NP connected with semi-leptonic  $b \rightarrow s$  transitions. In the light of this, many simplified models have been proposed that try to explain the experimental anomalies by supplementing the SM only by minimal amounts of NP. We have presented both approaches in this thesis considering CHMs and LQs.

The electroweak scale can be stabilized if there are new strong interactions such that this scale is generated as a result of dimensional transmutation. A successful framework for this idea are models in which the Higgs boson appears as a composite bound state. The relative lightness of the Higgs can further be introduced in a natural way if the NP sector connected with the new strong interactions is subject to a global symmetry breaking from which the Higgs emerges as a NGB. By interactions with the SM-like elementary sector these global symmetries can be broken explicitly, such that the Higgs actually only is an approximate NGB that can obtain a mass dynamically via the Coleman-Weinberg mechanism.

If there is a new strong interaction then one also expects that there are heavy composite resonances at energies accessible at collider experiments. A phenomenologically successful framework for the interaction of these resonances with elementary fields is given by partial compositeness. In this one assumes linear mixings between composite and elementary fields such that SM fields, which are identified with the lightest linear combinations, necessarily have a composite admixture. These mixings also generate a potential for the NGBs at the loop level which, in turn, induces EWSB.

Demanding phenomenological success of such a model puts restrictions on model-building. To protect EWPOs one introduces a custodial symmetry such that the minimal coset allowing for an  $SU(2)_L$  doublet Higgs is given by  $SO(5)/SO(4)$ . A protection of  $Zbb$  couplings can be achieved by choosing certain representations of the composite fermion resonances under the global symmetries. For the above coset the minimal choice for the representations is the fundamental  $\mathbf{5}$ . Generally, as we are working with non-renormalizable effective theories, the calculability of the Higgs potential may not be given. To ensure this we are working with theories deconstructed from gauge theories on extra-dimensional spacetimes. As a last ingredient we include the full flavour structure into the model where we assume that the composite sector is invariant either under  $U(3)$  or  $U(2)$  flavour symmetries that are slightly broken by the interactions with elementary fields to generate the flavour structure of the SM.

We perform a dedicated numerical analysis of CHMs taking into account a large number of experimental constraints to have control over the global parameter space. In particular, we demand compatibility with precision measurements of EWPOs and the  $Z$  width; we include Higgs physics,  $CP$  violation showing up through the neutron EDM and contact interactions of light quarks. In the flavour sector we include experimental results on meson-antimeson mixing and rare  $B$  decays. We include direct searches for heavy resonances at hadron colliders, although these are not discussed in detail in this work (we rather refer to [28]). The last and crucial constraint that we include is a realistic EWSB through the Coleman-Weinberg effective potential that reproduces the correct Higgs mass

and vev. This allows us for the first time to perform a global analysis of CHMs including all relevant constraints at the same time while satisfying the correlations induced by the potential. Due to partial compositeness and the large dimensionality of the problem we were forced to implement elaborate numerical methods based on Markov Chain Monte Carlos on a high-performance computational cluster to sample the parameter spaces of the models.

The flavour structure as well as the effective Higgs potential are induced by the interactions of the composite and elementary sectors. Therefore, it is an interesting question whether this leads to non-trivial correlations between both phenomena. As estimated through a spurion analysis and verified in the numerical analysis, we do not find an obvious correlation between EWSB and flavour transitions in these models. However, we are able to exclude an  $U(3)_{LC}$  flavour structure since it is in conflict with CKM unitarity due to the large degree of compositeness of left-handed light quarks.

As expected we find that the main source of tuning in these models stems from the fact that a part of the elementary sector (the top quark) should be made heavy while a field of the composite sector (the Higgs) has to be made relatively light. Generally, we find that a fine-tuning better than the percent level is achievable for symmetry breaking scales  $f$  roughly below the TeV range. This shows that in the light of the current experimental status the main motivation for this model, giving a solution for the fine-tuning problem, is still a reasonable one, although there is increasing tension with naturalness if no resonances will be found.

Enlarging the minimal coset to the next-to-minimal one  $SO(6)/SO(5)$  introduces many new and interesting features. Most importantly a new pseudoscalar pNGB  $\eta$  appears. Because of this the effective potential becomes two-dimensional and a vev for  $\eta$  can be generated. This gives new contributions to EWSB such that, in particular, the vev of the doublet pNGB does not have to be small anymore. We find a slightly improved but overall similar picture regarding the fine-tuning in this model. The model based on the next-to-minimal coset gives rise to a limit in which it gets indistinguishable from the minimal model, but away from this limit there are new features can arise. In particular, the vev of  $\eta$  acts as a source of spontaneous  $CP$  violation. Therefore, large effects in neutron EDMs are generated which can be a clear discriminator between the two models. The vev also leads to a mixing between  $\eta$  and the Higgs which induces modifications of Higgs couplings. Flavour transitions, however, are in any case similar to the minimal case which confirms the small impact of the potential on these observables.

In recent years LQs have gained increasing theoretical interest as in these models one can give a simple solution to the anomalies observed in  $b \rightarrow s\ell^+\ell^-$  decays. Although LQs are a phenomenon appearing in many models we take a more general approach and consider simplified models in which the LQ is the only new field that is added to the SM. In this work we assume the standpoint that the  $b \rightarrow s\ell^+\ell^-$  anomalies are in fact due to NP neglecting the possibility of a hadronic effect. Under this assumption we investigated the impact on the related decays  $B \rightarrow K^{(*)}\bar{\nu}\nu$  and  $B_s \rightarrow \mu^+\mu^-$ . It is then interesting to see whether one can distinguish between different LQ scenarios (that allow for an explanation of the  $b \rightarrow s\ell^+\ell^-$  anomalies) using these related decays.

Assuming  $G_{SM}$  invariance of possible LQ contributions we find tight correlations between the dimuon and dineutrino mode leading to rather strong bounds. Although, given the  $b \rightarrow s\mu^+\mu^-$  anomalies, we find different predicted values for the different LQ representations, the estimated experimental uncertainty might not be enough to discriminate between the models using the dineutrino mode. If the LQs couple to first or third generation leptons then the bounds are significantly looser. Especially in the case of couplings to taus large effects are possible.

The rare decay  $B_s \rightarrow \mu^+\mu^-$  is sensitive to scalar operators which are generated by two vector LQ representations. We highlighted the particular benefit of the observable  $\mathcal{A}_{\Delta\Gamma}$  that in the not-too-far future will be measured to a good accuracy and will allow to lift degeneracies in the determination of Wilson coefficients that will not be resolvable by a measurement of the branching ratio alone.

Assuming the scenarios preferred by the  $b \rightarrow s\ell^+\ell^-$  anomalies we analyzed to current bounds given by direct searches for LQs. In general, these bounds strongly depend on the considered LQ scenario and on the values of the couplings. For certain scenarios (including one that allows to explain the  $b \rightarrow s\ell^+\ell^-$  anomalies) we find that small LQ masses as low as 500 GeV are still allowed.

An interplay between theory and experiment is crucial for the search of NP. Without a clear signal for a concrete NP scenario precise experimental measurements are essential for evaluating the still allowed



---

parameter spaces of hypothetical models. Even if at some point there will be a signal, investigating correlations between different experimental modes will be indispensable for differentiating between models. With the coming runs of the LHC and the upcoming Belle II experiment the future looks promising in that perspective.



# Appendix



# Appendix I

## Group theory

In this chapter we summarize results on the group theory of the groups SO(5) and SO(6) which are relevant for the analyses performed in chapters 4 and 5, respectively.

### I.1. SO(5)

#### Generators

The group SO(5) has  $\frac{1}{2} \cdot 5 \cdot (5 - 1) = 10$  generators. Of these, six can be associated to the subgroup SO(4) while the remaining 4 belong to the coset SO(5)/SO(4). For our purposes it is helpful to choose a basis for the generators in which the embedding of the subgroup SO(4) becomes transparent. As the group SO(4) is isomorphic to  $SU(2)_L \times SU(2)_R$  the basis of generators can be chosen in such a way that it decomposes into the generators of these two groups. We use the basis

$$\text{SO(5)} : \quad T^A = \left( \underbrace{T_L^a, T_R^a}_{\text{SO(4)}}, \underbrace{T_{(2,2)}^{\hat{a}}}_{\text{coset}} \right), \quad (\text{I.1})$$

where the generators take the explicit forms [60]

$$[T_L^a]_{ij} = -\frac{i}{2} \left( \frac{1}{2} \epsilon^{abc} (\delta_i^b \delta_j^c - \delta_j^b \delta_i^c) + (\delta_i^a \delta_j^4 - \delta_j^a \delta_i^4) \right), \quad (\text{I.2a})$$

$$[T_R^a]_{ij} = -\frac{i}{2} \left( \frac{1}{2} \epsilon^{abc} (\delta_i^b \delta_j^c - \delta_j^b \delta_i^c) - (\delta_i^a \delta_j^4 - \delta_j^a \delta_i^4) \right), \quad (\text{I.2b})$$

$$[T_{(2,2)}^{\hat{a}}]_{ij} = -\frac{i}{\sqrt{2}} (\delta_i^{\hat{a}} \delta_j^5 - \delta_j^{\hat{a}} \delta_i^5). \quad (\text{I.2c})$$

#### Fundamental representation

Relevant for this work is the **5**-dimensional fundamental representation. Under the SO(4) subgroup this decomposes as  $\mathbf{5} = \mathbf{4} \oplus \mathbf{1} = (\mathbf{2}, \mathbf{2}) \oplus (\mathbf{1}, \mathbf{1})$ , where in the last step we used the  $SU(2)_L \times SU(2)_R$  language. This means that the fundamental decomposes into a bidoublet and a singlet,

$$\mathbf{5} = \left( \begin{array}{c} \left[ \begin{array}{cc} Q^{++} & Q^{+-} \\ Q^{-+} & Q^{--} \end{array} \right] \\ S^{0,0} \end{array} \right), \quad (\text{I.3})$$

where the indices denote the quantum numbers under  $\hat{T}_L^3$  and  $\hat{T}_R^3$ .

We now want to embed the bidoublet into the fundamental **5**; this means we want to parametrize the fundamental **5** through components with defined  $T_L^3$  and  $T_R^3$  quantum numbers. For this we note that the coset operators form a bidoublet such that we can write

$$Q = Q^{\hat{a}} T_{(2,2)}^{\hat{a}} = Q^{++} T^{++} + Q^{+-} T^{+-} + Q^{-+} T^{-+} + Q^{--} T^{--}, \quad (\text{I.4})$$

where in the last step we introduced a basis of generators that have defined  $\hat{\mathbb{T}}_L^3$  and  $\hat{\mathbb{T}}_R^3$  quantum numbers. This means we have to find a mapping between the generators on the LHS and the RHS of the above equation. For this we note that, as generators are in the adjoint representation of the group, the operators  $\hat{\mathbb{T}}_L^3$  and  $\hat{\mathbb{T}}_R^3$  act on them via the commutator

$$\hat{\mathbb{T}}_{L,R}^3 \mathbb{T} := [\mathbb{T}_{L,R}^3, \mathbb{T}] = \mathbb{T}_{L,R}^3 \mathbb{T} - \mathbb{T} \mathbb{T}_{L,R}^3, \quad (\text{I.5})$$

such that the generators on the RHS of (I.4) are defined via

$$\hat{\mathbb{T}}_L^3 \mathbb{T}^{\pm X} = \mathbb{T}_L^3 \mathbb{T}^{\pm X} - \mathbb{T}^{\pm X} \mathbb{T}_L^3 = \pm \frac{1}{2} \mathbb{T}^{\pm X}, \quad (\text{I.6a})$$

$$\hat{\mathbb{T}}_R^3 \mathbb{T}^{X\pm} = \mathbb{T}_R^3 \mathbb{T}^{X\pm} - \mathbb{T}^{X\pm} \mathbb{T}_R^3 = \pm \frac{1}{2} \mathbb{T}^{X\pm}. \quad (\text{I.6b})$$

A suitable choice for this is given by

$$\mathbb{T}^{++} = \frac{1}{\sqrt{2}} (\mathbb{T}^{\hat{1}} + i\mathbb{T}^{\hat{2}}), \quad \mathbb{T}^{--} = \frac{1}{\sqrt{2}} (\mathbb{T}^{\hat{1}} - i\mathbb{T}^{\hat{2}}), \quad (\text{I.7a})$$

$$\mathbb{T}^{+-} = \frac{1}{\sqrt{2}} (\mathbb{T}^{\hat{3}} + i\mathbb{T}^{\hat{4}}), \quad \mathbb{T}^{-+} = -\frac{1}{\sqrt{2}} (\mathbb{T}^{\hat{3}} - i\mathbb{T}^{\hat{4}}). \quad (\text{I.7b})$$

Inverting these relations we find the sought embeddings

$$\Psi_5 = \begin{pmatrix} Q^{\hat{1}} \\ Q^{\hat{2}} \\ Q^{\hat{3}} \\ Q^{\hat{4}} \\ Q^{\hat{5}} \end{pmatrix} = \frac{1}{\sqrt{2}} \begin{pmatrix} Q^{++} + Q^{--} \\ iQ^{++} - iQ^{--} \\ Q^{+-} - Q^{-+} \\ iQ^{+-} + iQ^{-+} \\ \sqrt{2} S \end{pmatrix} \quad (\text{I.8})$$

for the bidoublet  $Q$  and the singlet  $S$ .

## I.2. SO(6)

### Generators

The group theory of SO(6) is very nicely explained in [212]. SO(6) has 15 generators: the usual 10 generators of SO(5) ( $\mathbb{T}_L^a, \mathbb{T}_R^a, \mathbb{T}_{(2,2)}^{\hat{a}}$ ) plus a bidoublet ( $\mathbb{T}_{(2,2)}^{\hat{a}}$ ) plus a singlet ( $\mathbb{T}_S$ ).

$$\text{SO(6)} : \quad \mathbb{T}^A = \left( \underbrace{\mathbb{T}_L^a, \mathbb{T}_R^a, \mathbb{T}_{(2,2)}^{1,a}}_{\text{SO(5)}}, \underbrace{\mathbb{T}_{(2,2)}^{2,\hat{a}}, \mathbb{T}_S}_{\text{coset}} \right), \quad (\text{I.9})$$

with

$$\begin{aligned} [\mathbb{T}_L^a]_{ij} &= -\frac{i}{2} \left( \frac{1}{2} \epsilon^{abc} (\delta_i^b \delta_j^c - \delta_j^b \delta_i^c) + (\delta_i^a \delta_j^4 - \delta_j^a \delta_i^4) \right), \\ [\mathbb{T}_R^a]_{ij} &= -\frac{i}{2} \left( \frac{1}{2} \epsilon^{abc} (\delta_i^b \delta_j^c - \delta_j^b \delta_i^c) - (\delta_i^a \delta_j^4 - \delta_j^a \delta_i^4) \right), \\ [\mathbb{T}_{(2,2)}^{\hat{a}}]_{ij} &= -\frac{i}{\sqrt{2}} (\delta_i^{\hat{a}} \delta_j^5 - \delta_j^{\hat{a}} \delta_i^5), \\ [\mathbb{T}_{(2,2)}^{\hat{a}}]_{ij} &= -\frac{i}{\sqrt{2}} (\delta_i^{\hat{a}} \delta_j^6 - \delta_j^{\hat{a}} \delta_i^6), \\ [\mathbb{T}_S]_{ij} &= -\frac{i}{\sqrt{2}} (\delta_i^5 \delta_j^6 - \delta_j^5 \delta_i^6), \end{aligned}$$

where  $a \in \{1, 2, 3\}$ ,  $\hat{a} \in \{1, 2, 3, 4\}$  and  $i, j \in \{1, 2, 3, 4, 5, 6\}$ .

---

## Representations and embeddings

Under the subgroup  $SO(5)$  the fundamental decomposes as  $\mathbf{6} = \mathbf{5} \oplus \mathbf{1}$ . As the generators of  $SO(6)$  were conveniently chosen to be a superset of those of  $SO(5)$ , the embeddings of the fundamental representation only have to be supplemented by an additional singlet,

$$\mathbf{6} = \begin{pmatrix} \begin{bmatrix} Q^{++} & Q^{+-} \\ Q^{-+} & Q^{--} \end{bmatrix} \\ S_1^{0,0} \\ S_2^{0,0} \end{pmatrix} = \frac{1}{\sqrt{2}} \begin{pmatrix} Q^{++} + Q^{--} \\ iQ^{++} - iQ^{--} \\ Q^{+-} - Q^{-+} \\ iQ^{+-} + iQ^{-+} \\ \sqrt{2} S_1 \\ \sqrt{2} S_2 \end{pmatrix}. \quad (\text{I.10})$$





## Appendix II

### CCWZ formalism

The goal of this section is to give a most general description of CHM's in four-dimensional theories. For this it is most helpful to use the language of phenomenological Lagrangians, i.e. of theories with a spontaneously broken global symmetry. The general classification of the structure of such Lagrangians was given in 1968 by Callan, Coleman, Wess and Zumino (CCWZ) [32, 33]. We will review their findings here and see in the following section how this general framework can be used to describe CHM's on a general ground.

The general procedure for writing Lagrangians with spontaneous symmetry breaking is based on the fact that the latter is a misnomer. The symmetries are not broken but rather hidden in non-linear realizations of the symmetry. Consider e.g. electroweak symmetry breaking in the Higgs sector. In the broken phase we do not see the  $SU(2)_L$  invariance looking just at the Higgs field  $h$ . But nevertheless, this symmetry is still physical (otherwise one could not go to  $R_\xi$  gauges); the Higgs field just does not transform linearly under it. What transforms linearly is the combination  $\Phi = (\phi_1 + i\phi_2, v + h + i\phi_3)^\dagger$ , that once was the full Higgs doublet. Thus, one can rephrase the problem. When considering theories with a symmetry breakdown  $\mathcal{G}/\mathcal{H}$  one actually considers *non-linear realizations of  $\mathcal{G}$  that become linear when restricted to the subgroup  $\mathcal{H}$* .

The general classification of this problem was given in [32]. The main point here is the construction of some standard form for describing the field content of this kind of theories. In general, we want to consider theories with pseudo-Nambu-Goldstone bosons, i.e. theories with a Lagrangian  $\mathcal{L} = \mathcal{L}_{\text{inv}} + \mathcal{L}_{\text{cov}}$ , that decomposes into an invariant part  $\mathcal{L}_{\text{inv}}$ , where the symmetry is realized non-linearly but becomes linear when restricted to the unbroken subgroup  $\mathcal{H}$ , and a covariant term  $\mathcal{L}_{\text{cov}}$  that describes an explicit breaking of  $\mathcal{G}$ .

As already mentioned, we want our theory to superficially appear invariant under linear  $\mathcal{H}$ -transformation. Therefore, let us introduce fields  $\psi$  transforming under  $h \in \mathcal{H}$ ,<sup>1</sup>

$$\psi \rightarrow \psi' = D(h)\psi, \quad (\text{II.1})$$

where  $D(h)$  is a representation. This describes the transformation under the unbroken subgroup  $\mathcal{H} \subset \mathcal{G}$ , but what about the transformation under the total group? Let us introduce generators of the global symmetry group  $\mathcal{G}$ . With  $T^a$  we denote the unbroken generators forming the subgroup  $\mathcal{H}$ , while we write  $T^{\hat{a}}$  for the broken generators parametrizing the coset  $\mathcal{G}/\mathcal{H}$ . We are then able to write a general element  $g \in \mathcal{G}$  uniquely as

$$g = \underbrace{\exp(\pi^{\hat{a}}T^{\hat{a}})}_{\in \mathcal{G}/\mathcal{H}} \underbrace{\exp(u^aT^a)}_{\in \mathcal{H}}. \quad (\text{II.2})$$

The (left) action of any  $g_0 \in \mathcal{G}$  on coset elements  $\mathcal{U} := \exp(\pi^{\hat{a}}T^{\hat{a}}) \in \mathcal{G}/\mathcal{H}$  then takes the form

$$g_0\mathcal{U} = g_0 \exp(\pi^{\hat{a}}T^{\hat{a}}) = \exp(\pi'^{\hat{a}}T^{\hat{a}}) \exp(u'^aT^a), \quad (\text{II.3})$$

where  $\pi' = \pi'(\pi, g_0)$  and  $u' = u'(\pi, g_0)$  are functions of the initial fields  $\pi^{\hat{a}}$  and  $g_0$ . Using this, we can then construct realizations

$$g_0 : \quad \pi \rightarrow \pi'(\pi, g_0), \quad \psi \rightarrow D(\exp(u'^aT^a))\psi, \quad (\text{II.4})$$

---

<sup>1</sup>Note that in general, the representation  $D(h)$  can be reducible. This means that  $\psi$  actually can be seen as a collection of *all* the particles in the theory that transform linearly under  $\mathcal{H}$ .

that are exactly what we were looking for: for a general  $g_0 \in \mathcal{G}$  the transformation  $\pi \rightarrow \pi'(\pi, g_0)$  is highly non-linear, but for the special case  $g_0 = h \in \mathcal{H}$  this reduces to linear representations.

To see this imagine for a short moment that  $g_0 = h$ . Then we can write

$$\mathcal{U} \xrightarrow{h} h\mathcal{U} = h\mathcal{U}h^{-1}h, \quad (\text{II.5})$$

showing that everything transforms linearly,<sup>2</sup>

$$\pi^{\hat{a}}\mathbb{T}^{\hat{a}} \rightarrow \pi'^{\hat{a}}\mathbb{T}^{\hat{a}} = h(\pi^{\hat{a}}\mathbb{T}^{\hat{a}})h^{-1}, \quad \psi \rightarrow \psi' = D(h)\psi. \quad (\text{II.6})$$

If, on the other hand, we transform with a general group element  $g_0 \in \mathcal{G}$ , the situation looks quite different. We then have to write

$$\mathcal{U} \xrightarrow{g} g\mathcal{U} \quad (\text{II.7})$$

$$= \exp(\pi'^{\hat{a}}\mathbb{T}^{\hat{a}}) \exp(u'^a\mathbb{T}^a) \quad (\text{II.8})$$

$$= \exp(\pi'^{\hat{a}}\mathbb{T}^{\hat{a}}) \exp(u'^a\mathbb{T}^a) \exp(-u'^a\mathbb{T}^a) \exp(u'^a\mathbb{T}^a) \quad (\text{II.9})$$

$$= g\mathcal{U}h^{-1}h, \quad (\text{II.10})$$

indicating highly non-linear transformation properties

$$\exp(\pi^{\hat{a}}\mathbb{T}^{\hat{a}}) \rightarrow g \exp(\pi^{\hat{a}}\mathbb{T}^{\hat{a}})h^{-1}, \quad \psi \rightarrow D(h)\psi, \quad (\text{II.11})$$

where  $h = h(\pi, g) \in \mathcal{H}$  is some function of  $g \in \mathcal{G}$ .

Let us summarize this. It is not enough to consider fields  $\psi$  in representations of  $\mathcal{H}$ . To write down a Lagrangian describing a symmetry breaking pattern  $\mathcal{G}/\mathcal{H}$  one additionally has to introduce new degrees of freedom  $\mathcal{U} = \exp(\pi^{\hat{a}}\mathbb{T}^{\hat{a}})$  taking values in the coset. These additional (but necessary) degrees of freedom we identify with *Goldstone bosons*. These then have transformation properties

$$g : \mathcal{U} \rightarrow g\mathcal{U}h(\mathcal{U}, g)^{-1}, \quad \psi \rightarrow D(h(\mathcal{U}, g))\psi, \quad (\text{II.12})$$

where  $h(\mathcal{U}, h) = h$  shows that these realizations become linear when restricted to unbroken subgroup. It is the main result of [32] that this constitutes a standard parametrization, in the sense that one can always describe symmetry breakdown by this form.

After discussing the occurring degrees of freedom let us now tackle the question of how to construct Lagrangians that respect the above transformation properties. The general procedure for doing this was described in [33]. The key question here is how to treat derivative terms that necessarily occur in Lagrangian densities. We will see that just as in gauge theories one has to introduce some kind of *covariant derivatives* that transform homogeneously under the given symmetries. In order to be as general as possible, we consider the case that additionally to the global symmetry  $\mathcal{G}$  that gets broken down to its subgroup  $\mathcal{H}$  there is also a local gauge symmetry  $\mathcal{G}_{\text{gauge}}$  under which the fields can transform. So we assume that the fields  $\psi$  couple to the gauge fields  $V_\mu$  via gauge covariant derivatives and we also allow the Goldstone fields to be charged under this symmetry,

$$D_\mu\psi = (\partial_\mu - iV_\mu)\psi, \quad (\text{II.13})$$

$$D_\mu\mathcal{U} = (\partial_\mu - iV_\mu)\mathcal{U}, \quad (\text{II.14})$$

where the exact form of these couplings depends on the representation of the fields under the gauge symmetry.

Let us now define the so-called *Maurer-Cartan form*,

$$\omega_\mu = i\mathcal{U}^\dagger D_\mu\mathcal{U}. \quad (\text{II.15})$$

---

<sup>2</sup>For the  $\pi$ -field we can see this easily by

$$\begin{aligned} \mathcal{U} &\rightarrow h\mathcal{U}h^{-1} = h \exp(\pi^{\hat{a}}\mathbb{T}^{\hat{a}})h^{-1} \\ &= h \left( \mathbb{1} + \pi + \frac{1}{2}\pi\pi + \dots \right) h^{-1} \\ &= \mathbb{1} + h\pi h^{-1} + \frac{1}{2}h\pi h^{-1}h\pi h^{-1} + \dots \\ &= \exp(h\pi h^{-1}) \end{aligned}$$

From (II.12) one sees that the Cartan-Maurer-form transforms similarly to a gauge field under  $\mathcal{H}$  (remember that  $g$  does not depend on  $x$ ):

$$\omega_\mu = i\mathcal{U}^\dagger D_\mu \mathcal{U} \rightarrow i (g\mathcal{U}h^\dagger)^\dagger D_\mu (g\mathcal{U}h^\dagger) \quad (\text{II.16})$$

$$= i (h\mathcal{U}^\dagger g^\dagger) g ((D_\mu \mathcal{U})h^\dagger + \mathcal{U}(\partial_\mu h^\dagger)) \quad (\text{II.17})$$

$$= h (i\mathcal{U}^\dagger D_\mu \mathcal{U} + i\partial_\mu) h^\dagger \quad (\text{II.18})$$

$$= h (\omega_\mu + i\partial_\mu) h^\dagger, \quad (\text{II.19})$$

where again  $h = h(\mathcal{U}, g)$  depends non-linearly on  $g$ . We further define the projections of  $\omega_\mu$  onto the broken and unbroken generators

$$\omega_\mu = i\mathcal{U}^\dagger D_\mu \mathcal{U} =: d_\mu + E_\mu = d_\mu^{\hat{a}} \mathbb{T}^{\hat{a}} + E_\mu^a \mathbb{T}^a \quad (\text{II.20})$$

with

$$d_\mu^{\hat{a}} = \text{tr} [\omega_\mu \mathbb{T}^{\hat{a}}], \quad E_\mu^a = \text{tr} [\omega_\mu \mathbb{T}^a]. \quad (\text{II.21})$$

Since  $h\partial_\mu h^\dagger \in \mathcal{H}$ , we can deduce the transformation properties of the  $d$ - and  $E$ -components:

$$E_\mu \rightarrow h (E_\mu + i\partial_\mu) h^\dagger, \quad d_\mu \rightarrow h d_\mu h^\dagger. \quad (\text{II.22})$$

We see that the  $d_\mu$ -components transform linearly while the  $E_\mu$ -components transform like a gauge connection. This suggests to define a covariant derivative for some field  $\psi$  that transforms in some representation  $r$  of  $\mathcal{H}$  (i.e.  $\psi \rightarrow \psi + \epsilon^a \mathbb{T}_r^a \psi$  infinitesimally, where  $\mathbb{T}_r^a$  are there the generators in the representation  $r$ ) as

$$\nabla_\mu \psi = (\partial_\mu - iE_\mu^a \mathbb{T}_r^a) \psi, \quad (\text{II.23})$$

Then one can easily see that this covariant derivative transforms linearly

$$\nabla_\mu \psi = \partial_\mu \psi - iE_\mu \psi \rightarrow \partial_\mu (h\psi) - i (h E_\mu h^\dagger + ih(\partial_\mu h^\dagger)) h\psi \quad (\text{II.24})$$

$$= (\partial_\mu h)\psi + h\partial_\mu \psi - ih E_\mu \psi + h(\partial_\mu h^\dagger)h\psi \quad (\text{II.25})$$

$$= h (\partial_\mu - iE_\mu) \psi + (\partial_\mu h)\psi + \underbrace{h(\partial_\mu h^\dagger)}_{=-(\partial_\mu h)h^\dagger} h\psi \quad (\text{II.26})$$

$$= h\nabla_\mu \psi \quad (\text{II.27})$$

If  $\psi$  also carries quantum numbers under the gauge symmetry  $\mathcal{G}_{\text{gauge}}$  then we have to modify the covariant derivative such that it is also covariant with respect to gauge transformations:

$$\nabla_\mu \psi = (\partial_\mu - iE_\mu - iV_\mu) \psi. \quad (\text{II.28})$$

Having made these definition, we can now state the main result of [33], namely that the most general Lagrangian realizing  $\mathcal{G}$  non-linearly, but  $\mathcal{H}$  linearly, is obtained writing down all terms consisting only of  $d_\mu$ ,  $\psi$  and  $\nabla_\mu \psi$  that are superficially invariant under  $\mathcal{H}$  using the transformations (II.22) and (II.27). An important consequence of this is the fact that there is no explicit occurrence of  $\mathcal{U}$  in the invariant part of the Lagrangian. In particular, this means that one cannot write down mass terms for the Goldstone bosons. Furthermore, Goldstone self-interactions are only included in the kinetic term

$$\mathcal{L} \supset \text{tr} [d_\mu^\dagger d^\mu] = (D_\mu \pi^{\hat{a}})^\dagger (D^\mu \pi^{\hat{a}}) + \dots, \quad (\text{II.29})$$

which shows that the self-interactions always carry powers of momentum. In turn, direct (Yukawa-type) interactions between Goldstones and matter fields can only occur if the Lagrangian contains terms breaking the  $\mathcal{G}$  symmetry explicitly.



## Appendix III

### Mass matrices of composite Higgs models

In this appendix we give the expressions for the mass mixing matrices that were used for the analyses of the M4dCHM (see chapter 4) and the NM4dCHM (see chapter 5).

#### III.1. M4dCHM

##### III.1.1. Boson sector

The pNGB structure of the M4dCHM Lagrangian leads to mixings between the elementary and composite vector bosons of equal charge. In particular, the composite triplets  $\rho_L^\mu$  and  $\rho_R^\mu$  as well as the axial resonances  $a^\mu$  will have neutral and charged components mixing with the elementary  $W_0^\mu$  and  $B_0^\mu$  gauge bosons. In addition, the neutral components will also mix with the  $U(1)_X$  resonance  $X^\mu$ .

For the neutral and charged vector bosons we find the mass matrices given in table III.1.

By the explicit mixings introduced in the Lagrangian (4.3) one finds the following mass matrices for the gluons and their composite resonances. By construction this does not spoil invariance under the SM  $SU(3)_c$ , which survives as a linear combination of the elementary and composite  $SU(3)$  symmetries as can be seen from the fact that the gluon mass matrices exhibit a massless eigenvalue.

$$M_{\text{Boson, Gluon}}^2 = \quad (III.3)$$

$$\left( \begin{array}{c|cc} & G_0^0 & \rho_{G\mu} \\ \hline G_0^\mu & \frac{1}{2}g_3^0 f_G^2 & -\frac{1}{2}g_3^0 g_G f_G^2 \\ \rho_G^\mu & & \frac{1}{2}g_{\rho_3}^2 f_G^2 \end{array} \right) \quad (III.4)$$

##### III.1.2. Fermion sector

After EWSB the elementary quarks mix with all resonances carrying the same electric charge. For the up- and down-type quarks we find the mass matrices given in table III.2.

For the exotically charged fermion resonances the mass matrices are independent of the Higgs field. Thus, they do not give a contribution to the Higgs potential, which is clear since they do not mix with elementary fields.

$$M_{\text{fermion}}^{+\frac{5}{3}} = \left( \begin{array}{c|cc} & Q_{uR}^{++} & \tilde{Q}_{uR}^{++} \\ \hline \overline{Q}_{uL}^{++} & m_U & m_{Y_u} \\ \tilde{\overline{Q}}_{uL}^{++} & 0 & \tilde{m}_U \end{array} \right), \quad M_{\text{fermion}}^{-\frac{4}{3}} = s \left( \begin{array}{c|cc} & Q_{dR}^{--} & \tilde{Q}_{dR}^{--} \\ \hline \overline{Q}_{dL}^{--} & m_D & m_{Y_d} \\ \tilde{\overline{Q}}_{dL}^{--} & 0 & \tilde{m}_D \end{array} \right) \quad (III.7)$$

Of course, the fields used above still carry flavour indices. As a consequence of this, all the entries in the fermionic mass matrices actually are  $3 \times 3$  matrices in flavour space, promoting the up- and down-type mass matrices to  $27 \times 27$  objects. The explicit form of the entries is model dependent and will be given in appendix IV.

Since we took the leptons as purely elementary, their mass matrices are just diagonal taking the SM values.

(III.1)

$$M_{\text{Boson,neutral}}^2 = \begin{pmatrix} W_\mu^{3\mu} & W_\mu^{03} & B_\mu^0 & \rho_{L,\mu} & \rho_{R,\mu} & \alpha_\mu^3 & \rho_{X,\mu} & \alpha_\mu^4 \\ \hline \frac{1}{2}g_0 f_1^2 & 0 & -\frac{1}{2}g_0 g_\rho f_1^2 \cos^2\left(\frac{h}{2f}\right) & -\frac{1}{2}g_0 g_\rho f_1^2 \sin^2\left(\frac{h}{2f}\right) & -\frac{1}{2\sqrt{2}}g_0 g_\rho f_1^2 \sin\left(\frac{h}{f}\right) & -\frac{1}{2\sqrt{2}}g_0 g_\rho f_1^2 \sin\left(\frac{h}{f}\right) & 0 & 0 \\ B_0^\mu & \frac{1}{2}g_0^2 (f_1^2 + f_X^2) & -\frac{1}{2}g_0 g_\rho f_1^2 \sin^2\left(\frac{h}{2f}\right) & -\frac{1}{2}g_0 g_\rho f_1^2 \cos^2\left(\frac{h}{2f}\right) & -\frac{1}{2\sqrt{2}}g_0 g_\rho f_1^2 \sin\left(\frac{h}{f}\right) & \frac{1}{2\sqrt{2}}g_0 g_\rho f_1^2 \sin\left(\frac{h}{f}\right) & -\frac{1}{2}g_0 g_X f_X^2 & 0 \\ \rho_{L,\mu}^\mu & \frac{1}{2}g_\rho^2 f_1^2 & \frac{1}{2}g_\rho^2 f_1^2 & 0 & 0 & 0 & 0 & 0 \\ \rho_{R,\mu}^\mu & \frac{1}{2}g_\rho^2 f_1^2 & \frac{1}{2}g_\rho^2 f_1^2 & \frac{1}{2}g_\rho^2 f_1^2 & 0 & 0 & 0 & 0 \\ \alpha^{3\mu} & \frac{1}{2}g_\rho^2 f_1^2 & \frac{1}{2}g_\rho^2 f_1^2 & \frac{1}{2}g_\rho^2 f_1^2 & \frac{1}{2}g_\rho^2 f_1^2 & \frac{1}{2}g_\rho^2 f_1^2 & 0 & 0 \\ \rho_{X,\mu}^\mu & \frac{1}{2}g_\rho^2 f_1^2 & \frac{1}{2}g_\rho^2 f_1^2 & \frac{1}{2}g_\rho^2 f_1^2 & \frac{1}{2}g_\rho^2 f_1^2 & \frac{1}{2}g_\rho^2 f_1^2 & \frac{1}{2}g_X^2 f_X^2 & 0 \\ \alpha^{4\mu} & \frac{1}{2}g_\rho^2 f_1^2 & \frac{1}{2}g_\rho^2 f_1^2 & \frac{1}{2}g_\rho^2 f_1^2 & \frac{1}{2}g_\rho^2 f_1^2 & \frac{1}{2}g_\rho^2 f_1^2 & \frac{1}{2}g_X^2 f_X^2 & \frac{1}{2}g_\rho^2 \frac{f_1^4}{f_1^2 - f^2} \end{pmatrix}$$

(III.2)

$$M_{\text{Boson,charged}}^2 = \begin{pmatrix} W_\mu^{0+} & W_\mu^{0-} & \rho_{L,\mu}^+ & \rho_{R,\mu}^+ & \alpha_\mu^+ \\ \hline W_0^{-\mu} & \frac{1}{2}g_0^2 f_1^2 & -\frac{1}{2}g_0 g_\rho f_1^2 \cos^2\left(\frac{h}{2f}\right) & -\frac{1}{2}g_0 g_\rho f_1^2 \sin^2\left(\frac{h}{2f}\right) & -\frac{1}{2\sqrt{2}}g_0 g_\rho f_1^2 \sin\left(\frac{h}{f}\right) \\ \rho_{L,\mu}^{-\mu} & \frac{1}{2}g_\rho^2 f_1^2 & \frac{1}{2}g_\rho^2 f_1^2 & 0 & 0 \\ \rho_{R,\mu}^{-\mu} & \frac{1}{2}g_\rho^2 f_1^2 & \frac{1}{2}g_\rho^2 f_1^2 & \frac{1}{2}g_\rho^2 f_1^2 & 0 \\ \alpha^{-\mu} & \frac{1}{2}g_\rho^2 f_1^2 & \frac{1}{2}g_\rho^2 f_1^2 & \frac{1}{2}g_\rho^2 f_1^2 & \frac{1}{2}g_\rho^2 \frac{f_1^4}{f_1^2 - f^2} \end{pmatrix}$$

**Table III.1.:** Mass matrices for the neutral and singly charged bosons in the M4DCHM5.

(III.5)

$$M_{\text{fermion}}^{(u)} = \begin{pmatrix} u_R^0 & Q_{uR}^{+-} & \tilde{Q}_{uR}^{+-} & Q_{uR}^{-+} & \tilde{Q}_{uR}^{-+} & Q_{dR}^{++} & \tilde{Q}_{dR}^{++} & S_{uR} & \tilde{S}_{uR} \\ 0 & -\Delta_{uL} \cos^2 \left( \frac{h}{2f} \right) & 0 & \Delta_{uL} \sin^2 \left( \frac{h}{2f} \right) & 0 & -\Delta_{dL} & 0 & \frac{i}{\sqrt{2}} \Delta_{uL} \sin \left( \frac{h}{f} \right) & 0 \\ 0 & m_U & m_{Y_u} & 0 & 0 & 0 & 0 & 0 & 0 \\ -\frac{i}{\sqrt{2}} \Delta_{uR}^\dagger \sin \left( \frac{h}{f} \right) & 0 & \tilde{m}_U & 0 & 0 & 0 & 0 & 0 & 0 \\ 0 & 0 & 0 & m_U & m_{Y_u} & 0 & 0 & 0 & 0 \\ -\frac{i}{\sqrt{2}} \Delta_{uR}^\dagger \sin \left( \frac{h}{f} \right) & 0 & 0 & 0 & \tilde{m}_U & 0 & 0 & 0 & 0 \\ 0 & 0 & 0 & 0 & 0 & m_D & m_{Y_d} & 0 & 0 \\ 0 & 0 & 0 & 0 & 0 & 0 & \tilde{m}_D & 0 & 0 \\ 0 & 0 & 0 & 0 & 0 & 0 & 0 & m_U & m_{Y_u} + Y_u \\ -\Delta_{uR}^\dagger \cos \left( \frac{h}{f} \right) & 0 & 0 & 0 & 0 & 0 & 0 & 0 & \tilde{m}_U \end{pmatrix}$$

(III.6)

$$M_{\text{fermion}}^{(d)} = \begin{pmatrix} d_R^0 & Q_{dR}^{+-} & \tilde{Q}_{dR}^{+-} & Q_{dR}^{-+} & \tilde{Q}_{dR}^{-+} & Q_{uR}^{++} & \tilde{Q}_{uR}^{++} & S_{dR} & \tilde{S}_{dR} \\ 0 & \Delta_{dL} \sin^2 \left( \frac{h}{2f} \right) & 0 & -\Delta_{dL} \cos^2 \left( \frac{h}{2f} \right) & 0 & -\Delta_{uL} & 0 & \frac{i}{\sqrt{2}} \Delta_{dL} \sin \left( \frac{h}{f} \right) & 0 \\ 0 & m_D & m_{Y_d} & 0 & 0 & 0 & 0 & 0 & 0 \\ -\frac{i}{\sqrt{2}} \Delta_{dR}^\dagger \sin \left( \frac{h}{f} \right) & 0 & \tilde{m}_D & 0 & 0 & 0 & 0 & 0 & 0 \\ 0 & 0 & 0 & m_D & m_{Y_d} & 0 & 0 & 0 & 0 \\ -\frac{i}{\sqrt{2}} \Delta_{dR}^\dagger \sin \left( \frac{h}{f} \right) & 0 & 0 & 0 & \tilde{m}_D & 0 & 0 & 0 & 0 \\ 0 & 0 & 0 & 0 & 0 & m_U & m_{Y_u} & 0 & 0 \\ 0 & 0 & 0 & 0 & 0 & 0 & \tilde{m}_U & 0 & 0 \\ 0 & 0 & 0 & 0 & 0 & 0 & 0 & m_D & m_{Y_d} + Y_d \\ -\Delta_{dR}^\dagger \cos \left( \frac{h}{f} \right) & 0 & 0 & 0 & 0 & 0 & 0 & 0 & \tilde{m}_D \end{pmatrix}$$

Table III.2.: Mass matrices for the up- and down-type fermions in the M4DCHM5.





and the ( $h$ - and  $\eta$ -dependent) composite-elementary mixings are

$$v_W^0 = \left( \begin{array}{c|c} & W_\mu^{03} \\ \hline \rho_{L\mu}^3 & -\frac{1}{4}f_1^2 g_0 g_\rho (c_h \tilde{c}_\eta^2 + \tilde{s}_\eta^2 + 1) \\ \rho_{R\mu}^3 & -\frac{1}{4}f_1^2 g_0 g_\rho (1 - c_h) \tilde{c}_\eta^2 \\ \mathbf{a}_{1\mu}^3 & \frac{f_1^2 g_0 g_\rho (1 - c_h) \tilde{s}_\eta \tilde{c}_\eta}{2\sqrt{2}} \\ \mathbf{a}_{2\mu}^3 & -\frac{f_1^2 g_0 g_\rho s_h \tilde{c}_\eta}{2\sqrt{2}} \\ X_\mu & 0 \end{array} \right), \quad (\text{III.10a})$$

$$v_B^0 = \left( \begin{array}{c|c} & B_\mu^0 \\ \hline \rho_{L\mu}^3 & -\frac{1}{4}f_1^2 g'_0 g_\rho (1 - c_h) \tilde{c}_\eta^2 \\ \rho_{R\mu}^3 & -\frac{1}{4}f_1^2 g'_0 g_\rho (c_h \tilde{c}_\eta^2 + \tilde{s}_\eta^2 + 1) \\ \mathbf{a}_{1\mu}^3 & -\frac{f_1^2 g'_0 g_\rho (1 - c_h) \tilde{s}_\eta \tilde{c}_\eta}{2\sqrt{2}} \\ \mathbf{a}_{2\mu}^3 & \frac{f_1^2 g'_0 g_\rho s_h \tilde{c}_\eta}{2\sqrt{2}} \\ X_\mu & -\frac{1}{2}f_X^2 g'_0 g_X \end{array} \right). \quad (\text{III.10b})$$

After the scalar fields assume their vevs the neutral boson mass matrices will have one massless and one rather light (as compared to the scale  $f$ ) eigenvalue. These we will identify with the photon and the  $Z$ -boson, respectively. The mass matrix of the charged vector bosons takes a similar (but simpler) form,

$$M_W^2(h, \eta) = \left( \begin{array}{c|ccc|cc} & W_\mu^{0+} & \rho_{L\mu}^+ & \rho_{R\mu}^+ & \mathbf{a}_{1\mu}^+ & \mathbf{a}_{2\mu}^+ \\ \hline W_\mu^{0-} & D_1^+ & & & & v_W^{+\dagger} \\ \hline \rho_{L\mu}^- & & & & & \\ \rho_{R\mu}^- & & & & & \\ \mathbf{a}_{1\mu}^- & & v_W^+ & & & \\ \mathbf{a}_{2\mu}^- & & & & D_2^+ & \end{array} \right). \quad (\text{III.11})$$

Here, the charged vector bosons  $V_\mu^\pm$  are given as linear combinations

$$V_\mu^\pm = \frac{1}{\sqrt{2}} (V_\mu^1 \mp iV_\mu^2), \quad (\text{III.12})$$

where the 1 and 2 refer to the  $SU(2)$  indices of the vector triplets. The mass matrix has diagonal elements

$$D_1^+ = \left( \begin{array}{c|c} & W_\mu^{0+} \\ \hline W_\mu^{0-} & \frac{f_1^2 g_0^2}{2} \end{array} \right), \quad (\text{III.13a})$$

$$D_1^+ = \left( \begin{array}{c|ccc|cc} & \rho_{L\mu}^+ & \rho_{R\mu}^+ & \mathbf{a}_{1\mu}^+ & \mathbf{a}_{2\mu}^+ \\ \hline \rho_{L\mu}^- & \frac{f_1^2 g_\rho^2}{2} & & & \\ \rho_{R\mu}^- & & \frac{f_1^2 g_\rho^2}{2} & & \\ \mathbf{a}_{1\mu}^- & & & \frac{f_1^2 g_\rho^2}{2} & \\ \mathbf{a}_{2\mu}^- & & & & \frac{f_1^4 g_\rho^2}{2(f_1^2 - f^2)} \end{array} \right), \quad (\text{III.13b})$$

and composite-elementary mixings

$$v_W^+ = \left( \begin{array}{c|c} & W_\mu^{0+} \\ \hline \rho_{L\mu}^- & -\frac{1}{4}f_1^2 g_0 g_\rho (c_h \tilde{c}_\eta^2 + \tilde{s}_\eta^2 + 1) \\ \rho_{R\mu}^- & -\frac{1}{4}f_1^2 g_0 g_\rho (1 - c_h) \tilde{c}_\eta^2 \\ \mathbf{a}_{1\mu}^- & \frac{f_1^2 g_0 g_\rho (1 - c_h) \tilde{s}_\eta \tilde{c}_\eta}{2\sqrt{2}} \\ \mathbf{a}_{2\mu}^- & -\frac{f_1^2 g_0 g_\rho s_h \tilde{c}_\eta}{2\sqrt{2}} \end{array} \right). \quad (\text{III.14})$$

This mass matrix also has a light eigenvalue which is the  $W$ -boson of the SM.

The mass matrices for gluons and their resonances are the same as in (III.4).

### III.2.2. Fermions

As for the vector bosons the fermion mass matrices are best grouped by the electrical charge of the fields, i.e. there is a mass matrix for up-type as well as for down-type quarks and quark resonances. The mass matrices for heavy resonances with exotic charges  $q = +\frac{5}{3}$  and  $q = -\frac{4}{3}$  are the same as (III.7).

The  $(h, \eta)$ -dependent mass matrix for up-type quarks is given as

$$M_u(h, \eta) = \begin{pmatrix} \begin{array}{c} \overline{u}_L^0 \\ \overline{Q}_{uL}^{+-} \\ \overline{Q}_{uL}^{-+} \\ \overline{Q}_{uL}^{++} \\ \overline{Q}_{dL}^{++} \\ \overline{S}_{uL}^1 \\ \overline{S}_{uL}^2 \end{array} & \begin{array}{c} u_R^0 \\ Q_{uR}^{+-} \quad \tilde{Q}_{uR}^{+-} \\ Q_{uR}^{-+} \quad \tilde{Q}_{uR}^{-+} \\ Q_{dR}^{++} \quad \tilde{Q}_{dR}^{++} \\ S_{uR}^1 \quad \tilde{S}_{uR}^1 \\ S_{uR}^2 \quad \tilde{S}_{uR}^2 \end{array} \\ \hline \begin{array}{c} \overline{u}_L^0 \\ \overline{Q}_{uL}^{+-} \\ \overline{Q}_{uL}^{-+} \\ \overline{Q}_{uL}^{++} \\ \overline{Q}_{dL}^{++} \\ \overline{S}_{uL}^1 \\ \overline{S}_{uL}^2 \end{array} & \begin{array}{c} 0 \\ \underline{\Delta}_{QuR}^{+-\dagger} \\ \underline{\Delta}_{QuR}^{-+\dagger} \\ 0 \\ \underline{\Delta}_{SuR}^{1\dagger} \\ \underline{\Delta}_{SuR}^{2\dagger} \end{array} \\ \hline \begin{array}{c} \overline{u}_L^0 \\ \overline{Q}_{uL}^{+-} \\ \overline{Q}_{uL}^{-+} \\ \overline{Q}_{uL}^{++} \\ \overline{Q}_{dL}^{++} \\ \overline{S}_{uL}^1 \\ \overline{S}_{uL}^2 \end{array} & \begin{array}{c} \underline{\Delta}_{QuL}^{+-} \\ \underline{M}_u \\ \underline{M}_u \\ \underline{\Delta}_{QdL}^{++} \\ \underline{M}_d \\ \underline{M}_u \\ \underline{\widehat{M}}_u \end{array} \end{pmatrix}. \quad (III.15)$$

By construction, the left-handed elementary quarks mix with heavy composite states  $\Psi$  while the right-handed ones mix with composites  $\tilde{\Psi}$ . Both composites mix via non-diagonal composite mass matrices

$$\underline{M}_u = \left( \begin{array}{c|cc} & \Psi_{uR} & \tilde{\Psi}_{uR} \\ \hline \overline{\Psi}_{uL} & m_U & m_{Y_u} \\ \overline{\Psi}_{uL} & 0 & m_{\tilde{U}} \end{array} \right), \quad (III.16a)$$

$$\underline{M}_d = \left( \begin{array}{c|cc} & \Psi_{dR} & \tilde{\Psi}_{dR} \\ \hline \overline{\Psi}_{dL} & m_D & m_{Y_d} \\ \overline{\Psi}_{dL} & 0 & m_{\tilde{D}} \end{array} \right), \quad (III.16b)$$

$$\underline{\widehat{M}}_u = \left( \begin{array}{c|cc} & \Psi_{uR} & \tilde{\Psi}_{uR} \\ \hline \overline{\Psi}_{uL} & m_U & m_{Y_u} + Y_u \\ \overline{\Psi}_{uL} & 0 & m_{\tilde{U}} \end{array} \right), \quad (III.16c)$$

$$\underline{\widehat{M}}_d = \left( \begin{array}{c|cc} & \Psi_{dR} & \tilde{\Psi}_{dR} \\ \hline \overline{\Psi}_{dL} & m_D & m_{Y_d} + Y_d \\ \overline{\Psi}_{dL} & 0 & m_{\tilde{D}} \end{array} \right). \quad (III.16d)$$

The composite-elementary mixings carry the  $h, \eta$ -dependence. These are given as

$$\underline{\Delta}_{QuL}^{+-} = \left( \frac{\parallel}{\bar{u}_L^0} \parallel \frac{Q_{uR}^{+-} \quad \tilde{Q}_{uR}^{+-}}{-\frac{1}{2}\Delta_{uL}(c_h\tilde{c}_\eta^2 + 1) \quad 0} \right), \quad (\text{III.17a})$$

$$\underline{\Delta}_{QuL}^{-+} = \left( \frac{\parallel}{\bar{u}_L^0} \parallel \frac{Q_{uR}^{-+} \quad \tilde{Q}_{uR}^{-+}}{\frac{1}{2}\Delta_{uL}\tilde{c}_\eta^2(1 - c_h) \quad 0} \right), \quad (\text{III.17b})$$

$$\underline{\Delta}_{QdL}^{++} = \left( \frac{\parallel}{\bar{u}_L^0} \parallel \frac{Q_{dR}^{++} \quad \tilde{Q}_{dR}^{++}}{-\Delta_{dL} \quad 0} \right), \quad (\text{III.17c})$$

$$\underline{\Delta}_{SuL}^1 = \left( \frac{\parallel}{\bar{u}_L^0} \parallel \frac{S_{uR}^1 \quad \tilde{S}_{uR}^1}{-\frac{i}{\sqrt{2}}\Delta_{uL}(1 - c_h)\tilde{s}_\eta\tilde{c}_\eta \quad 0} \right), \quad (\text{III.17d})$$

$$\underline{\Delta}_{SuL}^2 = \left( \frac{\parallel}{\bar{u}_L^0} \parallel \frac{S_{uR}^2 \quad \tilde{S}_{uR}^2}{\frac{i}{\sqrt{2}}\Delta_{uL}\tilde{c}_\eta s_h \quad 0} \right), \quad (\text{III.17e})$$

$$\underline{\Delta}_{QuR}^{+-} = \left( \frac{\parallel}{u_R^0} \parallel \frac{\bar{Q}_{uL}^{+-} \quad \tilde{\bar{Q}}_{uL}^{+-}}{0 \quad \frac{i}{\sqrt{2}}(\Delta_{uR}^5((1 - c_h)\tilde{s}_\eta\tilde{c}_\eta) + \Delta_{uR}^6 s_h \tilde{c}_\eta)} \right), \quad (\text{III.17f})$$

$$\underline{\Delta}_{QuR}^{-+} = \left( \frac{\parallel}{u_R^0} \parallel \frac{\bar{Q}_{uL}^{-+} \quad \tilde{\bar{Q}}_{uL}^{-+}}{0 \quad \frac{i}{\sqrt{2}}(\Delta_{uR}^5((1 - c_h)\tilde{s}_\eta\tilde{c}_\eta) + \Delta_{uR}^6 s_h \tilde{c}_\eta)} \right), \quad (\text{III.17g})$$

$$\underline{\Delta}_{SuR}^1 = \left( \frac{\parallel}{u_R^0} \parallel \frac{\bar{S}_{uL}^1 \quad \tilde{\bar{S}}_{uL}^1}{0 \quad -\Delta_{uR}^5(\tilde{c}_\eta^2 + c_h\tilde{s}_\eta^2) + \Delta_{uR}^6 s_h \tilde{s}_\eta} \right), \quad (\text{III.17h})$$

$$\underline{\Delta}_{SuR}^2 = \left( \frac{\parallel}{u_R^0} \parallel \frac{\bar{S}_{uL}^2 \quad \tilde{\bar{S}}_{uL}^2}{0 \quad -\Delta_{uR}^5 s_h \tilde{s}_\eta - \Delta_{uR}^6 c_h} \right). \quad (\text{III.17i})$$

The mass matrix for down-type states takes a form analogous to (III.15). One can get it by replacing  $u \leftrightarrow d$  and  $+ \leftrightarrow -$  (for the  $SU(2)_L \times SU(2)_R$  indices) in the up-type mass matrix.



# Appendix IV

## Composite-elementary mixings

In this appendix we summarize the explicit form of composite-elementary mixings in the fermion sector. The general form of flavour structures used in this work is discussed in section 2.2.3. For CHMs it is assumed that the composite sector is subject to an exact flavour symmetry that is only broken by interactions with the elementary sector. We consider two possibilities: left-compositeness, in which left-handed composite-elementary mixings respect the symmetry while it is broken explicitly by the right-handed couplings, and right-compositeness which marks the opposite case. The mixings that respect the flavour symmetry always have to take the form of a unity matrix in the respective flavour space<sup>1</sup> The structures of mixings that break the flavour symmetries have to be determined by a spurion analysis. For the case of a U(3) symmetry the breaking has to occur in terms of the SM CKM matrix in order to reproduce the SM in the MFV case. Assuming a U(2) symmetry the mixings are given by (2.85).

### IV.1. M4dCHM

In the case of the M4dCHM we consider four flavour structures:

- In  $U(3)_{LC}^3$ ,

$$\Delta_{uL} = \Delta_{uL}^{123} \mathbb{1}, \quad \Delta_{uR}^\dagger = V_{CKM}^\dagger \begin{pmatrix} \Delta_{uR}^1 & & \\ & \Delta_{uR}^2 & \\ & & \Delta_{uR}^3 \end{pmatrix}, \quad (IV.1a)$$

$$\Delta_{dL} = \Delta_{dL}^{123} \mathbb{1}, \quad \Delta_{dR}^\dagger = \begin{pmatrix} \Delta_{dR}^1 & & \\ & \Delta_{dR}^2 & \\ & & \Delta_{dR}^3 \end{pmatrix}. \quad (IV.1b)$$

Here,  $V_{CKM}$  is the CKM matrix with 3 angles and 1 phase.

- In  $U(3)_{RC}^3$ ,

$$\Delta_{uL} = V_{CKM}^\dagger \begin{pmatrix} \Delta_{uL}^1 & & \\ & \Delta_{uL}^2 & \\ & & \Delta_{uL}^3 \end{pmatrix}, \quad \Delta_{uR}^\dagger = \Delta_{uR} \mathbb{1}, \quad (IV.2a)$$

$$\Delta_{dL} = \begin{pmatrix} \Delta_{dL}^1 & & \\ & \Delta_{dL}^2 & \\ & & \Delta_{dL}^3 \end{pmatrix}, \quad \Delta_{dR}^\dagger = \Delta_{dR} \mathbb{1}. \quad (IV.2b)$$

---

<sup>1</sup>For the case of a U(2) flavour structure the “unity matrix” has the form  $\text{diag}(a, a, b)$ .

- In  $U(2)_{LC}^3$ ,

$$\Delta_{uL} = \begin{pmatrix} \Delta_{uL}^{12} & & \\ & \Delta_{uL}^{12} & \\ & & \Delta_{uL}^3 \end{pmatrix}, \quad \Delta_{uR}^\dagger = \begin{pmatrix} c_u \Delta_{uR}^1 & -s_u \Delta_{uR}^2 e^{i\alpha_u} & \\ s_u \Delta_{uR}^1 e^{-i\alpha_u} & c_u \Delta_{uR}^2 & \epsilon_u \Delta_{uR}^3 e^{i\phi_u} \\ & & \Delta_{uR}^3 \end{pmatrix}, \quad (IV.2ca)$$

$$\Delta_{dL} = \begin{pmatrix} \Delta_{dL}^{12} & & \\ & \Delta_{dL}^{12} & \\ & & \Delta_{dL}^3 \end{pmatrix}, \quad \Delta_{dR}^\dagger = \begin{pmatrix} c_d \Delta_{dR}^1 & -s_d \Delta_{dR}^2 e^{i\alpha_d} & \\ s_d \Delta_{dR}^1 e^{-i\alpha_d} & c_d \Delta_{dR}^2 & \epsilon_d \Delta_{dR}^3 e^{i\phi_b} \\ & & \Delta_{dR}^3 \end{pmatrix}. \quad (IV.2cb)$$

- In  $U(2)_{RC}^3$ ,

$$\Delta_{uL} = \begin{pmatrix} c_u \Delta_{uL}^1 & -s_u \Delta_{uL}^2 e^{i\alpha_u} & \\ s_u \Delta_{uL}^1 e^{-i\alpha_u} & c_u \Delta_{uL}^2 & \epsilon_u \Delta_{uL}^3 e^{i\phi_u} \\ & & \Delta_{uL}^3 \end{pmatrix}, \quad \Delta_{uR}^\dagger = \begin{pmatrix} \Delta_{uR}^{12} & & \\ & \Delta_{uR}^{12} & \\ & & \Delta_{uR}^3 \end{pmatrix}, \quad (IV.2d)$$

$$\Delta_{dL} = \begin{pmatrix} c_d \Delta_{dL}^1 & -s_d \Delta_{dL}^2 e^{i\alpha_d} & \\ s_d \Delta_{dL}^1 e^{-i\alpha_d} & c_d \Delta_{dL}^2 & \epsilon_d \Delta_{dL}^3 e^{i\phi_b} \\ & & \Delta_{dL}^3 \end{pmatrix}, \quad \Delta_{dR}^\dagger = \begin{pmatrix} \Delta_{dR}^{12} & & \\ & \Delta_{dR}^{12} & \\ & & \Delta_{dR}^3 \end{pmatrix}. \quad (IV.2e)$$

# Appendix V

## Markov Chain Monte Carlo techniques

In this appendix we want to lay out some basic properties of the Markov chains used in the numerical scans of chapters 4 and 5. Markov chains are very similar to Brownian motion in the sense that they describe a random walk through some space of dimension  $d$ . They are stochastic processes subject to the so-called Markov property: the probability for the next step does not depend on the previous steps. This means that at every step the Markov chain “starts new”.

Markov chains are usually used to sample some target probability distribution function  $f(\vec{\Theta})$  on some space of dimension  $d$  with points  $\vec{\Theta}$ . The Markov condition ensures that in the limit of infinitely many steps the distribution of samples coincides with the target function. In that sense, samples will be mostly drawn in regions of high likelihood producing an effective pull towards regions of maximal likelihood (or equivalently minimal  $\chi^2$ ). The standard approach for this is via the *Metropolis-Hastings algorithm* [102, 103]. The structure of this algorithm is very simple and it is shown in Table V.1. At every step of the stochastic process one is located at a current point  $\vec{\Theta}_0$  and a new point  $\vec{\Theta}$  is drawn randomly according to a given proposal density  $p(\vec{\Theta}; \vec{\Theta}_0)$ . If the value  $f(\vec{\Theta})$  at the new point is smaller than the value  $f(\vec{\Theta}_0)$  at the current point, then the step to the new point is made. Otherwise the new step is only performed with a transition probability  $f(\vec{\Theta}_0)/f(\vec{\Theta}) < 1$ . Then one starts again. This algorithm has the property that the chain does not go exclusively into the direction of the minimum of  $f$ , but there is also a non-vanishing probability to go to a point with worse  $f$  value. This is important for sampling the parameter space.

A crucial object for this procedure is the proposal density  $p(\vec{\Theta}; \vec{\Theta}_0)$ . Its concrete form depends very much on the target function  $f$  that is to be sampled. Imagine that  $f$  has a minimum with some intrinsic “width”  $w$ . If the proposal density mainly suggests new points  $\vec{\Theta}$  with  $\|\vec{\Theta} - \vec{\Theta}_0\| \gg w$ , then the chain will almost always “jump over” the minimum and it will be hard to find good points. On the other hand, if the proposal only gives new points with  $\|\vec{\Theta} - \vec{\Theta}_0\| \ll w$ , then the Markov Chain will have to make a large number of steps until it reaches the minimum. A priori the target function  $f$  is unknown and one has no information on how to choose the correct proposal density. The solution to this problem is to use adaptive Markov chains implemented in the package `pymc` [102]. The word “adaptive” here means that the Markov chain by itself has to learn somehow the optimal form of the proposal density [294, 295]. The details of such a self-adaptation are nicely explained in [296]. The basics are to use a multivariate normal distribution centered around the current point

$$p(\vec{\Theta}, \vec{\Theta}_0) \propto \exp\left(-\frac{1}{2}(\vec{\Theta} - \vec{\Theta}_0)^t \Sigma^{-1}(\vec{\Theta} - \vec{\Theta}_0)\right). \quad (\text{V.1})$$

Then, adaptation means tuning the covariance  $\Sigma$  to the optimal value. After  $n^1$  steps  $\Sigma$  is updated

---

<sup>1</sup>In our scans we use  $n = 500$ .

- 
1. Depending on the current points  $\vec{\Theta}_0$  generate a new point  $\vec{\Theta}$  according to the proposal density  $p(\vec{\Theta}; \vec{\Theta}_0)$ .
  2. Calculate the Hastings test ratio  $\alpha = \min\left\{1, \frac{f(\vec{\Theta}_0)}{f(\vec{\Theta})}\right\}$
  3. Draw a random number  $u$  uniformly distributed in  $[0, 1]$ .
  4. If  $u \leq \alpha$ , accept the new point and set  $\vec{\Theta}_0 = \vec{\Theta}$ . Otherwise do not make the step.
  5. Continue anew from 1.
- 

**Table V.1.:** Metropolis-Hastings algorithm

by

$$\Sigma' = (1 - a)\Sigma + aS, \tag{V.2}$$

where  $S$  is the covariance matrix calculated from the last  $n$  steps in the chain. The scale parameter  $a$  is chosen such that the acceptance rate  $\alpha$ , which is defined as the ratio of accepted steps to the total number of attempted steps, is optimal. If  $\alpha = 0$ , that means that no steps are made and the chain is stuck. On the other hand, if  $\alpha = 1$  it means that every step is accepted meaning that probably the step size is chosen too low. To obtain a good coverage of the parameter space the acceptance rate optimally takes a value  $\alpha \approx 0.25$  [296], showing that on average the chain does not stay at the best fit point, but also has a tendency to sample the region around it.



# Appendix VI

## Effective potential for NM4dCHM

In this appendix we will shortly present the calculation of the fermion contributions to the effective potential that was used in the arguments of section 5.4. For simplicity we give the calculation only for the top quark contributions, but the generalization to full flavour case is straight forward.

The starting point is the fermion Lagrangian of the NM4dCHM shown in (5.24). This leads to the mass matrices shown in appendix III.2.2. It is particularly useful to switch to a momentum space representation of the Lagrangian (this was also done e.g. in [41, 55] and integrate out the heavy resonances such that the effects of the composite sector are parametrized in terms of form factors,

$$\mathcal{L} \subset \bar{t}_L \not{p} \Pi_L t_L + \bar{t}_R \not{p} \Pi_R t_R - (\bar{t}_L \Pi_{LR} t_R + \text{h.c.}) \quad (\text{VI.1a})$$

$$= \bar{t}_L \not{p} t_L + \bar{t}_R \not{p} t_R + \bar{t}_L \not{p} (\Pi_L - 1) t_L + \bar{t}_R \not{p} (\Pi_R - 1) t_R - (\bar{t}_L \Pi_{LR} t_R + \text{h.c.}) \quad (\text{VI.1b})$$

The form factors are readily calculated from the mass matrices (in the gauge basis) and result in

$$\Pi_L(p^2, s_h, \tilde{s}_\eta) = \sum_I M_{1I} \frac{1}{p^2 - M_{II}} M_{I1}^* \quad (\text{VI.2a})$$

$$= \left[ 1 - \Delta_{uL} \pi_u(p^2) \Delta_{uL}^\dagger - \Delta_{dL} \pi_d(p^2) \Delta_{dL}^\dagger \right] - \frac{1}{2} s_h^2 \tilde{c}_\eta^2 \Delta_{uL} (\pi_{Su}(p^2) - \pi_u(p^2)) \Delta_{uL}^\dagger, \quad (\text{VI.2b})$$

$$\Pi_R(p^2, s_h, \tilde{s}_\eta) = \sum_I M_{I1} \frac{1}{p^2 - M_{II}} M_{I1}^* \quad (\text{VI.2c})$$

$$= \left[ 1 - \Delta_{uR}^5 \pi_{Su}(p^2) \Delta_{uR}^{5\dagger} - \Delta_{uR}^6 \pi_{Su}(p^2) \Delta_{uR}^{6\dagger} \right] + \tilde{c}_\eta^2 \Delta_{uR}^5 (\pi_{Su}(p^2) - \pi_u(p^2)) \Delta_{uR}^{5\dagger} \\ + (c_h \tilde{s}_\eta \Delta_{uR}^5 - s_h \Delta_{uR}^6) (\pi_{Su}(p^2) - \pi_u(p^2)) (c_h \tilde{s}_\eta \Delta_{uR}^{5\dagger} - s_h \Delta_{uR}^{6\dagger}), \quad (\text{VI.2d})$$

$$\Pi_{LR}(p^2, s_h, \tilde{s}_\eta) = \sum_I M_{1I} \frac{M_{II}}{p^2 - M_{II}} M_{I1} \quad (\text{VI.2e})$$

$$= i s_h \tilde{c}_\eta \Delta_{uL} \pi_{LR}(p^2) (s_h \tilde{s}_\eta \Delta_{uR}^{5\dagger} + c_h \Delta_{uR}^{6\dagger}), \quad (\text{VI.2f})$$

where  $M$  denotes the fermion mass matrix and the index  $I$  runs over the composite resonances. In the above equations we introduced the functions

$$\pi_q(p^2) = \frac{\cos^2(\theta_q)}{p^2 - m_{q1}^2} + \frac{\sin^2(\theta_q)}{p^2 - m_{q2}^2} \\ \pi_{LR}(p^2) = \frac{1}{\sqrt{2}} \left( \sin(\theta_{Su}) \cos(\theta_{Su}) \left( \frac{m_{Su1}}{p^2 - m_{Su1}^2} - \frac{m_{Su2}}{p^2 - m_{Su2}^2} \right) - \sin(\theta_u) \cos(\theta_u) \left( \frac{m_{u1}}{p^2 - m_{u1}^2} - \frac{m_{u2}}{p^2 - m_{u2}^2} \right) \right).$$

The angles  $\theta_i$  originate from diagonalizing the submatrices (III.16) (see also [55, appendix D.2]).

With these results one can either directly use the results of [55] for the effective potential or one can calculate the necessary one-loop vacuum diagrams using the vertices given in (VI.1b). In the end, one obtains the result

$$V_f(s_h, \tilde{s}_\eta) \sim \int \frac{d^E p_E}{(2\pi)^4} \log \text{tr} \left[ p_E^2 \Pi_L \Pi_R + |\Pi_{LR}|^2 \right], \quad (\text{VI.4})$$

where the index  $E$  denotes an integration over the euclidean momentum.



## Bibliography

- [1] W. Altmannshofer, C. Niehoff, P. Stangl, and D. M. Straub, *Status of the  $B \rightarrow K^* \mu^+ \mu^-$  anomaly after Moriond 2017*, [arXiv:1703.09189](#).
- [2] W. Altmannshofer, C. Niehoff, and D. M. Straub,  *$B_s \rightarrow \mu^+ \mu^-$  as current and future probe of new physics*, [arXiv:1702.05498](#).
- [3] C. Niehoff, P. Stangl, and D. M. Straub, *Electroweak symmetry breaking and collider signatures in the next-to-minimal composite Higgs model*, *JHEP* **04** (2017) 117, [[arXiv:1611.09356](#)].
- [4] C. Niehoff, P. Stangl, and D. M. Straub, *Direct and indirect signals of natural composite Higgs models*, *JHEP* **01** (2016) 119, [[arXiv:1508.00569](#)].
- [5] C. Niehoff, P. Stangl, and D. M. Straub, *Violation of lepton flavour universality in composite Higgs models*, *Phys. Lett.* **B747** (2015) 182–186, [[arXiv:1503.03865](#)].
- [6] A. J. Buras, J. Girrbach-Noe, C. Niehoff, and D. M. Straub,  *$B \rightarrow K^{(*)} \nu \bar{\nu}$  decays in the Standard Model and beyond*, *JHEP* **02** (2015) 184, [[arXiv:1409.4557](#)].
- [7] H. Fritzsch, M. Gell-Mann, and H. Leutwyler, *Advantages of the Color Octet Gluon Picture*, *Phys. Lett.* **B47** (1973) 365–368.
- [8] S. L. Glashow, *Partial Symmetries of Weak Interactions*, *Nucl. Phys.* **22** (1961) 579–588.
- [9] S. Weinberg, *A Model of Leptons*, *Phys. Rev. Lett.* **19** (1967) 1264–1266.
- [10] P. W. Anderson, *Plasmons, Gauge Invariance, and Mass*, *Phys. Rev.* **130** (1963) 439–442.
- [11] F. Englert and R. Brout, *Broken Symmetry and the Mass of Gauge Vector Mesons*, *Phys. Rev. Lett.* **13** (1964) 321–323.
- [12] P. W. Higgs, *Broken Symmetries and the Masses of Gauge Bosons*, *Phys. Rev. Lett.* **13** (1964) 508–509.
- [13] G. S. Guralnik, C. R. Hagen, and T. W. B. Kibble, *Global Conservation Laws and Massless Particles*, *Phys. Rev. Lett.* **13** (1964) 585–587.
- [14] D. J. Gross and F. Wilczek, *Ultraviolet Behavior of Nonabelian Gauge Theories*, *Phys. Rev. Lett.* **30** (1973) 1343–1346.
- [15] H. D. Politzer, *Reliable Perturbative Results for Strong Interactions?*, *Phys. Rev. Lett.* **30** (1973) 1346–1349.
- [16] N. Cabibbo, *Unitary Symmetry and Leptonic Decays*, *Phys. Rev. Lett.* **10** (1963) 531–533. [[648\(1963\)](#)].
- [17] M. Kobayashi and T. Maskawa, *CP Violation in the Renormalizable Theory of Weak Interaction*, *Prog. Theor. Phys.* **49** (1973) 652–657.
- [18] **ATLAS** Collaboration, G. Aad et al., *Observation of a new particle in the search for the Standard Model Higgs boson with the ATLAS detector at the LHC*, *Phys. Lett.* **B716** (2012) 1–29, [[arXiv:1207.7214](#)].
- [19] **CMS** Collaboration, S. Chatrchyan et al., *Observation of a new boson at a mass of 125 GeV with the CMS experiment at the LHC*, *Phys. Lett.* **B716** (2012) 30–61, [[arXiv:1207.7235](#)].

- [20] B. Pontecorvo, *Inverse beta processes and nonconservation of lepton charge*, *Sov. Phys. JETP* **7** (1958) 172–173. [*Zh. Eksp. Teor. Fiz.*34,247(1957)].
- [21] Z. Maki, M. Nakagawa, and S. Sakata, *Remarks on the unified model of elementary particles*, *Prog. Theor. Phys.* **28** (1962) 870–880.
- [22] C. Quigg, *Cosmic Neutrinos*, in *Proceedings, 35th SLAC Summer Institute on Particle Physics: Dark matter: From the cosmos to the Laboratory (SSI 2007): Menlo Park, California, July 30- August 10, 2007*, 2008. [arXiv:0802.0013](#).
- [23] C. Wetterich, *Fine Tuning Problem and the Renormalization Group*, *Phys. Lett.* **B140** (1984) 215–222.
- [24] L. Susskind, *Dynamics of Spontaneous Symmetry Breaking in the Weinberg-Salam Theory*, *Phys. Rev.* **D20** (1979) 2619–2625.
- [25] G. 't Hooft, *Naturalness, chiral symmetry, and spontaneous chiral symmetry breaking*, *NATO Sci. Ser. B* **59** (1980) 135–157.
- [26] G. F. Giudice, *Naturally Speaking: The Naturalness Criterion and Physics at the LHC*, [arXiv:0801.2562](#).
- [27] S. L. Glashow, J. Iliopoulos, and L. Maiani, *Weak Interactions with Lepton-Hadron Symmetry*, *Phys. Rev.* **D2** (1970) 1285–1292.
- [28] P. Stangl. PhD thesis, in preparation.
- [29] M. E. Peskin and D. V. Schroeder, *An Introduction to quantum field theory*. 1995.
- [30] O. Matsedonskyi, *On Flavour and Naturalness of Composite Higgs Models*, *JHEP* **02** (2015) 154, [[arXiv:1411.4638](#)].
- [31] R. Barbieri, C. W. Murphy, and F. Senia, *B-decay Anomalies in a Composite Leptoquark Model*, *Eur. Phys. J.* **C77** (2017), no. 1 8, [[arXiv:1611.04930](#)].
- [32] S. R. Coleman, J. Wess, and B. Zumino, *Structure of phenomenological Lagrangians. 1.*, *Phys. Rev.* **177** (1969) 2239–2247.
- [33] C. G. Callan, Jr., S. R. Coleman, J. Wess, and B. Zumino, *Structure of phenomenological Lagrangians. 2.*, *Phys. Rev.* **177** (1969) 2247–2250.
- [34] M. Bando, T. Kugo, S. Uehara, K. Yamawaki, and T. Yanagida, *Is rho Meson a Dynamical Gauge Boson of Hidden Local Symmetry?*, *Phys. Rev. Lett.* **54** (1985) 1215.
- [35] M. Bando, T. Kugo, and K. Yamawaki, *On the Vector Mesons as Dynamical Gauge Bosons of Hidden Local Symmetries*, *Nucl. Phys.* **B259** (1985) 493.
- [36] M. Bando, T. Kugo, and K. Yamawaki, *Nonlinear Realization and Hidden Local Symmetries*, *Phys. Rept.* **164** (1988) 217–314.
- [37] K. Yamawaki, *Hidden Local Symmetry and Beyond*, *Int. J. Mod. Phys.* **E26** (2017), no. 01n02 1740032, [[arXiv:1609.03715](#)].
- [38] K. D. Lane, *An Introduction to technicolor*, in *Theoretical Advanced Study Institute (TASI 93) in Elementary Particle Physics: The Building Blocks of Creation - From Microfermius to Megaparsecs Boulder, Colorado, June 6-July 2, 1993*, pp. 381–408, 1993. [hep-ph/9401324](#).
- [39] D. B. Kaplan, *Flavor at SSC energies: A New mechanism for dynamically generated fermion masses*, *Nucl. Phys.* **B365** (1991) 259–278.
- [40] R. Contino, T. Kramer, M. Son, and R. Sundrum, *Warped/composite phenomenology simplified*, *JHEP* **05** (2007) 074, [[hep-ph/0612180](#)].
- [41] R. Contino, *The Higgs as a Composite Nambu-Goldstone Boson*, in *Physics of the large and the small, TASI 09, proceedings of the Theoretical Advanced Study Institute in Elementary Particle Physics, Boulder, Colorado, USA, 1-26 June 2009*, pp. 235–306, 2011. [arXiv:1005.4269](#).

- 
- [42] Y. Grossman and M. Neubert, *Neutrino masses and mixings in nonfactorizable geometry*, *Phys. Lett.* **B474** (2000) 361–371, [[hep-ph/9912408](#)].
- [43] P. Sikivie, L. Susskind, M. B. Voloshin, and V. I. Zakharov, *Isospin Breaking in Technicolor Models*, *Nucl. Phys.* **B173** (1980) 189–207.
- [44] R. A. Diaz and R. Martinez, *The Custodial symmetry*, *Rev. Mex. Fis.* **47** (2001) 489–492, [[hep-ph/0302058](#)].
- [45] M. E. Peskin and T. Takeuchi, *A New constraint on a strongly interacting Higgs sector*, *Phys. Rev. Lett.* **65** (1990) 964–967.
- [46] **Gfitter Group** Collaboration, M. Baak, J. Cúth, J. Haller, A. Hoecker, R. Kogler, K. Mönig, M. Schott, and J. Stelzer, *The global electroweak fit at NNLO and prospects for the LHC and ILC*, *Eur. Phys. J.* **C74** (2014) 3046, [[arXiv:1407.3792](#)].
- [47] W. Skiba, *Effective Field Theory and Precision Electroweak Measurements*, in *Physics of the large and the small, TASI 09, proceedings of the Theoretical Advanced Study Institute in Elementary Particle Physics, Boulder, Colorado, USA, 1-26 June 2009*, pp. 5–70, 2011. [arXiv:1006.2142](#).
- [48] K. Agashe, R. Contino, and A. Pomarol, *The Minimal composite Higgs model*, *Nucl. Phys.* **B719** (2005) 165–187, [[hep-ph/0412089](#)].
- [49] K. Agashe, R. Contino, L. Da Rold, and A. Pomarol, *A Custodial symmetry for  $Zb\bar{b}$* , *Phys. Lett.* **B641** (2006) 62–66, [[hep-ph/0605341](#)].
- [50] D. B. Kaplan and H. Georgi,  *$SU(2) \times U(1)$  Breaking by Vacuum Misalignment*, *Phys. Lett.* **B136** (1984) 183–186.
- [51] B. Gripaios, A. Pomarol, F. Riva, and J. Serra, *Beyond the Minimal Composite Higgs Model*, *JHEP* **04** (2009) 070, [[arXiv:0902.1483](#)].
- [52] S. R. Coleman and E. J. Weinberg, *Radiative Corrections as the Origin of Spontaneous Symmetry Breaking*, *Phys. Rev.* **D7** (1973) 1888–1910.
- [53] E. J. Weinberg, *Radiative corrections as the origin of spontaneous symmetry breaking*. PhD thesis, Harvard U., 1973. [hep-th/0507214](#).
- [54] N. Arkani-Hamed, A. G. Cohen, and H. Georgi, *Electroweak symmetry breaking from dimensional deconstruction*, *Phys. Lett.* **B513** (2001) 232–240, [[hep-ph/0105239](#)].
- [55] D. Marzocca, M. Serone, and J. Shu, *General Composite Higgs Models*, *JHEP* **08** (2012) 013, [[arXiv:1205.0770](#)].
- [56] G. Panico, M. Redi, A. Tesi, and A. Wulzer, *On the Tuning and the Mass of the Composite Higgs*, *JHEP* **03** (2013) 051, [[arXiv:1210.7114](#)].
- [57] A. Pomarol and F. Riva, *The Composite Higgs and Light Resonance Connection*, *JHEP* **08** (2012) 135, [[arXiv:1205.6434](#)].
- [58] D. Pappadopulo, A. Thamm, and R. Torre, *A minimally tuned composite Higgs model from an extra dimension*, *JHEP* **07** (2013) 058, [[arXiv:1303.3062](#)].
- [59] A. Carmona and F. Goertz, *A naturally light Higgs without light Top Partners*, *JHEP* **05** (2015) 002, [[arXiv:1410.8555](#)].
- [60] G. Panico and A. Wulzer, *The Discrete Composite Higgs Model*, *JHEP* **09** (2011) 135, [[arXiv:1106.2719](#)].
- [61] O. Matsedonskyi, G. Panico, and A. Wulzer, *Light Top Partners for a Light Composite Higgs*, *JHEP* **01** (2013) 164, [[arXiv:1204.6333](#)].
- [62] C. Csaki, A. Falkowski, and A. Weiler, *The Flavor of the Composite Pseudo-Goldstone Higgs*, *JHEP* **09** (2008) 008, [[arXiv:0804.1954](#)].

- [63] M. Blanke, A. J. Buras, B. Duling, S. Gori, and A. Weiler,  $\Delta F=2$  Observables and Fine-Tuning in a Warped Extra Dimension with Custodial Protection, *JHEP* **03** (2009) 001, [[arXiv:0809.1073](#)].
- [64] M. Redi and A. Weiler, Flavor and CP Invariant Composite Higgs Models, *JHEP* **11** (2011) 108, [[arXiv:1106.6357](#)].
- [65] R. Barbieri, D. Buttazzo, F. Sala, and D. M. Straub, Flavour physics from an approximate  $U(2)^3$  symmetry, *JHEP* **07** (2012) 181, [[arXiv:1203.4218](#)].
- [66] G. D'Ambrosio, G. F. Giudice, G. Isidori, and A. Strumia, Minimal flavor violation: An Effective field theory approach, *Nucl. Phys.* **B645** (2002) 155–187, [[hep-ph/0207036](#)].
- [67] A. J. Buras, Minimal flavor violation, *Acta Phys. Polon.* **B34** (2003) 5615–5668, [[hep-ph/0310208](#)].
- [68] B. Grzadkowski, M. Iskrzynski, M. Misiak, and J. Rosiek, Dimension-Six Terms in the Standard Model Lagrangian, *JHEP* **10** (2010) 085, [[arXiv:1008.4884](#)].
- [69] G. Cacciapaglia, C. Csaki, J. Galloway, G. Marandella, J. Terning, and A. Weiler, A GIM Mechanism from Extra Dimensions, *JHEP* **04** (2008) 006, [[arXiv:0709.1714](#)].
- [70] R. Barbieri, D. Buttazzo, F. Sala, D. M. Straub, and A. Tesi, A 125 GeV composite Higgs boson versus flavour and electroweak precision tests, *JHEP* **05** (2013) 069, [[arXiv:1211.5085](#)].
- [71] G. Nordstrom, On the possibility of unifying the electromagnetic and the gravitational fields, *Phys. Z.* **15** (1914) 504–506, [[physics/0702221](#)].
- [72] T. Kaluza, On the Problem of Unity in Physics, *Sitzungsber. Preuss. Akad. Wiss. Berlin (Math. Phys.)* **1921** (1921) 966–972.
- [73] O. Klein, Quantum Theory and Five-Dimensional Theory of Relativity. (In German and English), *Z. Phys.* **37** (1926) 895–906. [Surveys High Energ. Phys.5,241(1986)].
- [74] J. M. Maldacena, The Large  $N$  limit of superconformal field theories and supergravity, *Int. J. Theor. Phys.* **38** (1999) 1113–1133, [[hep-th/9711200](#)]. [Adv. Theor. Math. Phys.2,231(1998)].
- [75] N. Arkani-Hamed, S. Dimopoulos, and G. R. Dvali, The Hierarchy problem and new dimensions at a millimeter, *Phys. Lett.* **B429** (1998) 263–272, [[hep-ph/9803315](#)].
- [76] L. Randall and R. Sundrum, A Large mass hierarchy from a small extra dimension, *Phys. Rev. Lett.* **83** (1999) 3370–3373, [[hep-ph/9905221](#)].
- [77] L. Randall and R. Sundrum, An Alternative to compactification, *Phys. Rev. Lett.* **83** (1999) 4690–4693, [[hep-th/9906064](#)].
- [78] S. J. Huber and Q. Shafi, Fermion masses, mixings and proton decay in a Randall-Sundrum model, *Phys. Lett.* **B498** (2001) 256–262, [[hep-ph/0010195](#)].
- [79] C. Csaki, C. Grojean, J. Hubisz, Y. Shirman, and J. Terning, Fermions on an interval: Quark and lepton masses without a Higgs, *Phys. Rev.* **D70** (2004) 015012, [[hep-ph/0310355](#)].
- [80] C. Csaki, J. Hubisz, and P. Meade, TASI lectures on electroweak symmetry breaking from extra dimensions, in *Physics in  $D=4$ . Proceedings, Theoretical Advanced Study Institute in elementary particle physics, TASI 2004, Boulder, USA, June 6-July 2, 2004*, pp. 703–776, 2005. [hep-ph/0510275](#).
- [81] Y. Hosotani, Dynamical Mass Generation by Compact Extra Dimensions, *Phys. Lett.* **B126** (1983) 309–313.
- [82] N. Haba, M. Harada, Y. Hosotani, and Y. Kawamura, Dynamical rearrangement of gauge symmetry on the orbifold  $S^1/Z(2)$ , *Nucl. Phys.* **B657** (2003) 169–213, [[hep-ph/0212035](#)]. [Erratum: *Nucl. Phys.*B669,381(2003)].

- 
- [83] H. Davoudiasl, J. L. Hewett, and T. G. Rizzo, *Bulk gauge fields in the Randall-Sundrum model*, *Phys. Lett.* **B473** (2000) 43–49, [[hep-ph/9911262](#)].
- [84] A. Pomarol, *Gauge bosons in a five-dimensional theory with localized gravity*, *Phys. Lett.* **B486** (2000) 153–157, [[hep-ph/9911294](#)].
- [85] L. Randall and M. D. Schwartz, *Quantum field theory and unification in AdS5*, *JHEP* **11** (2001) 003, [[hep-th/0108114](#)].
- [86] Y. Hosotani, *Dynamics of Nonintegrable Phases and Gauge Symmetry Breaking*, *Annals Phys.* **190** (1989) 233.
- [87] M. Kubo, C. S. Lim, and H. Yamashita, *The Hosotani mechanism in bulk gauge theories with an orbifold extra space  $S^{*1}/Z(2)$* , *Mod. Phys. Lett.* **A17** (2002) 2249–2264, [[hep-ph/0111327](#)].
- [88] L. J. Hall, H. Murayama, and Y. Nomura, *Wilson lines and symmetry breaking on orbifolds*, *Nucl. Phys.* **B645** (2002) 85–104, [[hep-th/0107245](#)].
- [89] G. Panico and A. Wulzer, *Effective action and holography in 5D gauge theories*, *JHEP* **05** (2007) 060, [[hep-th/0703287](#)].
- [90] M. Serone, *Holographic Methods and Gauge-Higgs Unification in Flat Extra Dimensions*, *New J. Phys.* **12** (2010) 075013, [[arXiv:0909.5619](#)].
- [91] R. Contino, L. Da Rold, and A. Pomarol, *Light custodians in natural composite Higgs models*, *Phys. Rev.* **D75** (2007) 055014, [[hep-ph/0612048](#)].
- [92] C. Csaki, Y. Grossman, P. Tanedo, and Y. Tsai, *Warped penguin diagrams*, *Phys. Rev.* **D83** (2011) 073002, [[arXiv:1004.2037](#)].
- [93] R. Malm, M. Neubert, K. Novotny, and C. Schmell, *5D Perspective on Higgs Production at the Boundary of a Warped Extra Dimension*, *JHEP* **01** (2014) 173, [[arXiv:1303.5702](#)].
- [94] M. Beneke, P. Dey, and J. Rohrwild, *The muon anomalous magnetic moment in the Randall-Sundrum model*, *JHEP* **08** (2013) 010, [[arXiv:1209.5897](#)].
- [95] M. Beneke, P. Moch, and J. Rohrwild, *Muon anomalous magnetic moment and penguin loops in warped extra dimensions*, *Int. J. Mod. Phys.* **A29** (2014) 1444011, [[arXiv:1404.7157](#)].
- [96] P. Moch and J. Rohrwild,  *$\bar{B} \rightarrow X_s \gamma$  with a warped bulk Higgs*, *Nucl. Phys.* **B902** (2016) 142–161, [[arXiv:1509.04643](#)].
- [97] N. Arkani-Hamed, A. G. Cohen, and H. Georgi, *(De)constructing dimensions*, *Phys. Rev. Lett.* **86** (2001) 4757–4761, [[hep-th/0104005](#)].
- [98] G. Munster and M. Walzl, *Lattice gauge theory: A Short primer*, in *Phenomenology of gauge interactions. Proceedings, Summer School, Zuoz, Switzerland, August 13-19, 2000*, pp. 127–160, 2000. [hep-lat/0012005](#).
- [99] S. De Curtis, M. Redi, and A. Tesi, *The 4D Composite Higgs*, *JHEP* **04** (2012) 042, [[arXiv:1110.1613](#)].
- [100] S. De Curtis, M. Redi, and E. Vigiani, *Non Minimal Terms in Composite Higgs Models and in QCD*, *JHEP* **06** (2014) 071, [[arXiv:1403.3116](#)].
- [101] D. M. Straub, *Anatomy of flavour-changing Z couplings in models with partial compositeness*, *JHEP* **08** (2013) 108, [[arXiv:1302.4651](#)].
- [102] N. Metropolis, A. Rosenbluth, M. Rosenbluth, A. Teller, and E. Teller, *Equation of State Calculations by Fast Computing Machines*, *Journal of Chemical Physics* **21** (1953) 1087.
- [103] W. K. Hastings, *Monte Carlo sampling methods using Markov chains and their applications*, *Biomatrica* **57(1)** (1970) 97–109.

- [104] S. G. Johnson, *The nlopt nonlinear-optimization package*. 2011, .  
<http://ab-initio.mit.edu/nlopt>.
- [105] T. Rowan, *Functional Stability Analysis of Numerical Algorithms*. PhD thesis, University of Texas at Austin, Department of Computer Sciences, 1990.
- [106] F. Beaujean and S. Jahn, *pypmc version 1.1*, August, 2016. DOI:10.5281/zenodo.61270.
- [107] <http://www.universe-cluster.de/c2pap/>.
- [108] **Particle Data Group** Collaboration, C. Patrignani et al., *Review of Particle Physics*, *Chin. Phys.* **C40** (2016), no. 10 100001.
- [109] S. Aoki et al., *Review of lattice results concerning low-energy particle physics*, *Eur. Phys. J.* **C74** (2014) 2890, [[arXiv:1310.8555](https://arxiv.org/abs/1310.8555)].
- [110] **Particle Data Group** Collaboration, K. A. Olive et al., *Review of Particle Physics*, *Chin. Phys.* **C38** (2014) 090001.
- [111] A. H. Hoang, *The Top Mass: Interpretation and Theoretical Uncertainties*, in *Proceedings, 7th International Workshop on Top Quark Physics (TOP2014): Cannes, France, September 28-October 3, 2014*, 2014. [arXiv:1412.3649](https://arxiv.org/abs/1412.3649).
- [112] K. G. Chetyrkin, J. H. Kuhn, and M. Steinhauser, *RunDec: A Mathematica package for running and decoupling of the strong coupling and quark masses*, *Comput. Phys. Commun.* **133** (2000) 43–65, [[hep-ph/0004189](https://arxiv.org/abs/hep-ph/0004189)].
- [113] A. Hoecker, *The Hadronic Contribution to the Muon Anomalous Magnetic Moment and to the Running Electromagnetic Fine Structure Constant at MZ - Overview and Latest Results*, *Nucl. Phys. Proc. Suppl.* **218** (2011) 189–200, [[arXiv:1012.0055](https://arxiv.org/abs/1012.0055)].
- [114] A. Crivellin and S. Pokorski, *Can the differences in the determinations of  $V_{ub}$  and  $V_{cb}$  be explained by New Physics?*, *Phys. Rev. Lett.* **114** (2015), no. 1 011802, [[arXiv:1407.1320](https://arxiv.org/abs/1407.1320)].
- [115] M. Gronau and D. London, *How to determine all the angles of the unitarity triangle from  $B(d)0 \rightarrow D K(s)$  and  $B(s)0 \rightarrow D0$* , *Phys. Lett.* **B253** (1991) 483–488.
- [116] M. Gronau and D. Wyler, *On determining a weak phase from CP asymmetries in charged B decays*, *Phys. Lett.* **B265** (1991) 172–176.
- [117] J. C. Hardy and I. S. Towner, *Superaligned  $0^+ \rightarrow 0^+$  nuclear  $\beta$  decays: 2014 critical survey, with precise results for  $V_{ud}$  and CKM unitarity*, *Phys. Rev.* **C91** (2015), no. 2 025501, [[arXiv:1411.5987](https://arxiv.org/abs/1411.5987)].
- [118] S. Aoki et al., *Review of lattice results concerning low-energy particle physics*, *Eur. Phys. J.* **C77** (2017), no. 2 112, [[arXiv:1607.00299](https://arxiv.org/abs/1607.00299)].
- [119] **Fermilab Lattice, MILC** Collaboration, J. A. Bailey et al.,  *$|V_{ub}|$  from  $B \rightarrow \pi \ell \nu$  decays and  $(2+1)$ -flavor lattice QCD*, *Phys. Rev.* **D92** (2015), no. 1 014024, [[arXiv:1503.07839](https://arxiv.org/abs/1503.07839)].
- [120] **BaBar** Collaboration, J. P. Lees et al., *Study of  $\bar{B} \rightarrow X_u \ell \bar{\nu}$  decays in  $B\bar{B}$  events tagged by a fully reconstructed B-meson decay and determination of  $\|V_{ub}\|$* , *Phys. Rev.* **D86** (2012) 032004, [[arXiv:1112.0702](https://arxiv.org/abs/1112.0702)].
- [121] **Fermilab Lattice, MILC** Collaboration, J. A. Bailey et al., *Update of  $|V_{cb}|$  from the  $\bar{B} \rightarrow D^* \ell \bar{\nu}$  form factor at zero recoil with three-flavor lattice QCD*, *Phys. Rev.* **D89** (2014), no. 11 114504, [[arXiv:1403.0635](https://arxiv.org/abs/1403.0635)].
- [122] **CMS** Collaboration, V. Khachatryan et al., *Measurement of the t-channel single-top-quark production cross section and of the  $|V_{tb}|$  CKM matrix element in pp collisions at  $\sqrt{s} = 8$  TeV*, *JHEP* **06** (2014) 090, [[arXiv:1403.7366](https://arxiv.org/abs/1403.7366)].
- [123] J. Charles et al., *Current status of the Standard Model CKM fit and constraints on  $\Delta F = 2$  New Physics*, *Phys. Rev.* **D91** (2015), no. 7 073007, [[arXiv:1501.05013](https://arxiv.org/abs/1501.05013)].



- 
- [124] M. E. Peskin and T. Takeuchi, *Estimation of oblique electroweak corrections*, *Phys. Rev.* **D46** (1992) 381–409.
- [125] T. Hahn and M. Perez-Victoria, *Automatized one loop calculations in four-dimensions and D-dimensions*, *Comput. Phys. Commun.* **118** (1999) 153–165, [[hep-ph/9807565](#)].
- [126] D. M. Pierce, J. A. Bagger, K. T. Matchev, and R.-j. Zhang, *Precision corrections in the minimal supersymmetric standard model*, *Nucl. Phys.* **B491** (1997) 3–67, [[hep-ph/9606211](#)].
- [127] R. Barbieri, B. Bellazzini, V. S. Rychkov, and A. Varagnolo, *The Higgs boson from an extended symmetry*, *Phys. Rev.* **D76** (2007) 115008, [[arXiv:0706.0432](#)].
- [128] A. Orgogozo and S. Rychkov, *The S parameter for a Light Composite Higgs: a Dispersion Relation Approach*, *JHEP* **06** (2013) 014, [[arXiv:1211.5543](#)].
- [129] **SLD Electroweak Group, DELPHI, ALEPH, SLD, SLD Heavy Flavour Group, OPAL, LEP Electroweak Working Group, L3** Collaboration, S. Schael et al., *Precision electroweak measurements on the Z resonance*, *Phys. Rept.* **427** (2006) 257–454, [[hep-ex/0509008](#)].
- [130] J. D. Wells and Z. Zhang, *Precision Electroweak Analysis after the Higgs Boson Discovery*, *Phys. Rev.* **D90** (2014), no. 3 033006, [[arXiv:1406.6070](#)].
- [131] C. Grojean, O. Matsedonskyi, and G. Panico, *Light top partners and precision physics*, *JHEP* **10** (2013) 160, [[arXiv:1306.4655](#)].
- [132] G. F. Giudice, C. Grojean, A. Pomarol, and R. Rattazzi, *The Strongly-Interacting Light Higgs*, *JHEP* **06** (2007) 045, [[hep-ph/0703164](#)].
- [133] I. Low and A. Vichi, *On the production of a composite Higgs boson*, *Phys. Rev.* **D84** (2011) 045019, [[arXiv:1010.2753](#)].
- [134] A. Azatov and J. Galloway, *Light Custodians and Higgs Physics in Composite Models*, *Phys. Rev.* **D85** (2012) 055013, [[arXiv:1110.5646](#)].
- [135] C. Delaunay, C. Grojean, and G. Perez, *Modified Higgs Physics from Composite Light Flavors*, *JHEP* **09** (2013) 090, [[arXiv:1303.5701](#)].
- [136] The CMS collaboration, *Precise determination of the mass of the Higgs boson and tests of compatibility of its couplings with the standard model predictions using proton collisions at 7 and 8 TeV*, Dec, 2014. CMS-HIG-14-009.
- [137] The ATLAS collaboration, *Measurements of the Higgs boson production and decay rates and coupling strengths using pp collision data at  $\sqrt{s} = 7$  and 8 TeV in the ATLAS experiment*, March, 2015. ATLAS-CONF-2015-007.
- [138] **ATLAS, CMS** Collaboration, G. Aad et al., *Measurements of the Higgs boson production and decay rates and constraints on its couplings from a combined ATLAS and CMS analysis of the LHC pp collision data at  $\sqrt{s} = 7$  and 8 TeV*, *JHEP* **08** (2016) 045, [[arXiv:1606.02266](#)].
- [139] I. Dunietz and J. L. Rosner, *Time Dependent CP Violation Effects in  $B_0$  anti- $B_0$  Systems*, *Phys. Rev.* **D34** (1986) 1404.
- [140] A. J. Buras, *Flavor physics and CP violation*, in *2004 European School of High-Energy Physics, Sant Feliu de Guixols, Spain, 30 May - 12 June 2004*, pp. 95–168, 2005. [hep-ph/0505175](#).
- [141] R. Fleischer, *Flavour Physics and CP Violation: Expecting the LHC*, in *High-energy physics. Proceedings, 4th Latin American CERN-CLAF School, Vina del Mar, Chile, February 18-March 3, 2007*, pp. 105–157, 2008. [arXiv:0802.2882](#).
- [142] U. Nierste, *Three Lectures on Meson Mixing and CKM phenomenology*, in *Heavy quark physics. Proceedings, Helmholtz International School, HQP08, Dubna, Russia, August 11-21, 2008*, pp. 1–38, 2009. [arXiv:0904.1869](#).

- [143] A. J. Buras, *Weak Hamiltonian, CP violation and rare decays*, in *Probing the standard model of particle interactions. Proceedings, Summer School in Theoretical Physics, NATO Advanced Study Institute, 68th session, Les Houches, France, July 28-September 5, 1997. Pt. 1, 2*, pp. 281–539, 1998. [hep-ph/9806471](#).
- [144] A. J. Buras, S. Jager, and J. Urban, *Master formulae for Delta F=2 NLO QCD factors in the standard model and beyond*, *Nucl. Phys.* **B605** (2001) 600–624, [[hep-ph/0102316](#)].
- [145] **Fermilab Lattice, MILC** Collaboration, A. Bazavov et al.,  *$B_{(s)}^0$ -mixing matrix elements from lattice QCD for the Standard Model and beyond*, *Phys. Rev.* **D93** (2016), no. 11 113016, [[arXiv:1602.03560](#)].
- [146] **ETM** Collaboration, V. Bertone et al., *Kaon Mixing Beyond the SM from  $N_f=2$  tmQCD and model independent constraints from the UTA*, *JHEP* **03** (2013) 089, [[arXiv:1207.1287](#)]. [Erratum: *JHEP*07,143(2013)].
- [147] D. Straub et al., *flav-io/flavio v0.21*, April, 2017. DOI:10.5281/zenodo.555949.
- [148] **Heavy Flavor Averaging Group (HFAG)** Collaboration, Y. Amhis et al., *Averages of b-hadron, c-hadron, and  $\tau$ -lepton properties as of summer 2014*, [arXiv:1412.7515](#).
- [149] Y. Amhis et al., *Averages of b-hadron, c-hadron, and  $\tau$ -lepton properties as of summer 2016*, [arXiv:1612.07233](#).
- [150] **LHCb** Collaboration, R. Aaij et al., *Precision measurement of CP violation in  $B_s^0 \rightarrow J/\psi K^+ K^-$  decays*, *Phys. Rev. Lett.* **114** (2015), no. 4 041801, [[arXiv:1411.3104](#)].
- [151] P. Frings, U. Nierste, and M. Wiebusch, *Penguin contributions to CP phases in  $B_{d,s}$  decays to charmonium*, *Phys. Rev. Lett.* **115** (2015), no. 6 061802, [[arXiv:1503.00859](#)].
- [152] A. J. Buras and D. Guadagnoli, *Correlations among new CP violating effects in  $\Delta F = 2$  observables*, *Phys. Rev.* **D78** (2008) 033005, [[arXiv:0805.3887](#)].
- [153] J. Brod and M. Gorbahn, *Next-to-Next-to-Leading-Order Charm-Quark Contribution to the CP Violation Parameter  $\epsilon_K$  and  $\Delta M_K$* , *Phys. Rev. Lett.* **108** (2012) 121801, [[arXiv:1108.2036](#)].
- [154] M. König, M. Neubert, and D. M. Straub, *Dipole operator constraints on composite Higgs models*, *Eur. Phys. J.* **C74** (2014), no. 7 2945, [[arXiv:1403.2756](#)].
- [155] G. Buchalla, A. J. Buras, and M. E. Lautenbacher, *Weak decays beyond leading logarithms*, *Rev. Mod. Phys.* **68** (1996) 1125–1144, [[hep-ph/9512380](#)].
- [156] A. J. Buras, L. Merlo, and E. Stamou, *The Impact of Flavour Changing Neutral Gauge Bosons on  $\bar{B} \rightarrow X_s \gamma$* , *JHEP* **08** (2011) 124, [[arXiv:1105.5146](#)].
- [157] P. Gambino and M. Misiak, *Quark mass effects in anti- $B \rightarrow X(s \text{ gamma})$* , *Nucl. Phys.* **B611** (2001) 338–366, [[hep-ph/0104034](#)].
- [158] A. J. Buras, M. Misiak, M. Munz, and S. Pokorski, *Theoretical uncertainties and phenomenological aspects of  $B \rightarrow X(s) \text{ gamma}$  decay*, *Nucl. Phys.* **B424** (1994) 374–398, [[hep-ph/9311345](#)].
- [159] W. Altmannshofer, P. Ball, A. Bharucha, A. J. Buras, D. M. Straub, and M. Wick, *Symmetries and Asymmetries of  $B \rightarrow K^* \mu^+ \mu^-$  Decays in the Standard Model and Beyond*, *JHEP* **01** (2009) 019, [[arXiv:0811.1214](#)].
- [160] M. Czakon, P. Fiedler, T. Huber, M. Misiak, T. Schutzmeier, and M. Steinhauser, *The  $(Q_7, Q_{1,2})$  contribution to  $\bar{B} \rightarrow X_s \gamma$  at  $\mathcal{O}(\alpha_s^2)$* , *JHEP* **04** (2015) 168, [[arXiv:1503.01791](#)].
- [161] K. De Bruyn, R. Fleischer, R. Kneijens, P. Koppenburg, M. Merk, A. Pellegrino, and N. Tuning, *Probing New Physics via the  $B_s^0 \rightarrow \mu^+ \mu^-$  Effective Lifetime*, *Phys. Rev. Lett.* **109** (2012) 041801, [[arXiv:1204.1737](#)].

- 
- [162] C. Bobeth, M. Gorbahn, T. Hermann, M. Misiak, E. Stamou, and M. Steinhauser,  *$B_{s,d} \rightarrow l^+l^-$  in the Standard Model with Reduced Theoretical Uncertainty*, *Phys. Rev. Lett.* **112** (2014) 101801, [[arXiv:1311.0903](#)].
- [163] W. Altmannshofer and D. M. Straub, *New Physics in  $B \rightarrow K^*\mu\mu$ ?*, *Eur. Phys. J.* **C73** (2013) 2646, [[arXiv:1308.1501](#)].
- [164] **LHCb, CMS** Collaboration, V. Khachatryan et al., *Observation of the rare  $B_s^0 \rightarrow \mu^+\mu^-$  decay from the combined analysis of CMS and LHCb data*, *Nature* **522** (2015) 68–72, [[arXiv:1411.4413](#)].
- [165] M. Pospelov and A. Ritz, *Neutron EDM from electric and chromoelectric dipole moments of quarks*, *Phys. Rev.* **D63** (2001) 073015, [[hep-ph/0010037](#)].
- [166] M. Jung and A. Pich, *Electric Dipole Moments in Two-Higgs-Doublet Models*, *JHEP* **04** (2014) 076, [[arXiv:1308.6283](#)].
- [167] C. A. Baker et al., *An Improved experimental limit on the electric dipole moment of the neutron*, *Phys. Rev. Lett.* **97** (2006) 131801, [[hep-ex/0602020](#)].
- [168] J. R. Espinosa, B. Gripaios, T. Konstandin, and F. Riva, *Electroweak Baryogenesis in Non-minimal Composite Higgs Models*, *JCAP* **1201** (2012) 012, [[arXiv:1110.2876](#)].
- [169] O. Domenech, A. Pomarol, and J. Serra, *Probing the SM with Dijets at the LHC*, *Phys. Rev.* **D85** (2012) 074030, [[arXiv:1201.6510](#)].
- [170] M. de Vries, *Four-quark effective operators at hadron colliders*, *JHEP* **03** (2015) 095, [[arXiv:1409.4657](#)].
- [171] **ATLAS** Collaboration, G. Aad et al., *Search for New Phenomena in Dijet Angular Distributions in Proton-Proton Collisions at  $\sqrt{s} = 8$  TeV Measured with the ATLAS Detector*, *Phys. Rev. Lett.* **114** (2015), no. 22 221802, [[arXiv:1504.00357](#)].
- [172] **ATLAS** Collaboration, G. Aad et al., *Search for new phenomena in dijet mass and angular distributions from pp collisions at  $\sqrt{s} = 13$  TeV with the ATLAS detector*, *Phys. Lett.* **B754** (2016) 302–322, [[arXiv:1512.01530](#)].
- [173] M. Aliev, H. Lacker, U. Langenfeld, S. Moch, P. Uwer, and M. Wiedermann, *HATHOR: HAdronic Top and Heavy quarks crOss section calculator*, *Comput. Phys. Commun.* **182** (2011) 1034–1046, [[arXiv:1007.1327](#)].
- [174] S. Dawson, *The Effective W Approximation*, *Nucl. Phys.* **B249** (1985) 42–60.
- [175] M. S. Chanowitz and M. K. Gaillard, *Multiple Production of W and Z as a Signal of New Strong Interactions*, *Phys. Lett.* **B142** (1984) 85–90.
- [176] G. Altarelli, B. Mele, and F. Pitolli, *Heavy Higgs Production at Future Colliders*, *Nucl. Phys.* **B287** (1987) 205–224.
- [177] D. Pappadopulo, A. Thamm, R. Torre, and A. Wulzer, *Heavy Vector Triplets: Bridging Theory and Data*, *JHEP* **09** (2014) 060, [[arXiv:1402.4431](#)].
- [178] P. Stangl, *peterstangl/svg2data: v0.1*, Feb., 2017. [[doi:10.5281/zenodo.292635](#)].
- [179] R. Barbieri and G. F. Giudice, *Upper Bounds on Supersymmetric Particle Masses*, *Nucl. Phys.* **B306** (1988) 63–76.
- [180] H. Baer, V. Barger, D. Mickelson, and M. Padeffke-Kirkland, *SUSY models under siege: LHC constraints and electroweak fine-tuning*, *Phys. Rev.* **D89** (2014), no. 11 115019, [[arXiv:1404.2277](#)].
- [181] M. R. Buckley, A. Monteux, and D. Shih, *Precision Corrections to Fine Tuning in SUSY*, [arXiv:1611.05873](#).

- [182] G. G. Ross, K. Schmidt-Hoberg, and F. Staub, *Revisiting fine-tuning in the MSSM*, *JHEP* **03** (2017) 021, [[arXiv:1701.03480](#)].
- [183] J. Barnard and M. White, *Collider constraints on tuning in composite Higgs models*, *JHEP* **10** (2015) 072, [[arXiv:1507.02332](#)].
- [184] R. Arthur, V. Drach, M. Hansen, A. Hietanen, R. Lewis, C. Pica, and F. Sannino, *Composite (Goldstone) Higgs Dynamics on the Lattice: Spectrum of  $SU(2)$  Gauge Theory with two Fundamental Fermions*, *PoS LATTICE2014* (2014) 249, [[arXiv:1412.7302](#)].
- [185] CMS Performance Note, *Updates on Projections of Physics Reach with the Upgraded CMS Detector for High Luminosity LHC*, Oct., 2016. CMS DP -2016/064.
- [186] Trovatelli, Monica, *Prospects for future precision measurements of Higgs properties at HL-LHC*, 2015. Talk at 25th International Workshop on Weak Interactions and Neutrinos, Heidelberg.
- [187] Savin, Alexander, *Prospects for Higgs and SM measurements at the HL-LHC*, *EPJ Web of Conferences* **95** (2016) 04060.
- [188] CMS Collaboration, *Projected Performance of an Upgraded CMS Detector at the LHC and HL-LHC: Contribution to the Snowmass Process*, in *Proceedings, Community Summer Study 2013: Snowmass on the Mississippi (CSS2013): Minneapolis, MN, USA, July 29-August 6, 2013*, 2013. [arXiv:1307.7135](#).
- [189] R. Barbieri, G. Isidori, J. Jones-Perez, P. Lodone, and D. M. Straub,  *$U(2)$  and Minimal Flavour Violation in Supersymmetry*, *Eur. Phys. J.* **C71** (2011) 1725, [[arXiv:1105.2296](#)].
- [190] LHCb Collaboration, R. Aaij et al., *Test of lepton universality using  $B^+ \rightarrow K^+ \ell^+ \ell^-$  decays*, *Phys. Rev. Lett.* **113** (2014) 151601, [[arXiv:1406.6482](#)].
- [191] S. L. Bifani, “Search for new physics in  $b \rightarrow s \ell^+ \ell^-$  decays at lhcb.” CERN Seminar, 18 April 2017.
- [192] A. J. Buras, D. Buttazzo, J. Girrbach-Noe, and R. Knegjens,  *$K^+ \rightarrow \pi^+ \nu \bar{\nu}$  and  $K_L \rightarrow \pi^0 \nu \bar{\nu}$  in the Standard Model: status and perspectives*, *JHEP* **11** (2015) 033, [[arXiv:1503.02693](#)].
- [193] A. J. Buras, D. Buttazzo, and R. Knegjens,  *$K \rightarrow \pi \nu \bar{\nu}$  and  $\epsilon'/\epsilon$  in simplified new physics models*, *JHEP* **11** (2015) 166, [[arXiv:1507.08672](#)].
- [194] A. J. Buras, D. Buttazzo, J. Girrbach-Noe, and R. Knegjens, *Can we reach the Zeptouniverse with rare  $K$  and  $B_{s,d}$  decays?*, *JHEP* **11** (2014) 121, [[arXiv:1408.0728](#)].
- [195] E949 Collaboration, A. V. Artamonov et al., *New measurement of the  $K^+ \rightarrow \pi^+ \nu \bar{\nu}$  branching ratio*, *Phys. Rev. Lett.* **101** (2008) 191802, [[arXiv:0808.2459](#)].
- [196] E391a Collaboration, J. K. Ahn et al., *Experimental study of the decay  $K0(L) \rightarrow \pi0 \nu \nu\text{-bar}$* , *Phys. Rev.* **D81** (2010) 072004, [[arXiv:0911.4789](#)].
- [197] B. Bellazzini, C. Csáki, and J. Serra, *Composite Higgses*, *Eur. Phys. J.* **C74** (2014), no. 5 2766, [[arXiv:1401.2457](#)].
- [198] E. Katz, A. E. Nelson, and D. G. E. Walker, *The Intermediate Higgs*, *JHEP* **08** (2005) 074, [[hep-ph/0504252](#)].
- [199] J. Galloway, J. A. Evans, M. A. Luty, and R. A. Tacchi, *Minimal Conformal Technicolor and Precision Electroweak Tests*, *JHEP* **10** (2010) 086, [[arXiv:1001.1361](#)].
- [200] J. Barnard, T. Gherghetta, and T. S. Ray, *UV descriptions of composite Higgs models without elementary scalars*, *JHEP* **02** (2014) 002, [[arXiv:1311.6562](#)].
- [201] G. Ferretti and D. Karateev, *Fermionic UV completions of Composite Higgs models*, *JHEP* **03** (2014) 077, [[arXiv:1312.5330](#)].
- [202] G. Cacciapaglia and F. Sannino, *Fundamental Composite (Goldstone) Higgs Dynamics*, *JHEP* **04** (2014) 111, [[arXiv:1402.0233](#)].

- 
- [203] F. Sannino, A. Strumia, A. Tesi, and E. Vigiani, *Fundamental partial compositeness*, *JHEP* **11** (2016) 029, [[arXiv:1607.01659](#)].
- [204] J. Galloway, A. L. Kagan, and A. Martin, *A UV complete partially composite-pNGB Higgs*, *Phys. Rev.* **D95** (2017), no. 3 035038, [[arXiv:1609.05883](#)].
- [205] A. Agugliaro, O. Antipin, D. Becciolini, S. De Curtis, and M. Redi, *UV complete composite Higgs models*, *Phys. Rev.* **D95** (2017), no. 3 035019, [[arXiv:1609.07122](#)].
- [206] M. Frigerio, A. Pomarol, F. Riva, and A. Urbano, *Composite Scalar Dark Matter*, *JHEP* **07** (2012) 015, [[arXiv:1204.2808](#)].
- [207] H. Georgi and D. B. Kaplan, *Composite Higgs and Custodial SU(2)*, *Phys. Lett.* **B145** (1984) 216–220.
- [208] J. Serra, *Beyond the Minimal Top Partner Decay*, *JHEP* **09** (2015) 176, [[arXiv:1506.05110](#)].
- [209] M. Low, A. Tesi, and L.-T. Wang, *A pseudoscalar decaying to photon pairs in the early LHC Run 2 data*, *JHEP* **03** (2016) 108, [[arXiv:1512.05328](#)].
- [210] B. Bellazzini, R. Franceschini, F. Sala, and J. Serra, *Goldstones in Diphotons*, *JHEP* **04** (2016) 072, [[arXiv:1512.05330](#)].
- [211] M. Redi and A. Tesi, *Implications of a Light Higgs in Composite Models*, *JHEP* **10** (2012) 166, [[arXiv:1205.0232](#)].
- [212] J. Mrazek, A. Pomarol, R. Rattazzi, M. Redi, J. Serra, and A. Wulzer, *The Other Natural Two Higgs Doublet Model*, *Nucl. Phys.* **B853** (2011) 1–48, [[arXiv:1105.5403](#)].
- [213] J. Wess and B. Zumino, *Consequences of anomalous Ward identities*, *Phys. Lett.* **37B** (1971) 95–97.
- [214] E. Witten, *Global Aspects of Current Algebra*, *Nucl. Phys.* **B223** (1983) 422–432.
- [215] D. Parganlija, *Quarkonium Phenomenology in Vacuum*. PhD thesis, Frankfurt U., 2011. [[arXiv:1208.0204](#)].
- [216] Parganlija, Denis, *Pion-Pion-Streuung in einem geeichten linearen Sigma-Modell mit chiraler  $U(2)_R \times U(2)_L$ -Symmetrie*, Dec, 2006. Diplomarbeit at Johann Wolfgang Goethe-Universität Frankfurt am Main.
- [217] A. Banerjee, G. Bhattacharyya, and T. S. Ray, *Improving Fine-tuning in Composite Higgs Models*, [[arXiv:1703.08011](#)].
- [218] I. Doršner, S. Fajfer, A. Greljo, J. F. Kamenik, and N. Košnik, *Physics of leptiquarks in precision experiments and at particle colliders*, *Phys. Rept.* **641** (2016) 1–68, [[arXiv:1603.04993](#)].
- [219] **LHCb** Collaboration, R. Aaij et al., *Differential branching fraction and angular analysis of the decay  $B^0 \rightarrow K^{*0} \mu^+ \mu^-$* , *JHEP* **08** (2013) 131, [[arXiv:1304.6325](#)].
- [220] **LHCb** Collaboration, R. Aaij et al., *Measurement of Form-Factor-Independent Observables in the Decay  $B^0 \rightarrow K^{*0} \mu^+ \mu^-$* , *Phys. Rev. Lett.* **111** (2013) 191801, [[arXiv:1308.1707](#)].
- [221] **LHCb** Collaboration, R. Aaij et al., *Angular analysis of the  $B^0 \rightarrow K^{*0} \mu^+ \mu^-$  decay using  $3 \text{ fb}^{-1}$  of integrated luminosity*, *JHEP* **02** (2016) 104, [[arXiv:1512.04442](#)].
- [222] The ATLAS collaboration, *Angular analysis of  $B_d^0 \rightarrow K^* \mu^+ \mu^-$  decays in pp collisions at  $\sqrt{s} = 8 \text{ TeV}$  with the ATLAS detector*, Apr, 2017. ATLAS-CONF-2017-023.
- [223] The CMS collaboration, *Measurement of the  $P_1$  and  $P'_5$  angular parameters of the decay  $B^0 \rightarrow K^{*0} \mu^+ \mu^-$  in proton-proton collisions at  $\sqrt{s} = 8 \text{ TeV}$* , March, 2017. CMS-PAS-BPH-15-008.
- [224] C. Bobeth, G. Hiller, and G. Piranishvili, *Angular distributions of  $\bar{B} \rightarrow \bar{K} \ell^+ \ell^-$  decays*, *JHEP* **12** (2007) 040, [[arXiv:0709.4174](#)].

- [225] **LHCb** Collaboration, R. Aaij et al., *Differential branching fractions and isospin asymmetries of  $B \rightarrow K^{(*)}\mu^+\mu^-$  decays*, *JHEP* **06** (2014) 133, [[arXiv:1403.8044](#)].
- [226] **LHCb** Collaboration, R. Aaij et al., *Angular analysis and differential branching fraction of the decay  $B_s^0 \rightarrow \phi\mu^+\mu^-$* , *JHEP* **09** (2015) 179, [[arXiv:1506.08777](#)].
- [227] S. Descotes-Genon, J. Matias, and J. Virto, *Understanding the  $B \rightarrow K^*\mu^+\mu^-$  Anomaly*, *Phys. Rev.* **D88** (2013) 074002, [[arXiv:1307.5683](#)].
- [228] F. Beaujean, C. Bobeth, and D. van Dyk, *Comprehensive Bayesian analysis of rare (semi)leptonic and radiative  $B$  decays*, *Eur. Phys. J.* **C74** (2014) 2897, [[arXiv:1310.2478](#)]. [Erratum: *Eur. Phys. J.*C74,3179(2014)].
- [229] T. Hurth and F. Mahmoudi, *On the LHCb anomaly in  $B \rightarrow K^*\ell^+\ell^-$* , *JHEP* **04** (2014) 097, [[arXiv:1312.5267](#)].
- [230] J. Lyon and R. Zwicky, *Resonances gone topsy turvy - the charm of QCD or new physics in  $b \rightarrow s\ell^+\ell^-$ ?*, [arXiv:1406.0566](#).
- [231] M. Ciuchini, M. Fedele, E. Franco, S. Mishima, A. Paul, L. Silvestrini, and M. Valli,  *$B \rightarrow K^*\ell^+\ell^-$  decays at large recoil in the Standard Model: a theoretical reappraisal*, *JHEP* **06** (2016) 116, [[arXiv:1512.07157](#)].
- [232] V. G. Chobanova, T. Hurth, F. Mahmoudi, D. Martinez Santos, and S. Neshatpour, *Large hadronic power corrections or new physics in the rare decay  $B \rightarrow K^*\ell\ell$ ?*, [arXiv:1702.02234](#).
- [233] J. C. Pati and A. Salam, *Lepton Number as the Fourth Color*, *Phys. Rev.* **D10** (1974) 275–289. [Erratum: *Phys. Rev.*D11,703(1975)].
- [234] H. Georgi and S. L. Glashow, *Unity of All Elementary Particle Forces*, *Phys. Rev. Lett.* **32** (1974) 438–441.
- [235] G. F. Giudice and R. Rattazzi,  *$R$ -parity violation and unification*, *Phys. Lett.* **B406** (1997) 321–327, [[hep-ph/9704339](#)].
- [236] P. W. Angel, Y. Cai, N. L. Rodd, M. A. Schmidt, and R. R. Volkas, *Testable two-loop radiative neutrino mass model based on an  $LLQd^cQd^c$  effective operator*, *JHEP* **10** (2013) 118, [[arXiv:1308.0463](#)]. [Erratum: *JHEP*11,092(2014)].
- [237] B. Gripaios, M. Nardecchia, and S. A. Renner, *Composite leptoquarks and anomalies in  $B$ -meson decays*, *JHEP* **05** (2015) 006, [[arXiv:1412.1791](#)].
- [238] W. Buchmuller, R. Ruckl, and D. Wyler, *Leptoquarks in Lepton - Quark Collisions*, *Phys. Lett.* **B191** (1987) 442–448. [Erratum: *Phys. Lett.*B448,320(1999)].
- [239] G. Hiller and M. Schmaltz,  *$R_K$  and future  $b \rightarrow s\ell\ell$  physics beyond the standard model opportunities*, *Phys. Rev.* **D90** (2014) 054014, [[arXiv:1408.1627](#)].
- [240] M. Bauer and M. Neubert, *Minimal Leptoquark Explanation for the  $R_{D^{(*)}}$ ,  $R_K$ , and  $(g-2)_g$  Anomalies*, *Phys. Rev. Lett.* **116** (2016), no. 14 141802, [[arXiv:1511.01900](#)].
- [241] **BaBar** Collaboration, J. P. Lees et al., *Measurement of an Excess of  $\bar{B} \rightarrow D^{(*)}\tau^-\bar{\nu}_\tau$  Decays and Implications for Charged Higgs Bosons*, *Phys. Rev.* **D88** (2013), no. 7 072012, [[arXiv:1303.0571](#)].
- [242] **Belle** Collaboration, M. Huschle et al., *Measurement of the branching ratio of  $\bar{B} \rightarrow D^{(*)}\tau^-\bar{\nu}_\tau$  relative to  $\bar{B} \rightarrow D^{(*)}\ell^-\bar{\nu}_\ell$  decays with hadronic tagging at Belle*, *Phys. Rev.* **D92** (2015), no. 7 072014, [[arXiv:1507.03233](#)].
- [243] **LHCb** Collaboration, R. Aaij et al., *Measurement of the ratio of branching fractions  $\mathcal{B}(\bar{B}^0 \rightarrow D^{*+}\tau^-\bar{\nu}_\tau)/\mathcal{B}(\bar{B}^0 \rightarrow D^{*+}\mu^-\bar{\nu}_\mu)$* , *Phys. Rev. Lett.* **115** (2015), no. 11 111803, [[arXiv:1506.08614](#)]. [Addendum: *Phys. Rev. Lett.*115,no.15,159901(2015)].

- 
- [244] L. Calibbi, A. Crivellin, and T. Ota, *Effective Field Theory Approach to  $b \rightarrow sl\ell^{(\prime)}$ ,  $B \rightarrow K^{(*)}\nu\bar{\nu}$  and  $B \rightarrow D^{(*)}\tau\nu$  with Third Generation Couplings*, *Phys. Rev. Lett.* **115** (2015) 181801, [[arXiv:1506.02661](#)].
- [245] S. Fajfer and N. Košnik, *Vector leptoquark resolution of  $R_K$  and  $R_{D^{(*)}}$  puzzles*, *Phys. Lett.* **B755** (2016) 270–274, [[arXiv:1511.06024](#)].
- [246] D. Bečirević and O. Sumensari, *A leptoquark model to accommodate  $R_K^{\text{exp}} < R_K^{\text{SM}}$  and  $R_{K^*}^{\text{exp}} < R_{K^*}^{\text{SM}}$* , [arXiv:1704.05835](#).
- [247] R. Barbieri, G. Isidori, A. Pattori, and F. Senia, *Anomalies in  $B$ -decays and  $U(2)$  flavour symmetry*, *Eur. Phys. J.* **C76** (2016), no. 2 67, [[arXiv:1512.01560](#)].
- [248] P. Colangelo, F. De Fazio, P. Santorelli, and E. Scrimieri, *Rare  $B \rightarrow K^{(*)}$  neutrino anti-neutrino decays at  $B$  factories*, *Phys. Lett.* **B395** (1997) 339–344, [[hep-ph/9610297](#)].
- [249] Y. Grossman, Z. Ligeti, and E. Nardi, *New limit on inclusive  $B \rightarrow X_s$  anti-neutrino neutrino decay and constraints on new physics*, *Nucl. Phys.* **B465** (1996) 369–398, [[hep-ph/9510378](#)]. [Erratum: *Nucl. Phys.*B480,753(1996)].
- [250] D. Melikhov, N. Nikitin, and S. Simula, *Right-handed currents in rare exclusive  $B \rightarrow (K, K^*)$  neutrino anti-neutrino decays*, *Phys. Lett.* **B428** (1998) 171–178, [[hep-ph/9803269](#)].
- [251] G. Buchalla and A. J. Buras, *QCD corrections to rare  $K$  and  $B$  decays for arbitrary top quark mass*, *Nucl. Phys.* **B400** (1993) 225–239.
- [252] M. Misiak and J. Urban, *QCD corrections to FCNC decays mediated by  $Z$  penguins and  $W$  boxes*, *Phys. Lett.* **B451** (1999) 161–169, [[hep-ph/9901278](#)].
- [253] G. Buchalla and A. J. Buras, *The rare decays  $K \rightarrow \pi\nu\bar{\nu}$ ,  $B \rightarrow X\nu\bar{\nu}$  and  $B \rightarrow l^+l^-$ : An Update*, *Nucl. Phys.* **B548** (1999) 309–327, [[hep-ph/9901288](#)].
- [254] J. Brod, M. Gorbahn, and E. Stamou, *Two-Loop Electroweak Corrections for the  $K \rightarrow \pi\nu\bar{\nu}$  Decays*, *Phys. Rev.* **D83** (2011) 034030, [[arXiv:1009.0947](#)].
- [255] W. Altmannshofer, A. J. Buras, D. M. Straub, and M. Wick, *New strategies for New Physics search in  $B \rightarrow K^*\nu\bar{\nu}$ ,  $B \rightarrow K\nu\bar{\nu}$  and  $B \rightarrow X_s\nu\bar{\nu}$  decays*, *JHEP* **04** (2009) 022, [[arXiv:0902.0160](#)].
- [256] **HPQCD** Collaboration, C. Bouchard, G. P. Lepage, C. Monahan, H. Na, and J. Shigemitsu, *Rare decay  $B \rightarrow K\ell^+\ell^-$  form factors from lattice QCD*, *Phys. Rev.* **D88** (2013), no. 5 054509, [[arXiv:1306.2384](#)]. [Erratum: *Phys. Rev.*D88,no.7,079901(2013)].
- [257] R. R. Horgan, Z. Liu, S. Meinel, and M. Wingate, *Lattice QCD calculation of form factors describing the rare decays  $B \rightarrow K^*\ell^+\ell^-$  and  $B_s \rightarrow \phi\ell^+\ell^-$* , *Phys. Rev.* **D89** (2014), no. 9 094501, [[arXiv:1310.3722](#)].
- [258] P. Ball and R. Zwicky, *New results on  $B \rightarrow \pi, K, \eta$  decay formfactors from light-cone sum rules*, *Phys. Rev.* **D71** (2005) 014015, [[hep-ph/0406232](#)].
- [259] P. Ball and R. Zwicky,  *$B_{d,s} \rightarrow \rho, \omega, K^*, \phi$  decay form-factors from light-cone sum rules revisited*, *Phys. Rev.* **D71** (2005) 014029, [[hep-ph/0412079](#)].
- [260] A. Bharucha, D. M. Straub, and R. Zwicky,  *$B \rightarrow V\ell^+\ell^-$  in the Standard Model from light-cone sum rules*, *JHEP* **08** (2016) 098, [[arXiv:1503.05534](#)].
- [261] J. A. Bailey et al.,  *$B \rightarrow K\ell^+l^-$  decay form factors from three-flavor lattice QCD*, *Phys. Rev.* **D93** (2016), no. 2 025026, [[arXiv:1509.06235](#)].
- [262] **Belle** Collaboration, J. Grygier et al., *Search for  $B \rightarrow h\nu\bar{\nu}$  decays with semileptonic tagging at Belle*, [arXiv:1702.03224](#).
- [263] Nakamura, Katsuro, *Status of Belle II Detector*, Dec, 2016. BELLE2-TALK-CONF-2017-007.

- [264] Urquijo, Phillip, *Extrapolation of  $B \rightarrow K^{(*)}\nu\bar{\nu}$  to the full Belle II dataset*, Feb, 2016. BELLE2-MEMO-2016-008.
- [265] Atmacan, Hulya, *Rare B Decay at Belle II*, Dec, 2016. BELLE2-TALK-CONF-2017-008.
- [266] W. Buchmuller and D. Wyler, *Effective Lagrangian Analysis of New Interactions and Flavor Conservation*, *Nucl. Phys.* **B268** (1986) 621–653.
- [267] **BaBar** Collaboration, J. P. Lees et al., *Measurement of the  $B \rightarrow X_s l^+ l^-$  branching fraction and search for direct CP violation from a sum of exclusive final states*, *Phys. Rev. Lett.* **112** (2014) 211802, [[arXiv:1312.5364](#)].
- [268] **CDF** Collaboration, T. Aaltonen et al., *Search for the Decays  $B_s^0 \rightarrow e^+ \mu^-$  and  $B_s^0 \rightarrow e^+ e^-$  in CDF Run II*, *Phys. Rev. Lett.* **102** (2009) 201801, [[arXiv:0901.3803](#)].
- [269] **CMS** Collaboration, S. Chatrchyan et al., *Measurement of the  $B(s)$  to  $mu+$   $mu-$  branching fraction and search for  $B^0$  to  $mu+$   $mu-$  with the CMS Experiment*, *Phys. Rev. Lett.* **111** (2013) 101804, [[arXiv:1307.5025](#)].
- [270] **LHCb** Collaboration, R. Aaij et al., *Measurement of the  $B_s^0 \rightarrow \mu^+ \mu^-$  branching fraction and effective lifetime and search for  $B^0 \rightarrow \mu^+ \mu^-$  decays*, [arXiv:1703.05747](#).
- [271] **LHCb** Collaboration, R. Aaij et al., *Search for the decays  $B_s^0 \rightarrow \tau^+ \tau^-$  and  $B^0 \rightarrow \tau^+ \tau^-$* , [arXiv:1703.02508](#).
- [272] **BaBar** Collaboration, J. P. Lees et al., *Search for  $B^+ \rightarrow K^+ \tau^+ \tau^-$  at the BaBar experiment*, *Phys. Rev. Lett.* **118** (2017), no. 3 031802, [[arXiv:1605.09637](#)].
- [273] **BaBar** Collaboration, B. Aubert et al., *Measurements of branching fractions, rate asymmetries, and angular distributions in the rare decays  $B \rightarrow K l^+ l^-$  and  $B \rightarrow K^* l^+ l^-$* , *Phys. Rev.* **D73** (2006) 092001, [[hep-ex/0604007](#)].
- [274] **LHCb** Collaboration, R. Aaij et al., *Search for the lepton-flavor violating decays  $B_s^0 \rightarrow e^\pm \mu^\mp$  and  $B^0 \rightarrow e^\pm \mu^\mp$* , *Phys. Rev. Lett.* **111** (2013) 141801, [[arXiv:1307.4889](#)].
- [275] **BaBar** Collaboration, J. P. Lees et al., *A search for the decay modes  $B^{+-} \rightarrow h^{+-} \tau^+ l^-$* , *Phys. Rev.* **D86** (2012) 012004, [[arXiv:1204.2852](#)].
- [276] O. J. P. Eboli, R. Zukanovich Funchal, and T. L. Lungov, *Signal and backgrounds for leptoquarks at the CERN LHC*, *Phys. Rev.* **D57** (1998) 1715–1729, [[hep-ph/9709319](#)].
- [277] A. Belyaev, C. Leroy, R. Mehdiyev, and A. Pukhov, *Leptoquark single and pair production at LHC with CalcHEP/CompHEP in the complete model*, *JHEP* **09** (2005) 005, [[hep-ph/0502067](#)].
- [278] J. Blumlein, E. Boos, and A. Kryukov, *Leptoquark pair production in hadronic interactions*, *Z. Phys.* **C76** (1997) 137–153, [[hep-ph/9610408](#)].
- [279] J. L. Hewett and T. G. Rizzo, *Much ado about leptoquarks: A Comprehensive analysis*, *Phys. Rev.* **D56** (1997) 5709–5724, [[hep-ph/9703337](#)].
- [280] S. Dulat, T.-J. Hou, J. Gao, M. Guzzi, J. Huston, P. Nadolsky, J. Pumplin, C. Schmidt, D. Stump, and C. P. Yuan, *New parton distribution functions from a global analysis of quantum chromodynamics*, *Phys. Rev.* **D93** (2016), no. 3 033006, [[arXiv:1506.07443](#)].
- [281] A. Buckley, J. Ferrando, S. Lloyd, K. Nordström, B. Page, M. Rüfenacht, M. Schönherr, and G. Watt, *LHAPDF6: parton density access in the LHC precision era*, *Eur. Phys. J.* **C75** (2015) 132, [[arXiv:1412.7420](#)].
- [282] **ATLAS** Collaboration, G. Aad et al., *Searches for scalar leptoquarks in  $pp$  collisions at  $\sqrt{s} = 8$  TeV with the ATLAS detector*, *Eur. Phys. J.* **C76** (2016), no. 1 5, [[arXiv:1508.04735](#)].
- [283] **ATLAS** Collaboration, M. Aaboud et al., *Search for scalar leptoquarks in  $pp$  collisions at  $\sqrt{s}=13$  TeV with the ATLAS experiment*, *New J. Phys.* **18** (2016), no. 9 093016, [[arXiv:1605.06035](#)].



- 
- [284] **CMS Collaboration**, V. Khachatryan et al., *Search for pair production of first and second generation leptoquarks in proton-proton collisions at  $\sqrt{s} = 8$  TeV*, *Phys. Rev.* **D93** (2016), no. 3 032004, [[arXiv:1509.03744](#)].
- [285] **CMS Collaboration** Collaboration, *Search for pair-production of second-generation scalar leptoquarks in  $pp$  collisions at  $\sqrt{s} = 13$  TeV with the CMS detector*, Tech. Rep. CMS-PAS-EXO-16-007, CERN, Geneva, 2016.
- [286] C. McNeile, C. T. H. Davies, E. Follana, K. Hornbostel, and G. P. Lepage, *High-Precision  $f_{B_s}$  and HQET from Relativistic Lattice QCD*, *Phys. Rev.* **D85** (2012) 031503, [[arXiv:1110.4510](#)].
- [287] **HPQCD Collaboration**, R. J. Dowdall, C. T. H. Davies, R. R. Horgan, C. J. Monahan, and J. Shigemitsu, *B-Meson Decay Constants from Improved Lattice Nonrelativistic QCD with Physical  $u$ ,  $d$ ,  $s$ , and  $c$  Quarks*, *Phys. Rev. Lett.* **110** (2013), no. 22 222003, [[arXiv:1302.2644](#)].
- [288] F. Beaujean, C. Bobeth, and S. Jahn, *Constraints on tensor and scalar couplings from  $B \rightarrow K \bar{\mu} \mu$  and  $B_s \rightarrow \bar{\mu} \mu$* , *Eur. Phys. J.* **C75** (2015), no. 9 456, [[arXiv:1508.01526](#)].
- [289] R. Alonso, B. Grinstein, and J. Martin Camalich,  *$SU(2) \times U(1)$  gauge invariance and the shape of new physics in rare  $B$  decays*, *Phys. Rev. Lett.* **113** (2014) 241802, [[arXiv:1407.7044](#)].
- [290] A. J. Buras, R. Fleischer, J. Girrbach, and R. Knegjens, *Probing New Physics with the  $B_s \rightarrow \mu^+ \mu^-$  Time-Dependent Rate*, *JHEP* **07** (2013) 77, [[arXiv:1303.3820](#)].
- [291] **LHCb Collaboration**, R. Aaij et al., *Measurement of the  $B_s^0 \rightarrow \mu^+ \mu^-$  branching fraction and search for  $B^0 \rightarrow \mu^+ \mu^-$  decays at the LHCb experiment*, *Phys. Rev. Lett.* **111** (2013) 101805, [[arXiv:1307.5024](#)].
- [292] The LHCb Collaboration, *Impact of the LHCb upgrade detector design choices on physics and trigger performance*, Aug, 2014. LHCb-PUB-2014-040.
- [293] **CMS Collaboration**, C. Collaboration, *B Physics analyses for the Phase-II Upgrade Technical Proposal*, .
- [294] H. Haario, E. Saksman, and J. Tamminen, *An Adaptive Metropolis Algorithm.*, *Bernoulli* **7.2** (2001) 223–242.
- [295] D. Wraith, M. Kilbinger, K. Benabed, O. Cappe, J.-F. Cardoso, G. Fort, S. Prunet, and C. P. Robert, *Estimation of cosmological parameters using adaptive importance sampling*, *Phys. Rev.* **D80** (2009) 023507, [[arXiv:0903.0837](#)].
- [296] F. Beaujean, *A Bayesian analysis of rare  $B$  decays with advanced Monte Carlo methods*. Dissertation, Technische Universität München, München, 2012.



## Acknowledgments

First of all, I want to express my deep gratitude to my supervisor, David Straub. For the last 3.5 years it has always been a pleasure to collaborate with you, to discuss with you and to profit from your deep physical understanding. Thank you so much for giving me all the opportunities for traveling. And thank you for all your advises and for all the answers to the many physics questions I had.

I also want to thank Martin Beneke for supervising my diploma thesis and later agreeing to act as my official Doktorvater.

For the warm welcome in Cincinnati I want to thank Stefania Gori and Wolfgang Altmannshofer. Thank you for the nice time I spent there.

Very special thanks go to Peter Stangl for sharing three offices with me in the past 4.5 years. Thank you for the many, many discussions we had and for tolerating me and all the silly things I do over such a long time.

For proofreading I want to thank Philipp Meyer and very, very especially Gal Ben Porath, who read this thesis in such great detail! I also want to thank David for valuable comments on the manuscript.

I want to thank all my friends who accompanied me in the past years, gave me confidence and made the last years such a nice time. And most important of all, I want to thank you, Micki, for everything. And for everything that is coming.